Alma Mater Studiorum – Università di Bologna

DOTTORATO DI RICERCA

SCIENCE FOR CONSERVATION

Ciclo XXII

Settore/i scientifico disciplinari di afferenza: CHIM/12

TITOLO TESI

Transmission and Reflection (ATR) Far-Infrared Spectroscopy Applied in the Analysis of Cultural Heritage Materials

Presentata da: **KENDIX Elsebeth Langholz**

Coordinatore Dottorato **Relatore**

Prof. R. Mazzeo **Prof. R. Mazzeo**

Esame finale anno 2009

TRANSMISSION & REFLECTION (ATR) FAR-INFRARED SPECTROSCOPY APPLIED IN THE ANALYSIS OF CULTURAL HERITAGE MATERIALS

ELSEBETH LANGHOLZ KENDIX

This project has been carried out at:

Università di Bologna, Ravenna Campus,
M2ADL - Microchemistry & Microscopy Art Diagnostic Laboratory,
Via Guaccimanni 42
48100 Ravenna
Italy

M2ADL homepage: http://www.tecore.unibo.it/html/Lab_Microscopia/M2ADL/

This project has been carried out with the support of the European Union, within the VI Framework Programme under Marie Curie Early Stage Training (EST) action, as part of the EPISCON project, contract no MEST-CT-2005-020559.

When You Eliminate The Impossible, Whatever Remains,
However Improbable, Must Be The Truth.

Sherlock Holmes
(Aka. Sir Arthur Conan Doyle,
1859-1930)

ABSTRACT

Most infrared analysis is performed in the Mid-IR (MIR) range (4000-400 cm^{-1}). In the case of inorganic components, the normal frequency of an organic stretching vibration decrease as the molecular weight increase, because the frequency of a vibration is inversely proportional to the square-root of the reduced mass. Thus, for high molecular-weight species such as metallic complexes or some halides, oxide and sulphides, this relationship shifts the vibrations into the Far-IR (FIR) region, roughly defined as below 400 cm^{-1}. FIR spectroscopy is thus an alternative way of collecting spectra of many inorganic pigments and corrosion products found on art objects, which is not normally observed in the MIR region. Most FIR spectra are traditionally collected in transmission mode but as a real novelty it is now also possible to record FIR spectra in ATR (Attenuated Total Reflectance) mode.

In FIR transmission we employ polyethylene (PE) for preparation of pellets by embedding the sample in PE using much the same procedure as for preparing KBr pellets. Unfortunately, the preparation requires heating of the PE in order to produces at transparent pellet. This will affect compounds with low melting points, especially those with structurally incorporated water. Another option in FIR transmission is the use of thin films. We test the use of polyethylene thin film (PETF), both commercial and laboratory-made PETF. Here there is no heating of the sample and almost no preparation time, as the powdery sample is merely brushed onto the surface of the PETF and then the spectrum can be collected.

ATR collection of samples is possible in both the MIR and FIR region on solid, powdery or liquid samples. Changing from the MIR to the FIR region is easy as it simply requires the change of detector and beamsplitter (which can be performed within a few minutes). No preparation of the sample is necessary, which is a huge advantage over the PE transmission method. The only concern with ATR is the need for good contact between the ATR crystal and the sample. This can be a problem especially with solid samples as not all solid samples have a planar surface that can come into good contact with the ATR crystal. In this case micro-sampling from the sample surface is necessary.

In most cases comparison of standard spectra collected in FIR transmission and FIR ATR mode leads to only a few differences. The most obvious, when comparing transmission with ATR, is the distortion of band shape. The ATR band shape appears asymmetrical in the lower wavenumber region when compared to spectra collected in transmission mode. Also, intensity differences are noticed. However, the biggest difference can be the shift of strong absorbing

bands moving to lower wavenumbers in ATR mode. In the majority of compounds, the shifts observed are small, approximately 1-10 cm^{-1}, but for very strong absorbing compounds the shifts observed can be as big as 30-50 cm^{-1}. These observed changes are in accordance with the established theory of ATR spectroscopy. It necessitates the collection of library standard samples in both FIR transmission and ATR modes, provided these two methods of collecting are to be employed for analyses of unknown samples.

Standard samples of 150 pigment and corrosion compounds are thus collected in both FIR transmission and ATR mode in order to build up a digital library of spectra for comparison with unknown samples. XRD, XRF and Raman spectroscopy assists us in confirming the purity or impurity of our standard samples. Focus of our attention are on the oxides and sulphides of metals, as they are not normally observed in the MIR region, but are visible in the FIR region. Many of these pigments and corrosion standards, particularly those originating from minerals, are available in FIR transmission libraries and literature. However, ATR spectra of pigments and minerals, are hardly available in the literature. This can complicate ATR identification of unknown samples in the FIR region.

24 didactic test tables, with known pigment and binder painted on the surface of a limestone tablet, are used for testing the established library and different ways of collecting in ATR and transmission mode. In ATR, micro samples are scratched from the surface and examined in both the MIR and FIR region. Additionally, direct surface contact of the didactic tablets with the ATR crystal are tested together with water enhanced surface contact. A drop of water on the ATR crystal before contact with the solid sample can enhance the signal intensity when there are problems achieving contact due to planarity issues. But the question is if the sample can tolerate the exposure to water. When the binding media on our test tablet is glue, it is not advisable to use water. Oil binding medium seem to be less affected by contact with the water drop. In FIR transmission we compare the powder from our test tablet on the laboratory PETF and embedded in PE. We also compare the PE pellets collected using a 4x beam condenser, focusing the IR beam area from 8 mm to 2 mm. In theory, this should make it possible to use less sample amount in our pellets. In practice we experience an increase in noise sensitivity in the FIR region compared to spectra of PE pellets collected without the beam condenser.

A few samples collected from a mural painting in a Nepalese temple, corrosion products collected from archaeological Chinese bronze objects and samples from a mural paintings in an Italian abbey, are examined by ATR or transmission spectroscopy.

ABBREVIATIONS & ACRONYMS:

μATR	Micro-Attenuated Total Reflectance
ATR	Attenuated Total Reflectance
CH	Cultural Heritage
CsI	Cesium Iodide
DSC	Differential Scanning Calorimetry
DTGS	Deuterated TriGlycine Sulfate
EM	Electro Magnetic
FIR	Far-InfraRed
FPA	Focal Plane Array
FTIR	Fourier Transform InfraRed
GPG	Gas Purging Generator
HDPE	High Density PolyEthylene
IR	InfraRed
IRE	Internal Reflection Element
KBr	Potassium Bromide
LOD	Limit Of Detection
M2ADL	Microchemistry and Microscopy Art Diagnostic Laboratory
MCT	Mercury Cadmium Telluride
MIR	Mid-InfraRed
n_{21}	ratio n_2/n_1
OPD	Optical Path Difference
PE	PolyEthylene
PETF	PolyEthylene Thin Film
S/N	Signal-to-Noise ratio
Std	Standard
UHMWPE	Ultra High Molecular Weight PolyEthylene
ZPD	Zero Path Difference

CONTENTS

CHAPTER 1 INTRODUCTION

1.1 FROM ARCHAEOLOGY TO CONSERVATION SCIENCE

Archaeology has been described using the demoralising words "…archaeology is a science which destroys its evidence in order to achieve the needed realisation" [1]. This statement is still valid in most cases although development in the field of analytical investigation has altered this to the better through the past decades.

Why is the scientific examination of cultural heritage materials important? The question can be answered in many ways, but the most true answer is probably, because we are curious. Curious what materials the artist have used compared to his contemporary colleagues or to historical written documents. Curious, as to the artistic choice behind choosing those particular materials and in what manner did he used them. Did he used them like historic documents suggests or did he invent another use for them. Can we by gathering both historical written documents and scientific examination of artworks create a living image of the artist, of the materials, the techniques, the thought process that went into his creations, centuries after the artists death? Why do we need to know this? Not all artworks can survive unchanged for centuries. Some do, and why is that? Again it comes down to the materials and the techniques that was used. If they don't survive the passage of time, if they deteriorate and degrade, can we repair them? Should we? That is a philosophical question still under heavy debate, but in order to prevent further degradation we should at least try to stop the degradations so future generations can still enjoy the artworks. And how do we do that? This requires knowledge of the materials. Without identifying the materials used, it is very difficult to start a preventive intervention. Let alone to start at complete restoration of an artwork. Previous interventions have been carried out with catastrophically results because of improper knowledge of the artwork, the artist and his materials.

This all bring us back to identification of materials. If any intervention is to be performed identification of the materials used is of uttermost importance. Identification of materials can be conducted in many different ways. Visually, we can observe with our eyes the materials used and historically we can gain as much knowledge as possible about the period, the artist, the artwork etc. and technically there are instruments available for all kinds of examinations. There are the non-invasive, non-destructive instruments like multi-scanning imaging systems, X-ray fluorescence, and Raman spectroscopy, which can collect pictures or spectra, without as much as taking a microscopically sample.

They can to a large extend gives us information about the surface, the upper paint layers on a picture or the corrosion patina on a bronze figurine. But they cannot tell us in what order the paint

layers was applied or how the corrosion patina grows on the figurine. In order to acquire this kind of information we need to take samples from the artwork, not necessary large samples. Small microscopic samples can in most cases gives us the information required.

There are now non-destructive and non-invasive instruments available to the conservation scientist which were not available 10 years ago thanks to the high-speed development in computer and laser technologies during the last decades. The development of said instruments means that they are becoming cheaper to buy, easier to use and produce better results than ever before at an even quicker pace, making the scientific investigations more accurate and less time consuming.

In the case of necessary sampling, the amount taken from Cultural Heritage (CH) object or artworks is becoming increasingly smaller as time goes on. Most of the samples taken from artworks are microscopically small and thus it is necessary to use an analytical technique with high sensitivity. Infrared (IR) spectroscopy is such a technique. It is still the most used analytical technique, partly because of the sensitivity and the price of a new IR instrument, but the main reason is the information achieved by applying this technique which for instance can be applied in the knowledge of a painters techniques and his choice in materials. Other techniques, such as Raman spectroscopy, a complimentary technique to IR, is quickly gaining popularity, despite the teething troubles especially with fluorescence when using the visual lasers. But the Raman instrument is still more expensive than an IR instrument and therefore it is still not so common as the relatively cheaper IR instruments.

1.2 INFRARED SPECTROSCOPY

The analytical method of infrared (IR) spectroscopy has been applied to the Cultural Heritage (CH) field for many decades since the non-visual IR region of the electromagnetic spectrum (see ***Figure 1.1***.)) was first discovered by the astronomer Sir William Herschel [2] in 1800. However, it took a little while before the first industrial produced dispersive IR spectrometer (model D83) from Adam Hilger Ltd. saw the light of day in 1913 [3].

Interpretation of bands in IR and Raman spectra have been a difficult task, which were not really developed until the quantum theory was in place, predicting molecular and lattice bands, just before World War II. From that time forward the developments in IR spectroscopy have been colossal. In particular the development and application of the Michelson Interferometer in the Fourier Transform IR (FTIR) spectrometers, together with the PC assisted spectrometer control, have participated in the development of newer, faster and more advanced methods of applying IR spectroscopy, like Micro-ATR (Attenuated Total Reflectance) mapping, Step-Scan Time-Resolved

FTIR Spectroscopy (S2TRS), Polarization Modulation FTIR Spectroscopy, and Two Dimensional Infrared (2D-IR) Correlation Spectroscopy [4]. These methods are all advanced spectroscopic methods requiring as a basis the simple FTIR spectrometer and then additional modules attached to the spectrometer.

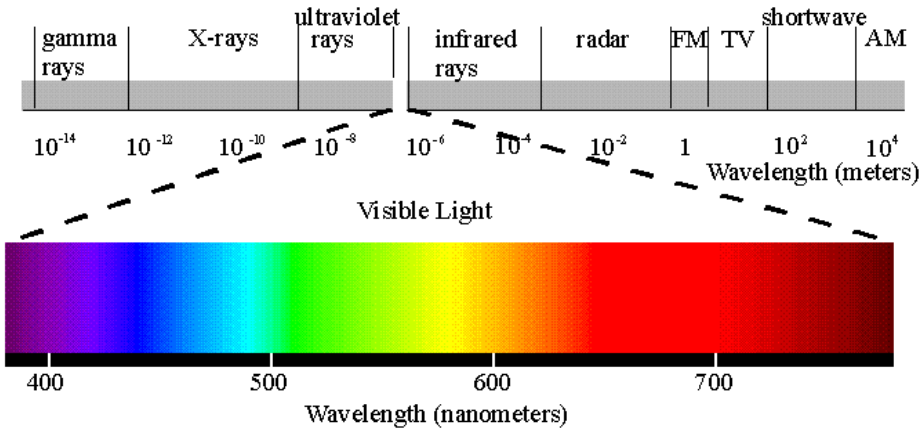

Figure 1.1: The Electromagnetic Spectrum as we know it today, showing the visual range, which was already known by the time the astronomer Sir William Herschel in 1800 concluded there were non-visual ranges of the EM spectrum. He discovered the Near-IR region of the IR range [2].

However, the most used form of IR spectroscopy are still transmission and ATR spectroscopies. In transmission spectroscopy the sample is usually embedded in a KBr pellet for investigations in the mid-IR (MIR) region, which was firstly described by Stimson in 1952 [5] and later described in arduous detail by Dent [6]. The IR spectrometers before 1960 where all dispersive prisms instruments, while the Fourier Transform IR (FTIR) spectrometers only slowly began being industrially produced in the 1960s after the availability of computers became widespread, employing the Cooley-Tukey algorithm [7][1] which converts analogue-to-digital signals. All FTIR instrument are build on the Michelson interferometer, which was invented already in 1887[2] but it was not applied industrially until the FTIR instrument was a reality in the 1960s. ATR spectroscopy is equally based on the FTIR instrument and originally though to be used to calculate effective thickness of thin films on surfaces. The theory behind ATR spectroscopy is well described by Harrick as early as the mid-sixties [9, 10]. The applications of these two basic methods of spectroscopy have thus been applied for many years for identifying covalent bonds in molecules also in the field of CH materials and artworks.

[1] Also known as the Fast Fourier Transform (FFT) algorithm or just Fourier Transform (FT) algorithm.
[2] Michelson received the Nobel prize in physics in 1907 for the Michelson Interferometer [8. Homepage of Nobel Prizes http://nobelprize.org/. (Access Date: June 4th 2009), .

The use of transmission and ATR spectroscopy are combined with the fact that in the CH field it is commonplace that only small amounts of sample are available as most owners of CH objects or artworks do not allow sampling (unless there is some visual form of degradation and an investigative diagnosis is desirable or the artwork is already undergoing restoration). The allowed sampling is in most cases at the microscopical level and thus usually only a few grains are lifted from the CH object or, in some cases, a micro cross-section is removed (this is becoming more usual). The development of cross-sectional sample investigation by means of micro-ATR spectroscopy has in many cases been employed [11, 12]. However, here we touch upon the limits of IR spectroscopy. The more demands are set for sensitivity and versatility of microscopic samples, the more limits we observe in the IR instruments, particularly regarding the detector.

The desire for better elaboration and understanding of structural cross-sections in CH samples are also heavily influenced by the desire to minimize the time spent collecting these spectra. Minimizing the collection time requires better detectors, faster processors, friction-free (x,y,z)-motorized stages etc. And this development is understandable. This is the way of modern scientific progress, in which we make as much investigations and elaborations in as little time as possible. But these technical demands have sacrifices, which comes in the form of detectors with higher cut-off than the traditionally old fashioned detectors and IR instruments.

A normal old fashioned DTGS detector has a cut-off at 400 cm^{-1}, while the faster and more sensitive MCT and FPA detectors used for FTIR microscopic mapping and imaging has a cut-off at approximately 650 and 750 cm^{-1}, respectively. This means that the lower part of the infrared spectrum (where the inorganic components have strong bands) are left largely undetected; unless you have a Raman instrument to cover this region.

However, Raman spectroscopy also have problems when conducting investigation of old CH materials. The very nature of the CH samples is that they are old and many of them are seriously degraded. Degradation, for example of organic binding media in a paint layer, can cause fluorescence in the Raman spectra. This often makes it very difficult to examine CH samples by Raman spectroscopy, especially if you use visual lasers. The problem of fluorescence is not so outspoken if you use an near-Infrared or infrared (i.e.1064 nm) laser source [13], however here other technical limitations (for instance resolution and time needed to record a spectrum) become important.

When investigating organic components such as the binding material or organic pigment with IR spectroscopy in paint layers, we observe spectral bands in the region 4000-1000 cm^{-1}, whereas inorganic components such as inorganic pigments and corrosion product mainly have their spectral bands below 1500 cm^{-1}. If we are thinking about inorganic oxides and sulphides most of these

compounds have bands below 700 cm^{-1}. This makes it difficult to identify these compounds by normal micro-ATR spectroscopy as a MCT detector has a cut-off limit at 650 cm^{-1}.

Alternatively, or maybe it is rather poetic justice so to say, we have the possibility of returning to the old fashion DTGS detectors. A modified DTGS detector with solid substrate beamsplitter is capable of collecting spectra in the region 700-90 cm^{-1} and thus we have the possibility to elaborate inorganic CH samples like oxides and sulphides, in the lower region of the electromagnetic spectrum. The lower region of the IR range is generally considered as the Far-IR (FIR) region. The newest literature from 2007 defines the FIR region as below 600 cm^{-1} [4]. This definition is closely linked with the development of the faster and more sensitive MCT detectors, which collect spectra faster than the old-type DTGS detectors.

In our case we define the FIR region, as the region where we collect spectra using the modified DTGS detector (with PE windows) and employing the solid substrate beamsplitter for data collection. Similarly, we define the MIR spectral range as the region where we collect data using the normal standard DTGS detector and applying the KBr beamsplitter. In both transmission and ATR there is a small overlap of regions.

The switch between the MIR and FIR region, both for transmission and ATR spectroscopy, is accomplished with remarkable ease if you posses a 'flexible' FTIR instrument.

1.3 VIBRATIONS IN FIR SPECTROSCOPY

There are many ways of acquiring information on chemicals compounds including pigments, upon which this thesis is focused. Many techniques are purely elemental, like XRF (x-ray fluorescence) and SEM (scanning electron microscopy) analysis. These techniques will give you only the elements of you chemical compositions, how those chemicals are bonded together is merely an educated guess. They can tell you your compound contains lead (Pb) and oxide (O). Such a result can be interpreted as both minium (Pb_3O_4) a red pigment, or as one of two yellow pigments, massicot (PbO – orthorhombic structure) or litharge (PbO – tetragonal structure).

All three are typical pigments used as paint material on artworks. The colour can give you a hint but only a technique such as IR or Raman spectroscopy can tell you the composition. In IR and Raman spectroscopy the information that you acquire is directly related to the covalent bond between atoms; how the atoms bond to each other and vibrate internally in the molecule (called internal vibrations) and how the entire molecule vibrates with it's neighbouring molecules (called external vibration or lattice vibrations). This level of information acquired using these methods are

the main reason why IR and Raman spectroscopy are such successful, universally employed investigative methods, compared to other elementary investigative methods.

Commercially available pigments that pre-dates 1850s are as a main thumb-rule inorganic pigments, while pigments that dates after 1850s are mainly industrialized synthesized organic pigments. Organic pigments are mainly observed in the region 4000-1000 cm^{-1}, while most inorganic substances are observed below 1500 cm^{-1}, i.e. sulphates, silicates, carbonates etc. in the IR region; unless they contain bonded hydroxide (OH), then they are observed throughout the IR region. But the pure oxides or sulphides of inorganic compounds are usually only observed below 700 cm^{-1}. Therefore, if we wish to identify the presence of oxides and sulphides in CH materials and artworks we must perform collection in the FIR region.

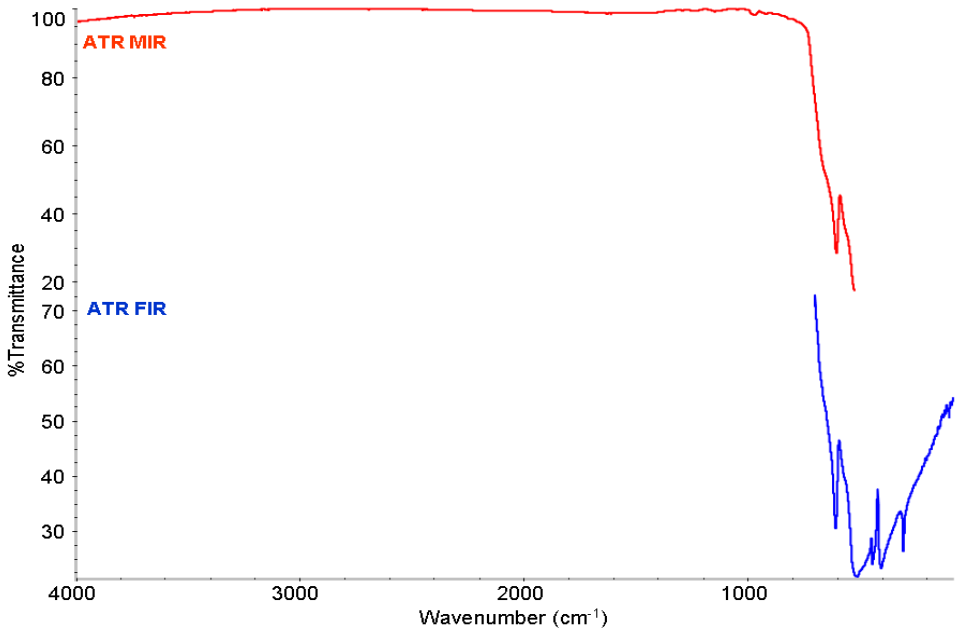

Figure 1.2: ATR spectra of a green chrome oxide (Cr_2O_3) pigment collected in the MIR and FIR region. As can be observed all the bands are below 700 cm^{-1}.

Figure 1.2 shows an example of green chrome oxide (Cr_2O_3) pigment[3], which only has bands below 700 cm^{-1}. There is a small overlapping region between the two spectra. The bands that we observe originate from the stretching and bending vibrations of the molecule as well as the crystalline lattice vibration. They are distributed across a region with much shorter wavenumbers than that of organic compounds due to the fact that inorganic substances have a higher molecular weight than the relatively lighter organic substances. Organic compounds have atoms consisting of mainly carbon, hydrogen, oxygen, sulphur and halides (fluoride, chloride, bromide, iodide), which are all considered light atoms compared to the inorganic substances. The inorganic compounds

[3] The green chrome oxide pigment is from W. G. Ball Ldt., their Artist Pigment Range (APR) no. 6630.

usually contain some metallic atoms like chrome, iron, mercury, copper, etc., which, due to their heavier atomic weight, are observed at lower frequencies than the organic substances. This means that in order to identify both organic and inorganic compounds in CH samples or artwork, we must work in the entire IR region from 4000-50 cm^{-1}. However, this is not possible with most IR instruments, mainly due to cut-off limits of detectors and beamsplitters, as already mentioned above.

Therefore, if we wish to focus our attention to oxides and sulphides of inorganic pigments, we must focus our attention to the region 700-90 cm^{-1}. This is the very region we have defined as the FIR region, because we have in our IR spectrometer installed a secondary modified DTGS detector and a beamsplitter, collecting in just this region.

1.4 AIMS & OBJECTIVE OF THESIS

This thesis is focused on the elaboration of inorganic pigments and corrosion products collected from CH materials in the FIR region. Both transmission and ATR spectroscopy has been employed for these investigations. Although FIR transmission spectroscopy has already in the past been applied on pigments [14] and minerals and corrosion products [15] down to 200 cm^{-1}. In this thesis we have the extended region from 200-90 cm^{-1} as part of our FIR region. This extended region is only published for very few pigments and minerals in literature and only in transmission.

ATR spectroscopy has been applied for many years with more and more success but the focus has always been in the MIR region. ATR spectroscopy applied in the FIR region is a real novelty in the field of spectroscopy. However, there are very few databases with ATR spectra. The focus of this thesis has therefore also been to build a standard ATR spectroscopic library database in both the MIR and FIR region for comparison with unknown samples.

During the development of our spectral library database it has been necessary to optimize the spectrometer for collecting in the FIR region. Also, for collection in transmission mode, sample preparation and optimization has been necessary. With ATR spectroscopy it is much easier to collect sample spectra as no sample preparation is required.

The library database has been tested on test tablets, where also different ways of collecting in ATR and transmission have been applied and compared. Finally, also collection of sample spectra originating from various CH case studies are used to validate the methods in the FIR region.

During the research of this thesis articles have been published in peer-reviewed journals [16-20] and the subject has been presented to relevant scientific congresses:

Published articles:

- E. L. Kendix, S. Prati, E. Joseph, G. Sciutto & R. Mazzeo**,** *ATR and transmission analysis of pigments by means of far infrared spectroscopy,* Anal. Bioanal. Chem. 2009, 394(4), 1023-1032.
- E. L. Kendix, S. Prati, R. Mazzeo, E. Joseph, G. Sciutto, *Far Infrared Spectroscopy of pigments in Art*, Meddelelser om Konservering (Announcement about Conservation), 2009, **2**, 3-10.
- E. Kendix, S. Prati, R. Mazzeo, E. Joseph, G. Sciutto, C. Fagnano, *Far Infrared Spectroscopy in the Field of Cultural Heritage*, Accepted for ePRESERVATIONScience (IRUG8 conference proceedings) (http://www.morana-rtd.com/e-preservationscience/index.html).
- R. Mazzeo, S. Prati, M. Quaranta, E. Joseph, E. Kendix, M. Galeotti, *Attenuated total reflection micro FTIR characterisation of pigment-binder interaction in reconstructed paint films*, Anal Bioanal Chem. 2008, **392**, 65-76.
- E. Kendix, G. Moscardi, R. Mazzeo, P. Baraldi, S. Prati, E. Joseph, S. Capelli, *Far Infrared and Raman spectroscopy analysis of inorganic pigments*, J. Raman spectroscopy, 2008, **39(8)**, 1104-1112.

Scientific Presentations To Congresses (Invited Speaker):

- **2009:** E. L. Kendix, E. Joseph, G. Sciutto, D. Prandstaller, S. Prati, R. Mazzeo **"The Application of Far IR Spectroscopy Methods in the Characterization of Pigments and Corrosion Products"** CNR Workshop, Tecniche avanzate (PEM. IRRAS, VCD, TRS) di Spettroscopia FTIR e Microscopia IR/Raman per la caratterizzazione di materiali e superfici**,** Thermo Scientific, May 12 2009, Padova (Italy).
- **2008:** E. Kendix, E. Joseph, G. Sciutto, S. Prati, Vanna Minguzzi, R. Mazzeo, **"Application of Far Infrared Spectroscopy Methods in the Chemical Characterization of Pigments and Corrosion Products"** ISLS 2008 (XIII International Symposium on Luminescence Spectrometry), September 7-11, 2008, Bologna (Italy).
- **2007:** R. Mazzeo, E. L. Kendix, **"FROM CURRIC …….. TO EPISCON (European PhD in Science for Conservation)"** "Scienza e Beni Culturali. La Diagnostica: Formatione e Professtione" ($AIED_{BC}$), Universitá di Roma, Jan 31 2007, Rome (Italy).

Scientific Presentations To Congresses (Posters):

- **2009:** E. Kendix, G. Sciutto, S. Prati, R. Mazzeo, **Far-IR Spectroscopy Applied for Identification of Pigments and Corrosion Products**, *presented at XXIII Congressi National della Società Chimica Italiana,* July 5-11 2009, Sorronto (Italy).
- **2008:** E. Kendix, E. Joseph, S. Prati, R. Mazzeo, **Macroscopic and microscopic ATR – FTIR spectroscopy for the study of painting materials in FIR and MIR regions**, *presented at YOCOCU08 (Youth in Conservation of Culturel Heritage)*, November 24-25 2008, Rome (Italy).
- **2008:** E. Gurini, E. Joseph, G. Sciutto, A. Cagnini, E. Kendix, S. Porcinai, D. Prandstraller, S. Prati, Y. Junchang, R. Mazzeo, **Compositional and Microstructural Study of Archaeological Bronzes Excavated from the Zhou Dynasty (1046 Bc-221 Bc) Aristocratic Cemetery in Liangdai Village, Shaanxi Province, China**, *presented at ISA08 (37th Int. Symposium on Archaeometry),* May 12-16, 2008, Siena (Italy).
- **2008:** E. Kendix, S. Capelli, E. Joseph, G. Sciutto, S. Prati, R. Mazzeo, **Far Infrared Spectroscopy Methods in the Field of Cultural Heritage**, *presented at IRUG8 (8th International conference on Infrared and Raman Users' group)*, March 26-29 2008, Vienna (Austria).
- **2007:** E. Joseph, S. Capelli, E. Kendix, S. Prati, R. Mazzeo**, Alternative sample preparation methods using ATR-MIR- and FIR-spectroscopy for the study of Cultural Heritage Materials,** *Presented at HSC5 (Hercules Specialised Course 5) at ESRF- European Synchrotron Radiation Facility,* Oct. 2007, Grenoble (France).
- **2007:** P. Baraldi, E. Joseph, E. Kendix, R. Mazzeo, S. Prati, S. Capelli. **Far Infrared And Raman scpectroscopy analysis of inorganic pigment,** *presented at RAA07 (the IV International Conference on the Application of Raman Spectroscopy in Art and Archaeology),* September 5-11 2007, Modena (Italy).
- **2007:** R. Mazzeo, S. Prati, E. Joseph, E. Kendix, **Mapping ATR-FTIR nella Caratteriz-Zazione E Localizzazione Stratigrafica Di Materiali Artistici ed Archeologici,** *Presented at the X Congresso Nazionale di Chimica dell'Ambiente E dei Beni Culturali - CONOSCENZA E CREATIVITÀ,* June 12-15 2007, Lecce (Italy).

CHAPTER 2 THEORY: TRANSMISSION & ATR SPECTROSCOPY

2.1 INFRARED SPECTROSCOPY

Infrared (IR) spectroscopy is a very important non-destructive technique for gaining structural information and identifying the chemical bonds in unknown compounds. This information is important for qualitative as well as quantitative determination of the chemical compounds used in various scientific areas of research, among others the private industry, forensic science and the cultural heritage sector.

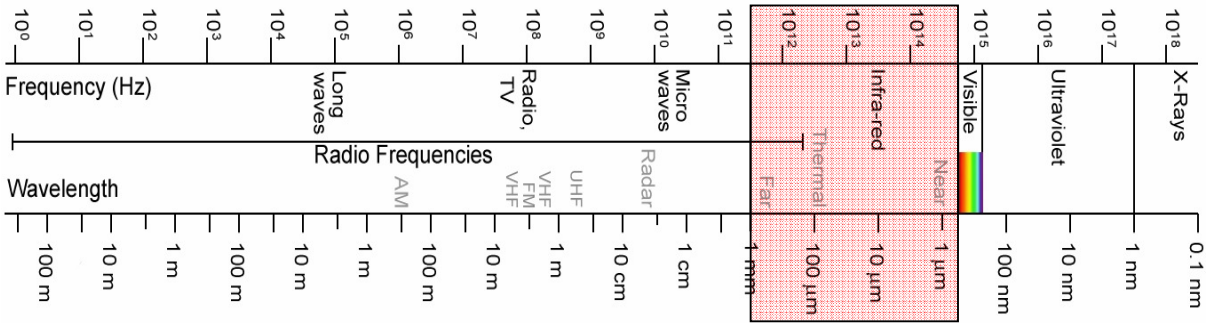

Figure 2.1: The electromagnetic spectrum showing the Infrared region.

The infrared range of the electromagnetic spectrum covers the wavelength region from 25 µm to 1 mm, which conforms to the wavenumber range 40.000-100 cm^{-1}. It is split in the Near-IR (NIR), the Midt-IR (MIR) and the Far-IR (FIR) region. It is neighbour to the visible region on one side and the microwave region on the other. All regions in the electromagnetic region can be described by energy E and its relationship with frequency ν measured in hertz (Hz), which is the number of waves per second:

Equation 2.1 $E = h\nu$

where h is Planck's constant (6.63×10^{-34} J s).

We can convert the frequency ν to wavenumber $\bar{\nu}$, the units employed in IR spectroscopy, by $\nu = c\bar{\nu}$, this transforms the equation into:

Equation 2.2 $E = hc\bar{\nu}$

where the wavenumber $\bar{\nu}$ is measured in cm^{-1} and c is the speed of light (3.0x10 cm/s). Through these equations we learn that an increase in energy is equal to an increase in wavenumber.

The energy difference between organic and inorganic bond excitation, is caused by the atoms involved in the bond. With increased atomic mass the bond length between the atoms will be increasingly longer, and the vibrational excitation energy becomes lower.

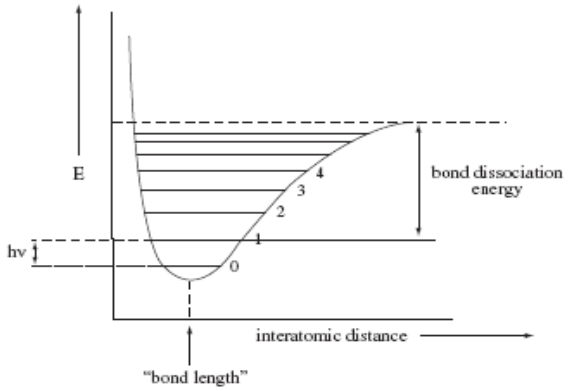

Figure 2.2: The anharmonic oscillator model for interatomic distances between bond length as a function of energy.

A typical inorganic bond requires 1.6 x 10^{-20} J in order to be vibrationally excited [21] and it will be visible in the IR spectrum as a fundamental vibration at a wavenumber of approx. 800 cm^{-1}. A typical organic vibrationally excited bond will have an energy of 3.0 x 10^{-20} J and will be visible in the IR spectrum as a fundamental vibration with a wavenumber frequency of approx. 1500 cm^{-1}. For comparison, the energy require to break the C-H bond in methane (bond disassociation energy) is approximately 7.29 x 10^{-19} J (439 $kJ \cdot mol^{-1}/N_A$) [22], which is the equivalent of 36650 cm^{-1}. The excitation energy is generally a factor of 10 lower than the bond disassociation energy.

2.1.1 THE HARMONIC APPROXIMATION

The vibration between two molecules can be expressed by Hook's spring law. The potential energy *U* of the vibration, is dependent on the spring constant *k* and the distance *x,* that the spring has been stretched or compressed away from the equilibrium position.

Equation 2.3 $U = \frac{1}{2}kx^2$

Compressed ***Equilibrium*** ***Stretched***

We know from the anharmonic oscillator model that a vibration between two atoms only can compress and stretch to a certain limit before either colliding or breaking bonds. Stretching vibrations in diatomic molecules together with the reduced atomic mass μ $((m_1m_2)/(m_1+m_2))$, the

force constant *k* between the bond, and the frequency of the vibration *v,* changes Hook's equation to:

Equation 2.4 $$\nu = \frac{1}{2\pi}\sqrt{\frac{k}{\mu}}$$

Diatomic stretching vibration in equilibrium.

This is the classical harmonic oscillating spring model. In this simplified model a molecule could absorb energy at any given wavelength. The IR vibration must however, follow the rules of quantum mechanics, as the vibrational motion is a quantized function, which states that only certain transitions are allowed:

Equation 2.5 $$E_n = (n + ½)h\nu$$

Where *v* is the frequency of the vibration, *n* is the quantum number (0, 1, 2, 3, …..) and *h* is Planck's constant. $E_0 = ½h\nu$ is the lowest energy level, $E_1 = {}^3/_2 h\nu$ the next lowest and so on. As the selection rule only allow the energy to go from one level to the next the molecule will absorb energy equal to $E_1 - E_0 = h\nu$. The *Equation 2.5* is fundamental for the harmonic approximation, showing the quantized fundamental vibration bond between two atoms in a molecule.

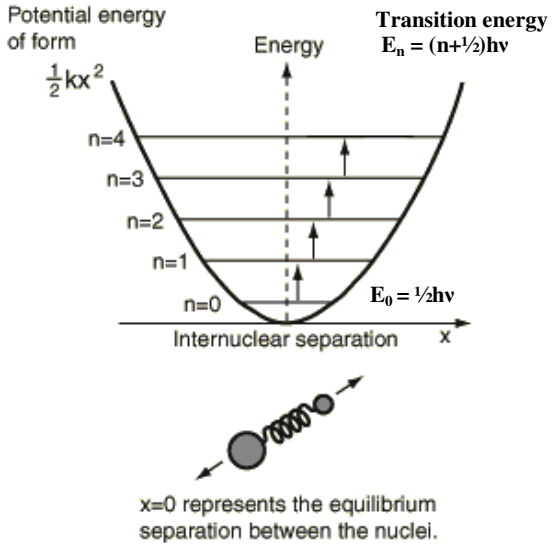

Figure 2.3: The harmonic oscillator model in which the quantized fundamental vibrations are shown

Transitions of 2hν or 3hν are sometimes observed, these transitions are called overtones or combination band. They have lower intensity than the fundamental vibrations. The interactions between vibrations can occur if the vibrating bonds are coupled to a single, central atom. Vibrational

coupling is influenced by a number of factors. Coupling between stretching or bending vibrations occurs when there is a common atom or bond between the two vibrating groups: A coupling is strongest when the coupling groups have approximately equal energy in the anharmonic approximation; no coupling is observed when the groups are separated by two or more bonds. Overtone and combination bands are observed at higher wavenumbers than the fundamental vibrations.

2.2 VIBRATIONS OF THE MOLECULES

We know now that the vibrations observed in molecules are fundamental vibrations, which are quantized in specific energy levels. The fundamental vibrations of molecules can be divided into to main categories: Internal and external vibrations. While internal vibrations happen within a single molecule, while the external vibrations happen between two or more units of molecules (these are also called lattice or crystal vibrations).

2.2.1 INTERNAL VIBRATIONS

The internal vibration can be subdivided into stretching (ν) and bending (δ) vibrations. Change in the inter-atomic distance along the bond axis is called symmetric and asymmetric stretching vibrations and can be seen in *Figure 2.4.*

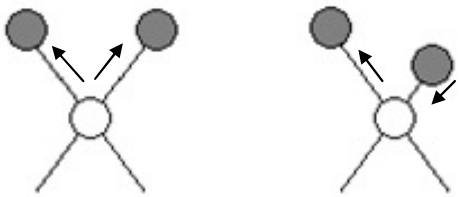

Figure 2.4: Symmetric and asymmetric stretching vibration of a molecule are changes along the interatomic bond axis [23].

If the motion does not involve changes along the bond axis but involves changes between bond angles the vibration is called bending. Here there are two types of bending vibrations; in-plane (ip) bending vibrations and out-of-plane (oop) bending vibrations.

The (ip)-bending vibrations are thus named because they happen in the plane of the molecule. Anti-symmetric and symmetric bending vibrations are known as rocking and scissoring vibrations.

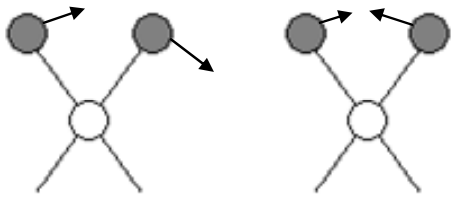

Figure 2.5: The two in-plane (ip) bending vibrations known as rocking and scissoring bending vibrations [23].

The oop-bending vibrations are a change in bond angles across the plane of the molecule and these vibrations are known as wagging and twisting bending vibrations and can be observed in *Figure 2.6.*

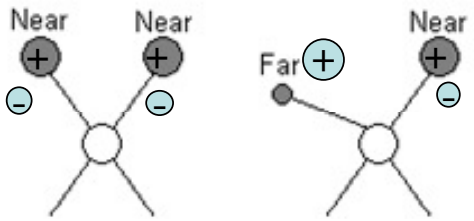

Figure 2.6: The two out-of-plane (oop) bending vibrations known as wagging and twisting [23].

2.2.2. EXTERNAL VIBRATIONS

The internal vibrations shown above, are the vibrations between the atoms in a molecule while the external molecular vibrations are the vibrations between the atoms in the crystal also known as lattice vibrations.

Lattice vibrations have lower frequencies than the internal vibrations. The lattice vibrations for organic compounds are usually at a lower frequency than 400 cm^{-1}. For inorganic compounds the lattice vibrations are at even lower frequencies than for the organic compounds, again due to the heavier atoms present in the inorganic molecules.

If we look at a diatomic molecule, consisting of a cation and anion, we will have 4 different kinds of vibrations, shown in *Figure 2.7.* Acoustic vibrations, are vibrations where the two atoms in the unit cell vibrate in the same direction in the lattice. In the optical vibrations the two atoms in the unit cell vibrate in opposite motions. These two different kinds of motions can appear both transversely and longitudinal in the crystal cell. The naming of these four vibrations are LO (longitudinal optical), TO (transversely optical), LA (longitudinal acoustical) and TA (transversely acoustical) vibrations [24].

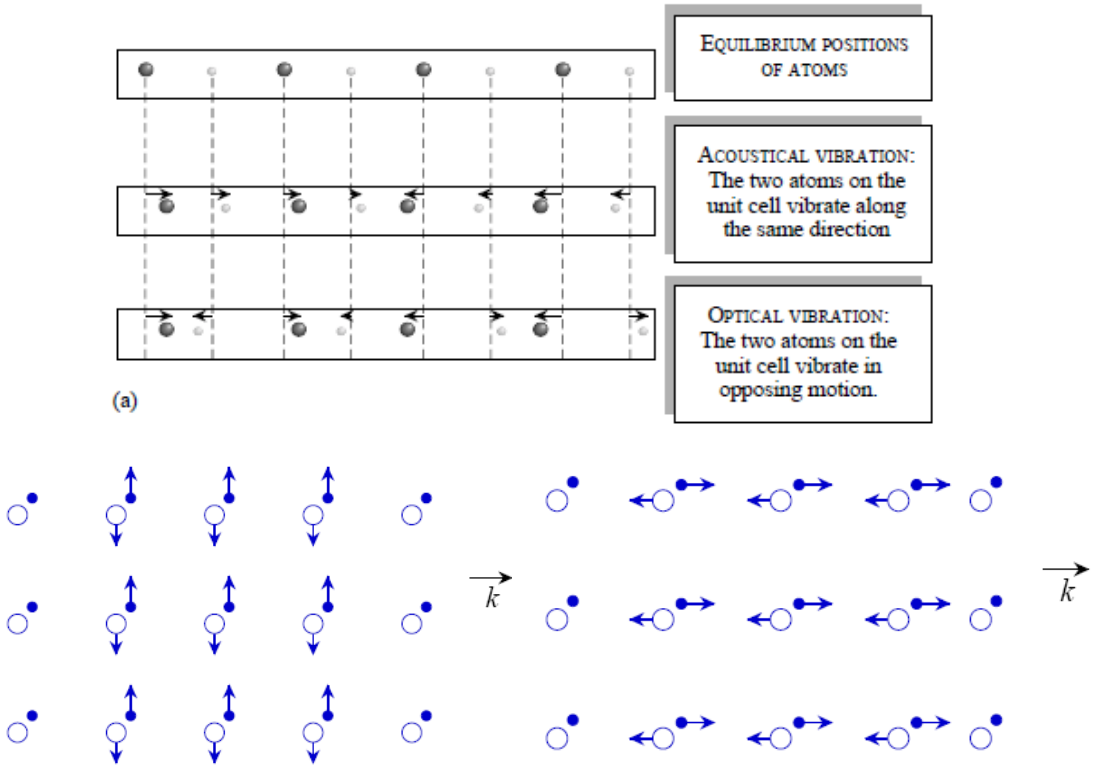

Figure 2.7: The lattice vibrations of a diatomic molecule (of uneven masses, with the big atom as the cation and the small atom as the anion). A) show the acoustical and optical vibrations compared to the equilibrium. B) Transverse vibrations and C) longitudinal vibration. Reprinted from [24].

When more than two atoms are in the unit cell of the crystal, the vibrations of cause becomes more complicated, but the lattice motions will still consist of these four basic vibrations.

2.3 TRANSMISSION VS. ATR SPECTROSCOPY

Since Stimson in 1952 [5] first applied KBr pellets in IR spectroscopy of solid samples transmission spectroscopy [6, 25-29] has been one of the most used IR techniques. ATR spectroscopy [9-11, 17, 20, 30-36] is equally a much employed technique. The theory behind them is quite different considering that they are based on the same principle. In transmission, the light source goes through the sample (embedded in an inert medium) to the detector. The sample is normally embedded in KBr for the MIR region and in CsI for the FIR region, as these are inert in the respective regions. The ATR (Attenuated Total Reflectance) technique is a surface examination technique. An internal reflecting element (IRE) crystal is used to focus and direct the light beam to the surface of investigation. Usually the beam only penetrates about 1-5 µm into the sample. The

beam is absorbed by the sample and is reflected back out to the crystal and the beam continues to the detector.

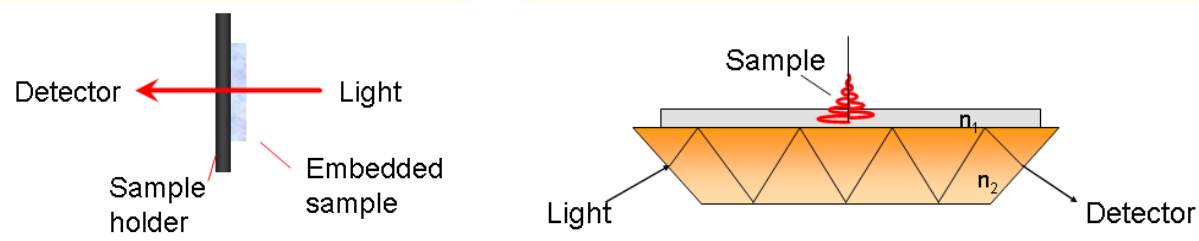

Figure 2.8: Schematic of transmission and ATR techniques. Images © Thermo Fisher

Not only the theory behind the techniques are different but also the output spectra look different. There are several distinct features that differentiate ATR spectra from transmission spectra when comparing the two techniques. The ATR spectra looks more distorted than the transmission spectrum, especially changes in intensity are observed and some bands, particularly the very strong bands, appear to shift to a lower frequency. These ATR distortion are quite known from the MIR region [34, 37, 38]. Band shift between the two methods can be anywhere from 1-50 cm^{-1}, where 1-10 cm^{-1} is normal, and 40-50 cm^{-1} appears only in very extreme cases (which will be shown in chapter 5). A typical example of differences can bee seen in ***Figure 2.9***, which shows the mineral cerussite collected in transmission and ATR mode. We observe in particular the band at 1400 cm^{-1}, which in transmission is the strongest band but in ATR the intensity has decreased considerably. Small shifts in band frequency are also noticed.

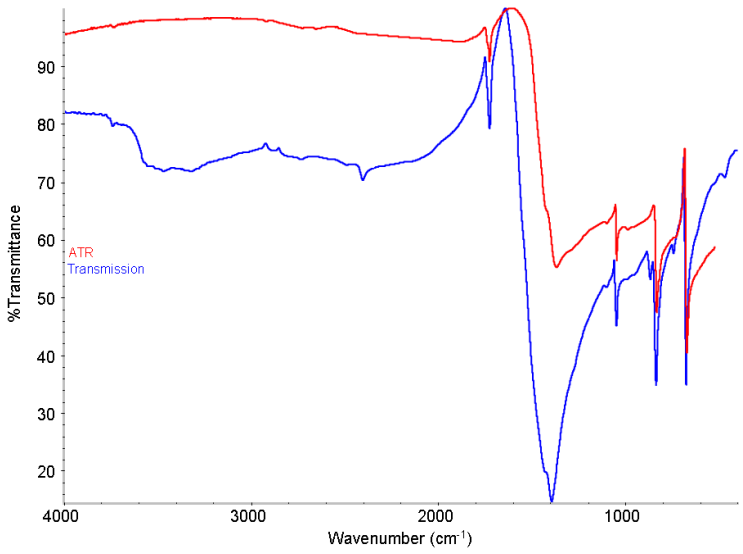

Figure 2.9: ATR and Transmission spectra of Cerussite collected in the normal MIR region. In transmission (blue spectrum) the mineral is embedded in a KBr pellet, while in ATR (red spectrum) it has been collected directly on the powder mineral. Both spectra have been background subtracted and baseline corrected.

To explain these phenomena, it is necessary to examine the theory behind the two different spectroscopic techniques more closely and evaluate the potential benefits by applying ATR to the FIR region.

These next paragraphs are heavily influenced by the works of Harrick [9, 10] and Averett [34] as they both explain in excellent terms the theory behind ATR compared to that of transmission spectroscopy.

2.4 TRANSMISSION SPECTROSCOPY

Infrared transmission spectroscopy can be explained by Lambert-Beer's law. *Lambert's* law states that the fraction of the incident light absorbed is independent of the intensity of the source. *Beer's* law states that the absorption is proportional to the number of absorbing molecules. In combining the two law's we express the Lambert-Beer Law [39]:

Equation 2.6 $A = \varepsilon c l$

Where A is absorbance (dimensionless), c is the concentration of the sample and l is the path length travelled by the light through the sample and ε is the absorptivity (given in units concentration x path length) [39, 40]. In older literature ε was also called extinction coefficient. Various units for path length and concentration can be applied as longs as they are consistent, depending on whether you investigate liquid or solid samples. The absorptivity ε is a fundamental physical property of the specific molecule under investigation, which varies with wavenumber. For quantitative analysis absorbance is applied as it is proportional to concentration, as stated in the Lambert-Beer Law.

For qualitative work transmission T can be employed, as traditionally (before 1980) grating or prismatic instruments have been employed, which gave a directly readable output-signal as a difference between sample and no-sample in the pathway of the IR beam, according to ***Equation 2.7:***

Equation 2.7 $T = I/I_0$ **(or** $\%T = (I/I_0) \times 100$**),**

where T is transmittance, I is light Intensity with sample in the beam, and I_0 is the light Intensity with no sample (background) in the beam. The relationship between absorbance and transmission is as follows:

Equation 2.8 $A = -\log T$

This relationship can also be observed in *Figure 2.10*.

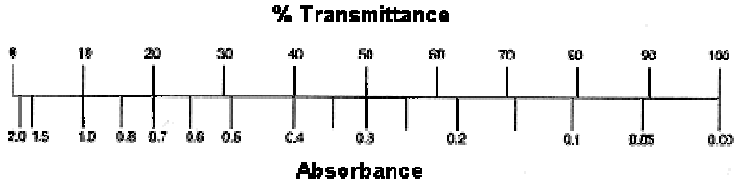

Figure 2.10: The relationship between Absorbance and transmission as explained by Equation 2.8.

Here we observe that if all the light passes through a sample *without* any absorption, then absorbance is zero, and percent transmittance is 100%. If all the light is absorbed by the molecules in the sample, the percent transmittance is zero, and absorption is 2.

Which scale is most convenient to use in IR spectroscopy is still heavily debated by the spectroscopists and both scales are equally used in literature. In this laboratory all spectra are conventionally shown in transmittance (*%T*). However, if quantitative analysis is performed absorbance spectra is always shown, as absorbance is proportional to the concentration as stated by *Equation 2.6*. Transmission is not equally proportional to concentration, as stated in *Equation 2.7 and 2.8*.

2.5 ATR - DEPTH OF PENETRATION

In ATR we work with effective thickness d_e and depth of penetration d_p. Harrick [9, 10] and Averett [34] explain as follows:

Equation 2.9 $$\mathbf{d_p}= \frac{\lambda}{2\pi\sqrt{\sin^2\theta - (n_2/n_1)^2}}$$

Depth of penetration d_p for ATR spectroscopy is dependent on wavelength λ, incident angle θ of the IR beam, n_1 and n_2, which are the refractive index of the rarer medium and the denser medium, respectively, also called the refractive ratio n_{21} [34, 37, 38]. *Equation 2.9* states that *dp* is dependant on the ratio n_{21} of the refractive index of the rare (n_1) and denser (n_2) medium. This can also be observed in *Figure 2.11* when the refractive ratio n_{21} approaches 1, a considerable increase in depth of penetration is observed in the FIR region compared to that of the MIR region [34].

This means that if you wish to penetrate deeper into the sample than normal surface penetration of about 1-5 µm, you can attempt to alter the refractive ratio n_{21}, and thus achieve bigger penetrations depths. This however, is only possible for the FIR region, not for the MIR region.

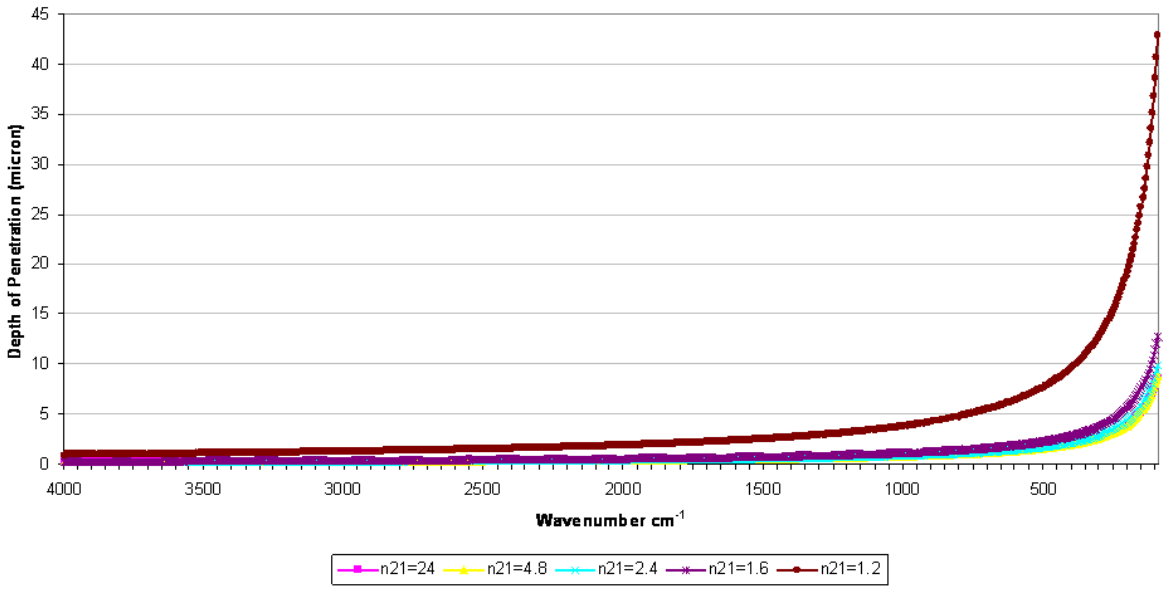

Figure 2.11: Depth of Penetration (dp) as a function of wavenumber, with the angle of incident θ = 45°, at variable n_{21} ratio. We observe higher penetration in the FIR region (~500-90 cm^{-1}) when $n_{21} \rightarrow 1$.

Equation 2.9 assumes that the ratio n_{21} is constant throughout the infrared region. However, this is not always true, as in the case of very strong absorbing bands present in the sample. This can be observed in *Figure 2.12*, which show the refractive index spectrum of a compound that have very strong absorbing bands in the region 1400-500 cm^{-1}.

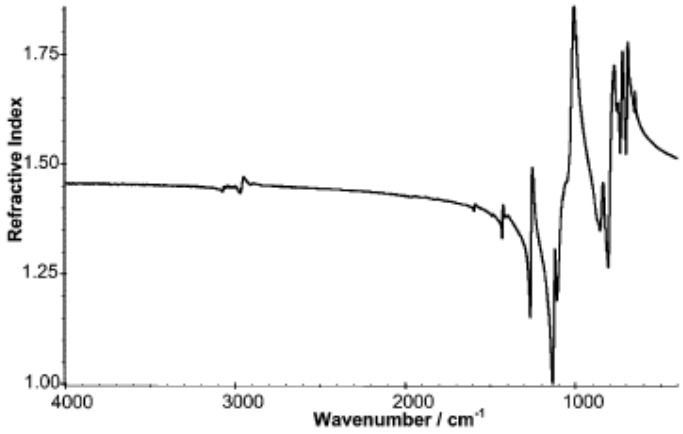

Figure 2.12: Refractive index spectrum of poly(phenyl methyl siloxane). Reprinted from 1..

When a compound has so strong absorbing bands also the d_p will be influenced, causing an increase in d_p in the region where the strong absorbing bands appear [34]. For the majority of materials where the thickness of the rarer medium is much greater than the penetration depth of the evanescent field E_0^2, the effective thickness d_e can be approximated for low absorption bands [9]:

Equation 2.10

$$\mathbf{d_e}=\frac{n_{21}E_0^2 d_p}{2\cos\theta}$$

Because the electric field amplitudes in the rarer medium are different for equal incident amplitudes of perpendicular (⊥) and parallel (∥) polarization, the effective thicknesses are different for the two polarizations, in that $d_{e\parallel}$ is bigger than $d_{e\perp}$ [9]:

Equation 2.11

$$d_{e\perp}=\frac{\lambda_1 n_{21}\cos\theta}{\pi\left(1-n_{21}^2\right)\left(\sin^2\theta-n_{21}^2\right)^{1/2}}$$

Equation 2.12

$$d_{e\parallel}=\frac{\lambda_1 n_{21}\cos\theta\left(2\sin^2\theta-n_{21}^2\right)}{\pi\left(1-n_{21}^2\right)\left[\left(1+n_{21}^2\right)\sin^2\theta-n_{21}^2\right]\left(\sin^2\theta-n_{21}^2\right)^{1/2}}$$

The depth of penetration d_p is proportional to the wavelength λ, which means the effective thickness d_e increases with wavelength. The effective thickness is dependant on four factors

1) the penetration depth d_p which is proportional to the wavelength and decreases with increasing angle of incident.
2) the Electric field amplitude E_0^2 in the rarer medium, which decrease with increasing angle of incident.
3) Sampling area which varies with angle of incident (1/cosθ).
4) Refractive index, wherein the ratio n_2/n_1 is less than unity but the closer the index of the sample match that of the Internal Reflecting Element (IRE) the grater is the interaction.

These are the four reasons that absorption bands at the shorter wavenumber are relatively stronger in intensity in ATR spectroscopy, compared to transmission spectroscopy. This also results in greater absorption on the shorter wavenumber side of a single band and thus creating distortion of the band, compared to the same band collected in transmission spectroscopy [9].

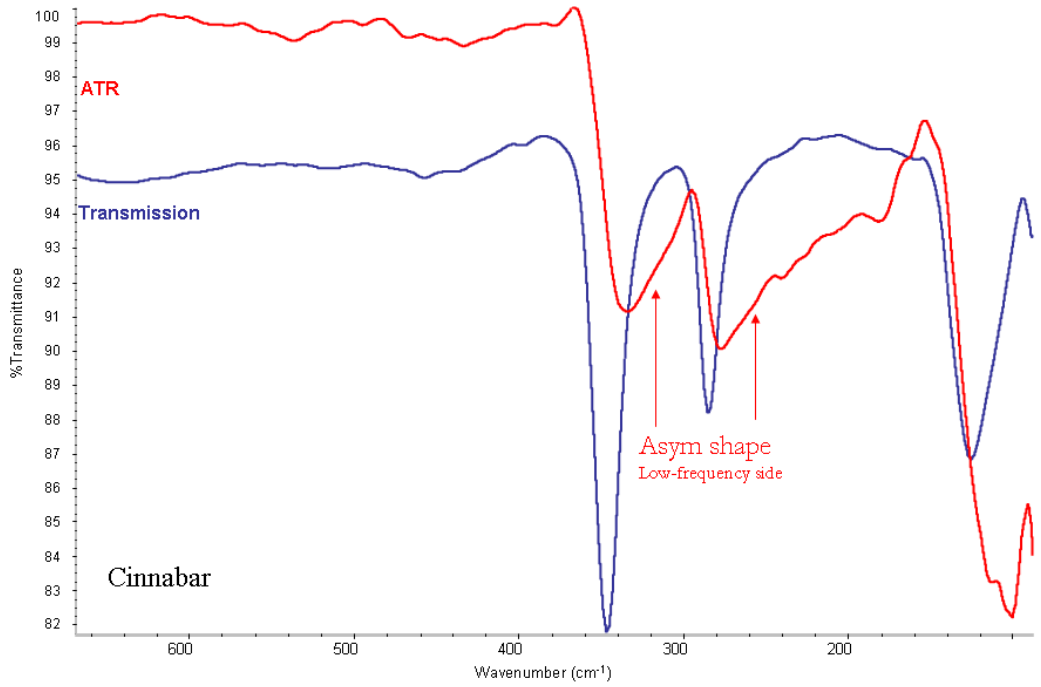

Figure 2.13: FIR spectra of the red pigment cinnabar (HgS) collected in transmission (blue) and ATR (red), showing quite clearly the differences between transmission and ATR spectra, intensity differences, band shift to lower frequency and distortion of the ATR band shape.

The distortions of the ATR bands, can be observed very clearly in *Figure 2.13*, which shows the transmission and ATR FIR spectra of the red pigment cinnabar (HgS). Also differences in intensity and shift of bands to lower frequency are observed for the cinnabar pigment. The observed wavenumber differences are in the case of cinnabar (*Figure 2.13*) approximately 5 cm^{-1}. It has been observed that the stronger the band absorption, the bigger the relative shift between bands observed in transmission and ATR. The differences observed here in the FIR region are observed in the entire IR region. Due to the depth of penetration being significantly larger in the FIR region the asymmetrical band shape (distortion of band shape on the low wavenumber side) is more prominent in the FIR region than in the MIR region.

CHAPTER 3 OPTIMISATION OF THE SPECTROMETER FOR FIR SPECTROSCOPY

3.1 THE IR SPECTROMETER

The spectrometer used for these experiments is a Nicolet Nexus 5700 from Thermo Electron Corporation. By changing a few components the spectrometer is capable of collecting spectra in the normal IR range as well as in the FIR range using both transmission and Attenuated Total Reflection (ATR) spectroscopy.

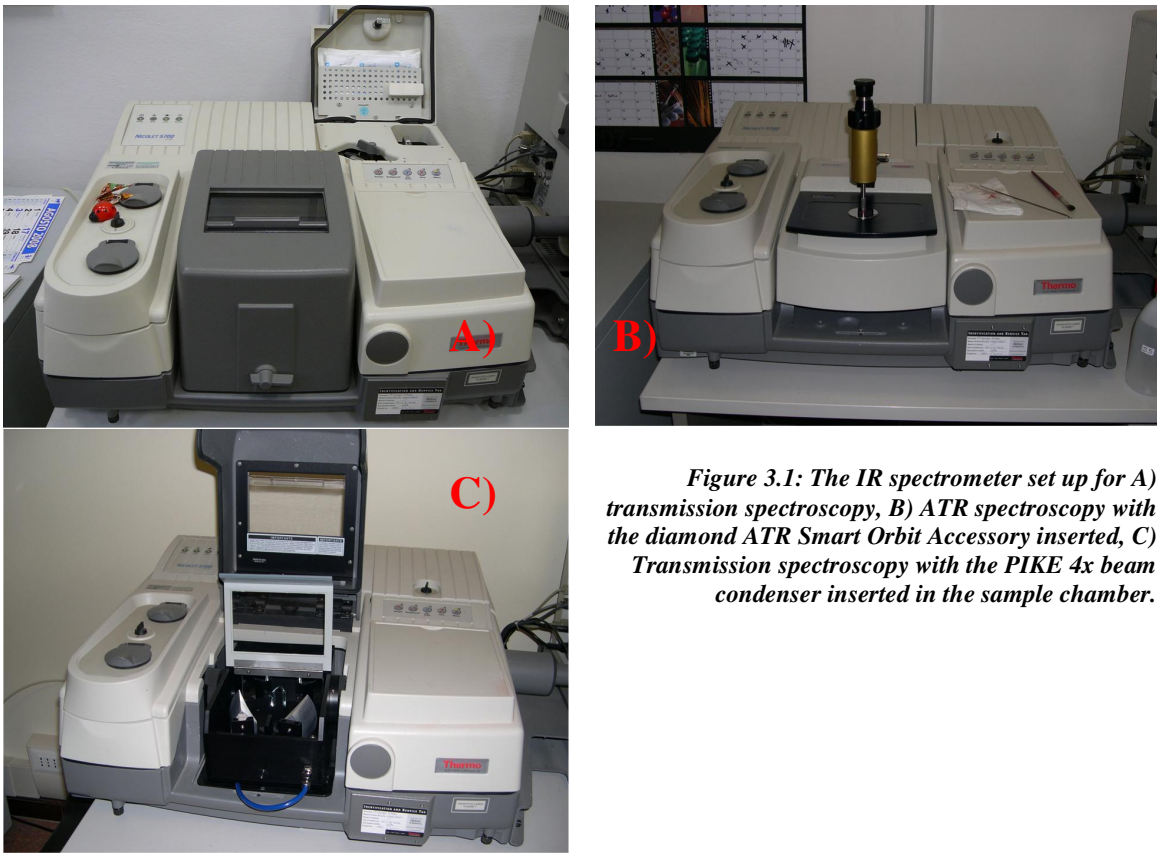

Figure 3.1: The IR spectrometer set up for A) transmission spectroscopy, B) ATR spectroscopy with the diamond ATR Smart Orbit Accessory inserted, C) Transmission spectroscopy with the PIKE 4x beam condenser inserted in the sample chamber.

Furthermore the instrument has the option to make microscopic FTIR investigations as a Continuum IR microscope fitted with a MCT type A detector (cooled by liquid nitrogen) and a X,Y,Z-motorised stage. This is an accessory attached to the spectrometer enabling micro-investigations of cross-sections. However, this part of the instrumentation is not employed or discussed in this thesis.

The IR spectrometer is controlled by OMNIC 7.3, a software from Thermo Electron Scientific Instruments Corporation.

Figure ***3.1*** show the FTIR spectrometer set-up for collection in transmission and ATR investigation with the diamond ATR smart Orbit accessory, respectively. Also by use of the most

resent accessory addition to the instrument, the PIKE beam condenser, we are able to collect spectra with a 4x condensed beam thus enabling the use of smaller sample sizes.

The schematic of our FTIR spectrometer is presented below in ***Figure 3.2***. The red line shows the optical pathway of the IR beam in the spectrometer, through the interferometer, reflected off the mirrors, through the sample compartment (and the sample) to the detector. The spectrometer has been fitted with two DTGS detectors, one for MIR collection, the other DTGS detector has additionally polyethylene windows enabling the detector for collection in the FIR region.

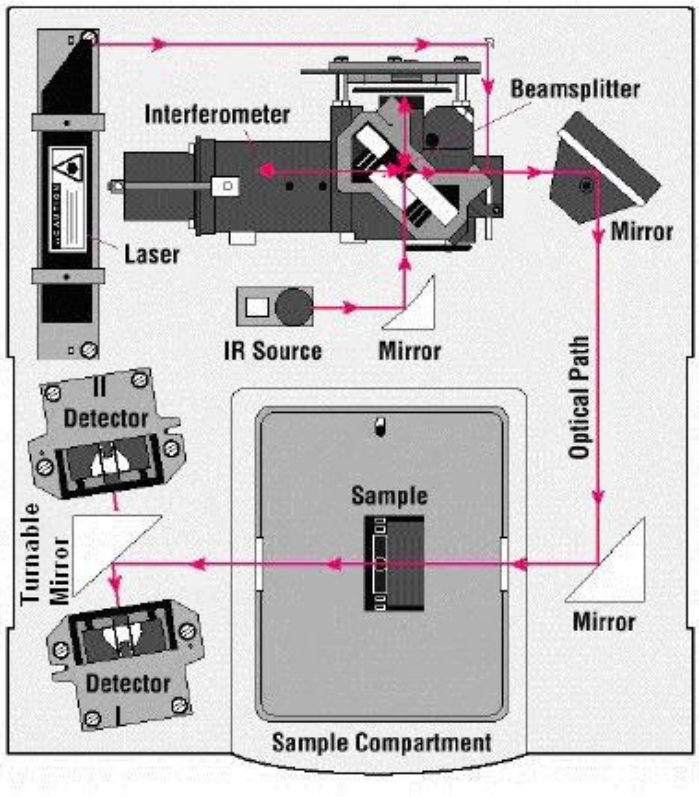

Figure 3.2: Schematic of a FTIR spectrometer with two detectors.

A Parker/Balston Self-Contained Gas Purge Generator (GPG) is attached, purging the spectrometer with dry air for minimizing interference bands generated from ambient moisture. The outlet pressure is set to 30 psig/bar and the outlet flow control is set to 9 (dimensionless) during collection of spectra.

3.1.1 LIGHT SOURCES

There are several options for a light source, which can provide radiant energy in the infrared region of the electromagnetic spectrum. An air cooled source is the simplest and cheapest infrared

source used in old type instruments. It typically runs at temperature from 1100-1400 K. Air cooled sources may not provide enough infrared intensity for all applications. The second type of infrared radiation source is the Globar source. It consist of a silicon carbide rod, which typically heats to temperatures above 1400K. The increased temperature means that the Globar IR source also gives off more infrared radiation than the old type air cooled sources. More radiation will supply a higher throughput and a lower noise [39]. Globars are nowadays the most common IR light source and are also present in our spectrometer.

3.1.2 INTERFEROMETER

A Fourier transform Infrared (FTIR) spectrometer has at its heart a Michelson interferometer. The purpose of an interferometer, is to split a beam of light into two beams, and make one of the light beams travel a different distance than the other (called *Optical Path Difference*, OPD, denoted by δ) [39].

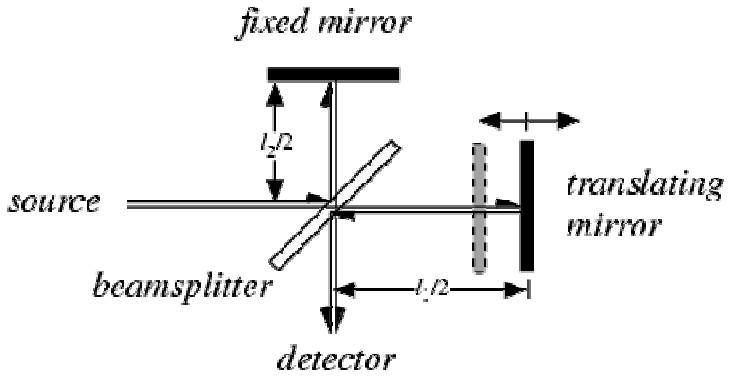

Figure 3.3: Schematic of the Michelson interferometer where the arrows shows the optical pathway for the IR beam.

The interferometer consists of two mirrors located at a right angle to each other and oriented perpendicularly, with a beamsplitter placed at the vertex of the right angle and oriented at a 45° angle relative to the two mirrors. The beamsplitter splits the incident beam in two equal part. One part is going through the beamsplitter to the translating mirror. The other part of the beam is reflected to the fixed mirror. Both the fixed and translating mirror reflects the incident beam. The two beams are then recombined and transmitted to the detector. If the translating mirror and the fixed mirror are the same distance from the beamsplitter, the distance travelled by the two light beams are the same. This is called Zero Path Difference (ZPD) denoted by Δ. The relationship between mirror displacement with optical path difference is:

Equation 3.1 $\delta = 2\Delta$

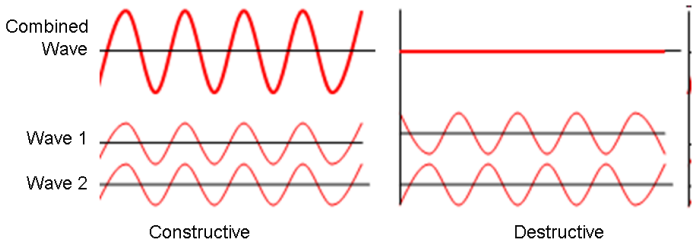

Figure 3.4: Destructive and constructive interference pattern for light travelling in an interferometer.

If an optical path difference is introduced between the two light beams, by moving the translating mirror away from ZPD position. Then the light reflecting from the translating mirror will travel further than the light off the fixed mirror. If the light travel a specific wavelength λ further, this will recombine to give a constructive wave pattern, which gives an intense light beam leaving the interferometer. We know that amplitudes of light is additive, so the amplitudes of the two light beams travelling between the fixed and translating mirror will be greater than the amplitude of the individual beams.

Equation 3.2 $\delta = n\lambda$ *where n = 0, 1, 2, 3, ….*

Where ZPD corresponds to n = 0, and constructive wave pattern will take place when OPD is equal to multiples of λ. If however, the ZPD is ¼ λ out of phase the OPD will recombine to give ½ λ, a destructive wave pattern (meaning weak or no) signal, following from ***Equation 3.3***:

Equation 3.3 $\delta = (n + ½)\lambda$ *where n = 0, 1, 2, 3, ….*

The interferometer observed in IR spectroscopy is a multitude of amplified wave pattern. A typical interferogram is seen in *Figure 3.5*. The centerburst ZPD is the highest spike (addition of all constructive wave amplitudes) observed in the interferogram, while the destructive wave pattern is observed in the wings, where the amplitudes cancels each other out, to give weak or no signal.

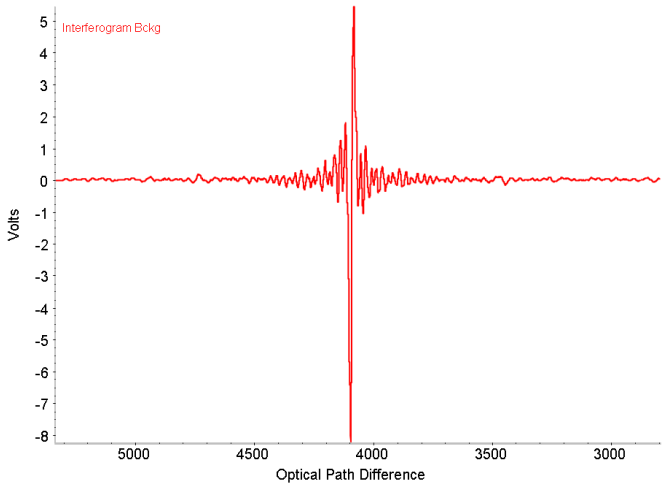

Figure 3.5: Interferogram collected of the background, with OPD as a function of voltage. ZPD is the highest amplitude of constructive waves.

This is the signal originally observed in FTIR spectroscopy. Later, when the signal arrives to the detector it is mathematically Fourier transformed from a function of mirror path differences to a function of wavelength/wavenumbers.

The normal running mirror velocity of the translating mirror is 0.4747, 0.6329 or 0.9329 cm/s, depending on which experimental method is applied. The low mirror velocity employed is due to the type of detector, which works best under these running conditions.

3.1.3 BEAMSPLITTER

The beamsplitter used in the MIR region is a thin coating of Germanium (Ge) sandwiched between two KBr plates; It is normally referred to as a KBr beamsplitter. It acts similar to a semitransparent silver mirror which partly reflects and partly transmits the light source. The KBr serves to protect the Ge from the environment. The KBr beamsplitter is transparent for the IR beam in the region 4000-400 cm^{-1}. Cesium Iodide (CsI) is another possible beamsplitter, which works until 200 cm^{-1}, which is lower wavenumbers than the KBr beamsplitter. However, the CsI is a soft material and very hygroscopic, which tends to become fogged over in time due to its hygroscopicity. A beamsplitter made of CsI must be expected to be replaced more often than the KBr beamsplitter [39]. The purging of the spectrometer with dry air serves to protect the beamsplitter from a humid environment and prolong its life expectancy.

Figure 3.6: The beamsplitter compartment with easily exchangeable beamsplitter for MIR and FIR region.

At lower wavenumbers in the FIR region, there are two other options for beamsplitters. The classical Mylar beamsplitter, which has been used since the 1960s, and the Solid Substrate beamsplitter, which is a relatively new beamsplitter that has been used since 1998.

The classical Mylar beamsplitter is the trade name of a very thin biaxially-oriented polyethylene terephthalate (boPET) polyester film. Depending on its thinness it can collect spectra in different low wavenumber regions, as can be observed in *Table 3.1*. The Mylar is not equally transparent in all the mentioned ranges. At low and high ends of the ranges mentioned, the Mylar is less transparent than in the middle-range mentioned [41].

Table 3.1: IR Spectral Range as a function of the Thickness of PET films. Reprinted from [42].

Film Thickness (μm)	Spectral Range (cm^{-1})
6.25	80–450
12.5	40–220
25.5	20–100
50	12–50
100	8–25

The Mylar beamsplitter has several great disadvantages. One of the biggest disadvantages is that in order to collect spectra in the entire FIR region at optimum condition with equally transparency, different beamsplitters with different thickness's of the Mylar is required [42]. *Figure 3.7* shows the FIR spectrum of calcite recorded with three different Mylar beamsplitters (with different thickness) in order to collect the entire region of 500-50 cm^{-1} [43].

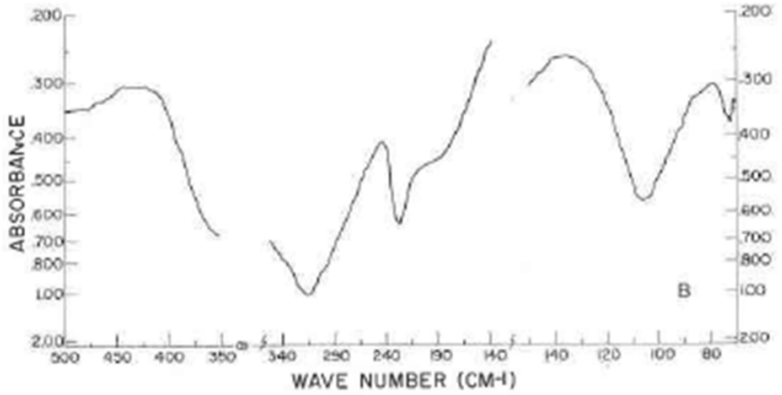

Figure 3.7: FIR transmission spectrum of calcite collected in the region at 500-50 cm^{-1} using Mylar beamsplitters. In order to colect this entire region the same sample needs to be recorded 3 times with different Mylar beamsplitters. Reprinted from [43].

Another problem is that due to the thinness of the mylar beamsplitter it is highly sensitive to noise vibrations, including those originating from the GPG (necessary for purging the spectrometer for water vapours). The thinner the Mylar film is, the more sensitive it is to vibrations. Despite these problems the Mylar beamsplitters are still one of the most used beamsplitters for the FIR region.

The second possible option as a FIR beamsplitter, is the solid substrate beamsplitter commercially produced by Nicolet. The Solid substrate beamsplitter is an approximately 2 mm thick silicon wafer [44], which is much thicker than the Mylar and as such it is much less sensitive to noise vibration than the Mylar. It also functions in just one working region, which is 700-50 cm^{-1} with equal efficiency over the entire region.

Another difference between the two types of beamsplitters is in the amount of energy absorbed. The solid substrate absorbs more energy than the Mylar beamsplitter due to its larger thickness. It is therefore necessary to turn up the energy input when applying the solid substrate beamsplitter. Otherwise there is not enough output energy properly registered by the detector [45]. This is accomplished by employing a Globar IR light source, while for the Mylar beamsplittet an air cooled light source would be enough.

In our instrument we use the solid substrate beamsplitter together with the higher energy output of the Globar light source. This combines to give the option of collecting better spectra in the FIR region with less noise interference than ever seen before in the literature. Only one collection of spectrum is necessary for the FIR region, not three collections, as observed in *Figure 3.7*. The manual changing of beamsplitters from the MIR to the FIR region takes no more than 30 seconds.

3.1.4 SAMPLE CHAMBER

The sample chamber is the place where the actual sample is inserted and investigated. As already mentioned, we have the option of collecting samples using transmission and ATR spectroscopy. This requires a different setup of the instrument as shown in the ***Figure 3.8***.

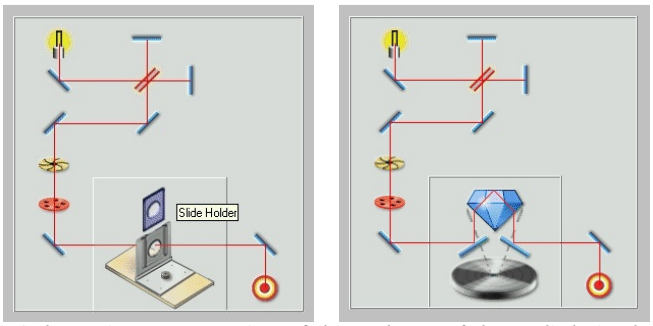

Figure 3.8: Schematic representation of the pathway of the IR light in the sample chamber for both transmission and ATR spectroscopy

Collection of samples in normal transmission requires the sample to be in powder form either embedded in an inert material. For the MIR region this material is KBr, for the FIR region we apply PE. The pellet is placed into the sample holder, which is then placed in the slide holder. The path

way of the light goes strait through the sample to the detector. For transmission collection with the IR card, where the powder is placed on the IR card, the card itself is placed into the slide holder.

The ATR (Attenuated Total Reflection) measurements were performed by means of an ATR Smart Orbit™ accessory from Thermo Scientific, which allows recording of ATR spectra directly on a sample without mixing it with an inert material such as KBr or PE. By changing the beamsplitter and the detector we can collect sample spectra both in the MIR and in the FIR region. The Smart Orbit™ can collect the spectra directly on a small fragment, on powders, semi-solids, and thin films as well as on liquids. The crystal used is transparent to the IR beam, it is a so-called internal reflecting element (IRE) with a high refractive index. Typical materials used are *zinc selenide*, *KRS-5*, *germanium* and *diamond*, whose refractive index and range of transparency are all listed in *Table 3.2* together with other typical window or crystal material frequently employed in IR spectroscopy. Our ATR crystal is a *diamond* crystal with a refractive index of 2.4 and a region of transparency from 45000-50 cm^{-1}.

Table 3.2: List of window material [46]. In bold italic the materials relevant for FIR region.

Material	***Refractive index (n)***	***Transmission (cm^{-1})***
AMTIR, GeAsSe glass	2.5	11,000-1,000
Arsenic triselenide, $As2Se_3$	2.8	12,500-600
Arsenic trisulfide, AsS_3	2.4	14,000-1,200
Barium fluoride, BaF_2	1.45	50,000-1,000
BK-7 glass	1.5	31,000-4,300
Cadmiun telluride, CdTe	2.65	10,000-350
Calcium fluoride, CaF_2	1.39	66,000-1,300
Cesium bromide, CsBr	1.65	33,000-250
Cesium iodide, CsI	1.72	33,000-150
Crystal quartz, SiO_2	1.5	50,000-3,600; 250-30
Diamond, C	2.4	45,000-2,500; 1,600-30
Gallium arsenide, GaAs	3.14	10,000-600
Germanium, Ge	4	5,000-600
Lithium fluoride, LiF	1.33	90,000-1,500
Magnesium oxide, MgO	1.68	25,000-1,300
Polyethylene, HDPE	1.55	600-10
Potassium bromide, KBr	1.52	33,000-400
Potassium chloride, KCl	1.47	33,000-500
Quartz, SiO_2	1.44	57,000-3,000
Sapphire, Al_2O_3	1.75	66,000-2,000
Silicon, Si	3.42	10,000-100
Silver bromide, AgBr	2.2	20,000-300
Silver chloride, AgCl	2	23,000-400
Sodium chloride, NaCl	1.5	28,000-700
Strontium fluoride, SrF_2	1.44	66,000-1,000
Strontium titinate, $SrTiO_3$	2.41	25,000-1,700
Thallium bromoiodide, KRS-5	2.35	16,000-200
Titanium dioxide, TiO_2	2.6-2.9	24,000-1,700
Zinc selenide, ZnSe	2.42	20,000-500
Zinc sulfide, ZnS	2.22	22,000-750
Zirconium dioxide, ZrO_2	2.15	27,000-1,500

Mirrors in the Smart Orbit accessory bring the IR beam into the crystal (incident beam) focussing on the crystal surface with an incident angle, normally 45º. Once the infrared radiation is inside the crystal a standing evanescent wave of radiation is created. An unique property of the evanescent wave is that it is slightly larger than the crystal, which means it will penetrate a small fraction of distance beyond the crystal surface. When a sample is brought into contact with the crystal it can interact with the evanescent wave, absorb the infrared radiation and reflect it's own absorbance spectrum together with the evanescent wave back into the crystal and out to the detector [39].

Good contact between the crystal and the sample is crucial for insuring the evanescence wave penetrates into the sample. Hence, pressure is very often applied, pressing the sample into contact with the crystal. In the MIR region the evanescent wave penetrates 0.1-5 µm into the sample, while in the FIR region the penetration is much deeper as explained in chapter 2.

The depth of penetration decreases as the refractive index of the crystal increases. A Ge crystal with $n_{Ge} = 4.0$ has a significantly smaller depth of penetration than a ZnSe crystal with $n_{ZnSe} = 2.5$. If you change the crystal material during investigation of the same sample it is possible to collect spectra from different depth in the sample. This is called *depth profiling*. This is especially useful with laminated thin film with different thin layers.

In the last few month a new addition to our laboratory has arrived. It is the PIKE 4x beam condenser whose schematics is observed in ***Figure 3.1***, which is inserted into the sample chamber and applied in transmission mode.

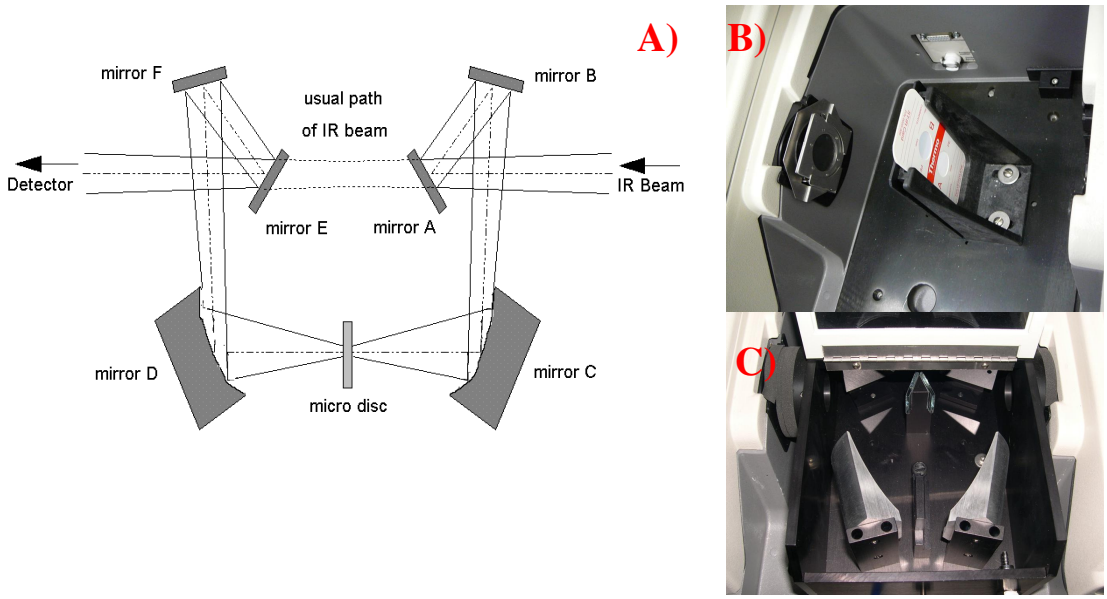

Figure 3.9: A) Schematics of the beam condenser shown here together with a photo of B) the normal transmission chamber (with an IR card inserted) and C) the sample chamber with the beam condenser inserted.

Collection with the PIKE 4x beam condenser is very similar to collection in the normal transmission mode. The function of the PIKE is to focus the beam from a previous normal transmission area of 8 mm area to a 2 mm area, which is accomplised by a sequential series of fucussing mirrors, which can be observed in *Figure 3.9a*. This should in theory make it possible to use smaller size pellet and hence, use smaller amount of sample to make the pellet.

The sample pellet is then inserted in the micro holder and the collection of a spectrum can begin. A small amount of sample is of cause always an advantage when working with cultural heritage material, as usually there are only very small amounts to investigate.

One very important consideration must be taken into accout when optimizing the sample compartment. The manufacture of FTIR instrument tend to offer the sample compartment as either sealed and desiccated or unsealed and with a GPG. Sealed and desiccated compartment means that a window material (usually KBr) is placed on either side of the sample chamber, thus sealing off the sample chamber from the rest of the instrument. This has the advange of not requiring a GPG to purge the instrument for humid air, but only requiring desiccant packs stategically placed in the sample chamber, and the rest of the instrument, to absorb the water from the air. The disadvantage with using a window material in the pathway of the light is that it usually lowers the signal intensity by 20% [39]. Another disadvantage is of course when collecting spectra and changing the spectral region in the instrument, these windows must also be changed. KBr windows are transparent in the MIR but not in the FIR region, while polyethylene windows are transparent in the FIR but not in the MIR region, as can be observed in *Table 3.1*. They must thus be continuously changed if you are changing the region during recording of spectra.

In our instrument we have thus removed the windows for optimising signal intensity, and to make it easier to change between spectral regions. A GPG is attached for removing humid air from the sample chamber (and the rest of the instrument).

3.1.5 DETECTOR

Both in the MIR and FIR region the detector employed in our FTIR instrument is DTGS (Deuterated TriGlycine Sulfate) detector. The detector element is usually protected by a small infrared transparent window to protect it from the environment. However, as already mentioned, the window material can also decrease the signal intensity coming from the sample chamber by 20%. In the case of the MIR region we have therefore removed the KBr window, which used to protect the detector element. In the FIR region this detector element is still protected by a Polyethylene (PE) window.

The DTGS detector is a pyroelectric bolometer. It works by registering changes in the amount of infrared radiation striking the detector element, which causes a temperature change in the DTGS element. This is quantifiable as the change in capacitance with temperature measured in voltage across the detector element. The DTGS detectors are cheap, simple and stable. The only drawback is that they are less sensitive than other detectors available, i.e. the MCT (Mercury Cadmium Telluride) detector. The translating mirror cannot move as fast collecting the interferogram as with the MCT detector. The normal operating mirror velocity for the DTGS detector is 0.4747, 0.6329 or 0.9329 cm/s, while for the MCT detector the normal mirror velocity is 1.2659, 1.8988, or 2.5317 cm/s. This makes DTGS a slow detector compared to the more modern MCT detector. Collecting time is the reason why the MCT detector is used for 2D IR mapping of areas and DTGS is normally used only for 1D point investigation.

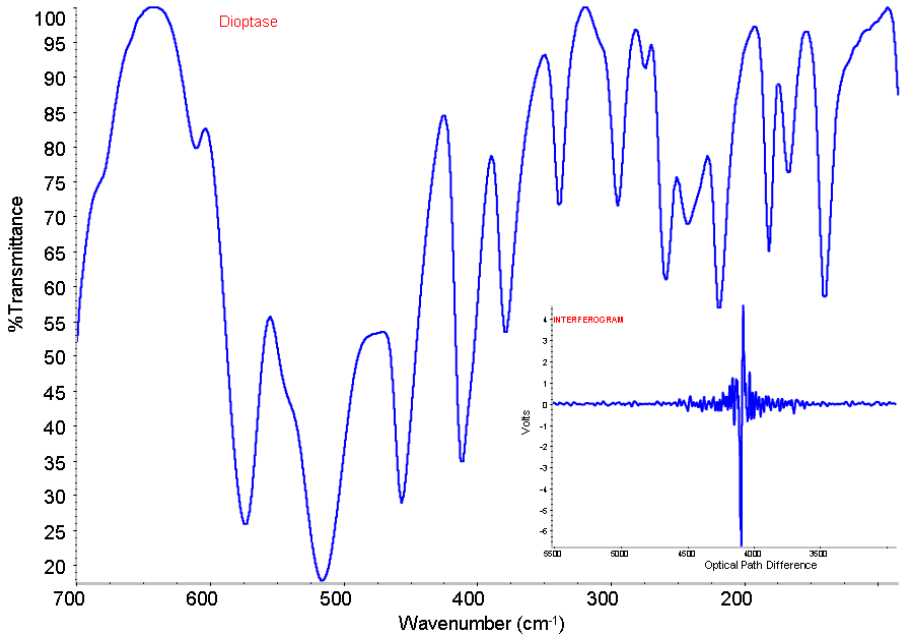

Figure 3.10: FIR spectrum of the mineral Dioptase and its interferogram (inserted) collected in transmission mode. The Cooley-Tukey algorithm transform the interferogram into a readable IR spectrum.

An interferogram is the sum of sinusoidal waves, each of which contains informtions about the wavenumber of a given infrared peak and amplitude information about the peak intensity at that specific mirror posision [39]. The interferogram measures the temperature fluctuations in the detector in voltage as a function of OPD. It is transformed into transmittance as a function of wavenumbers by applying the Fourier transformation (FT). The FT was originally developed by the French mathematician Joseph Fourier in the 19th century and developed further in the 1960 [7] to the so-called Cooley-Tukey algorithm, which is generally the algorithm applied in IR spectroscopy nowadays.

Our Instrument has two DTGS detectors, one optimized for MIR region the other for the FIR. The definition of the MIR and FIR region depends on the literature that your read. Early literature, which employ a DTGS (or even an older type) detector and a CsI beamsplitter define the FIR region as below 200 cm^{-1} as this was the cut-off limit of those detectors and the beamsplitter in the past [14]. The CsI beamsplitter was made from a much more soft and hygroscopic material than the later and more popular KBr beamsplitters, and thus the CsI beamsplitter tended to need replacement more often than the KBr one. Hence, the KBr beamsplitter quickly became more popular and have been almost universally employed since these early days; They have a cut-off limit at 400 cm^{-1} and thus the FIR region has been defined for many years now as below 400 cm^{-1}. Most literature still define the FIR region as below 400 cm^{-1} [39]. The newest literature from 2007 defines the FIR region as below 600 cm^{-1} [4]. This definition is closely linked with the development of the more sensitive MCT detectors, which collect spectra faster than the old DTGS detectors. This detector has quickly become the most employed detectors in advanced spectroscopy, including micro-spectroscopy. But the MCT detectors has a cut-off limit at 650-600 cm^{-1} and hence the author of Ref [4] defines everything below 600 cm^{-1} as the FIR range.

In our case we define the FIR region, as the region where we collect spectra using the modified DTGS detector (with PE windows) and employing the solid substrate beamsplitter for data collection. Similarly, we define the MIR spectral range as the region where we collect data using the normal standard DTGS detector and applying the KBr beamsplitter. For transmission spectroscopy the MIR range in our instrument is 4000-400 cm^{-1} and the FIR range is 670-90 cm^{-1}, for ATR spectroscopy the MIR range is 4000-525 cm^{-1} and the FIR range is 700-90 cm^{-1}. In both cases there is a small overlap of regions.

The switch between the MIR and FIR region, both for transmission and ATR spectroscopy, is accomplished with remarkable ease if you posses a ‘flexible’ FTIR instrument. The change between the two regions, the MIR region and the FIR region, is facilitated by the manual change of beamsplitter and the PC controlled change of detector.

3.2 OPTIMIZATION MESUREMENTS.

This section is dedicated to optimizing the spectral appearance, for best signal-to-noise (S/N) ratio in the spectrum. Once the hardware, the beamsplitter, the detector and the accessory is in place in the instrument, how do we achieve a good S/N ratio? The optimization is mainly conducted from the PC by using functions in the OMNIC software, which controls the Thermo Nicolet 5700 spectrometer. Focus is on achieveing good S/N ratio in the FIR region.

3.2.1 ALIGNMENT, GAIN AND MIRROR VELOCITY

The first problem encountered is the aligning of the signal to its maximum performance. The aligning is performed in practice by having a set of four small electromagnets apply a small pressure on the back of the fixed mirror. The pressure on the back of the mirror turns the fixed mirror slightly, in such a way that the IR beam arriving at the detector is focused. Normally, when using the spectrometer, the interferometer should align itself automatically depending on which experiment is being run. However, if you change beamsplitter or insert (or remove) the smart orbit accessory in order to change the experimental set-up, the alignment is not always performed automatically. It is therefore necessary to align the interferometer (i.e. tell the PC to do it) in order to obtain maximum peak value (output energy measured in the detector). The process takes about 2 min.

The setting of the gain is important to improve the peak values by factors of 1, 2, 4, 8 and 'autogain'. Normally the 'autogain' is applied allowing the software itselfto find the best possible peak value in every experiment. It is very important that the peak value does not exceed the value of 7-8 (depending on which experiment is chosen). If the peak value is higher the detector will be overloaded when running an experiment and effectively stop the collection of spectra for several minutes. There is no damage to the detector if the peak value is lower than 7-8 but this can give bad quality spectra with more noise.

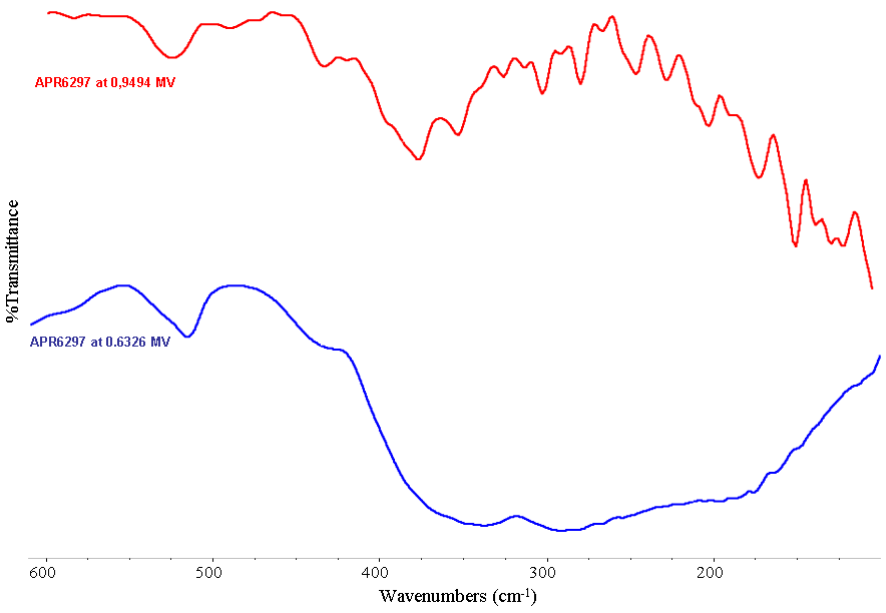

Figure 3.11: Spectra of APR6297 Cobalt Green at 0.9494cm/s (red) and 0.6326 cm/s (blue) Mirror Velocity. The baseline noise observe in the fast moving mirror is not coming from water vapour.

From the detector paragraph in section 3.1.5 we know that the DTGS detector works best at slow mirror velocities. Collection of spectra at various mirror velocities is compared in order to obtain the best possible S/N ratio in the spectra using 'autogain' to obtain optimum peak value. A considerable signal increase and noise reduction is achieved when slowing the mirror velocity from 0.9494 to 0.6326 cm/s as can be observed in *Figure 3.11,* which shows the spectrum of cobalt green (CoO, ZnO)[4], before and after the mirror velocity change. Collecting the pigment spectrum with 0.6326 cm/s mirror velocity instead of the faster mirror velocity really improves the FIR spectrum, giving a significant increase in band vibrations and a significant reduction in visible water bands in the range 400-100 cm^{-1}.

The same improvement is not observed when investigating PE thin film. This is partly due to the thinness of the PE thin film, and partly due to the amount of absorbed radiation by the sample. The sample is only applied on the PE thin film in a very thin layer, and therefore the IR radiation penetrating the film is faster through. This gives a higher output peak value of about 14, which totally drowns out the detector. Thus, it is necessary to apply faster mirror velocity and also lower the gain, to achieve spectra with optimal S/N ratio.

3.2.2 GAS PURGING GENERATOR (GPG)

Optimization experiments are also conducted in order to establish how long before collecting a spectrum the Gas Purging Generator (GPG) has to be switched on to achieve a good spectrum without noise bands.

The GPG purges the spectrometer with dry air to force out any moisture from inside the spectrometer during collection. This is especially necessary for collection of spectra in the FIR region, where gaseous water bands are highly visible, but also necessary for ATR collection in the MIR region.

Figure 3.12 shows a close-up of the background collected in the FIR region 400-240 cm^{-1}. The red spectrum is collected without the GPG switched on. In this case the water vapour bands are highly visible, compared to just minutes (or hours) later, where the water bands are less poignant.

[4] Cobalt green (CoO, ZnO) standard pigment from W. G. Ball Ltd, Artist Pigment Range (APR) n° 6297, available from http://www.wgball.com/artists-pigments.htm

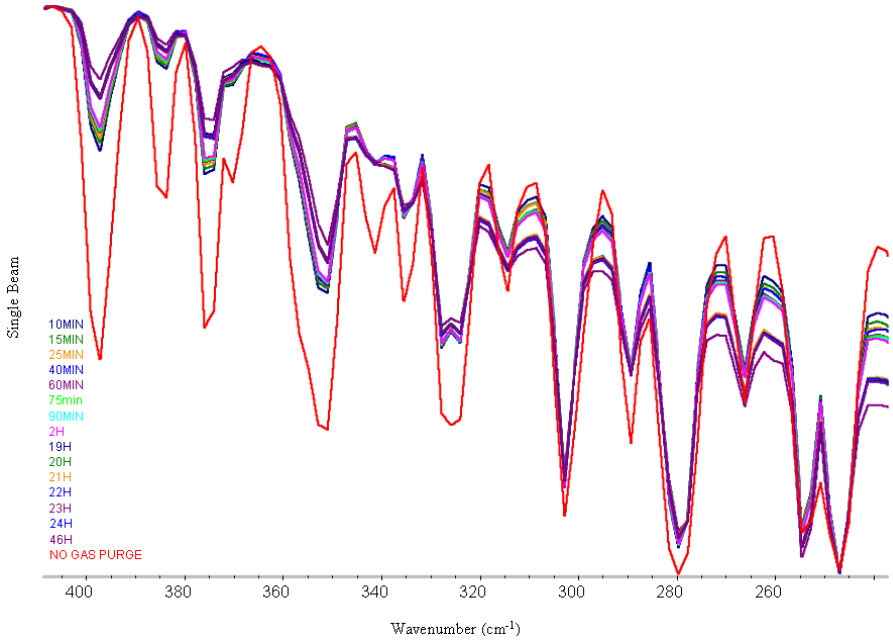

Figure 3.12: FIR spectra collected of the background over 0-46 hours with the GPG switched on, in the region 400-240 cm^{-1}. The red spectrum is collected without the GPG switched on.

Especially going from 0-10 minutes purge time, a considerable reduction of the water bands is noticed, while only a small reduction is visible going from 2 hours to 19 hours, and again from 24 hours to 46 hours. All through the 46 hours of collecting the background we observe decreasing intensity of the gaseous water bands. We must conclude that with the new optimized settings the background is not stable over a long period of time and that the background is especially sensitive in the first hour of collecting spectra. However, this is not surprising as the environment that surrounds the spectrometer is constantly changing. People walk in and out of the laboratory (more/less gaseous water in the room) and also i.e. the temperature, humidity and sun influence the laboratory environment, in which the spectrometer is placed. Additionally it has been noted that opening a window or having wind draught trough the laboratory affects the visibility of water in the spectra and must thus be avoided. The unstable environment over a long period of time makes it necessary to always subtract the background spectrum just before or after collecting the sample spectrum rather than subtracting a single background spectrum recorded at the beginning of the day.

When commencing collection of spectra it is necessary to wait some time after the GPG has been switched on to achieve stable environment inside the spectrometer, as can be observed from the spectra in *Figure 3.13.* Here the spectrum of Cobalt Green (CoO, ZnO) APR6297 can be observed before switching on the GPG, after 2 minutes and again after 30 minutes.

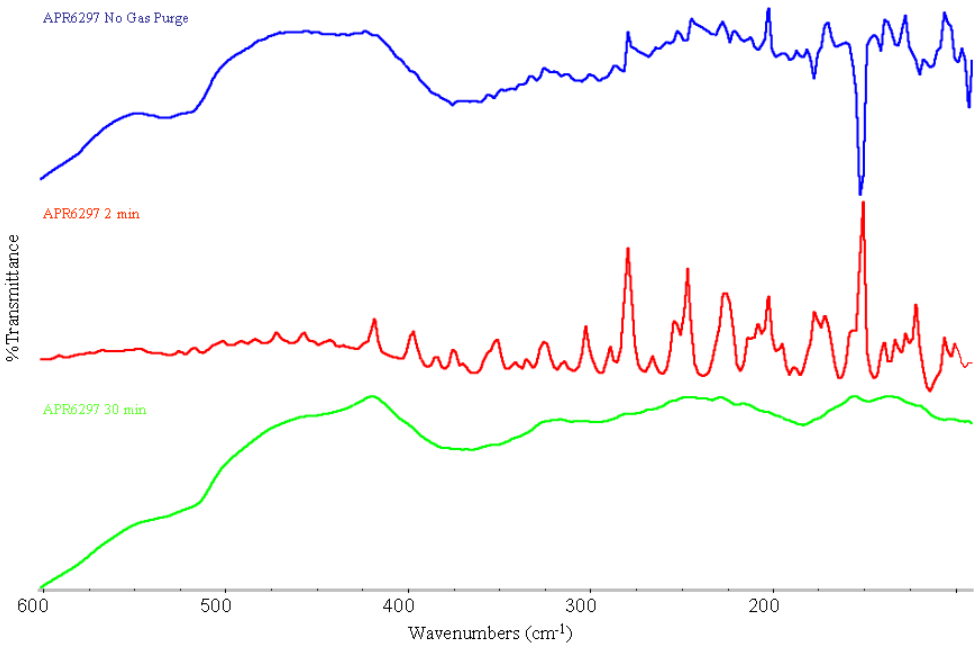

Figure 3.13: FIR spectra of cobalt green (CoO, ZnO) APR6297, collected before the GPG was switched on and 2 min and 30 min, respectively, after it was switched on. After 2 min we observe negative water vapour as the spectrometer has not yet achieved a stable environment. After 30 min the environment inside the spectrometer is stable enough to observe weak bands of cobalt green.

After 2 minutes we observe negative water bands in the spectrum. This is due to the gaseous water background subtraction, which is still not stable inside the spectrometer, hence the background is still adapting during collection of the sample spectrum. First after 20-30 min is the background stable enough to provide a spectrum without the presence of neither positive nor negative water bands. The observed bands for cobalt green (CoO, ZnO) are weak and an assignation of bands will be difficult. But at least there will be no interference from the environment when trying to interpret the bands in the spectrum.

From the supplier of the spectrometer we were informed not to use the GPG when collecting ATR-spectra with the smart orbit accessory in the MIR region. This, we where told, would not be necessary as all water bands are easily removed from the sample spectrum when collecting the background spectrum. Initially, as with the ATR spectra collected in the FIR region, we collected the background spectrum in the MIR region over a period of time with the ATR smart orbit accessory. We concluded as before, that the background inside the spectrometer is not stable over time and the background subtraction must take place when collecting sample spectra. However this is not a surprise. In theory, as water and CO_2 in the background is automatically subtracted from the sample spectrum, it should not be necessary to apply the GPG in the MIR region. In practice, we

examine this further by looking closer at the MIR spectrum of barium chromate[5] in ***Figure 3.1***. Here we observe a little noise when there is no GPG switched on in the region of 2400-1400 cm^{-1}. This noise will make assignment of bands in this region a little more difficult especially if the bands are weak (as can be observed here). With the GPG switched on for 12 minutes (like with ATR-FIR collection) we observe negative water and CO_2 bands, indicating that GPG has not yet stabilized the environment inside the spectrometer. After 35 min the internal environment in the spectrometer is clearly stabilized. We still observe a little noise in the spectra from 2400-1900 cm^{-1}, however, this region has very few important bands so noise here is of little importance.

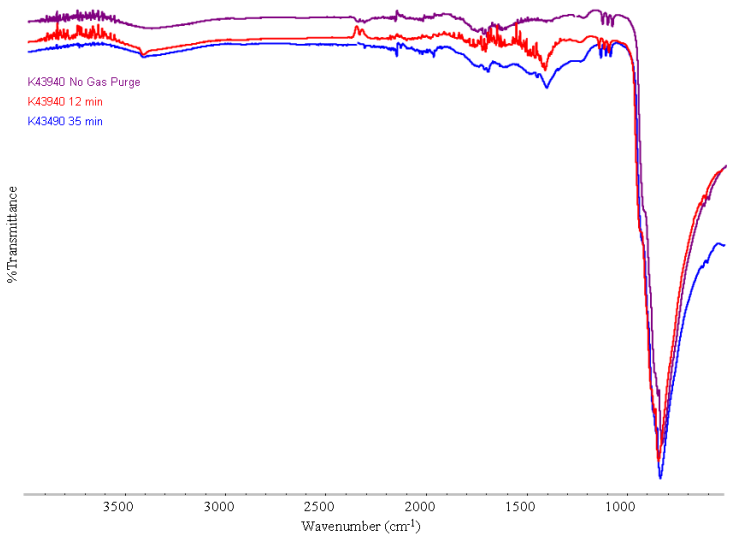

Figure 3.14: ATR-MIR spectra of pigment Barium yellow (K43940) without GPG switched on, and 12 min and 35 minutes after purging has commenced. After 12 min we observe negative water vapour as the spectrometer has not yet achieved a stable environment. After 35 min the environment inside the spectrometer is stable enough to observe weak overtone bands of barium yellow in the 1800-1200 cm^{-1} region.

These experiments with the GPG in both the MIR and the FIR region leads us to two conclusions. Firstly, the background is not stable over a long period of time, which means the background must be subtracted every time we collect a sample spectrum. Secondly, after the GPG has been turned on for approximately 30 minutes, the background in the spectrometer is stable enough to collect optimal spectra with minimum interference from water or CO_2 in the background.

3.2.3 COLLECTING THE BACKGROUND 1ST OR 2ND

During these optimizations experiments we noticed some peculiarities in the order of collecting spectra. The experimental set-up in the PC allows you to collect the background before or after

[5] Barium yellow ($BaCrO_4$) from Kremer Pigmente GmbH, id no 43940, available at http://kremer-pigmente.de/en

collecting the sample spectrum. There should in theory be no difference in what order you subtract the background from the sample spectrum but in practice we observe that occasionally there is. Figure 3.15 shows two spectra of leather collected at the same place on the sample. But spectrum *leather 1* is collected 1st, the background 2nd and then subtracted. Spectrum *leather 1 corrected* is the same spectrum merely corrected (removing the CO_2 band and applying smooth 9 on the spectrum). We notice it is not possible to remove the observed water vapours in the spectrum. However, the order of recording is reversed with spectrum *leather 2 corrected*, where the background is collected 1st, the leather sample is collected 2nd, and then the background is subtracted and corrected (CO_2 band is removed and smooth 9 is applied). All three spectra has been baseline corrected and the GPG has been switched on during the experiments.

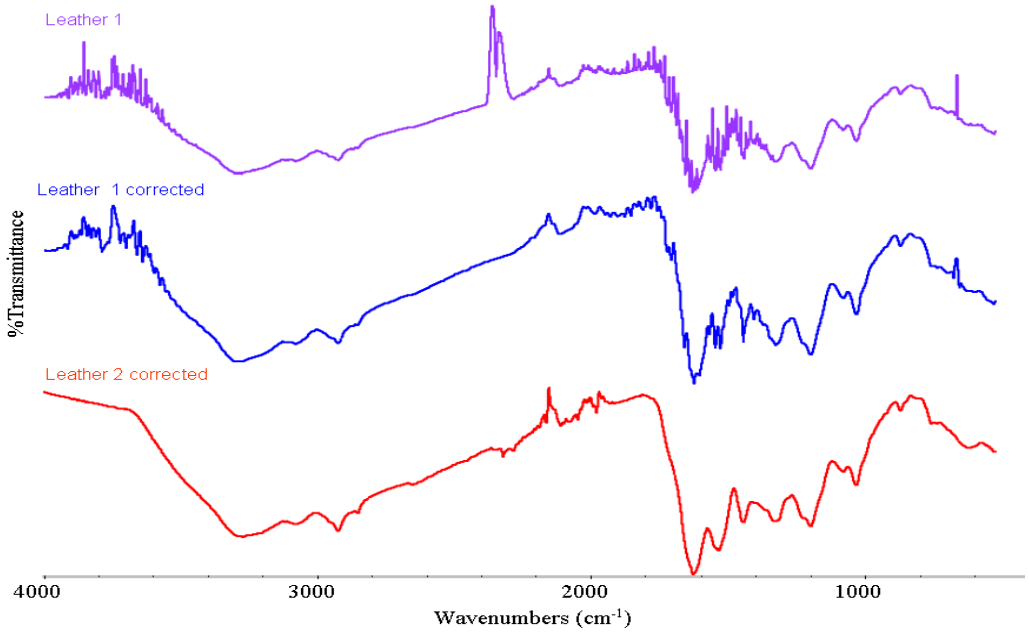

Figure 3.15: Spectra of leather 1 & leather 1 corrected which has the sample collected first, background collected second. Leather 2 corrected have the background collected first, sample collected second. Notice the noise at 2000-1300 cm^{-1} for leather 1 & leather 1 corrected compared to Leather 2 corrected.

But as it can be observed in *Figure 3.15* we notice similar noise as we observed during the GPG experiments, the presence of what appears to be water vapour bands covering the region from 2000-1300 cm^{-1} in spectrum *leather 1* (corrected as well as uncorrected). These bands influence the interpretation of the bands as well as the wavenumber assignment. Whereas, in *leather 2 corrected* we observe only typical water vapour in the 2400-1900 cm^{-1} region as expected. This observation means that the order in which we collect the background spectrum, 1st or 2nd, can influence the resulting spectrum. However, this observation appears to be random as it is not observed every time we collect the background 2nd to the sample spectrum. The possibility of this random noise must be taken into account when collecting spectra in reverse order.

It has been observed when collecting the background 1st that the 'autogain' has a starting peak value of about 7,2-7,5 and the following sample collection is slightly lower, about 5-7 in peak value (as the energy normally becomes lower upon investigating the sample itself). But when reversing the order of collecting spectra, the sample spectrum has a much lower peak value which starts about 3-5, and the subsequent collection of the background spectrum is equally lower in peak value (about 2-4). It is therefore believed that this lower energy, when collecting the background 2nd, significantly reduces the signal intensity and increases the noise intensity, and hence, we observe more noise coming from ambient surroundings than by reversing the order of background collection. This could very well be a side effect to using the 'autogain' (letting the computer decide the energy output) instead of manually determining the gain before commencing spectral collection.

These spectral observations, although random, has also been observed during collection of FIR transmission spectra as well as with the ATR smart orbit accessory in the MIR and FIR region. Hence, the standard experimental set-up collects the background 1st and the sample 2nd for best S/N ratio in the spectrum.

3.2.4 CALIBRATION OF SPECTROMETER

The purpose of calibrating the spectrometer is to immediately see if there is anything wrong with the set-up of the instrument, with the hardware or with the alignment of the instrument. Calibration is performed by finding one or more very sharp and intense bands, that are always the same when collected, at the same resolution, no matter how much time (month or years) has passed in between collection of spectra. Very often simple crystals are used because they often appear to have just that very sharp band, which can be employed for calibration. Previously, HgO [47] have been used, but it is poisonous. Also Sulfur (S_8) has been used [48] but mainly for Raman calibration since there are 11 active Raman vibrations, of which some are extremely sharp [49].

For collection in both ATR and transmission in the FIR region the easiest way of calibrating the spectrometer is to collect the ambient background and compare the wavenumbers with a previous collected spectrum of the background. For the FIR region the spectrum of the bands in the ambient background is very reproducible, as can be observed in *Figure 3.16*.

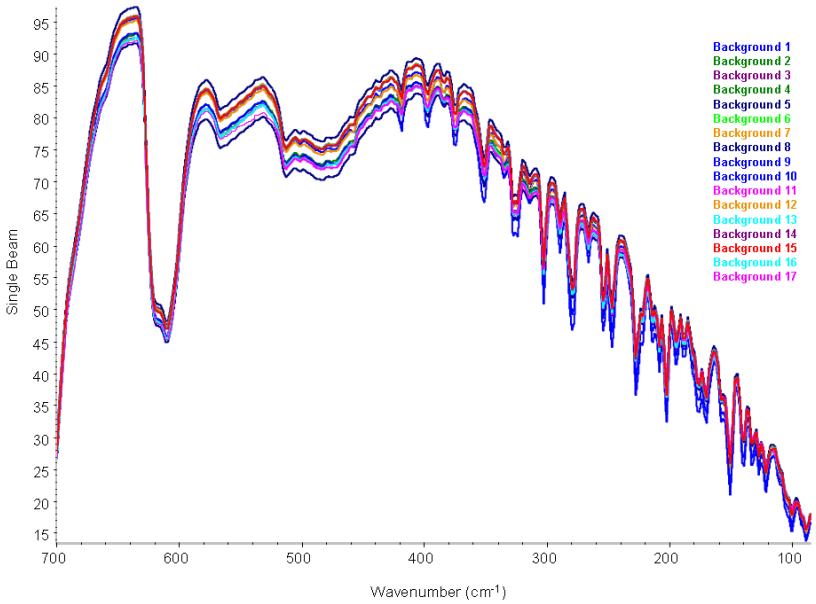

Figure 3.16: The ambient background collected 17 times over a period of 4 weeks in the ATR FIR region. No baseline correction has been performed. As can be observed the water vapour bands are very reproducible.

Many of the water vapour bands are so sharp that even when collecting 26 spectra with a spectral resolution of 4 cm^{-1}, the majority of the water vapour peaks only varies from 0.0-0.4 cm^{-1}, as can be observed in ***Table 3.3***. Here are listed 40 bands of which most originates from water. A few bands, the band at 55 and 72 cm^{-1} originate from the instrument, in this case the PE window in the detector. The sharpness and repeatability of water vapour is quite exceptional and thus can be used for checking and calibrating the spectrometer. Water vapour calibration is generally applied for gaseous spectrometer calibration because of the extreme sharpness of the water vapour bands [47].

In transmission, another way of directly collecting a spectrum of water vapour (besides collecting the natural background), is by inserting a cup of boiling hot water in the sample compartment (after collecting the instrument background first). Allow the water vapour to fill the sample compartment for a few minutes and then collect a spectrum. This gives only the very sharp and intense water vapour bands, without the bands originating from the instrument itself.

In the MIR region many once again use the natural background for calibration, as it contains CO_2 vapours. When collecting in ATR mode with the smart orbit accessory CO_2 has sharp and intense peaks at 2323, 2286 and 2156 cm^{-1}. In the case of transmission spectroscopy breathing into the sample chamber should be enough to be able to collect the CO_2 vapour bands.

Table 3.3: Peak list of 26 collected background spectra; average wavenumber, maximum and minimum wavenumber, wavenumber interval and standard deviation of the 40 observed peaks. All background spectra are collected with a spectral resolution of 4 cm^{-1}.

Peak	*Average*	*Max*	*Min*	*Interval*	*Std.Dev.*
1	*55.72*	*59.4*	*52.3*	*7.1*	*0.9852*
2	*72.93*	*74.7*	*70.2*	*4.5*	*0.5379*
3	*88.49*	*88.7*	*88.3*	*0.4*	*0.0426*
4	*100.06*	*100.1*	*100.0*	*0.1*	*0.0452*
5	*121.24*	*121.3*	*121.2*	*0.1*	*0.0452*
6	*126.97*	*127.0*	*126.9*	*0.1*	*0.0515*
7	*132.40*	*132.4*	*132.4*	*0.0*	*0.0000*
8	*139.66*	*139.8*	*139.5*	*0.3*	*0.0452*
9	*150.62*	*150.7*	*150.6*	*0.1*	*0.0000*
10	*157.36*	*157.6*	*157.3*	*0.3*	*0.0900*
11	*170.32*	*170.4*	*170.2*	*0.2*	*0.0000*
12	*176.46*	*176.6*	*176.3*	*0.3*	*0.0389*
13	*188.09*	*188.1*	*188.0*	*0.1*	*0.0289*
14	*194.52*	*194.6*	*194.4*	*0.2*	*0.0000*
15	*202.49*	*202.5*	*202.3*	*0.2*	*0.0577*
16	*208.30*	*208.3*	*208.3*	*0.0*	*0.0000*
17	*213.60*	*213.7*	*213.6*	*0.1*	*0.0000*
18	*227.10*	*227.1*	*227.1*	*0.0*	*0.0000*
19	*246.97*	*247.0*	*246.9*	*0.1*	*0.0000*
20	*253.89*	*253.9*	*253.6*	*0.3*	*0.0866*
21	*266.20*	*266.2*	*266.2*	*0.0*	*0.0000*
22	*279.25*	*279.5*	*279.0*	*0.5*	*0.0000*
23	*289.37*	*289.4*	*289.3*	*0.1*	*0.0492*
24	*302.70*	*302.7*	*302.7*	*0.0*	*0.0000*
25	*314.40*	*314.5*	*314.2*	*0.3*	*0.0289*
26	*324.66*	*324.7*	*323.7*	*1.0*	*0.0000*
27	*327.08*	*327.1*	*327.0*	*0.1*	*0.0452*
28	*334.93*	*335.0*	*334.9*	*0.1*	*0.0289*
29	*351.56*	*351.8*	*351.4*	*0.4*	*0.0000*
30	*375.07*	*375.2*	*375.0*	*0.2*	*0.0568*
31	*384.21*	*384.4*	*384.1*	*0.3*	*0.0452*
32	*397.57*	*397.6*	*397.5*	*0.1*	*0.0522*
33	*418.89*	*418.9*	*418.6*	*0.3*	*0.0866*
34	*436.43*	*436.7*	*435.2*	*1.5*	*0.2392*
35	*457.80*	*458.0*	*456.0*	*2.0*	*0.5734*
36	*483.99*	*484.1*	*483.8*	*0.3*	*0.0515*
37	*501.82*	*502.0*	*501.6*	*0.4*	*0.0900*
38	*512.90*	*513.1*	*512.8*	*0.3*	*0.0389*
39	*566.57*	*566.7*	*566.4*	*0.3*	*0.0515*
40	*610.33*	*610.4*	*610.3*	*0.1*	*0.0492*

3.2.5 REPRODUCIBLITY

According to the producer, with interchangeable detector and beamsplitter, it is possible to collect spectral information in the range 4000-50 cm^{-1}.

In order to verify the lower range we collect 5 spectra of limestone in both ATR and transmission mode, which can be seen in *Figure 3.17.*

We observe from both experimental modes that reproducibility in the lower region stops around 90-80 cm^{-1}. In ATR mode we observe in 4 out of 5 spectra a band at 73 cm^{-1}, which comes from the PE window in the detector. This band is present with varying intensity in the 4 spectra and is lacking in the 5th spectrum. Equally in transmission mode we observe arbitrary fluctuations in the region 80-50 cm^{-1}.

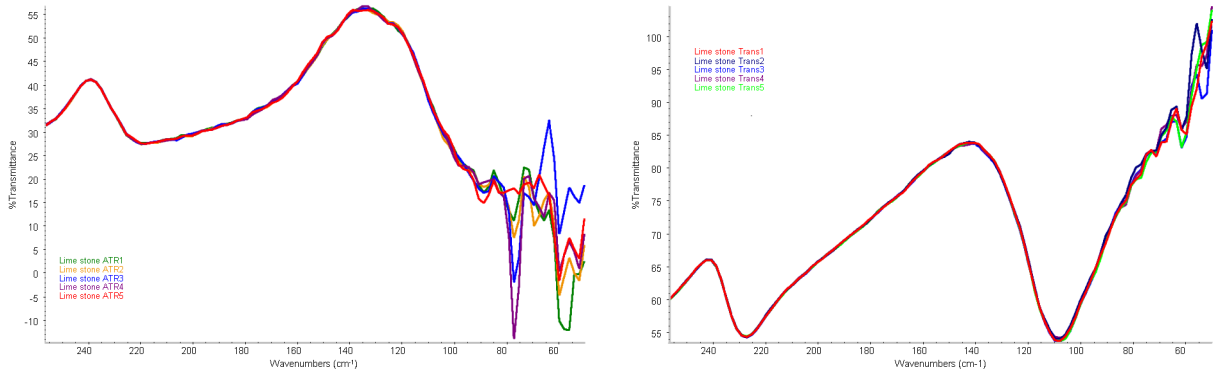

Figure 3.17: Reproducibility test of 5 times spectral collection of lime stone in the FIR region 250-50 cm^{-1} collected in ATR and transmission mode, respectively. Reproducibility stops below 90 cm^{-1} due to fluctuation and unreliable instrument noise in the 90-50 cm^{-1} region.

From these spectra we observe that reproducibility for collection of spectra in the lower IR range stops below 90 cm^{-1}. This is because the signal arriving from the detector is very close to the detector cut-off, which makes it a very weak signal.

3.3 MANIPULATION OF SPECTRA IN THE FIR REGION

It is quite common in all areas of spectroscopy to manipulate the spectrum to achieve a spectrum with less noise and better signal intensity. However, some manipulation is part of the set-up before collection of spectra begins, like zero filing and apodisation, while others are conducted after collection of spectra, like baseline correction and smoothing. Only in the last case, with post-collection corrections, is it possible to retain your original spectra, while in the first case scenario, it is no longer possible to remove the spectral manipulation and retrieve the original spectrum.

3.3.1 ZERO FILLING & APODISATION

Zero filling is a manipulation of data which improves the defined line shape of a spectrum by adding data points (zero's) between collected data points in the wings of the interferogram. This manipulation must be set-up before collection of spectra commence. It is not possible to un-do the manipulation at a later time.

The process aims at smoothing sharp and edgy features into becoming smoother and more rounded. The zero filling takes place before the data are Fourier transformed. The Fourier Transformation of data will take longer because data points are added to the interferogram. No increase of the actual spectral resolution takes place, as this is determined solely by the number of data points collected .

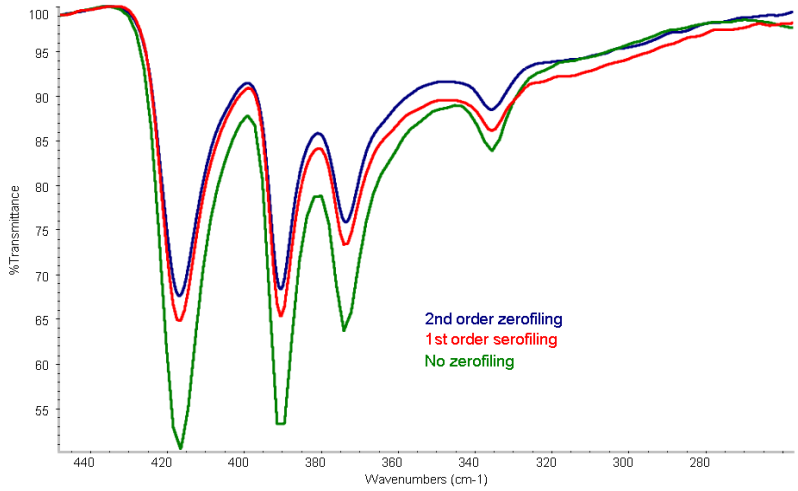

Figure 3.18: The three possible zero filing options available in OMNIC collected of Barium Yellow in ATR mode; No zero filing, 1st order zero filing and 2nd order zero filing.

In the OMNIC software it is possible to choose 3 different zero filling options. A) No zero filling; B) 1st order zero filling, in which one data point is added between each collected data point in the wings of the interferogram; C) 2nd order zero filling, in which three data points are added between each collected data point in the wings of the interferogram. *Figure 3.18* show an example of zero filling in the FIR region for the powder pigment barium yellow ($BaCrO_4$) collected in ATR mode. As can be observed the zero filling makes the spectra more round and smooth but it also decreases signal intensity.

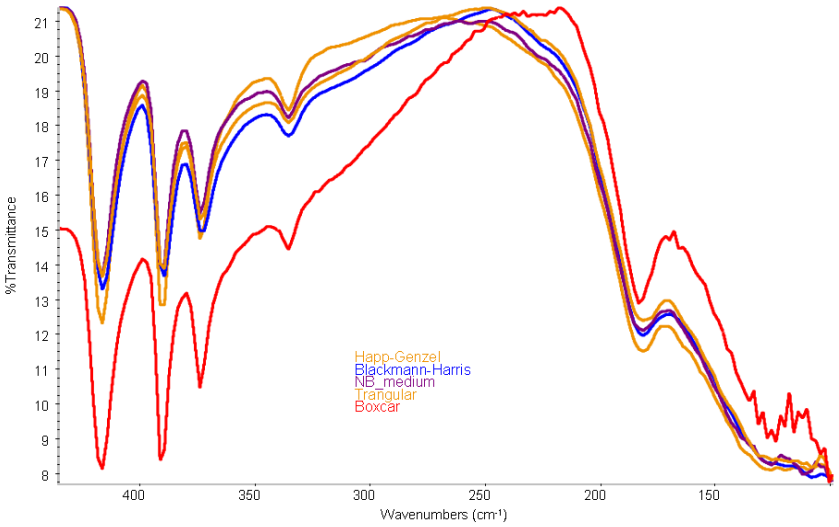

Figure 3.19: Various apodisation algorithms applied to powder of Barium Yellow collected in ATR mode. Happ-Genzel, Blackmann-Harris, Norton-Beer (NB)-Medium and Triangular are all quite similar algorithms, while Boxcar (meaning very weak apodisation) shows distinct difference from the other 4 algorithms.

Another spectral manipulation which must be determined prior to collecting the spectra is apodisation. Apodisation removes small "feets", which is peaks that can occur because the interferogram is not an infinite set of data, as it is limited by the length of the translating mirror. In order to mathematical pretend that the translating mirror has infinite length we basically apply an algorithm to the interferogram, which removes the little "feet". Without the apodisation the baseline of the spectra becomes very noisy as can be observed in *Figure 3.19,* in which the boxcar apodisation (meaning very weak apodisation) has a much more unsteady baseline with amplified noise [39]. Almost no matter which of the other 4 possible algorithmic options is selected, we get an baseline with less noise. Some of the other algorithms available can cause band broadening. This laboratory use no-zero-filling and employ the Happ-Genzel algorithm to all collected spectra.

3.3.2 BASELINE CORRECTION & SMOOTHING

Normally a spectrum needs baseline correction. This spectral manipulation is performed post-collection of the sample spectrum. The baseline is affected by many factors; the colour of the sample, the sample quality as well as the quality of the background spectrum. Also the preparation of the sample can cause baseline problems [39]. Larger particles (more than 5 µm) can cause scattering effects due to insufficient grinding of the sample in transmission mode. This results in decreased transmittance. Also difference in thickness of the sample pellet compared to the thickness

of the background pellet can cause significant baseline differences. Figure 3.20 show an example of baseline correction collected in ATR mode.

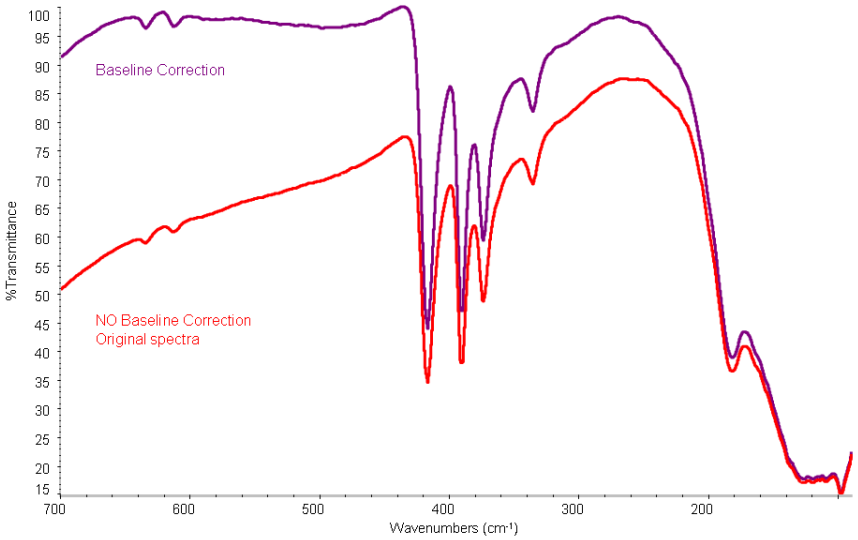

Figure 3.20: Original and Baseline Corrected spectrum of powder Barium Yellow collected in ATR mode in the FIR region 700-90 cm^{-1}.

Table 3.4: Smoothing over averaging neighboring data point using the Savitzky-Golay algorithm.

Smooth	Average (cm^{-1})
5	9.642
7	13.499
9	17.356
11	21.213
13	25.070
15	28.927
17	32.784
19	36.641
21	40.498
23	44.355
25	48.212

The original spectrum is preserved when smoothing a spectrum as it is a post-collection manipulation.

Smooth uses the Savitzky-Golay algorithm whereby one data point is averaged over a selected region, basically by averaging over a specific amount of neighbouring data point [39] as listed in *Table 3.4*. Smooth is used to improve the appearance of the selected spectrum and is especially useful for improving spectra when random noise obscures the peaks.

The higher the smooth algorithm is applied in a spectrum, the more information can be lost as smoothing also makes sharp bands broader and less intense. Small spectral features can effectively degraded the spectral resolution to a point where the peaks can be completely lost. Even sharp and intense peaks can at high smooth be shifted and melted together with neighbouring bands as can be observed of the pigment barium yellow[5] spectra in *Figure 3.21*.

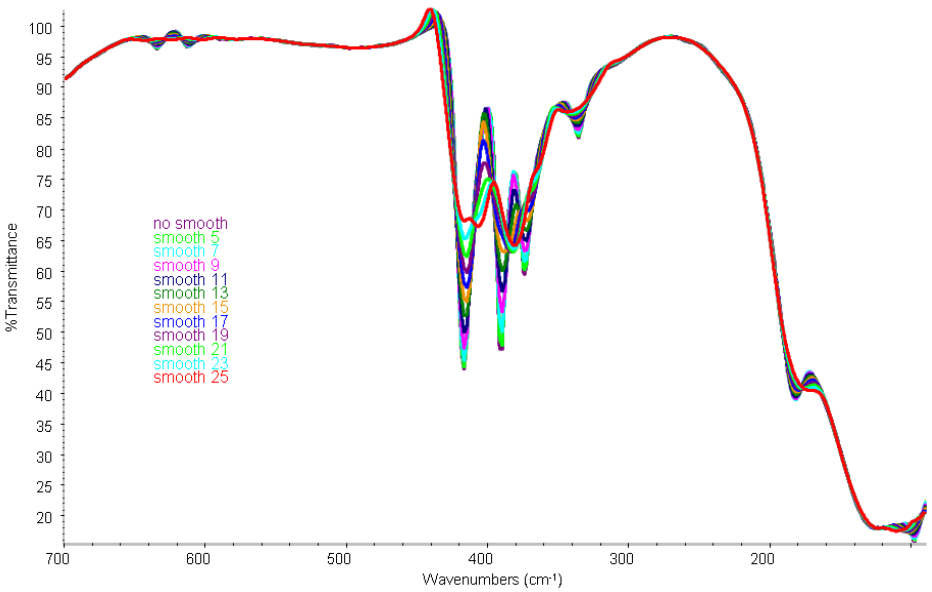

Figure 3.21: Spectrum of Barium Yellow[5] collected in ATR exposed to various smoothing. With high smoothing weak bands degenerate and disappear; Sharp bands lose intensity, they becomes broader, melt together with the neighbouring band and shift wavenumber position.

Normally smooth 5-9 is applied in the FIR region, in the normal IR region smooth 7-13 is applied. Smooth is especially applied when water bands are present in the spectrum or when harmonic noise vibrations disturb the spectrum.

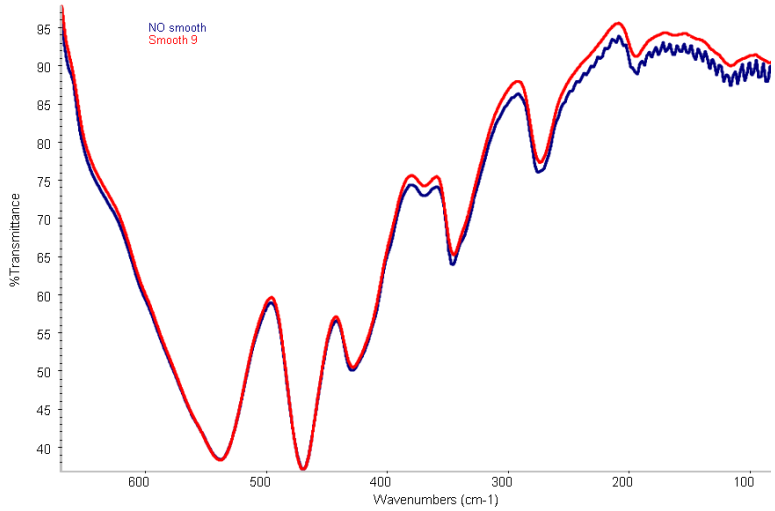

Figure 3.22: Spectrum of Pencil Clay, original (no smoothing) and after smooth 9. The original spectrum clearly show harmonic noise in the lower wavenumber region 250-90 cm^{-1} coming from the GPG, which is evened-out by the smooth 9 Savitzky-Golay algorithm.

Figure 3.22 shows an example of harmonic noise vibration coming from the GPG, which occasionally vibrates in such a way that the vibration interferes with the collection of spectra. This particular vibration was caused by a drilling machine, drilling a hole in a wall close to the IR

instrument. These noise vibrations can sometimes be observed in the lower region of the spectrum at 250-90 cm^{-1}; at other times the harmonic noise vibration is more serious (the source of the vibration is closer and more intense) and can be observed in the entire Far-IR range. Smooth 9 is enough to remove this particular noise observed in *Figure 3.22* from the sample spectrum.

3.4 ATR TRANSFORMATION OF SPECTRA

ATR spectra can be, as explained in the theory section, considerably different from transmission spectra with respect to intensities, band shift and band distortions. These differences are due to difference in the collection technique and prevailing theory. Using both techniques for detecting and identifying unknown pigment samples in the FIR region therefore requires spectral databases of standard pigment collected employing both techniques. Perhaps it would be less time consuming and more convenient to try to correct the ATR spectra to simulate a transmission spectra by using a correction algorithm. One such transformation is the advanced ATR correction algorithm (from Thermo) or to try applying the Kramers-Kronig transformation on the ATR spectra.

Already before attempting these transformations of the spectra scepticism was the prevailing emotion, as the transformation of spectra usually are problematic. The advanced ATR correction is specially designed for ATR spectra to simulate transmission spectrum, while the Kramers-Kronig transformation is designed for reflectance spectra to transform into simulated transmission spectra.

3.4.1 ADVANCED ATR CORRECTIONS

Thermo Scientific in their OMNIC software endeavour to transform ATR spectra into transmission spectra with the use of an advanced correction algorithm [34, 38]. The correction algorithm mainly adjust for the shift towards lower wavenumber by incorporating:

Equation 3.4

$$A = LN\, e\, \frac{n_2 E_0^2 d_p}{n_1 \cos \varphi 2} \alpha$$

Into Harricks *Equation 2.9* [9, 10] mentioned in the previous chapter. The correction algorithm requires four types of input; the refractive index of the sample and the ATR crystal, the angle of incident and the number of bounces in the crystal. We test the advanced ATR correction algorithm on the FIR spectra of the pigment cinnabar (HgS). The refractive index of the ATR diamond is n_{diam}

$= 2.4$, the refractive indexs of the crystalline cinnabar are $n_\omega = 2.905$ *and* $n_\varepsilon = 3.256$ (uniaxal)[6], the angle of incident is 45^o and the number of bounces in the diamond ATR crystal is *1*. Thus armed with these information is should be easy to calculate the advanced ATR correction spectrum and have a spectrum that appear more as a transmission spectrum than an ATR spectrum. But, unfortunately, the Adv. ATR correction requires the refractive index of the sample to be 0.707 times less than that of the ATR crystal. This is a limit in the correction algorithm. As cinnabar has a larger refractive index ($n_\omega = 2.905$ *or* $n_\varepsilon = 3.256$) than the ATR crystal ($n_{diam} = 2.4$). This calculation is thus not possible according to the required input data for performing the calculation. Unless we cheat. We cheat by pretending the refractive index is exactly 0.707 times smaller than the ATR crystal, giving a 'corrected' refractive index for cinnabar which is $n_{cor} = 1.6968$. The result of this cheating 'correction' can be observed in ***Figure 3.23*** together with the original collected ATR spectrum and the original transmission collected spectrum of cinnabar.

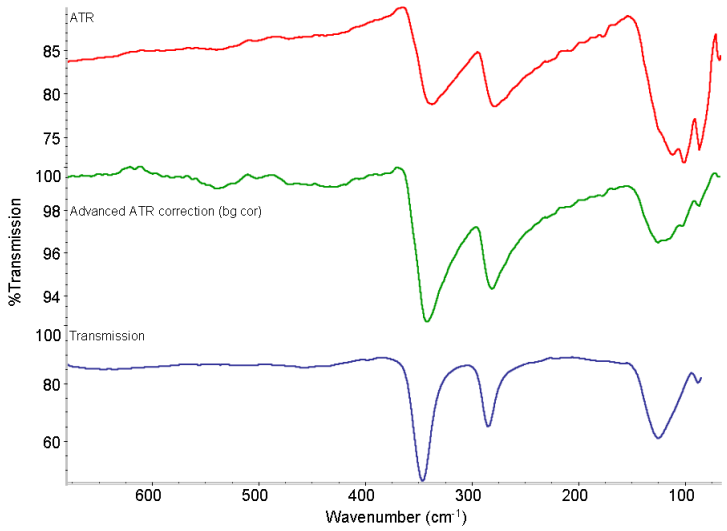

Figure 3.23: FIR spectra of cinnabar (HgS) collected in ATR mode (red) and transformed with the Adv. ATR correction algorithm with $n_{cor} = 1.6968$ (green), compared to transmission spectrum (blue).

The Advanced ATR corrected (cheat) spectrum appears to be a mixed spectrum, having less ATR distortion than the original ATR corrected spectrum, but still more ATR distortion than the original transmission spectrum. The frequency shift however, appears to be somewhat closer to bands in the transmission spectrum than the bands in the ATR spectrum.

[6] Information about refractive index of cinnabar available from Mineral Data's Homepage http://www.mindat.org/min-1052.html

However, this adv. ATR 'corrected' spectrum was achieved by inputting an arbitrary unit (0.707 times less than n_{diam}) and not the actual physical refractive index constant of the pigment. Thus, such correction is not trust worthy, especially as most times you are investigating an unknown sample, whose exact refractive index are unknown. So although the adv. ATR correction reduce the typical ATR spectral distortions, the algorithm behind the correction is adequate.

3.4.2 THE KRAMER-KRONIG TRANSFORMATION ALGORITHM

The Kramer-Kronig transformation algorithm is employed on specular reflectance spectra to get rid of reststrahlen. The Kramer-Kronig transformation will decompose the complex reflectance spectrum into its separate extinction coefficient according to $n^* = n + iK$; one component is the actual absorbance spectrum (K spectrum), and the other is the refractive index spectrum (n spectrum) [50-52]:

Equation 3.5
$$n = \frac{1 - R}{1 + R - 2\sqrt{R}\cos\varphi}$$

Equation 3.6
$$K = \frac{-2\sqrt{R}\sin\varphi}{1 + R - 2\sqrt{R}\cos\varphi}$$

Equation 3.7
$$\text{where } R = \frac{(n-1)^2 + k^2}{(n+1)^2 + k^2}$$

In specular reflectance spectroscopy the refractive index spectrum dominates the appearance of the spectrum, which makes the spectral interpretation difficult [53]. This information can then be used for qualitative evaluation of the sample. The refractive index of a typical medium strong IR absorbing compound tends to change rapidly in regions of strong absorbance [34]. This causes the major absorbance peaks to appear as strong first derivative shaped features in the measured reflectance data.

Figure 3.24 shows the Kramer-Kronig transformation performed on cinnabar (HgS), compared to the original collected ATR and transmission spectrum. Shape wise the bands in the Kramer-Kronig transformed spectrum are much more like the transmission collected spectrum of cinnabar. But the observed band shift has changed more than desired to higher wavenumbers than the actual bands observed in the transmission spectrum. For ATR collected spectra we are employing an incident angle of 45º, which is far away from the typical angles applied in reflectance spectroscopy, which normally uses angles near zero. Thus the Kramer-Kronig separation of the K and n components is overcompensating the n component in the spectrum, thereby resulting in too high

wavenumbers.

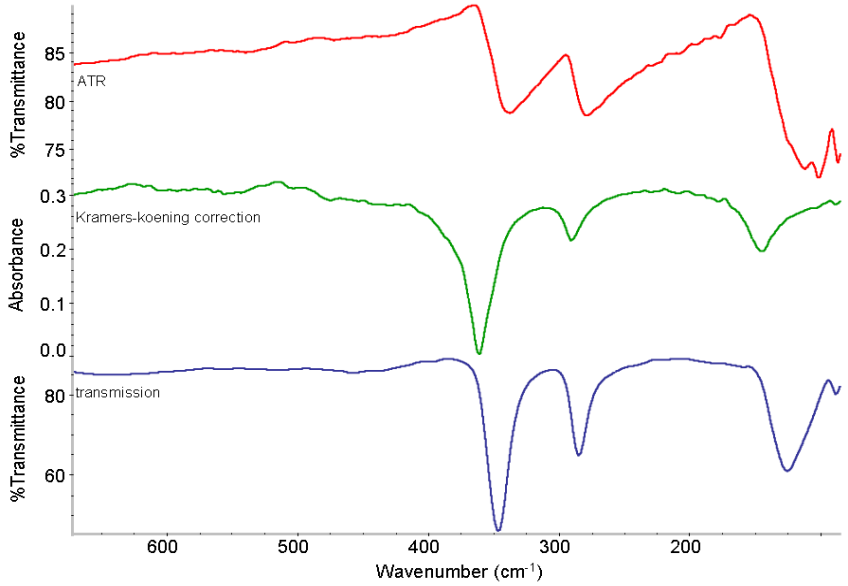

Figure 3.24: FIR spectra of cinnabar (HgS) collected in a ATR mode (red), transformed with the Kramer-Kronig correction (green), and collected in transmission (blue).

Neither the advanced ATR correction from the OMNIC software nor the Kramer-Kronig transformation can thus be applied in the attempt to transform the ATR spectrum of cinnabar to a transmission spectrum. A comparison of wavenumbers between the two transformations can be observed in *Table 3.5*. The advanced ATR 'correction' actually comes very close in achieving the desired wavenumbers of a simulated transmission spectrum, but the input data (the refractive index of cinnabar) necessary for achieving the spectral transformation is not accurate. On the other hand the Kramer-Kronig transformation comes very close in simulating the transmission spectrum, as the main ATR distortion features are gone. But the Kramer-Kronig transformation overcompensate causing an considerable increase in wavenumbers.

Table 3.5: Wavenumber (cm^{-1}) for Cinnabar collected with ATR and transmission spectroscopy, and transformed using the advances ATR correction and the Kramer-Kronig transformation algorithms.

Cinnabar	**Observed bands in the FIR region (cm^{-1})**				
ATR spectroscopy	338	279	112	101	87
Adv. ATR 'correction' algorithm	342	282	121	-	86
Kramer-Kronig transformation	360	290	145	-	-
Transmission spectroscopy	346	284	125	-	88

We are therefore forced to collect our standard pigments in both transmission as well as ATR spectroscopy, if we wish to build a database for comparison with unknown samples using both techniques as means of detection and identification.

CHAPTER 4 SAMPLE PREPARATION FOR FIR SPECTROSCOPY

4.1 PREPARATIONS FOR FIR SPECTROSCOPY

In this chapter we look at the sample preparation necessary for data collection in transmission and reflectance ATR spectroscopy in the FIR region.

In transmission we produce a pellet which must be transparent enough for the IR radiation to pass through. This means temperature and pressure dependence together with the size and thickness of the pellet. If the pellet is too thin we might expect to see artificial bands, i.e. interference fringes. Additionally, the possibility of applying the sample on a thin film is investigated and compared to embedding the sample in an inert material.

For collection in ATR mode no sample preparation should be necessary. Very small sample amounts can be examined by ATR spectroscopy.

4.2 TRANSMISSION SPECTROSCOPY

The first objective when thinking about transmission, is to choose a transparent or inert material in which the sample is embedded or applied onto. Below is listed materials employed as window materials in the instrument when collecting in the FIR region. The most logical choice would be to select one of these compounds as the inert transparent material, onto which our sample is applied or embedded.

Figure 4.1: List of materials used as window material transparent or inert in the FIR region [54].

Material	***Refractive index (n)***	***Transmission (cm^{-1})***
Cadmiun telluride, CdTe	2.65	10,000-350
Cesium bromide, CsBr	1.65	33,000-250
Cesium iodide, CsI	1.72	33,000-150
Crystal quartz, SiO_2	1.5	50,000-3,600; 250-30
Diamond, C	2.4	45,000-2,500; 1,600-50
Polyethylene, HDPE	1.55	600-10
Potassium bromide, KBr	1.52	33,000-400
Potassium chloride, KCl	1.47	33,000-500
Silicon, Si	3.42	10,000-100
Silver bromide, AgBr	2.2	20,000-300
Silver chloride, AgCl	2	23,000-400
Thallium bromoiodide, KRS-5	2.35	16,000-200

However, one of the most important criteria for selecting the material is the region of transparency and a material which is not influenced by a humid atmosphere.

Our solid substrate beamsplitter, which is made of a silicon material, is transparent in the region 700-50 cm^{-1}. Our aim would therefore be to have an embedding medium equally transparent in the same region. At the same time the FIR region can be very sensitive to humidity, as this is the

region where water vapour has its bands, so the next criteria would be to chose a non-hygroscopic material to have minimum interference from water bands. Another obvious criteria is the price of the inert material used.

The materials fitting the transparency criteria from Figure 4.1 are CsBr, CsI, quartz, silicon, high density polyethylene (HDPE) and KRS-5. KRS-5 is dismissed immediately do to its toxicity, and diamond and silicon due to their price. Quartz has broad bands from 3600-250 cm^{-1} but is otherwise transparent from 250-30 cm^{-1}. It could thus in theory be applied in the low FIR region, but not in the entire region where the solid substrate beamsplitter is transparent.

The last options available is CsBr, CsI, and HDPE. Of these options CsBr and CsI is considered to be extremely hygroscopic although literature [14] have applied these materials previously for collection of transmission spectra. They are, however not transparent in the very low FIR region in which the instrument allows us to collect, as can be observed in Figure 4.2.

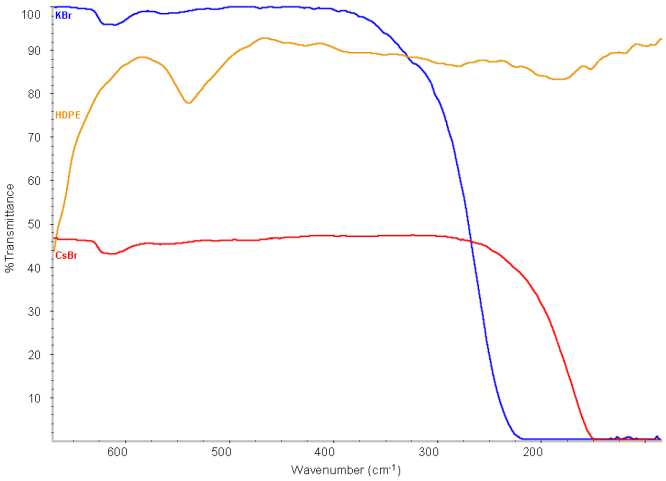

Figure 4.2: Spectra of KBr, CsBr and HDPE collected in transmission in the FIR region.

When in Figure 4.2 collecting spectra of KBr and CsBr pellets and comparing them to the transparency of a HDPE pellet we observe quite clearly that with PE we have the possibility of collecting spectra in the same region in which the beamsplitter is transparent. For KBr and CsBr we observe quite clearly the cut-off of the material, KBr beginning at 380 cm^{-1} and CsBr beginning at 240 cm^{-1}. Also we note that where KBr is close to 100% transparent until cut-off begins, CsBr is only 50% transparent until cut-off begins. PE is around 80-90% transparent in the 600-90 cm^{-1} region. The bands observed in PE at 525 cm^{-1}, and other small bands, are the crystal lattice bands of

PE. These bands can be subtracted by having a blank PE pellet inserted in the pathway of the IR beam when collecting the background.

The PE is not transparent in the normal IR region, as can be seen in Figure 4.3. Here it is observed that PE has many very strong bands in the region 4000-700 cm^{-1}. Any Cultural Heritage sample material investigated by FIR transmission spectroscopy by embedding in PE can thus not be used for investigation in the MIR region.

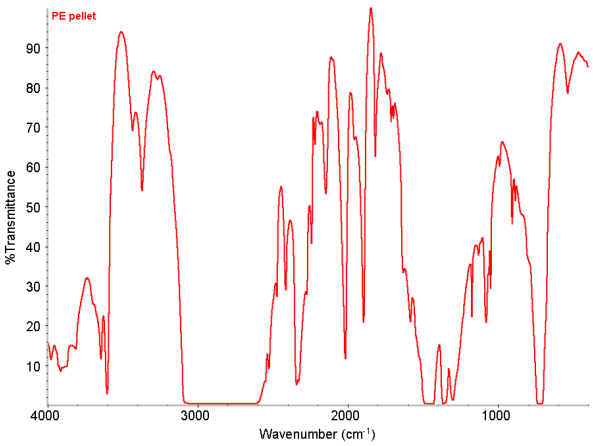

Figure 4.3: Spectrum of a PE pellet collected in the normal IR region 4000-400 cm-1.

Due to the range of transparency and the insensitivity to water vapours, PE is chosen as the material used in FIR transmission spectroscopy, instead of compounds like CsBr and CsI.

4.2.1 POLYETHYLENE (PE) PELLETS

Polyethylene (PE) is a polymerisation of the monomer ethylene (CH_2=CH_2), which opens up the double bond upon polymerisation to $–(CH_2\text{-}CH_2)_n\text{-}$. There are many different types of PE all dependent on the length of the chain (n = number of ethylene units) and the possible branching of a side chain. Each of these possible PE have different density, crystalline structure, molecular weight, glass transition, and melting point.

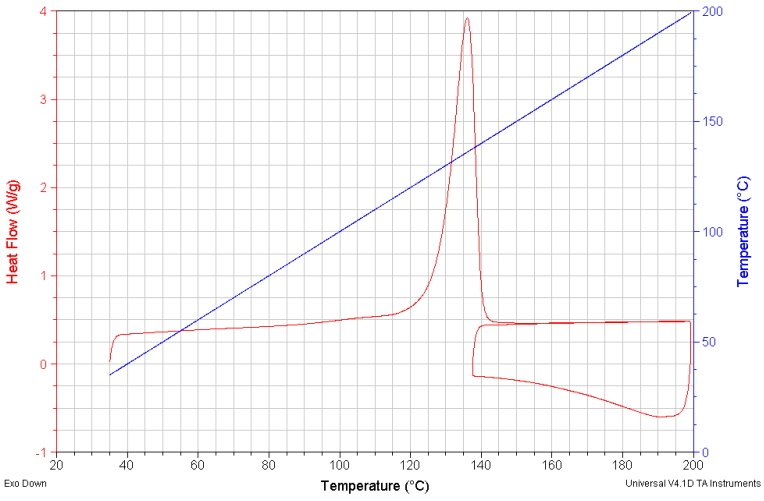

Figure 4.4: DSC of linear HDPE determining the exact melting temperature to be 136 ºC.

The polyethylene we use is a high density linear polyethylene powder, sold under the name of Microthene ® FA 75000 from Quantum Chemical Corporation, Cincinnati OH, USA (CAS nr. 25087-34-7). The supplier reports the melting point to be approximately 125-140ºC. By DSC experiment we determine the exact melting temperature to be 136 ºC.

All experiments in this thesis have been conducted with the same polyethylene and will hence only be mentioned as PE.

4.2.2 PRELIMINARY PE EXPERIMENTS

In the beginning, during the early experiments with the PE pellet, the FIR spectra was not very pretty. There were many harmonic oscillating noise bands known as interference fringes visible in the spectra, which can be seen in Figure 4.5a. Interference fringes are reflections produced at the sample surface which has a wave pattern [27, 55-58].

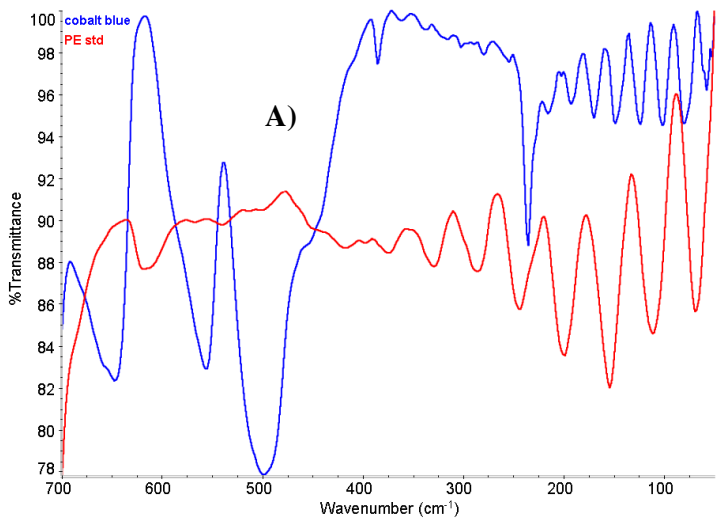

Figure 4.5: FIR spectra of pigment cobalt blue and PE standard A) when the pellets are approximately 280 µm thick; harmonic interference bands are clearly observed in the lower part (below 400 cm^{-1}) of the FIR region and B) when the pellets are 1 mm thick; no harmonic interference bands are observed.

This phenomenon occurs very often with thin pellets but not if the pellets are thicker. In the early experiments the anvil die was not used to standardise the thickness of the pellet. The PE pellet was melted directly on the magnetic hotplate as performed in early literature [59]. This resulted in a very thin PE pellet, in which very often the interference fringes was observed. In later experiments the PE was produced in an anvil die and interference fringes are no longer observed.

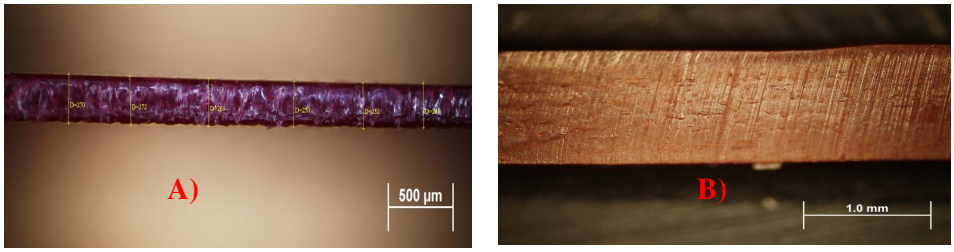

Figure 4.6: Cross-section of PE pellets with embedded std pigments as observed in optical microscope at 50x magnification a) melted directly on the hotplate measuring 280 µm in thickness b) pressured into form in the anvil die measuring 1 mm in thickness.

Figure 4.6a shows the pictures of the cross-section of the PE pellets when first making the PE pellets directly on the hotplate, which gave a pellet thickness of approximately 280 µm. Figure 4.6b shows the cross section of a PE pellet that has a homogeneous thickness all over the cross section of approximately 1,05-1,08 mm. No air bubbles, which could disturb the recording of the FIR spectra and create artificial noise bands in the spectra, are visible in the cross-section of the PE pellet. The harmonic interference fringes seen here are very strong and dominates the entire spectra. In the later spectra in Figure 4.5b collected of PE standard pellet and the pigments cobalt blue produced in the anvil die, no such harmonic oscillation interference bands are observed.

4.2.3 PREPARING THE PE PELLETS

When preparing PE pellets the normal procedure for preparing KBr pellets is followed [6], however with a few modifications.

The minimum amount of PE used in one pellet is 50 mg, which gives the normal standard thickness of approximately 1 mm. Usually a little more PE is used (60-70 mg). The amount of sample embedded is approximately 0,5-1.5 mg dependent on the pigment's covering ability; the stronger the colour the more intense the signal is in FIR spectra and hence less than 1 mg is necessary to record a good FIR spectra.

Figure 4.7: The heating of the Anvil Die on a hotplate of a magnetic stirrer.

The sample is ground in a mortar and mixed thoroughly with the PE powder in the mortar, not with the pestle as the PE powder is electrostatic, but with a spatula. The metallic anvil die accessory (in this case a 13 mm Die from SPECAC, Kent, UK, with maximum load of 10 tons), is used to form the PE pellets. Unlike KBr pellets, the anvil die is heated to 180ºC on a magnetic stirrer with a hotplate for approximately 5-10 min. The temperature of the die surface is expected to be approximately 150-170°C (above the melting temperature of PE, which is 136°C) but due to lack of a proper thermometer capable of

measuring the surface of the die, the actually temperature of the die surface and the hotplate are unknown. Unsuccessful experiment have been conducted with an infrared thermometer employed for surfaces analysis. This IR thermometer measured from 25-250°C on the surface of the heated die, depending on where on the surface you performed the measurements. These heavy fluctuations in the measured temperature lead to the conclusion the IR thermometer was unreliable.

After heating the die, the mixture of PE and sample are quickly added in the die while it is still hot. The die is assembled and put under 5 tons pressure for 3 minutes while the die is under vacuum. Afterwards, the die is disassembled and the resulting opaque (milky white) transparent PE pellet (with embedded sample the PE of cause changes colour) is ready for FIR collection in the 670-90 cm^{-1} region.

The PE pellet, when melted and exposed to pressure, has been formed into a hard plastic pellet. It can be investigated spectroscopically immediately or at a later date, it is of no importance, as the PE is insensitive to water vapours and can be stored indefinitely for later FIR collection. All samples and standards embedded in PE made in this laboratory has been stored for future reference.

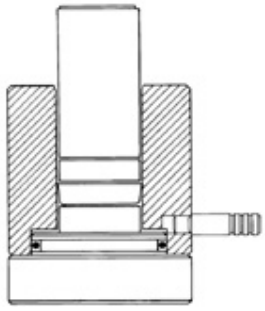

Figure 4.8: Drawing of a standard anvil die used for making the PE pellet.

Obviously the anvil die, though made of metals, has problems being heated to this high temperatures in the long run. Two problems must be mentioned. The first is the rubber rings in the die, they are usually the first to become degraded (brittle) and must be exchange on a regular yearly basis. The second is the glue keeping the vacuum evacuation nose firmly in the die, this must be replaced often, as most glues are not heat resistant. At the moment we are testing Teflon tape which hopefully will prove more heat resistant than glue.

The hot die is handled using heat resistant gloves and a pair of tongs.

Figure 4.9: Various sizes of O-rings employed as sample forms with inner diameter of 8, 10 and 13 mm and 1 mm thickness purchased from a everyday ironmonger shop.

An old anvil die has been used, which is missing the lower stopper, thus making it difficult to form the pellet to a specific thickness and size. Instead a flat metallic O-ring is placed in the bottom of the die to form the pellet. Preliminary test was performed on O-ring forms with an inner diameter

of 8, 10 and 13 mm and with a thickness of 1-1.5 mm. The smallest diameter form was favoured in order to minimise the amount of sample necessary, since often the amount of sample available in cultural heritage objects is very small.

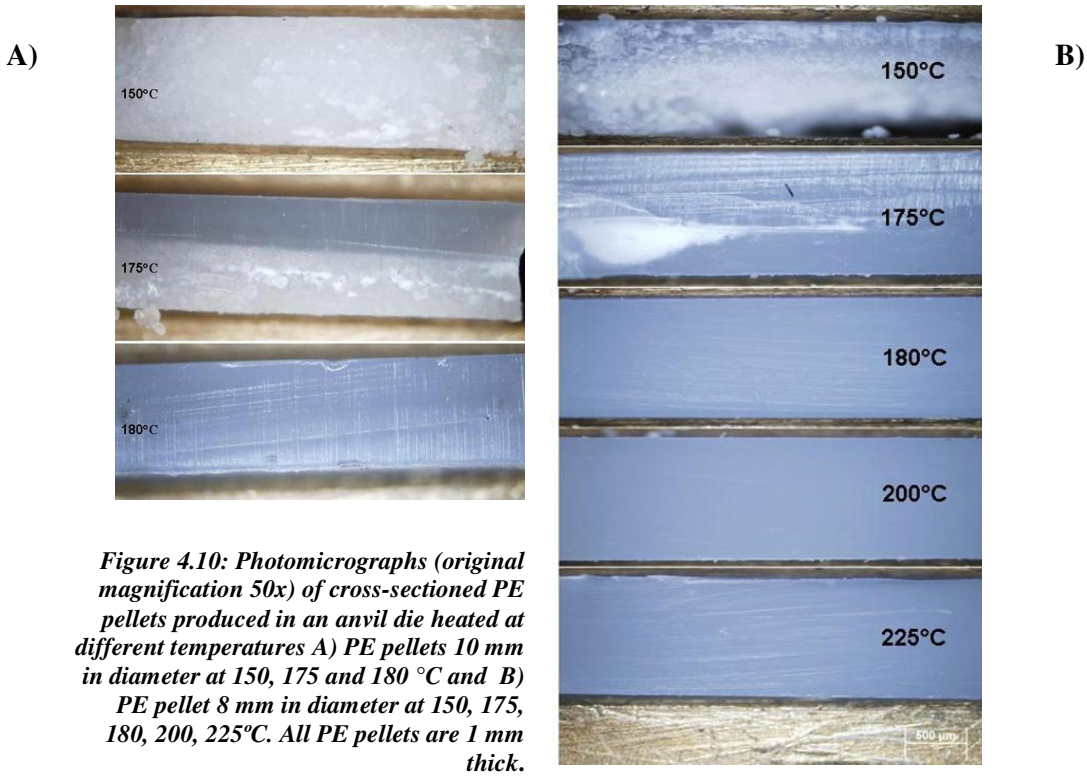

Figure 4.10: Photomicrographs (original magnification 50x) of cross-sectioned PE pellets produced in an anvil die heated at different temperatures A) PE pellets 10 mm in diameter at 150, 175 and 180 °C and B) PE pellet 8 mm in diameter at 150, 175, 180, 200, 225ºC. All PE pellets are 1 mm thick.

Figure 4.7 shows cross-sections of PE pellets pressed into O-ring shape with the heated anvil die. The temperature mentioned here is the temperature settings of the hotplate and not a measured temperature. For the 10 mm O-ring cross-sections of PE pellets produced by heating the hotplate to 150, 175 and 180°C respectively are show and for the 8 mm O-ring cross-sections of PE pellets produced at 150, 175, 180, 200, 225ºC is shown. For both PE pellet (with diameter 8 and 10 mm) it is observed at 150°C that the PE is not melted to the desired transparent pellet; at 175°C the pellet is becoming semitransparent or almost transparent. Only when the anvil die is heated to 180°C or higher on the hotplate, the produced PE pellet is fully homogeneous and transparent as can be seen in Figure 4.10.

For the PE pellet produced at 150°C the FIR spectra is NOT transparent and thus we would not be able to observe any components embedded in the PE. For the PE pellets produced at 175°C or higher temperatures, the PE pellets are transparent to the IR beam and thus we would observe a sample embedded in the PE matrix.

It is expected that some sample compounds could be heat sensitive, therefore it is preferred to keep the production temperature down to a minimum, in order not to induce any structural changes in the components. However, at the same time it is preferred to have as visually a transparent pellet as possible to prevent any possible artefact bands appearing in the spectrum. The preferred PE production temperature for the hotplate is thus set to 180°C and the preferred inner diameter of the O-ring is 8 mm.

4.2.3.1 BACKGROUND SUBTRACTION OF BLANC PE PELLETS

An important thing to mention is the fact that in MIR transmission it is normal standard procedure, when collecting the background, to have nothing inserted in the beam path [39]. This is because of the KBr material, with which is difficult to achieve identical transparency and thickness to that of the sample pellet. When subtracting the background (with a blank pellet) from the sample pellet you could thus occasionally observe strange baseline or bands due to either difference in thickness between the blank and the sample pellet or due to water bonded to the KBr, which was not completely subtracted because a different amount of water was present in the sample pellet compared to that of the blank pellet. The standard way of collecting is therefore without anything in the pathway (except atmospheric gaseous molecules which are unavoidable).

This was originally also the way our standard collection for FIR transmission was to be carried out. However, very quickly this procedure encountered a technical problem. When working in the FIR region the amount of infrared radiation required is higher than the energy required to work in the MIR region. For this reason we also insert a Carbon black filter in the pathway of the beam (just before the detector) in order to prevent overloading the detector. Once the detector is overloaded it shuts down and makes data collection impossible. This was exactly what happened the first time we tried to collect a spectrum of the background without the blank PE pellet inserted. The detector overloaded, shut down all collection and restart of the spectrometer is required. To avoid this, it is therefore necessary in FIR transmission spectroscopy to insert a blank PE pellet when subtracting the background from the sample pellet. This is different from accepted MIR transmission theory.

A small experiment with different blanc PE pellet is carried out in Figure 4.11. Firstly, to observe the differences in background with different thickness of the PE pellets. At approximately 620 cm^{-1} we notice a clear decrease of transparency caused by the appearance of a PE band at 710 cm^{-1} (outside the region). We clearly observe differences in the baseline of the PE pellets but no strange peaks appear despite the difference in thickness varying from 1.05-1.45 mm.

Table 4.1: PE pellets produced and their thcikness. The PE pellets are 8 mm in diameter.

PE Pellet	Production Date	Thickness (mm)	Order of transparency PE	Order of transparency PE + malachite
1	030308	1.45	6	3
2	270508	1.05	5	4
3	130109	1.45	**8**	**8**
4	190109	1.35	7	6
5	050209	1.40	4	7
6	060209	1.30	1	5
7	220509	1.30	2	1
8	080609	1.05	3	2
Malachite		1.25		

Where 1 is the highest order and 8 the lowers order of transparency

The difference in thickness is greatly dependant on how many times the metal form for producing the PE pellet has been used previously to make pellets. When the form has not been used previously, the PE pellets are usually 1.45-1.30 mm in thickness (and 8 mm in diameter). While, if the metal form has been used before, the thickness of the pellets are less, around 1.25-1.05 mm. This is of cause due to the 5 ton pressure applied on the forms during the making of the PE pellets, causing the forms to be slightly thinner than originally. The pellets 6, 7 and 8 are the most transparent, while the PE pellet number 3 is the least transparent.

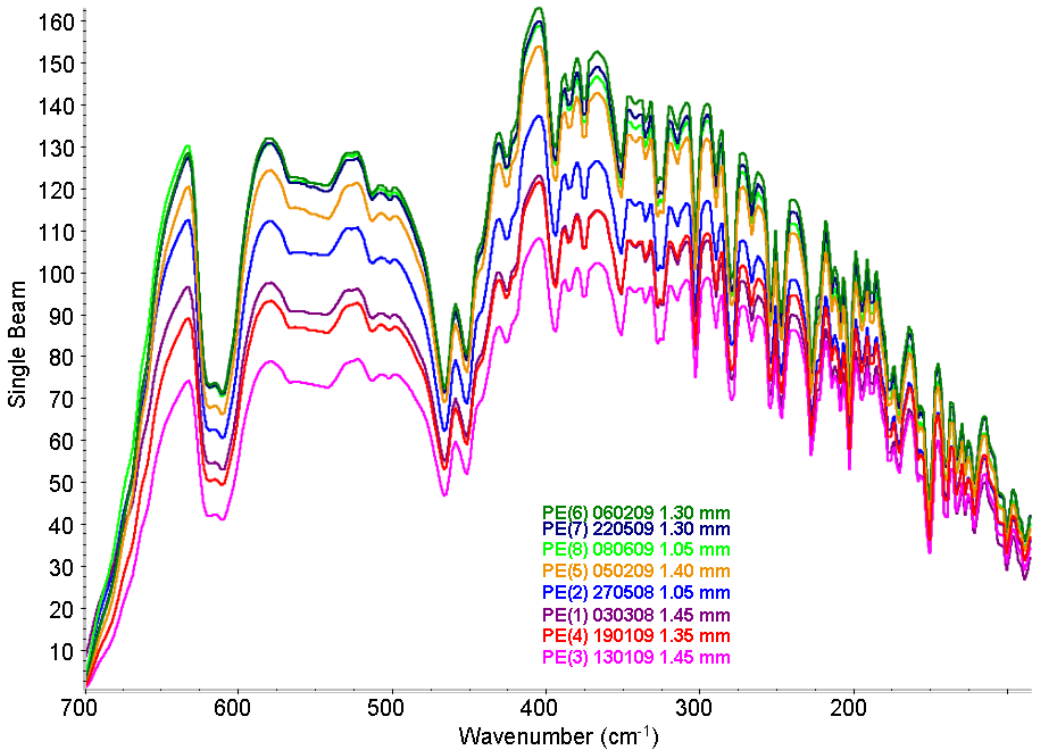

Figure 4.11: Background FIR spectra of the various PE pellet with different thickness.

One std. sample of malachite with a pellet thickness of 1.25 mm, has been subtracted with the 8 different PE pellets mentioned above inserted during background collection. This is performed to investigate the transparency and to see the effect in the spectra on the baseline and the appearance of any artefact bands, which can be seen in *Figure 4.12*. In the region from 600-90 cm^{-1} we observe only the difference in baseline i.e. transparency, between the different PE backgrounds. In the region 700-600 cm^{-1} we quite clearly observe differences and thus this region must be considered carefully. We notice a small band around 621 cm^{-1} which must be considered an artefact band. This band is occasionally observed during normal collection but it is not always present. The broad band appearing at 670 cm^{-1} in some but not all spectra is also an artefact caused by subtraction. This is considered the turning point where either to much or to little is subtracted with regards to the PE background and thus the region 700-670 cm^{-1} is not considered to be reliable in transmission. Normally the FIR region is thus cut off at 670 cm^{-1} in transmission because that is when interferance from PE bands are observed making problems with interpretation of the spectra.

However, some chemical compounds have strong bands in the region 670-600 cm^{-1} and therefore we keep this region when collecting FIR spectra in transmission, but interpretation of bands must be performed with caution and always remembering the artefact band at 621 cm^{-1}. Weak bands in this region are not expected to be free of PE subtraction artefact bands. The PE pellet No. 3 is not only the least transparent pellet but also the one giving the least transmittance of malachite as observed in *Figure 4.12*.

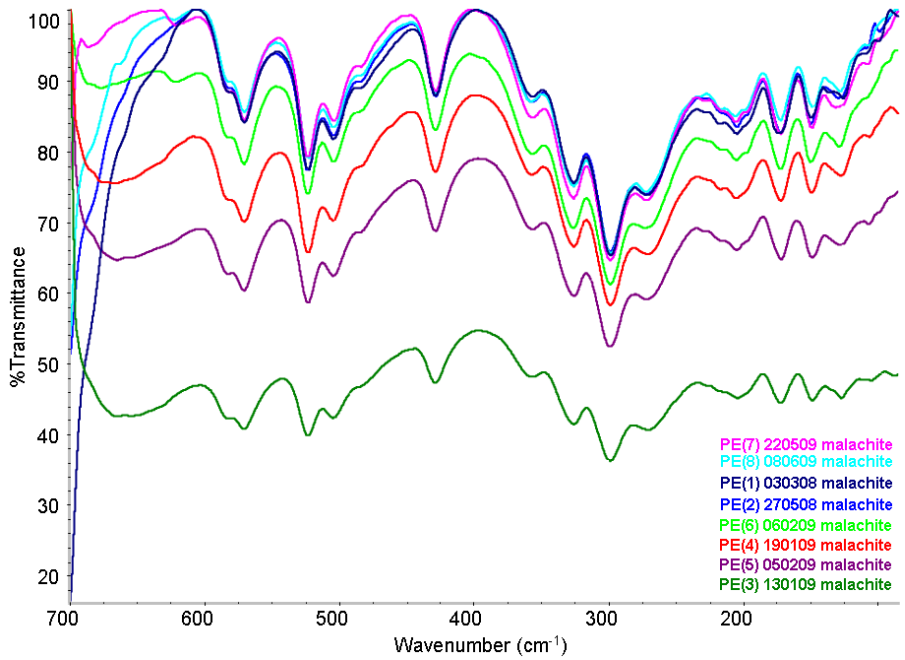

Figure 4.12: FIR spectra of malachite subtracted 8 different PE pellet backgrounds.

4.2.4 PE THIN FILMS

PE thin films are another option for spectral collection in transmission. The main advantage is no heat exposure of the sample, as the case is when embedding the sample in a PE pellet produced at 180 ºC. Also, the ease of use is a main advantage as the sample powder is gently brushed on the PE thin film (PETF). Main disadvantage is the PETF's are extreme sensitivity to water vapours and the high price of the commercially available PETF. The high price of the PETFs can be reduced drastically by producing your own PETF in the laboratory. The main advantage of this, besides the reduced cost, is that they are recyclable.

4.2.4.1 COMMERCIALLY AVAILABLE PE THIN FILMS

Preliminary test of PETF's in the FIR region gives good spectral results. The powder is applied to the PETF with a brush or it can be applied by adding a drop of organic solvent to the sample and then applying the solution to the PETF. The solvent must be allowed to evaporate before collecting spectra. In our case we only mainly apply samples without any solvent as there appears to be no problem with this. The powder must, however, be very fine or it will simply fall off the thin film when the thin film is inserted horizontally into the sample holder in the sample chamber. When the sample is a mixture of powder pigment and binding media, it is not possible to simply brush on the PETF, here an inert solvent is necessary.

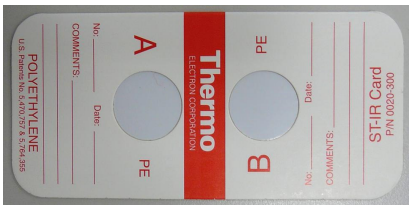

Figure 4.13: Picture of the PE thin film from Thermo Electron Corporation with two circular areas (21 mm diameter) for sample application.

The PETF is sold from Thermo Electron Corporation as a quick application method for MIR transmission spectroscopy[7]. The application is quick (since there is no sample pre-treatment) but the spectra achieved so far in the MIR region are not very pretty. Despite changing the mirror velocity and the gain setting the PE is too thin and the spectra are mainly dominated by interference fringes as can be observed in Figure 4.14 on a powder sample of milori blue standard pigment. Changing the settings in the experimental set-up cannot alter the presence of the interference fringes as they are a product due to reflection off the surface of the PETF. They are not a product of the instrumental set-up.

Interference fringes can be removed by mathematical methods [27, 55, 56], however, these calculations are not always reliable, they are usually very time consuming and in the end the time is usually better spent making a transmission spectrum in the MIR region by embedding the sample in

[7] Mentioned in the adjoining brochure for the ST-IR Card type 1, PE (code 0020-30).

KBr as described in the literature [6]. If necessary, the interference fringes can be manually removed by changing the surface of the PETF. By polishing the surface with some sandpaper or silicon-carbon cards (before you apply the sample) you change the reflection off the PETF and thereby you can reduce the interference fringes visible in the spectrum to an acceptable or non-existing level.

The spectrum of powdery Milori blue pigment standard collected in both FIR and MIR transmission on a PETF can be seen in Figure 4.14. For collection in MIR transmission we observe the appearance of intense interference fringes plus bands from the PETF itself. However, in FIR transmission we observe a very nice spectrum completely without the appearance of interference fringes. This is typical of this particular commercial PETF, the interference fringes are normally only visible in the MIR region, not in the FIR region.

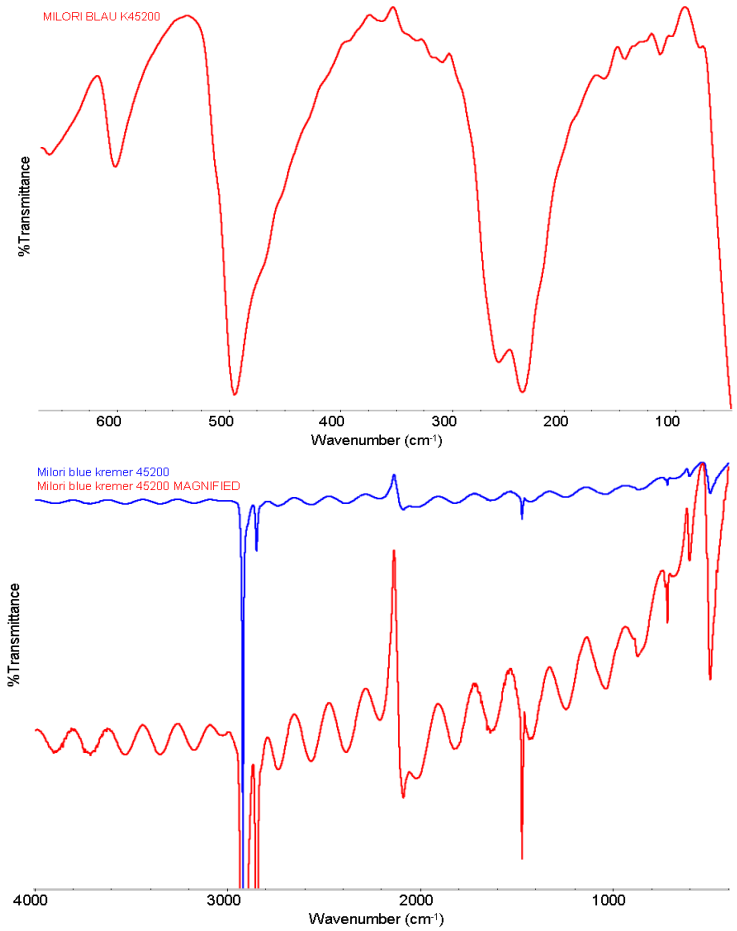

Figure 4.14: FIR and MIR transmission spectrum of Milori Blue collected on PE thin film.

The PETF seem also to be a lot more sensitive to ambient water vapour than the thicker PE pellets used for FIR transmission. It is therefore necessary to be very attentive to the humidity of the spectrometer as well as the laboratory when working with PETF.

After preliminary investigations of PETFs we must conclude that it can be used for recording spectra of a fine powder samples in the FIR region and not as the producer claim in the MIR region. The sample preparation time is short as we only require the sample to be a fine powder before applying it on the PETF with a brush. As the PETF is very thin (0.01 mm) the IR radiant energy required to traverse trough the thin film and the sample on the surface is less than by normal thick pellet transmission. We therefore have to lower the energy gain settings and change the mirror velocity to 0,9494 cm/s in order not to overload the detector when collecting these thin films in the FIR region.

4.2.4.2 LABORATORY-MADE PE THIN FILMS

When heating the magnetic hotplate to temperatures above 200°C it becomes increasingly difficult to produce homogeneous PE pellets. Probably a more reliable heat source than a normal hotplate is required for these higher temperatures. However, with a little patience we succeed in making a few thin PE pellets, which are more transparent to the naked eye, than the standard semitransparent PE pellets. The difference can be seen in Figure 4.15a. A higher temperature and a higher pressure are needed to make the laboratory-made PE thin films.

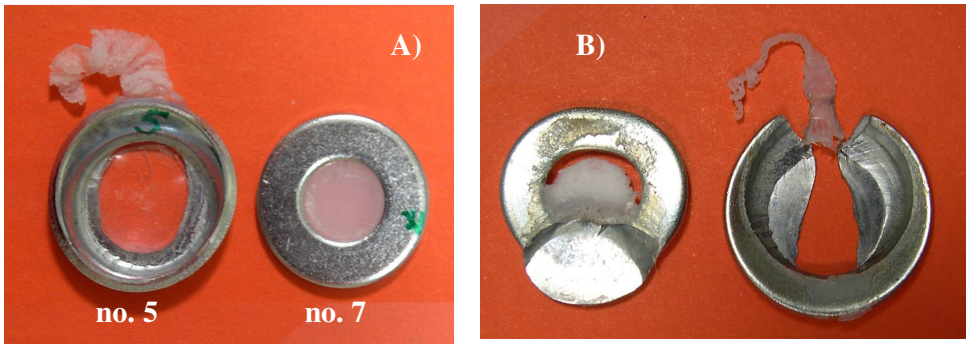

Figure 4.15: Photographs of A) transparent (no. 5) with surplus PE in shape of a tail and semitransparent 'milky white' (no.7) PE pellets, and B) failed pellet forming attempts (both after heating to 275C with 8 tons pressure for 2 min), non-melted PE and PE trust out of form with only PE tail visible.

The biggest problem encountered is the actual forms in which the PE pellets are cast. Occasionally they break due to the high temperature and/or pressure. Under high temperature the forms containing the PE powder seem to either spontaneous break during application of pressure or move around inside the anvil die, which causes the PE pellet to get an uneven distribution of pressure. This results in the failing of the PE to become plasticised as can be seen in Figure 4.15b. Also, the PE can be trust out of the form, when the form breaks, leaving the PE outside the form in

the anvil die, plasticised but not usable for application of samples (i.e. see the PE tail trust out of the broken O-ring in Figure 4.15b, no PE inside the ring).

It is thus necessary to keep temperature and/or pressure down in order to have an even homogeneous PE pellet formed. Table 4.2 shows the attempt to make 10 completely transparent PE thin films. Not all 10 pellets were completely transparent nor where they all thin films. They are all thicker than the commercial PETF. They have all succeeded in becoming homogeneous transparent or semitransparent after applying heat and pressure to form the plastic pellet. The semitransparent pellets has the same visual appearance as the PE pellets produced at 180ºC used for embedding sample. However, the thickness of the pellets are not homogeneous, the three visually most transparent pellets (no. 3, 5 and 8) are 0.75-0.35 mm thick, while the four semitransparent pellets (no. 6, 7, 9 and 10) are between 1.10-1.50 mm thick.

Table 4.2: Transparency of PE pellets at various temperature.

Number	Temp (°C)	Pressure (tons/2min)	Visual transparency	Thickness of pellets (mm)
1	225	8	Yes, but with some milky white spots	0.55
2	225	8	Yes, but with some milky white spots	0.40
3	225	8	Yes	0.75
4	225	8	Yes, but with air pockets	0.35
5	225	8	yes	0.35
6	225	8	Milky white	1.10
7	250	6	Milky white	1.35
8	250	8	Yes	0.35
9	300	5	Milky white	1.45
10	300	6	Milky white	1.50

Not only visual differences are observed of the PE thin films made under same conditions (i.e. hotplate heated to 225ºC and 8 tons pressure) between the transparent and semitransparent PE pellet, but also a spectroscopic difference is observed between the two plastic states, semitransparent and transparent as can be observed in Figure 4.16 of PE thin films number 5 and 6 compared to a normal PE standard pellet (produced at 180ºC and 5 tons pressure).

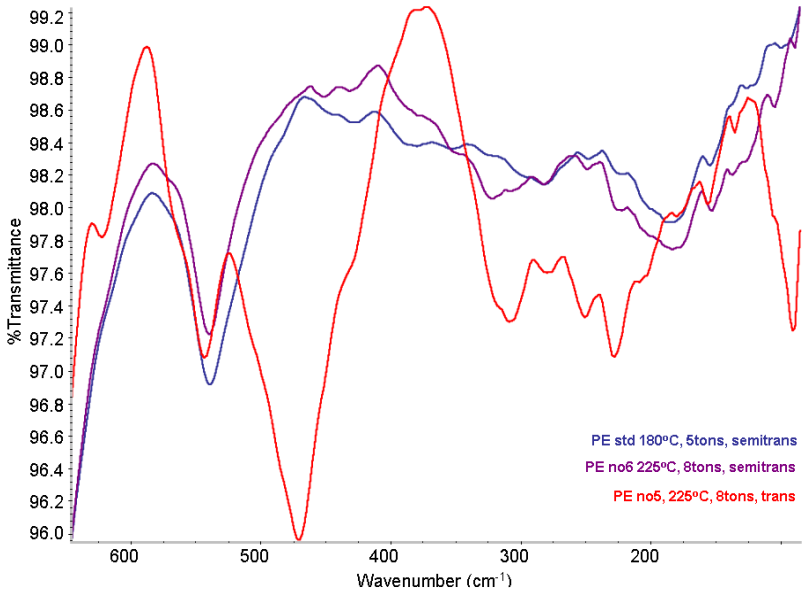

Figure 4.16: FIR spectra of PE pellet formed at various temperature and pressure. The two semitransparent PE pellets formed at 180ºC, 3 tons (std PE) and 225ºC, 8 tons (PE thin film no 6), respectively and the complete transparent PE thin film no 5 formed at 225ºC, 8 tons.

It is clearly observed that PE thin films 5 and 6, made under similar temperature and pressure conditions, but where one is semitransparent the other completely transparent, has two different plasticised phases. The spectrum of the completely transparent PE thin film no 5 has shift of bands and the appearance of other before not observed bands (most prominent the band at 469 cm^{-1}), when comparing it to spectra of the standard PE pellet or the semitransparent PETF no 6. These differences are also observed for the two other completely transparent film no 3 and 8, but the observations are most prominent for film no 5.

It is concluded firstly, that the hotplate is not stable enough at high temperatures to continuously produce the same quality PE thin film and second, that we probably have reached a temperature region where different transition phases of the PE plastic are formed. A phase transition diagram is described in the literature for ultra high molecular weigh PE (UHMWPE), which at low temperature and pressure has orthorhombic structure, while at higher temperature and higher pressure it has hexagonal structure along the chain length [60-62].

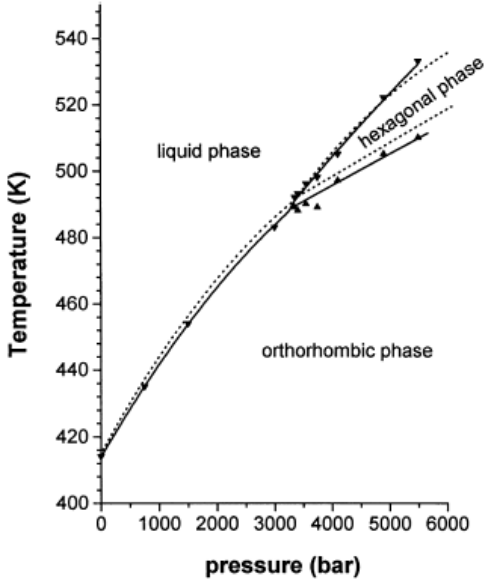

Figure 4.17: Phase diagram for UHMWPE. Reprinted from [60].

A phase transition state of our PE in two different structures is probably also what we observe in the FIR

spectra, as in this region we observe the crystal lattice vibrations. While the internal vibration of the molecule (visible in the MIR region) would show no significant difference. This is confirmed by MIR spectra of the same two PE thin film no 5 and 6, where no significant differences are observed in band shape or band shifts. Band intensities are very difficult to compare as the intensities in the MIR region are very very strong, as was already shown in *Figure 4.3*.

When collecting spectra of all laboratory made PETF's we observe that they are all transparent to the IR beam. However they are not all equally transparent, the semitransparent pellets are less transparent to the IR beam than the completely clear transparent PE pellet. The IR spectroscopic investigation thus confirms the visual impression of the PE pellets.

Spectra of Egyptian blue collected using a transparent (no. 5) and a semitransparent (no. 6) PETF as substrate can be observed in Figure 4.18. The difference observed is not in bands shift but in the shape of the bands. We observe in Egyptian blue on semitransparent PETF no 6 a tendency for asymmetric band shapes not unlike the asymmetric shapes observed in ATR spectroscopy. Also note the difference in band intensity of Egyptian blue below 200 cm^{-1} between the two PETF's. This tendency of semitransparent PE pellet to create asymmetric band shape and different intensity can cause problems in interpreting the spectra, and thus it is by far preferable that the PETF's are completely transparent and not milky white in appearance. The three PE pellets no 3, 5 and 8 are therefore selected for use as substrate for thin film transmission investigations.

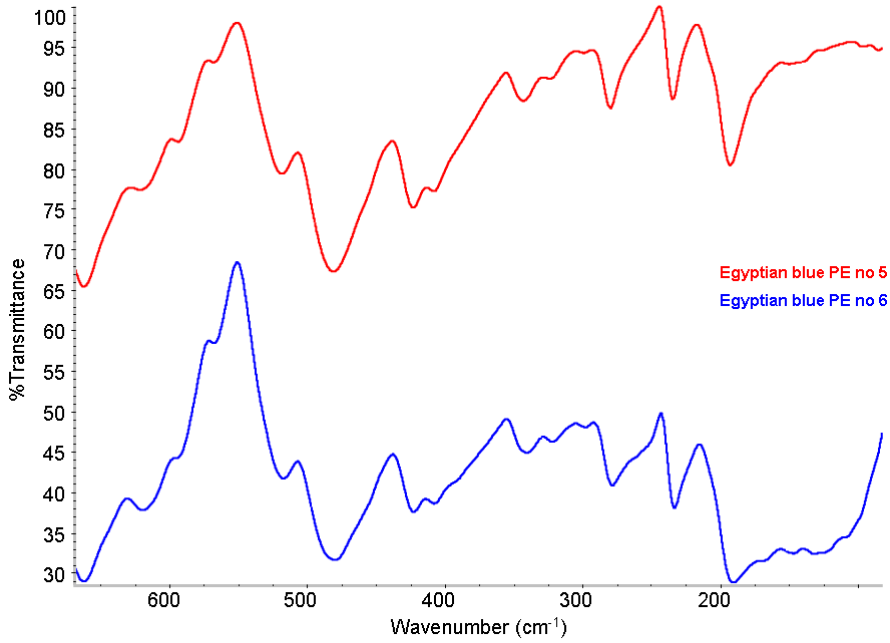

Figure 4.18: FIR spectra of Egyptian blue (pigment from W.G.Ball, APR no 6295) collected on laboratory-made PE thin film, no. 5 (red) and no. 6 (blue), respectively.

The thin films can be recycled repeatedly if they are cleaned properly after use. The pellet is first cleaned with a dry bush to remove as much powder as possible, then the pellet is cleaned with water with a wet brush and quickly dried in paper. If need be ethanol or ethanol-water solution can be applied for cleaning.

Care must be taken that the pellet does not have time to soak up the water (or the ethanol), because the pellet can contain liquid inside and this will show up in the spectrum. In fact if you wish to collect spectrum of a liquid component you can either brush the pellet surface with the liquid or leave the pellet 30-90 seconds in the liquid, after which you can collect the spectrum of the liquid (naturally first after having collected the background spectrum of the pellet without the liquid). The time necessary for the pellet to soak up the liquid depends on the thickness of the pellet. Ultrasonic bath can speed up the procedure. The PE pellets with liquid are left to evaporate either naturally or a bit more speedily in a oven at 60 degrees after which the pellet can be re-used as substrate for another sample.

4.2.5 COMPARISON

In theory, when we collect in transmission mode, whether embedding the sample in PE or applying the sample on the surface of a thin film, we should observe the same bands with the same intensity. In practice, this is not the case. Figure 4.19 show the FIR spectra of lead tin yellow (pigment from W. G. Ball, APR no. 6290) collected in transmission embedded in PE (red spectrum) and applied on a PETF (lab-made no. 3, blue spectrum). We observe almost the same bands, small shift are seen, but we also quite clearly detect differences in relative intensity between the two collection methods, note in particular the bands at 460 and 320 cm^{-1}, they have changed intensity. Also we notice the appearance of some weak bands in the sample spectra applied on PETF3. These weak bands do not originate from water vapour.

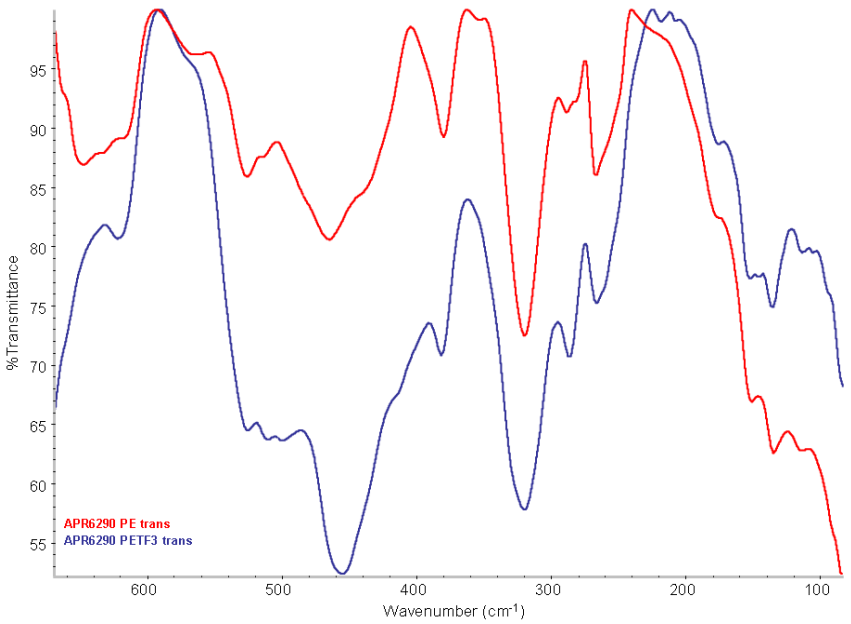

PE trans (cm^{-1})	PETF (3) trans (cm^{-1})
648	-
631	-
617	***622**
563	-
526	**525**
512	**510**
-	500
465	**456**
438	-
380	**382**
319	**320**
287	**289**
267	**267**
-	217
176	**175**
150	**152**
-	145
135	**136**
113	**112**

Figure 4.19: FIR spectra of lead tin yellow (APR6290, from W.G ball Ltd.) collected in transmission embedded in PE (red) and applied on a PETF, lab-made no. 3 (blue), together with a list of bands (bold marks the bands in common), * signifies artefact band.

These differences observed can be caused by differences in particle size and the distribution of the sample. We know from the literature, that bands become slimmer when smaller particles sizes are investigated by infrared spectroscopy [63, 64]. When the powder is brushed on to the PETF, it is of varying particle sizes, but as soon as the PETF is inserted vertically into the sample chamber the larger particle sizes falls off. This is quite evident when looking at the floor of the sample chamber. We can thus imagine that only the smallest particle sizes remains on the surface of the PETF, while when embedding in PE, the ground powder consist of heterogeneous particle sizes distributed throughout the thickness of the PE. These two differences are very likely explaining the reasons for observing intensity differences and small shift in the two transmission FIR spectra.

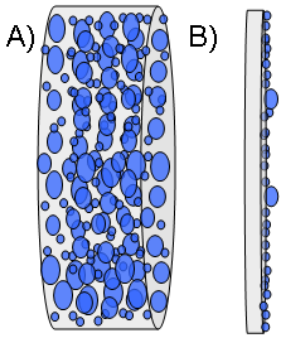

Figure 4.20: A) multilayer distribution of heterogeneous particles in all the PE and B) 1-layer distribution of homogeneous size particles on PETF

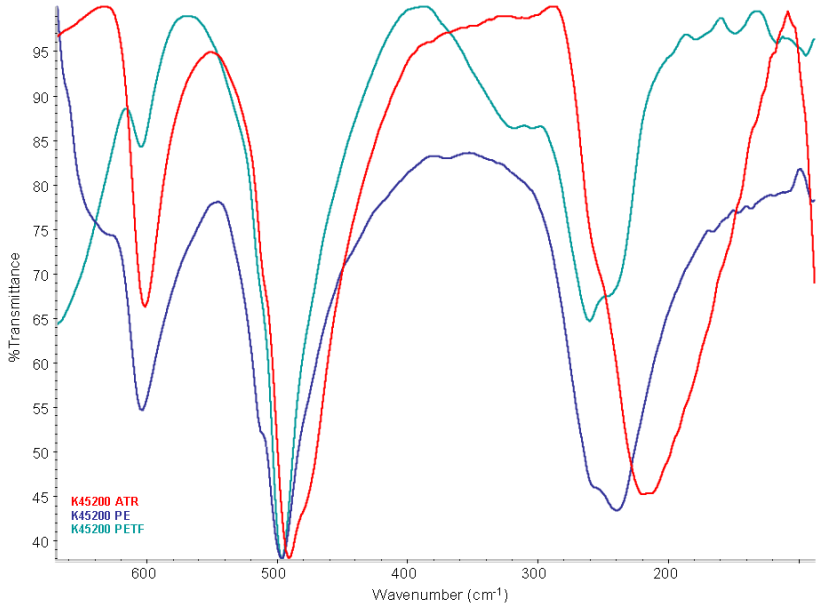

Figure 4.21: FIR spectra of Milori blue (from Kremer Pigmente no 45200) collected in ATR (red), and in transmission on a PE thin film (green) and embedded in PE (blue).

The same differences are observed in milori blue (Kremer Pigmente no 45200). Differences in intensity, small shift of bands and in the PETF (commercial) weak bands appear on the baseline. However, the observed differences between PETF and PE spectra are small when comparing them to milori blue FIR spectrum collected in ATR mode. Here, the disparities observed are not due to particle size but due to the difference in collection method as explained in chapter 2.

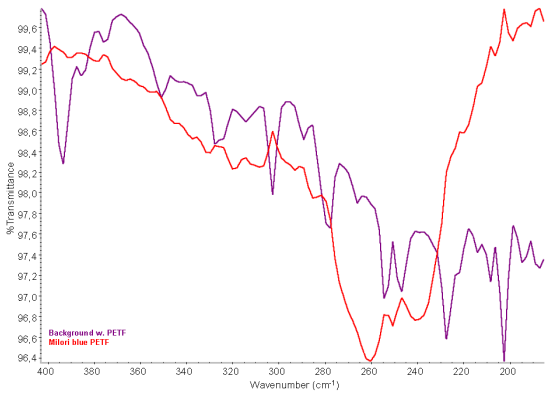

Figure 4.22: FIR spectra of Milori blue collected on PETF compared to the background with PETF inserted in the pathway in the 400-200 cm^{-1} region. We observe quite clearly water vapour bands present. No smoothing has been performed.

When using PETF we do notice that very often weak band appears on the baseline whether the PETF is commercial or lab-made. These small bands can originate from water vapour present in the sample compartment when collecting the spectrum. This can be confirmed in Figure 4.22 where we observe another spectrum of milori blue in the region 400-200 cm^{-1} shown together with the background spectrum. In the background spectrum water vapour bands are observed clearly. The same bands appear as maxima (or reverse) bands in the milori spectrum. It can be very difficult to remove these weak water vapour band from the spectrum even by smoothing the spectrum. After smoothing the small water vapour bands have also been smoothed out and since the water vapour

bands are reversed the wavenumbers are not recognisable with those of water vapour bands observed in Figure 4.22.

This is a common problem with the thin films. The are generally very sensitive to water vapours. Mistakes in interpretation of these weak band can easily occur and therefore interpretation must be performed with extreme caution always comparing to the water vapour bands in the background spectrum.

4.2.6 OTHER OPTIONS FOR COLLECTION IN FIR TRANSMISSION

There are other ways of preparing a sample for FIR transmission spectroscopy. One of these methods is to lower the melting point temperature of the PE by adding another substance with lower melting point. In literature it is suggested to add wax to the PE [47]. The general chemical formula of wax is C_nH_{2n+2}. It is a aliphatic hydrocarbon whose melting point temperature differs with varying chain length, branching and molecular weight. Two of the most known waxes are paraffin wax ($20 \leq n \leq 40$), which is an unbranched aliphatic hydrocarbon with low melting point temperature (47-92°C), and microcrystalline wax, which is a high molecular branched hydrocarbon with slightly higher melting point temperature (80-100°C) than paraffin.

The addition of another substance with a lower melting point than PE will act as an impurity in the PE. This will lower the overall melting point temperature needed for the mixture of sample, PE and wax. If a sample is heat sensitive this could be an excellent solution for transmission spectroscopy. Waxes do have vibrations in the FIR region but if strong absorbing bands are present they are usually very sharp (this is often observed in organic compounds). Most organic bands however, have weak intensity in this region. Regrettably, there has not been enough time to perform experiments with various types of wax mixed with PE.

In the literature another option is presented as the cold pressed PE pellet [65]. This particular linear PE requires no heating to be transparent for the IR beam. The pellet is thinner than our pellet and longer pressure time is required. The boiling point is reported as 50-70°C, and the optimum transparency is achieved by collecting spectra in cold surroundings, at -50 – 0°C [65] (this is unfortunately not possible with our detector type). It has not been possible to find any further information about this particular PE. But employing a cold pressed PE would solve the problem of exposing a low melting point sample to heat during production of the PE pellet preventing possible structural changes.

If very little sample is available, the option of using a beam condenser is available. The beam condenser focuses the beam on a much smaller area than with normal transmission spectroscopy,

thus making it possible to use much smaller pellets. The beam condenser is a late addition to our M2ADL laboratory and therefore only preliminary experiments have been completed. The minimum amount of sample and PE required, when using the beam condenser, has not yet been determined. Preliminary experiments have been focussing on collecting spectra of already existing samples in PE pellets and comparing them to normal transmission collection. These experiments are explained in chapter 6.

4.3 REFLECTION ATR SPECTROSCOPY

The general idea of using ATR spectroscopy is that no sample preparation is necessary, the actual sample is either investigated directly on the ATR crystal, or particles from the sample are removed from the object and then investigated on the ATR crystal. No embedding is necessary nor is any thin film required for collecting a spectrum. The ATR crystal, however, need good contact in order to achieve a high-quality spectrum with minimum noise. The sample can be in liquid as well as powder form. Also, solid samples can be investigated, for instance paint on a wood object, provided the investigated area have a flat region that can make contact with the ATR crystal.

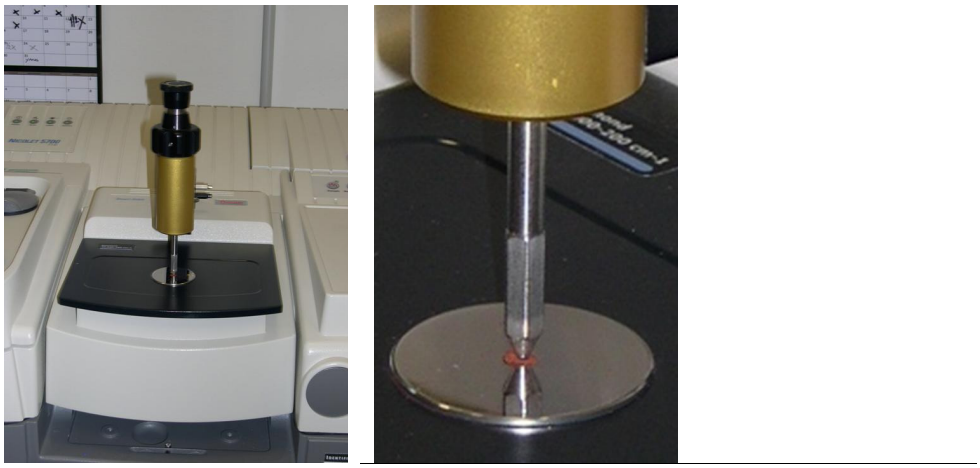

Figure 4.23: The ATR smart orbit inserted in the sample chamber with a red powder sample on the ATR crystal (close up). The pressure arm keeps the sample in constant contact with the ATR crystal. N. B. The amount of red sample is seriously exaggerated in this photo in order to better visualise placing the sample on the ATR crystal.

Pressure is applied on the solid sample in order to achieve optimal contact between the solid sample and the ATR crystal. This means that the sample also must be able to withstand the pressure applied. Normally, a sample made from wood, paper, stone, metals, porcelain or other artistic objects should be able to withstand the pressure. But, as many cultural heritage objects are degraded to a certain degree, the sample under investigation might not be able to withstand the pressure

applied for optimum ATR contact. This must always be taken into account from case to case, when working with cultural heritage objects. Also if the sample is small, i.e. a fraction removed from a larger piece of artwork, micro structural cracks would be present in the smaller fraction. And thus again, it might not be able to withstand the pressure applied in order to achieve the optimum contact with the crystal and the fragment would either become flat, deformed or completely crushed depending on its structure.

Sampling small particles from fragments or larger object is therefore an option. The particle sampling is usually performed under microscope, in order to have as uniform a sample as possible from a heterogeneous matrix. The same sample can be investigated both in the MIR and FIR region using the ATR Smart Orbit. Change between the two regions is very easy, it takes only a few minutes to change beamsplitter and align the interferometer.

4.3.1 COLLETION PROCEDURE ON SAME SAMPLE

In ATR mode it is possible to collect a spectrum of the exact same particles in the region 4000-525 and 700-90 cm^{-1}, gaining chemical information over a wide range similar to the range obtainable with Raman spectroscopy. This is the big advantage over the transmission method, where the sample is either embedded in KBr (for investigations in the MIR range) or embedded in PE (for the FIR range). If you have sufficient sample material you can remove enough particles to make both embeddings, but you cannot investigate the exact same particles in both regions. This is important when working with heterogeneous samples but not important when working with homogeneous sample materials.

In order to collect ATR spectra in both regions of the exact same particles the following procedure is recommended.

- Collection of the background spectrum in the MIR region.
- Placing the sample on the ATR crystal and applying pressure.
- Collecting the sample spectra in the MIR region.
- Changing the beamsplitter for the FIR region and aligning the interferometer (must always be performed when changing beamsplitter), while the ATR crystal is still in contact with the sample.
- Collect the sample spectrum in the FIR region.
- Remove the pressure arm from the crystal and sample (if you are lucky the sample will stick to the pressure arm so cleaning the crystal will be easier)
- Clean the crystal (do NOT remove the particles on the pressure arm)

- Collect background spectrum in the FIR region

This should, in theory, be the procedure for every sample thus ensuring that you have collected in both MIR and FIR region. Be alert that no false signals are visible in the spectrum (if you collect FIR region first and then the MIR region, very often water vapour bands will appear in the MIR spectrum which can significantly influence the spectrum quality).

False signals occasionally appear in the FIR region. Often a false band appearing at 621 cm^{-1} is observed. Also on occasion a sharp band at 630 cm^{-1} is observed, this band however, is so sharp that no mistake can be made that it is a false band. But if other false signals appear or water vapour bands appear a new collection is necessary. And this is where the sample on the pressure arm comes into play (and why you should not remove it).

- Change settings (reverse order of collecting background and sample from previously).
- Collect the background again.
- Put the pressure arm (with the sample sticking to the arm) in contact with the crystal.
- Collect again the sample spectrum in the FIR region.

You should now have a FIR spectrum without artefacts and still collected on the exact same particles as for MIR region.

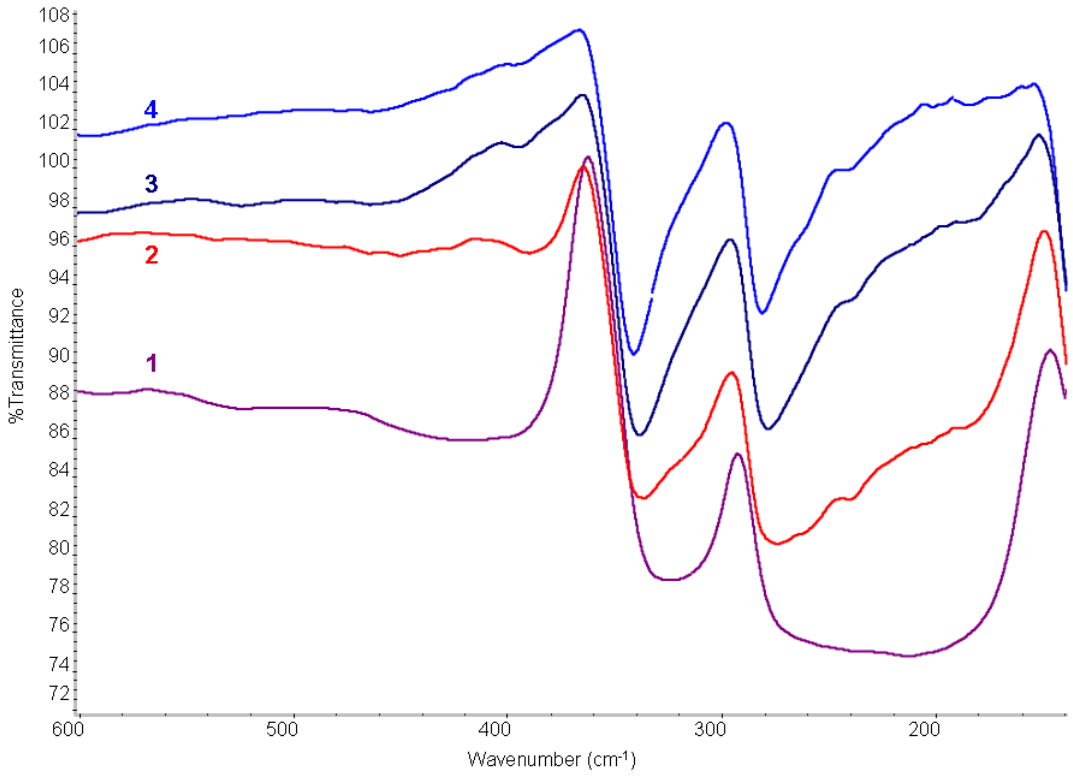

Figure 4.24: FIR spectra of cinnabar with less and less (1 →4) sample on the ATR crystal. As can be seen the less sample is placed on the ATR crystal the slimmer the spectrum becomes and also a shift is noticed. Band shift from 325 → 342 cm^{-1} and from 214 → 281 cm^{-1}.

Care must also be taken with the amount of sample placed on the ATR crystal. In theory it should not matter how much sample is placed on the ATR crystal. But as can be seen in the case of cinnabar in Figure 4.24, it does matter. The first collection of a cinnabar FIR spectrum is unusually broad banded (purple spectrum marked with 1 in Figure 4.24). Some of the sample powder is removed from the ATR crystal and a new spectrum (red, no 2) is collected on what is left on the ATR crystal. Immediately, a band shift and a slimming of the broadest band at 214 cm^{-1} is observed. Twice more some particles are removed from the ATR crystal and spectra are collected, dark blue and light blue spectra, marked 3 and 4, respectively in Figure 4.24. Again, it is observed that the bands shift slightly in wavenumber. The two bands of cinnabar shift from 325 → 342 cm^{-1} and from 214 → 281 cm^{-1} in the four spectra.

This phenomenon of band broadening and shifting of bands (loss of definition) when a larger amount of sample is present on the ATR crystal is occasionally observed, also in the MIR region, but it is most prominent in the FIR region. The same phenomenon, loss of definition, is observed in transmission with hematite when the sample is ground too much [66].

It is thus advisable to always try and minimise the sample amount investigated in order to minimise the effect of band broadening, loss of definition and band shifting.

4.3.2 TEMPERATURE EXPERIMENTS WITH ATR SMART ORBIT

One important question which arise during heating of the mixed PE and sample in the heated anvil die, is if the temperature is too high to affect the chemical structure of the sample. In the literature melting point temperature of 25 of our investigated standard inorganic pigments and corrosion products are available [22]. They are shown in Table 4.3. As can be seen many of them have really high melting point temperature or, like the hexagonal red pigment cinnabar with α-HgS structure, it transforms its chemical structure at 344°C to the black cubic β-HgS structure, which melts to a liquid phase at 850°C. Most of these listed melting points are much higher than the expected temperature of the heated anvil die (where we set the hotplate to 180°C), and therefore no structural change is anticipated for these inorganic components in the FIR region.

However, not all melting point temperatures of our standard samples are known. Information from the pigment supplier is usually very scarce in this aspect, especially as very often we do not even have a correct chemical formula for the pigments. Very often the pigments are a heterogeneous mixture of component (this is especially true of earth and umbra pigments). To

perform melting point analysis on all our 180 standard pigments and corrosion products is a very long, expensive and tedious task, which is still under consideration.

Table 4.3: Melting point (mp) of selected inorganic pigments and corrosion products (dec = decompose, trans = transformation of chemical structure) [22]. *individual mp temperature for one component in a mixture.

Pigment Name	**Brotto Formel**	**Colour**	**Mp (°C) [22]**
Anglesite	$PbSO_4$	White	1087
Aragonite + org. Subs.	$CaCO_3$	White	825
Bariumchromate	$BaCrO_4$	Yellow pale	1380
Bristol yellow pale	Blend Of Pigments ($BiVO_4$)	Yellow light	500 trans
Burnt umber	Fe_2O_3, MnO_2	Brown dark	1539*/1842*
Cadmium red	CdS, CdSe	Red dark	1480*/1240*
Cadmium yellow	CdS, ZnS	Yellow	1480*/1020* trans
Cassiterite	SnO_2	Brown	1630
Cerussite	$PbCO_3$	Grey light	315 dec
Chalcocite	Cu_2S	Black	1129
Chromium green oxide	Cr_2O_3	Green dark	2320
Cinnabar	α-HgS (hexagonal)	Red	344 β-trans
Cobalt green deep	CoO, ZnO	Green dark	1830*/1974*
Cuprite	Cu_2O	Red Brown	1244
Galena (galenite)	PbS	Black	1113
Hematite	Fe_2O_3	Red	1539
Lead white	$2PbCO_3,Pb(OH)_2$	White	400 dec
Calcite	$CaCO_3$	White	825
Malachite	$CuCO_3,Cu(OH)_2$	Green	200 dec
Massicot	PbO	Yellow	887
Minium	Pb_3O_4	Orange	830
Orpiment	As_2S_3	Yellow Beige	312
Quartz	α-SiO_2	Pale grey	573 β-trans
Realgar	α-As_4S_4	Orange	320
Titanium white	TiO_2 (anatase)	White	1560
Zinc white	ZnO	White	1974

Instead it was decided to use the ATR Smart Orbit as a possible means of validating the PE pellets in transmission. We know that the pigments are heated briefly inside the anvil die when producing the PE pellets but is the temperature employed enough to cause structural changes. Thus an experiment is conducted in which the pigments are heated in the exact same way "as if" the PE was present and spectral collection takes place immediately after heating, comparing the spectrum to one collected without heating. This temperature experiment is performed twice in order to collected the same results in both the FIR and MIR region.

The procedure is the standard procedure for making PE pellets but without the presence of the PE. The anvil die is heated on a hotplate for approximately 5-10 minutes to 180ºC. After heating the die, the die is removed from the hotplate and a spatula sized spoon of ground pigment is added in the standard form (first a few grains to observed visual changes in colour or sublimation, then the

rest is added), the die is then assembled and put under 5 tons of pressure for 3 minutes. The die is disassembled and a small amount of powder is quickly placed on the ATR crystal for collection of spectrum. The background spectrum (a 2 min process) was collected during application of pressure to make it possible to collect the sample spectrum immediately, while the powder was still hot, in order not to risk cooling (restructuring of the chemical structure) while collecting the background spectrum.

The temperature experiments are carried out on 19 pigments all from Kremer Pigmente listed in Table 4.4. The melting point, decomposition or sublimation temperature is only known for very few of the listed pigments from the internet or from the suppliers homepage (Kremer Pigmente) and all are reported higher than 200ºC except for Milori blue (a Prussian blue analogue), which reportedly liquefies at >140ºC.

Collection of spectra recorded before and after the heat treatment collected in both MIR and FIR region of each of the 19 pigments from Kremer Pigmente, are compared to determine if any structural change has occurred during heating in the anvil die, by evaluating changes in wavenumber, shape and intensity of the bands.

Table 4.4: List of pigments for temperature experiments all coming from Kremer Pigment GmbH. All information regarding chemical formula are available on the homepages of the supplier (www.kremerpigmente.de)

No.	Pigment name	Brutto Formel	Colour
12030	Atramentum neutraler	tannic acid (general formula $C_{76}H_{52}O_{46}$) from oak bark in a reaction with iron salts	Grey
43940	Barium yellow	$BaCrO_4$	Yellow
10180	Bremer blue	$2CuCO_3$, $Cu(OH)_2$	Blue
42100	Carmin naccarat	Aluminium lake of carminic acid; $C_{22}H_2OO_{13}$.	Red
43500	Cobalt yellow Aureolin	$2K_3(Co(NO_2)_6)_3H_2O$	Yellow
11100	Green earth bavarian	Fe^{2+} silicate	Green
40820	Green earth italian	Fe^{2+} silicate	Green
11000	Green earth veronese (Celadonite)	$K(Mg,Fe^{2+})(Fe^{3+},Al)[(OH)_2 \|Si_4 O_{10}]$	Green
37050	Gamboge	Resin derived from trees of the family *Guttiferae.*	Brown
36000-a	Indigo	$C_{16}H_{10}N_2O_2$	Blue
10110	Lead tin yellow type 1	Pb_2SnO_4	Yellow
10120	Lead tin yellow type 2	$Pb(Sn,Si)O_4$	Yellow
44400	Malachite synthetic	$CuCO_3$, $2Cu(OH)_4$	Green
45200	Milori blue	$Fe(CN)_6 \cdot Fe \cdot NH_4$	Blue
43130	Naples yellow reddish	$Pb_3(SbO_4)$	Orange
4096	Pencil clay	Clayous material	Grey
40450	Terra di Siena, burnt	Iron oxide, silicate	Brown
44250	Viridian green, Chromoxid hydrate green	Cr_2O_3 H_2O	Green
10400	Vivianit natural	$Fe_3(PO_4)_2 \cdot 8H_2O$	Blue

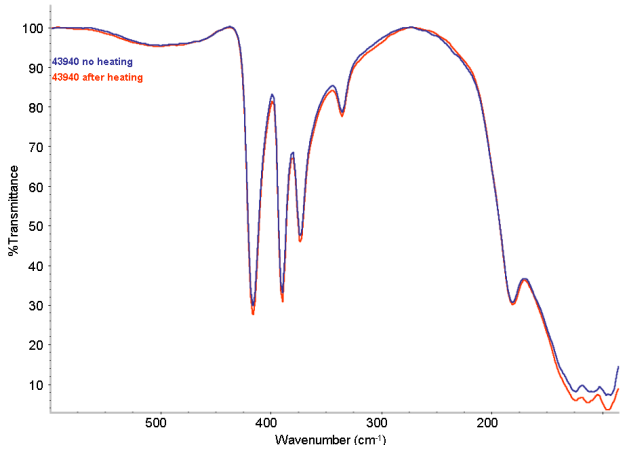

Figure 4.25: Spectra of Barium yellow from Kremer (ID no 43940) no heating (blue) and after heating (red) the pigment in the anvil die. No spectral differences are observed by the ATR method.

Figure 4.25 shows the spectra of barium yellow before and after exposing the pigment to the heat treatment. As can be observed in the FIR spectra, no significant change has occurred due to the temperature experiment to influence the bands of barium yellow. Similarly, no significant changes are observed in the MIR region.

Milori blue (also known as Prusian blue) has a melting point listed as >140°C (decomp.) in the Material Safety Data Sheet on Kremer Pigmente's Homepage. Milori blue has a very strong band at 2069 cm^{-1}, it is one of the few pigments to have a cyanide (-C≡N) stretching band (not shown). The chemical composition of milori blue from Kremers homepage is given as ($Fe(CN)_6 \cdot Fe \cdot NH_4$). It is not considered to be absolute true when we look in the spectra we observe the presence of water in the very broad band 3700-2600 cm^{-1}. Also most listings of Prussian blue has crystal water in the structure, anything from 1-20 H_2O, depending on the analogue and the metals involved (Prussian blue analogue can have Fe, Cu, K, Ca, Mg, Mn, Al etc incorporated into the $Fe(CN)_6$ complex). However, the broad band at 3700-2600 cm^{-1} is a mixture of both NH stretching and OH stretching vibrations. In the MIR region we notice, after the temperature experiment, a considerable slimming of this band in addition to 4 small bands appearing at 3694, 3309 (two O-H stretching vibration), 1670 (O-H bending vibration) and 715 cm^{-1} (O-H out-of-plane bending vibration), which can be observed in Figure 4.26a and Figure 4.26b, respectively. The NH- bending vibration is observed at 1413 cm^{-1}. Milori blue has thus both H_2O and NH_4 incorporated into the iron-cyanide complex ion, most probably the chemical composition is ($Fe(CN)_6 \cdot Fe \cdot NH_4$ xH_2O) and one could imagine both the $-NH_4$ and H_2O to be relatively easy to depart from the rest of the complex when exposed to heat, however, we only observe changes in water at this temperature.

No significant changes are observed in the FIR region, only small acceptable shifts in wavenumber and minor slimming of the band at 210 cm^{-1} are observed. This is due to differences in amount of powder placed on the ATR crystal [66]. In the case of Milori blue we conclude that some H_2O is freed from the Fe-complex as observed, but no change occurs in the lattice structure.

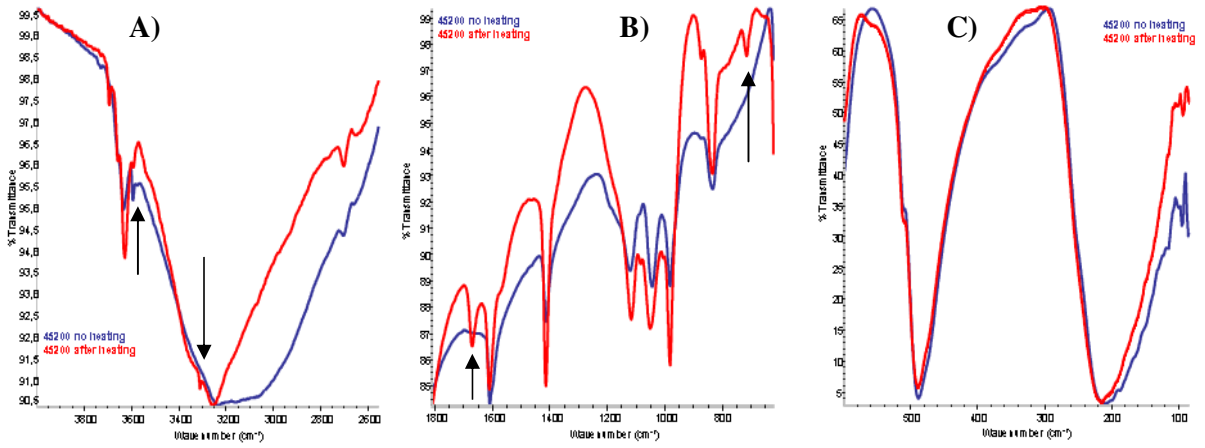

Figure 4.26: Spectra of Milori blue (Kremer Pigmente no. 45200) before (blue) and after (red) heating the pigment. Significant change is observed in the broad band centred at 3200 cm^{-1} and small bands appear after heating at A) 3694 and 3309 cm^{-1} and the broad band at 3100 cm^{-1} has lost intensity B) 1670 and 715 cm^{-1}. C) No significant changes are observed in the FIR region.

In the Italian green earth pigment, of which we know only it is a Fe^{2+} silicate, we only observe significant changes for the OH stretching region. Since we have no other information about this pigment from the supplier we can only speculate that the change can be caused by loss of H_2O or OH from complex bonded to free form, but at the same time, since we observe no change in the FIR region, the loss does not cause any change within the lattice vibrations of the crystal.

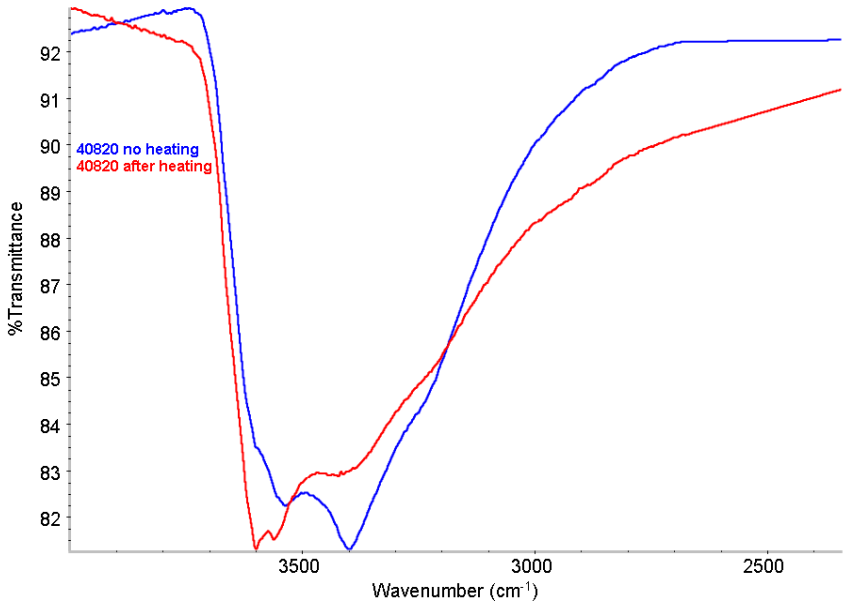

Figure 4.27: Close-up of the MIR spectral region 3900- 2400 cm^{-1} for the pigment Italian green earth (Kremer 40820). The only differences observed are in the 3700-3000 cm^{-1} MIR region. The OH bands are changing intensity due to heat exposure.

Iron phosphate, vivianit ($Fe_3(PO_4)_2 \cdot 8H_2O$) a pale light blue pigment, shows perhaps the greatest changes in the FIR spectra after heating. Bands in the region 600-400 cm^{-1}, bending vibrations from the phosphate, do not change all that much in band shifting but they do change significantly in intensity and shape of the bands. Important changes are observed in the 400-90 cm^{-1} region. Vivianit has structural bonded water. It is therefore very natural to assume that during the exposure to heat structural water is lost, and this is what is observed in the FIR region. This theory is confirmed by *Rodgers et al,* who have performed DTA on a vivianite sample, and observes that differential thermal responses includes a major endothermic band occurring at 115–235°C from loss of structural water combined with oxidation of Fe^{2+}; also, two small exothermic bands are observed with maxima at 605 and 780°C related to structural transformations [67]. From the DTA results [67] and the changes observed in the FIR spectra, we conclude that the 180°C degrees is enough to cause structural changes in vivianit, primarily related to the loss of structural water in the crystal lattice but that also an oxidation of the iron is taking place.

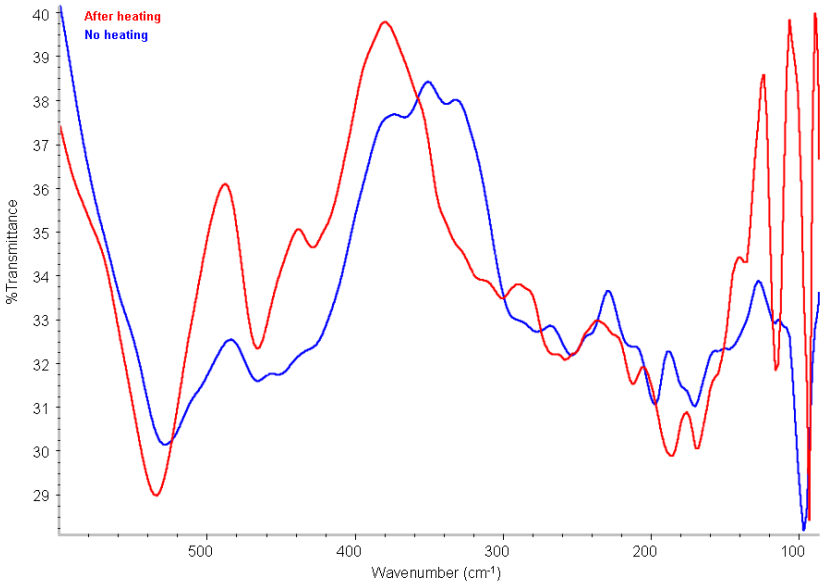

Figure 4.28: Spectra of Iron blue Vivianit ($Fe_3(PO_4)_2$, $8H_2O$) without (red) and after (blue) heating. The chemical structure of vivianit has clearly changed.

With this small experiment concerning inorganic pigments in ATR mode heated in a similar manner as when producing the PE pellets, we must conclude that there will be changes in the structure of some pigments embedded in PE for transmission spectroscopy in the FIR region.

Table 4.5 shows the results obtained by comparing heated pigments with not heated pigments both collected in ATR mode. 10 of the 19 pigments show no significant change (within acceptable limit dependant on the spectral resolution of 4 cm^{-1}). While the pigments containing OH, H_2O or NH_4 in the chemical structure show small changes, or like in the case of vivianit, the changes are

indeed significant and linked most specifically to the loss of structural water incorporated into the chemical structure. Thus, when examining inorganic pigments with water, OH or NH incorporated into the crystal structure, PE transmission is not an optimal method. Instead using the PETF for transmission or the ATR method would produce a result with no structural changes brought on by the heating procedure.

Table 4.5: List of pigments and the changes observed before and after heating the pigments in the MIR and FIR regions. All spectra are collected with 4 cm^{-1} resolution.

Kremer Id no	*Pigment name*	*ATR MIR region: Spectral changes comparing without and after heating*	*ATR FIR region: Spectral changes comparing without and after heating*
12030	Atramentum neutraler	**Band 3363 cm^{-1} intensity decrease, region of changes 1200-1000 cm^{-1} and 800-750 cm^{-1}, band shift 668→ 659 cm^{-1}.**	No significant change
43940	Barium yellow	No significant change	No significant change
10180	Bremer blue	No significant change	**Intensity changes and small acceptable shift for several bands in the region 120-90 cm^{-1}.**
42100	Carmin naccarat	No significant change	**Changes observed below 350 cm^{-1}, band 262 appear, broad band appear centered at 180, broad band disappear centered at 130 cm^{-1}, visible noise in the 'after' spectrum.**
43500	Cobalt yellow Aureolin	No significant change	No significant change
11100	Green earth bavarian	No significant change	No significant change
40820	Green earth italian	**Band 3400 cm^{-1} decrease intensity, 3558 + 3601cm^{-1} increase intensity.**	No significant change
11000	Green earth veronese (Celadonite)	**Decreased intensity of bands 3700-3000 cm^{-1} and 1630 cm^{-1}.**	No significant change
37050	Gamboge, Gummi gutti	No significant change	No significant change
36000a	Indigo	No significant change	No significant change
10110	Lead tin yellow type1	No significant change	No significant change
10120	Lead tin yellow type2	No significant change	No significant change
44400	Malachite synthetic	No significant change	No significant change
45200	Milori blue	**Broad band 3000 less intensive, and the appearance of weak bands 3694, 3309, 1670 and 715 cm^{-1}.**	No significant change
43130	Naples yellow reddish	No significant change	No significant change
4096	Pencil clay	**Band 3430 cm^{-1} decreases in intensity.**	**Shifts observed below 300 cm^{-1}, decreased intensity bands 137(w)→138(vw), 108(m)→107(w), 95(m)→92(vw) cm^{-1}**
40450	Terra di Siena, burnt	No significant change	**Noise below 200 cm^{-1}, possible small band shift in region 165 → 90 cm^{-1}.**
44250	Viridian green, Chromoxid-hydrate green	No significant change	No significant change
10400	Vivianit naturel	**Band appear 772 cm^{-1}**	**Several changes in the external region, band shift, change in intensitites ect.**

One could argue that as long as the standard pigments for the database is collected in the same manner as the unknown sample, the same amount of heat will have been applied in both standard and sample and the structural changes will be identical. It will thus still be possible to spectrally compare a standard pigment with a sample in order to identify an unknown sample despite any structural changes even if the unknown sample was vivianit, because we know what it looks like after the structural change. However, this is only true if the sample is pure and there are no other factors influencing the heating and the structural changes (like another compound). Other compounds present as impurities in a sample can significantly change the melting point temperature of the sample compared to that of the pure sample. They can either delay or hasten the melting point [68-70]. And if the melting point can be influence one could imaging that also the point where the impure sample starts to change structurally can be influenced. This is significant if that point is close to the temperature at which we produce the PE pellets. Thus we are back to status quo, where we need another method for collection in order to spectroscopically identify the impure sample correctly.

4.4 LIMIT OF DETECTION

A common misconception is that the smallest concentration that can be measured is identical to the limit of detection (LOD). Instead, LOD is the concentration where we can determine the presence of a substance or not, the point where it is possible to distinguish a specific signal from the background [71, 72].

In an attempt to determine the LOD or lowest possible amount investigated by FIR spectroscopy, we have selected the malachite standard (from Kremer Pigmente, no. 10300). Malachite ($CuCO_3$,$Cu(OH)_2$) as a representative of a inorganic compound with medium intensity bands in the FIR region but also as a sample which has bands both in the FIR as well as the MIR region.

For both transmission and ATR spectroscopy we do not reach the LOD, the lowest amount of sample that we investigate is 0.07 and 0.04 mg for malachite std, respectively, and in both cases we are able to identify our sample quite clearly. The LOD is thus much lower than the amounts mentioned. The reason that we are not able to go lower is the limit of our laboratory weight, which only has 5 digit after the decimal, and thus we can not weigh any smaller amounts.

When we investigate 0.04-0.07 mg it literally means only investigating a few powder particles from a sample. Although we have not reached the LOD we do observe background noise in the FIR spectra. In order to have FIR spectra without the presence of background noise it is therefore

necessary to estimate how low it is possible to go in concentration. This lower limit is found for both transmission as well as ATR spectroscopy.

Table 4.6: List of Malachite std and PE powder weight mixtures for lower limit experiments.

No	Malachite (g)	PE (g)	Total Weight (g)	% Malachite
1	0.00235	0.06726	0.06961	3.376
2	0.00150	0.06806	0.06956	2.156
3	0.00090	0.06780	0.06870	1.310
4	0.00072	0.06483	0.06555	1.098
5	0.00052	0.06379	0.06431	0.809
6	0.00021	0.07926	0.07947	0.264
7	0.00009	0.06619	0.06628	0.136
8	0.00007	0.06409	0.06416	0.109

To investigate the lower limit of FIR spectra collected in transmission various malachite standards are weighed, ground and mixed with PE (approximately 65-75mg) using the standard preparation method for PE pellets mentioned above. Table 4.6 lists the weight of malachite and PE. FIR spectra of some of the std malachite samples embedded in PE can be seen in Figure 4.29. Intensities are here shown in absorbance due to the Lambert-Beer law, which states that absorbance, not transmission, is proportional to concentration.

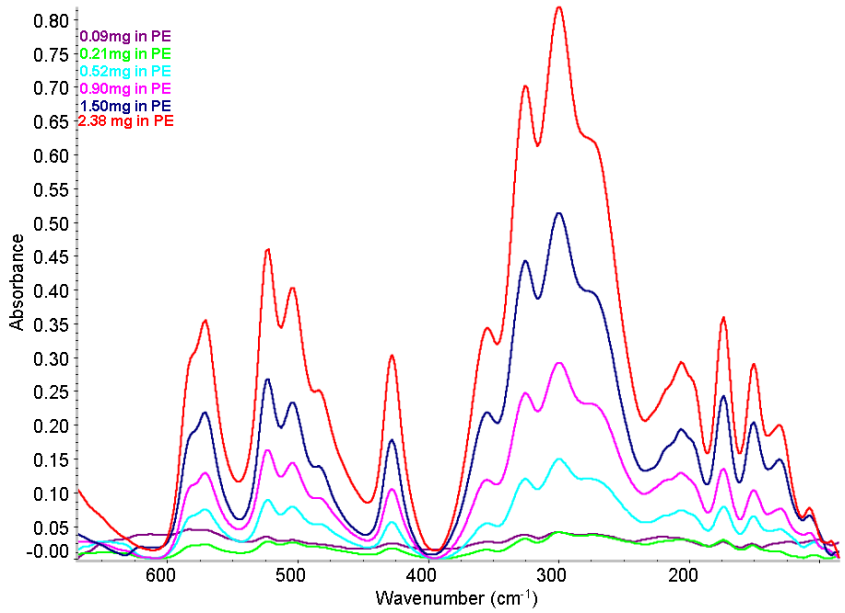

Figure 4.29: FIR spectra of weighed std. malachite embedded in PE and collected in transmission mode, the spectra are shown in absorbance due to proportionality with concentration (Lambert-Beer law).

We have no problems identifying the malachite bands in the FIR region in Figure 4.29, thus we have not reached the LOD. But at lower concentrations anomalies are observed in the spectra originating from the background (instrument, PE or scattering of light), which can be observed in Figure 4.31, where 0.09, 0.21 and 0.90 mg std. malachite are compared on a common scale. Here

we observe quite clearly, that with the lowest concentration 0.09 mg std. malachite in PE (purple spectrum), we are able to identify the pigment but we also observe spectral bands not originating from malachite; generally more noise is seen in this spectrum (observe the small noise band at 390 cm^{-1}) and also bands shifting are detected (most prominent the band at 220 cm^{-1}) and the change in baseline intensity below 150 cm^{-1}. The band at 617 cm^{-1} is a false signal as mentioned above.

As soon as we have a higher concentration, i.e. 0.21 mg malachite in PE, there are no anomalies appearing in the spectra. This means that the lower concentration limit without anomalies, changes in baseline or noise bands appearing in the spectra, is approximately 0.26% malachite as reported in Table 4.6. This is in good agreement with the standard method for making KBr pellets for transmission in the MIR region. Here 0.33-1% is suggested, the usual recommended concentrations are 1-3 mg sample per 300 mg KBr [39].

In ATR there is no embedding of the sample, and as such it is much easier to just weigh small amounts of std. malachite and record the spectra on the ATR crystal. The smallest amount weighed is 0.04 mg malachite, the largest amount 1.15 mg as can be seen in Table 4.7.

Table 4.7: list of weighed sample for ATR investigation.

Malachite (mg)
1.15
0.87
0.77
0.57
0.44
0.24
0.20
0.11
0.08
0.04

The amounts 1.15 – 0.5 mg of malachite, which is normal for collection in MIR transmission in KBr pellets, is too much powder for the ATR crystal. The entire crystal is covered in sample (and also outside the crystal). It means that we might apply 1.15 mg on the crystal but we are not collecting on that same amount. It is quite impossible to contain all that powder on the crystal, hence the absorbance is not proportional to the concentration.

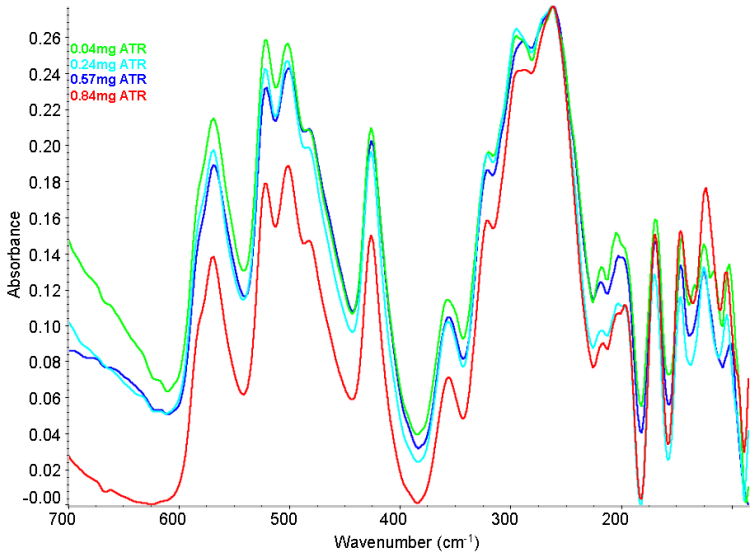

Figure 4.30: FIR spectra of malachite weighing 0.04, 0.24, 0.57 and 0.84 mg (unified scale) collected in ATR

Figure 4.30 shows the spectra of malachite of 0.04, 0.24, 0.57 and 0.87 mg (on a unified scale). The baselines for the four shown spectra are different in the region 700-600 cm^{-1}. However, in the rest of the FIR spectra we observe no difference in relative band intensities, band shape and no significant band shifts. Even at so low a concentration as 0.04 mg (virtually only 1-2 powder particles) we observe no background noise, which means we can identify and assign bands from the std. malachite without any interference.

Following the procedure for standard ATR collection mentioned in section 4.3 the exact same amounts have also been collected in the MIR region and here the conclusion is the same as for the FIR region. With ATR spectroscopy it is possible to go lower in concentration than with traditional transmission spectroscopy; ATR is a factor of 10 better than transmission spectroscopy. We actually believe it is possible to go even lower in concentration. However, the eye is the limit, as placing the sample on the ATR crystal is limited by how well you can see. (Even with the help of a magnifying glass) it can be difficult to place 1-2 particles of sample.

Normally for ATR collection of standards, between 0.1-0.2 mg of sample is applied on the crystal. For investigation of cultural heritage samples less is usually applied.

The smaller the amount of standard or sample applied to the crystal, the more you have to be attentive to the presence of water bands. However, this is not necessary with 0.2-0.4 mg sample. Here the bands are usually too strong to be influenced by water bands. However, if your sample has abnormally weak bands in the FIR region it is advisable to apply larger a amount (but no larger than 0.5 mg as there is simple not enough space on the crystal) in order to better distinguish the signal

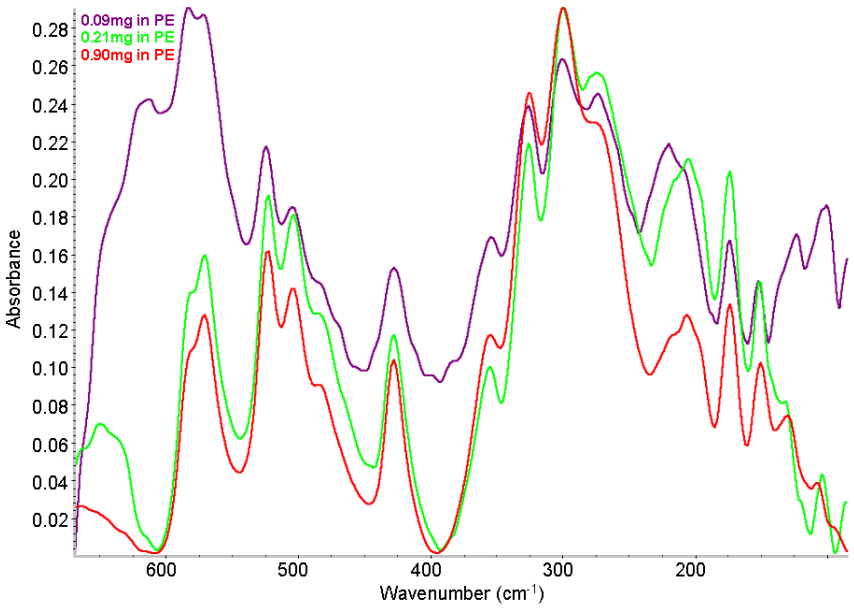

Figure 4.31: FIR spectra of malachite standard at 0.09, 0.21 and 0.90 mg embedded in PE, shown here in absorbance (unified scale).

from the noise bands. If the bands are abnormally broad this usually implies too much sample has been applied on the crystal and less is better, like with the cinnabar std in Figure 4.24, which will usually shift the bands. However, broad bands are quite common for some oxides and sulphides in the FIR region.

The setting up of a sample preparation procedure for collection in the FIR region, both in transmission and ATR mode, are now complete.

CHAPTER 5 DEVELOPMENT OF STANDARD LIBRARY DATABASE

5.1 STANDARD PIGMENTS

The M2ADL laboratory has many standard pigments available. Many of these have already been examined by μATR or transmission spectroscopy but only in the MIR region (4000-650 cm^{-1}). In order for the FIR region to be of any use in identifying inorganic pigments in samples, it is therefore necessary to build up a database in the FIR region.

Initially, the idea was only to collect spectra of those pigments and corrosion products which would be of interest in the FIR region, the ones expected to have active bands in the FIR region, like certain oxides and sulphides. However, that would make identification of unknown samples difficult, firstly because we would not have spectra of other pigments in the database and therefore it would be difficult to know which bands were from the oxides and sulphides we were looking for and which bands were coming from the other pigments in a mixture of an unknown sample. Secondly, pigments and corrosion products have previously only been analysed in the FIR region in transmission spectroscopy [14], not in ATR.

Table 5.1: List of standard pigment suppliers.

Short name	Supplier	Contact adress	Number of pigments investigated
APR	W.G Ball, Artist Pigment Range (APR)	W.G Ball Ltd., Anchor road, Longton, Stoke-on-Trent, Staffordshire, ST3 1JW, UK http://www.wgball.com/	**27**
ICCROM	ICCOM research	ICCROM, Via di San Michele 13, I-00153 Rome, Italy. http://www.iccrom.org/	**8**
Kremer	Kremer Pigmente	Kremer Pigmente GmbH & Co. KG, Hauptstr. 41 – 47, DE 88317 Aichstetten, Germany. http://kremer-pigmente.de/en	**47**
OPD	Opificio delle Pietre Dure	Opificio delle Pietre Dure, Via Alfani 78, 50121 Firenze, Italy. http://www.opificiodellepietredure.it/	**18**
Phase	Phase - Prodotti per il Restauro	Phase prodotti per il restauro. Via T. Cremona 7, 40139 Bologna, Italy. http://www.phaseitalia.it/	**8**
UNIBO	Geological Museum	Geological Museum, University of Bologna, Faculta di Scienze Matematiche Fisiche e Naturali, Piazza di Porta S. Donato, 1 Bologna, Italy. http://www.scienze.unibo.it/Scienze+Matematiche/default.htm	**20**
Zecchi	Zecchi Colori e Belle Arti	Zecchi colori e belle arti, via dello Studio 19r, 50122 Firenze, Italy. http://www.zecchi.it/	**16**
Unknown		No supplier name given or synthesised in lab	**16**

ATR from our point of view, is easier to use as it requires less preparation time, and there is no heating involved. But unfortunately, no database exists. Yet. Therefore, the decision to collect

spectra of pigments and corrosion products in the FIR region focusing on ATR spectroscopy, in order to make a usable library database to identification of unknown samples, was an easy decision.

The collected standard pigment spectra come from various sources. Some of the standards have been collected by other scientists, who have kindly loaned or given us their pigments in order for us to collect FIR spectra. We are deeply indebted to them for this. The most important pigment sources are listed in ***Table 5.1***.

In total we have collected spectra of close to 180 standard pigments and corrosion products using ATR spectroscopy in the MIR and FIR region. In transmission mode, due to the longer preparation time of the PE pellet, we have collected approximately 80 standard pigments. Many of the standards that are available to us are the same, i.e. we have 6 lead tin yellow standards (with different shades of yellow) coming from 2 different suppliers.

The chemical compositions that are available to us are information given by the supplier of that pigment. This information is not considered complete as in many instances the impurities are not mentionen, therefore many of the compound have also been investigated by XRF, XRD or Raman spectroscopy, in order to better known which impurities (if any) are present in the standards. Also, standards from OPD are listed in ***Table 5.1*** although we have no information about the chemical composition or from where the 18 investigated OPD pigments originate. In this case the primary composition of the pigment is an educated guess based on the observed IR vibrations.

It is not possible to show all the collected spectra in this chapter. A few of them have already been shown in the previous chapters. A small number of the collected spectra will be shown and discussed in this chapter, with the main focus on the FIR spectra as the MIR spectra are relatively easily available in literature (although only collected in transmission, not in ATR). Main focus will also be on ATR collection of the oxides and sulphides that we originally set out to investigate.

5.2 THE OMNIC LIBRARY

The instrument is controlled by the OMNIC 7.3 software from Thermo Scientific Corporation. All collected ATR spectra have been collected into the OMNIC library 'ATR FIR library' and 'ATR MIR library'. These libraries contain all the spectra collected of our standards together with name of the standards pigment, possible alternative names, chemical formula (when known), colour, and comments about the collection procedure. Searching the library is easy. Either one can select the library and search a specific pigment. Or in order to make it more easy to compare an unknown spectrum of a sample, the library can search for the closest match. In *Figure 5.1* we match a unknown sample with that of illite from our library database. There is 66.79% congruence

between the two spectra, and the two spectra indeed has a lot of bands in common. As illite is part of a very large family of silicates, which can be very similar in IR spectra, it is thus not surprising that the two spectra have a lot in common. The 9 other hits that the library had are all of silicates (earth, ochre, umbra and clay silicates) with 65.52-54.85% congruency. But there are also a few bands which do not match, they can come from a different type of silicate or from and impurity. Further investigations, both spectral comparison with other standards and/or other possible examinations are necessary in order to completely identify this unknown sample. The same sample has also been collected in the MIR region and compared to the 'ATR MIR library'. Here the same answer appear, that the unknown sample is mainly a silicate.

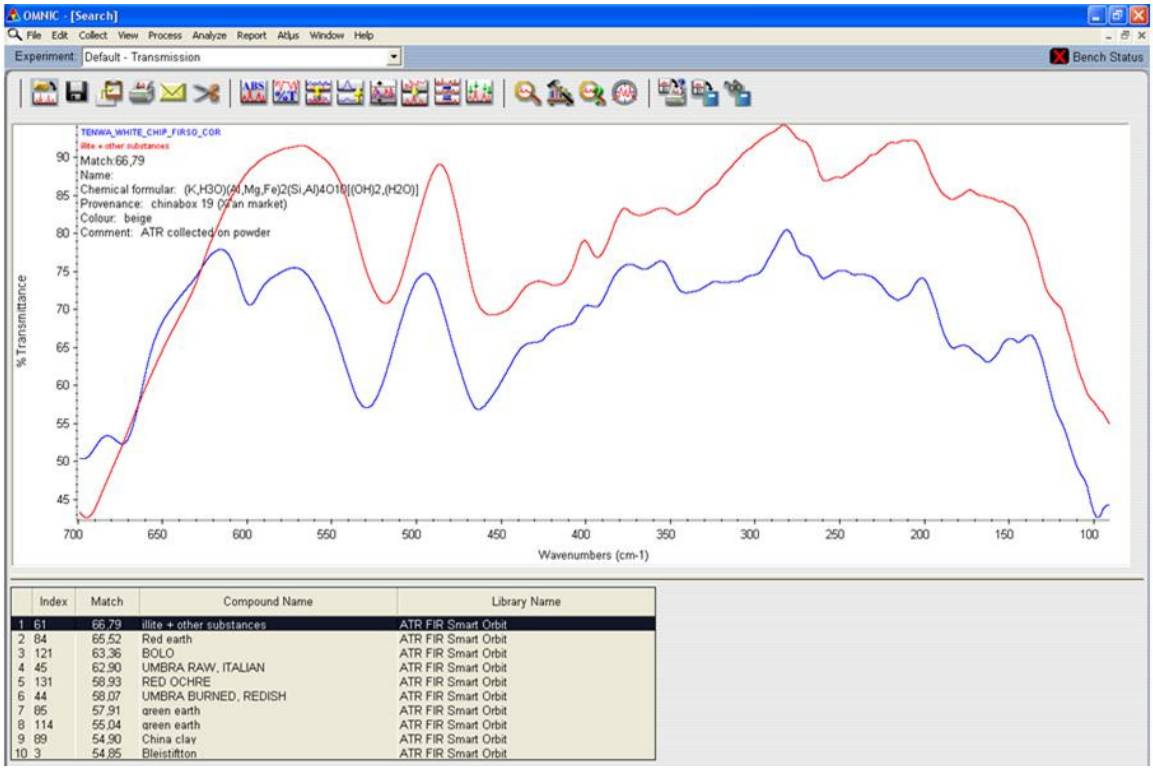

Figure 5.1: Screen capturing of comparison between a white unknown sample (TENWA) and one selected pigment in the library with 66,79 congruence. In this case the best congruence is with the silicate mineral illite.

One problem with this type of spectral comparison is of course that the library can only find a matching spectrum of the major component present in the unknown sample. Once you have found the major components you have to look for the other bands manually and search the literature for information about these specific bands for confirmation if they are not available in our libraries.

5.3 SELECTED PIGMENTS FROM THE LIBRARY

It can be very difficult to identify unknown bands in the FIR range as not many articles or books exist citing bands or showing FIR spectra of inorganic pigments. One of the few recent books available which focus on inorganic and complex components is written by Nakamoto [73]. However this book mainly focusses on halide connections and there are hardly any pigments mentioned. Concerning older literature we have some luck with Afremow [14], Nyquist [74], Karr [15] and Farmer [75]. Afremow [14] has published an article with 79 pigments collected in 1500-200 cm^{-1} range. Nyquist [74] a book of numerous inorganic component mainly minerals collected in the region 3800-45 cm^{-1}, where many oxides and sulphides are shown, however, many of these spectra are of a poor quality. Karr's [15] book focuses on both Lunar and Terrestrial minerals in the region 4000-300 cm^{-1}, where Farmer [75] (editor) focuses on Terrestrial minerals down to 200 cm^{-1}. All of them [14, 15, 74, 75] have been collected in transmission mode. As we know from ATR theory in chapter 2 that there can be substantial differences between transmission and ATR spectra in form of intensity, shift of bands and asymmetrical band shape. One of the few (very recent) publication about ATR application on paints in the 500-230 cm^{-1} region, focuses only on red pigments, hematite, cinnabar, minium and cadmium red [32]. And they conclude their research by adding "*Before spectroscopic analysis in the far infrared region can spread widely it is necessary to compile spectral databases of the spectra of pigments"* [32]. Thus the biggest problem we have when collecting samples with the ATR smart orbit is that no digital library exist and only a few references are found in literature for comparison with unknown samples.

This chapter is focused on showing the ATR spectra of pigments and minerals, since, with a little literature search, some pigments and minerals are available collected in transmission mode down to 400, 300 or even 200 cm^{-1}, but only few are available in ATR mode.

5.3.1 WHITE PIGMENTS

The most common white pigments used in paints consist of carbonates, sulphates, silicates and oxides. Here we look at calcite, lead white, gypsum, quartz, China clay, titanium white and zinc white. The gypsum, quartz, smithsonite and calcite are mineral samples whose purity has all been confirmed by powder XRD analysis to be approximately 95-99%. Smithsonite is not a pigment but included here for comparison with calcite. Lead white, China clay, titanium and zinc white comes from the standard pigment suppliers mentioned in ***Table 5.1***.

The observed vibration for these pigment in the MIR region do not always corresponds to the one found in literature. This is mainly due to the differences in collection between ATR and transmission mode, since the known literature only describes transmission spectra.

5.3.1.1 CARBONATES

Our calcite mineral has been collected in both transmission (embedded in KBr and PE) and ATR mode. The spectra are in good accordance with the transmission spectra observed by Afremow [14] and Nyquist [74], and Karr [15] (who list frequency ranges for 8 mineral calcite crystals) but not with the ones listed by Nakamoto [73], see list of vibrations in *Table 5.2*.

Afremow [14] show two transmission spectra of calcite, where the one listed in square brackets is precipitated calcite. Afremow observes a shift of bands here particularly in the C-O stretching band at 1428 [1445] cm^{-1}, where Nakamoto [73] observes the same stretching band at 1484 cm^{-1} and Nyquist at 1450 cm^{-1} (very broad strong band). Karr [15] observes (for 8 minerals) the stretching vibration between 1440-1420 cm^{-1}. Our carbonate stretching band of the almost pure mineral is observed at 1428 cm^{-1} in transmission mode and at 1391 cm^{-1} in ATR mode. The difference observed between Nakamoto and Karr/Nyquist is so big that one could speculate the Nakamoto's sample was precipitated calcite (not mentioned in [73]). The stretching vibration shown by Nyquist [74] is extremely broad. This could indicate that too much sample was applied to make the pellet. Broad bands can make exact reading of the band frequency difficult, perhaps this is also the case for Nakamoto.

Nakamoto [73] also mentions a translatory lattice band active in the FIR region at 182 cm^{-1}. This band is neither observed by Afremow, Nyquist nor us but also Angino [43] reports a shoulder at 190 cm^{-1}. We do, however, observe a band at 228 (217 in ATR) cm^{-1}, which match that reported by Nyquist at 230 cm^{-1}, Angino [43] at 228 cm^{-1} and Afremow's at 233 [240] cm^{-1}. Afremow show again that precipitated calcite moves this band to a higher wavenumber, from 233 to 240 cm^{-1}, it is thus difficult to speculate on what Nakamoto and Angino are observing at 182 and 190 cm^{-1}, respectively, other than possibly an impurity.

The bending vibration observed by Nakamoto at 885 cm^{-1} is observed at a lower wavenumber by Afremow at 876 [874] cm^{-1}, by Nyquist at 877 cm^{-1}, by Karr [15] for 8 minerals the bending vibrations are between 877-870 cm^{-1} and us at 875 (871 in ATR) cm^{-1}.

From these observations we learn that precipitated calcite moves the vibrations to a higher wavenumber, while the mineral moves the same vibration to a lower wavenumber.

For smithsonite Karr [15] reports the frequency range of 3 minerals as 1435-1415, 871-867, 744-743 and 300 cm^{-1} collected in transmission mode. This is in very good agreement with our smithsonite mineral collected in transmission configuration, which has major bands at 1423, 870, 743, 303 and 202 cm^{-1}. Basic lead white is reported by Afremow [14] as having bands at 1412, 1047, 848, 695, 683 and 404 cm^{-1}. We notice considerable changes between the basic lead white collected in transmission and the one collected in ATR.

Table 5.2: List of IR-active molecular and lattice vibrations (cm^{-1}) for Calcite as reported by Nakamoto [73], Afremow [14], Nyquist [74], Karr [15] (range of 8 minerals) and observed by us, all in tranmsission mode.

Intermolecular vibration [73]	**Nakamoto [73] transmission**	**Afremow [14] transmission**	**Angino [43] transmision**	**Nyquist [74] transmission**	**Karr [15] transmission**	**Observed Transmission**
E_u	1484	1428 [1445]	-	1450	1440-1420	1428
E_u	706	714 [716]	-	715	715-708	712
A_{2u}	885	876 [874]	-	877	877-870	875
Lattice translatory [73]	**Nakamoto [73] transmission**	**Afremow [14] transmission**	**Angino [43] transmision**	**Nyquist [74] transmission**	**Karr [15] transmission**	**Observed Transmission**
E_u	330	326 [330]	315	325	315-307	317
E_u	-	233 [240]	228	230	-	228
?	182	- -	190(sh)			
A_{2u}	357	- [355]	-	-	-	356
Lattice rotatory [73]	**Nakamoto [73] transmission**	**Afremow [14] transmission**	**Angino [43] transmision**	**Nyquist [74] transmission**	**Karr [15] transmission**	**Observed Transmission**
E_u	106	-	106	110	-	109
A_{2u}	106	-	106	110	-	109

In the spectrum of our calcite mineral standard we observe ATR bands at 1392 and 288 cm^{-1}, which in transmission are observed at 1428 and 326 cm^{-1} [14]. These differences are expected as this is part of the differences between the two methods. Bands observed in ATR will, however, always appear lower than those observed in transmission mode. But not all bands will shift. The bands at 875 and 711 cm^{-1} observed in transmission mode are also observed in ATR at almost the same frequency. Again, this can be explained by the difference between the two theories, which states that only the very strong absorbing bands are expected to shift frequency. Although the bands at 875 and 711 cm^{-1} are strong, they are less strong than the observed transmission bands at 1428 and 326 cm^{-1}.

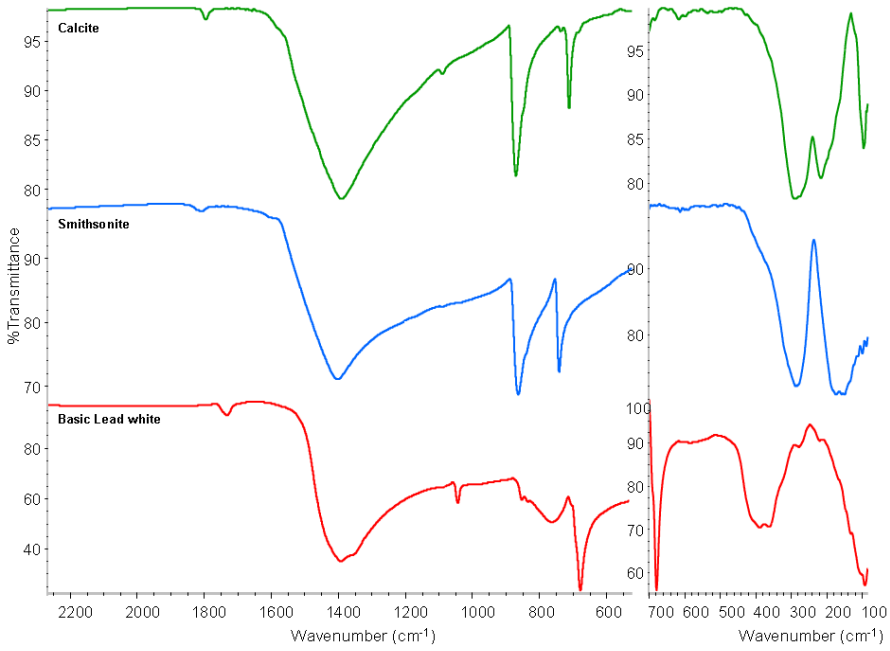

Figure 5.2: ATR MIR and FIR spectra of Calcite ($CaCO_3$, greens pectrum), smithsonite ($ZnCO_3$, blue spectrum) and Basic lead white ($(PbCO_3)_2 \cdot Pb(OH)_2$, red spectrum)

The ATR spectra collected of calcite, smithsonite and basic lead white, all carbonate pigmentes, are observed in *Figure 5.2*. The carbonate are very similar in the MIR region, particular the calcite and the smithsonite, which also have the same crystal system, hexagonal (rhombohedral) calcite structure. The difference observed here are approximately 5-15 cm^{-1} between the spectra of the two mineral carbonate. The differences in shifts observed between calcite and basic lead carbonate are much larger. Due to the band shifts observed both in the MIR and FIR region it is relatively easy to tell the 3 carbonates apart.

Table 5.3: List of wavenumber freqeuncies for calcite, smithsonite and basic lead white collected in ATR mode.

Calcite ($CaCO_3$)	**Smithsonite ($ZnCO_3$)**	**Basic lead white [$(PbCO_3)_2$, $Pb(OH)_2$]**
2516(w)	2490(w)	3532(m)
1797(w)	1808(w)	1732(w)
1391(s,br)	**1402(s,br)**	**1392(s,br)**
1090(m,sh)	**-**	1043(m)
871(s)	**863(s)**	852(m)
736(w)	**741(s)**	763(m)
711(m)	**-**	**678(s)**
288(s,br)	**288(s)**	389(m,br)
216(s)	**173(s,br)**	278(w,br)
96(m)	**149(s,br)**	**92(s,br)**
	99(w)	

For calcite and smithsonite which both have calcite structure, there is a small difference in the metalion. The zinc atom is a little heavier than the calcium atom and therefore molecular and lattice vibrations that involves the calcium or zinc atom is observed shifting frequency. This happens for all vibrations except for the lattice vibrations at 288 cm^{-1}. Basic lead white do not have the same crystal structure as calcite (or smithsonite) and hence here we observe many large differences (as expected) both in the MIR and FIR region.

5.3.1.2 CHINA CLAY, GYPSUM AND QUARTZ

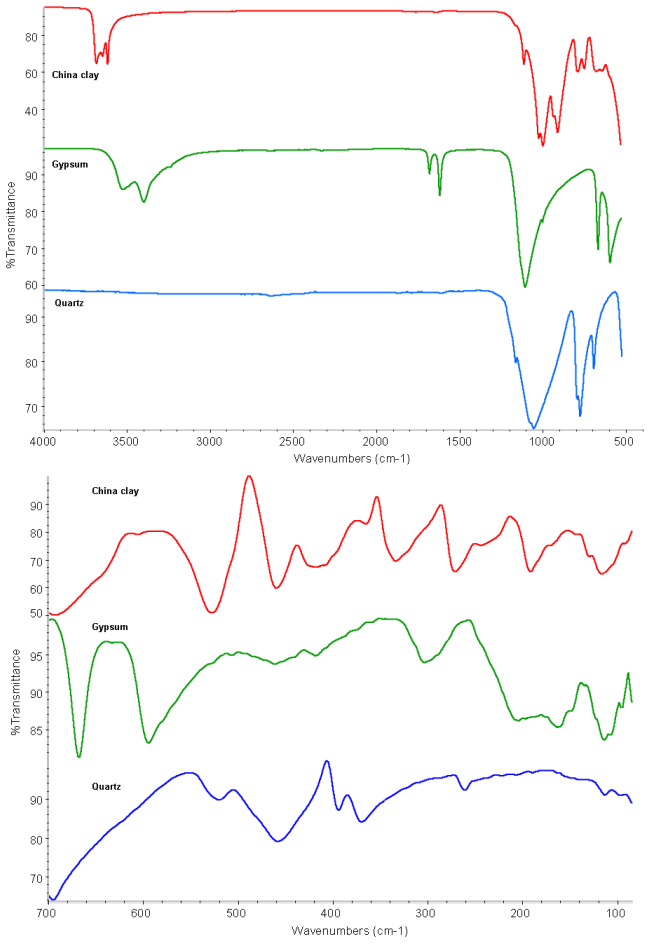

China clay (kaolinite)	Gypsum	Quartz
$Al_2Si_2O_5(OH)_4$	$CaSO_4$, $2H_2O$	SiO_2
3685(m)	3524(m)	1162(sh)
3649(m)	3401(m)	**1056(s)**
3618(m)	3243(w,sh)	794(m)
1162(w,sh)	1682(m)	776(m)
1114(m)	1619(m)	693(m)
1025(s)	**1107(s,br)**	520(m)
1001(s)	1003(w,sh)	**458(m,br)**
935(s,sh)	**668(s)**	394(m)
910(s)	**596(s)**	370(m)
792(m)	461(w)	261(w)
750(m)	302(m)	113(w)
678(m)	**205(s,br)**	
642(m)	**163(s,br)**	
527(s)	**112(s)**	
459(s)		
418(m)		
365(w)		
334(m)		
271(m)		
243(w,sh)		
192(m)		
172(w,sh)		
143(w,sh)		
129(w,sh)		
117(m)		
93(w)		

Figure 5.3: ATR MIR and FIR spectra of China clay (red), gypsum(green) and quartz (blue), together with the wavenumber frequencies collected in ATR mode.

Gypsum and quartz are minerals samples 95-99% pure as confirmed by powder XRD analysis, while the China clay has not yet been analysed for purity. China clay is a common name for a clay material containing an aluminium silicate normally with Al_2O_3 and SiO_2 coordinated to give kaolinite [$Al_4Si_4O_{10}(OH)_8$], which is a generalised formula. The collection of ATR spectra for

China clay, gypsum and quartz match extremely well the transmission frequencies given by Afremow [14] and Karr [15] even taking into account the possible band shift and intensity differences between transmission and ATR bands. The observed differences between transmission and ATR spectra are very little for these three compounds. Figure 5.3 show the ATR spectra of China clay, gypsum and quartz in the MIR and FIR region and also list the observed wavenumber frequencies in ATR mode.

5.3.1.3 ZINC AND TITANIUM OXIDE

Our Zinc oxide 'lead free' comes from our Kremer Pigmente supplier. *Figure 5.4* shows the spectra of zinc white collected on PETF (assumed to be only small particles), embedded in PE (mixture of particle sizes) both in transmission and on a powder sample collected in ATR mode. Both on transmission PETF and in ATR mode we detect background noise from water in the spectra below 300 cm^{-1} giving a unsteady baseline, which is not present when embedded in PE.

On PETF we observe two bands at 560 and 410 cm^{-1}, while in PE we observe a very broad band centred at 422 cm^{-1} with a shoulder band at 526 cm^{-1}. In ATR mode we observe a band at 365 cm^{-1}. The difference between bands observed in transmission and ATR mode are among the biggest observed so far ~50 cm^{-1}.

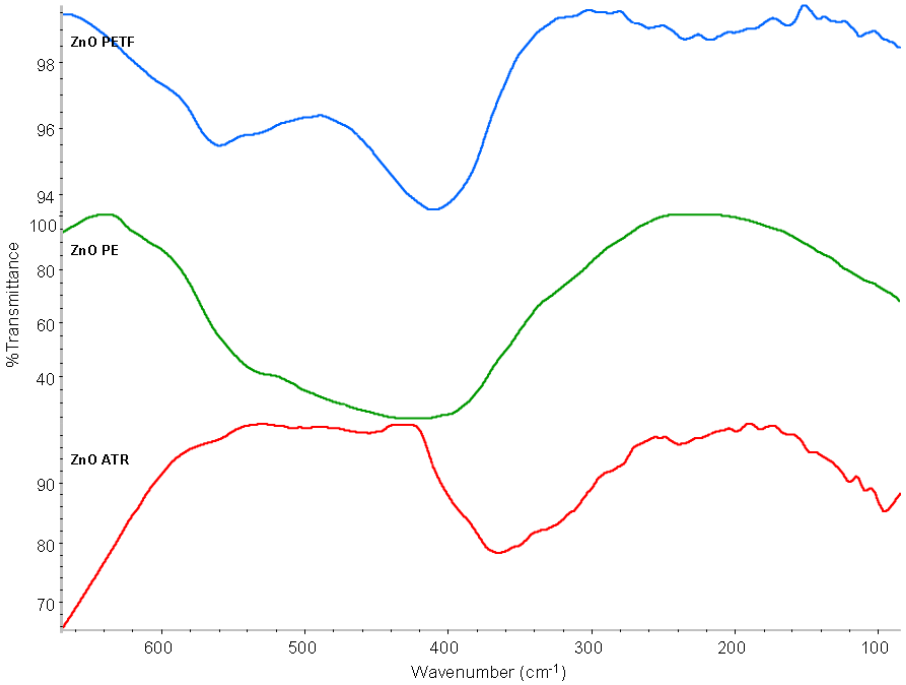

Figure 5.4: FIR spectra of zinc white (ZnO) collected on PETF (blue spectrum), in PE (green spectrum) both in transmission and on powder (red spectrum) in ATR mode.

Afremow [14] observe ZnO in transmission for two different production procedures. Both have broad bands between 550-400 cm^{-1} centred at 520, 501 and 400 cm^{-1} (lead free procedure) and

523, 470 and 440 cm^{-1} (French process), whose intensity and bands shift according to fabrication procedure. In McDervit [76] one very broad band is observed at 430 cm^{-1} in transmission (no mentioning of any shoulder bands) and in Nyquist [74] the broad band is between 550-400 cm^{-1} centred at 450 cm^{-1}, with shoulder bands at 550, 500 and 400 cm^{-1}. Karr [15] observe for 2 zincite minerals bands in the range 540-535 and 440-435 cm^{-1}.

Common for all literature descriing zinc white is the very broad band observed, whose frequencies seems to greatly depend on the method by which it is produced. In this case it seems to been an advantage to collect the spectrum in transmission mode using the PETF as here we observe a splitting of the otherwise very broad band into two separate bands at 560 and 410 cm^{-1}.

The zinc white standard has also been recorded by Raman spectroscopy (at 785 nm) for verification and here the bands are in complete accordance with those observed in Raman literature [77-79].

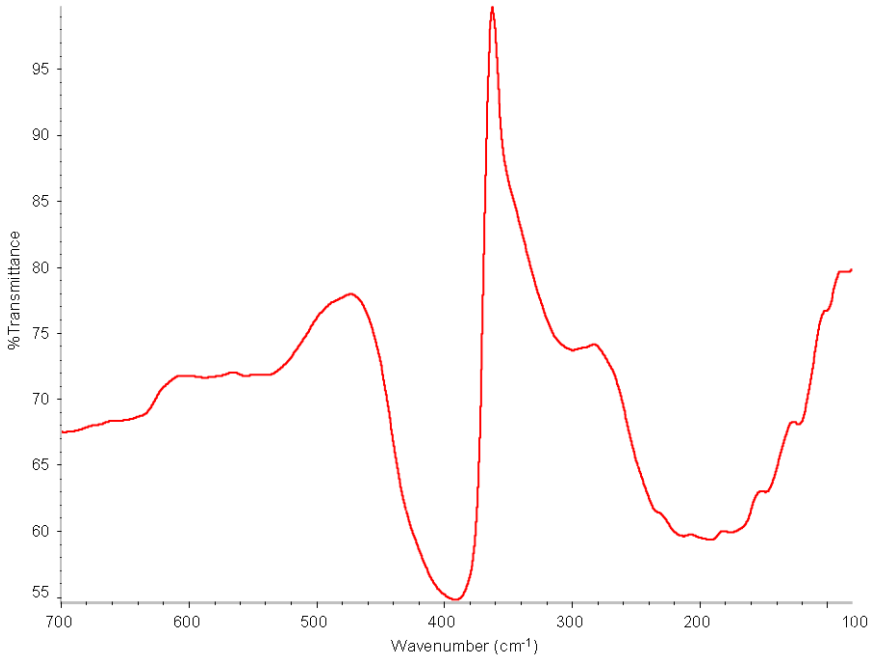

Figure 5.5: FIR spectrum of titanium white (TiO_2) collected in the FIR region in ATR mode.

Also, our standard of titanium white (TiO_2), which comes from APR, is ground to a fine powder by the suppliers. It has been examined by micro-Raman spectroscopy in order to verify the structure. Titanium dioxide as a pigment has two different crystal structures, rutile and anatase. By Raman spectroscopy we confirm that the titanium white from APR has anatase structure as observed in Raman literature [78, 79]. *Figure 5.5* shows the ATR spectrum of powder titanium white.

In the infrared spectrum of anatase we observe a maxima at approximately 365 cm^{-1}, which vaguely resembles of a 1st order reflectance band. This maxima is often observed in reflectance spectra, where the reflectance peak ν_{LO} arise from the polar $\varepsilon \perp C$ (electric field normal to the surface of the C-axis) which couples with the vibration mode of an actual ν_{LO} phonon frequency [80, 81]. The 1st order reflectance phenomenon has previously been observed in cubic structures [82]. We observe the same phenomenon in some oxide and sulphide pigments when working in the FIR region in both ATR and transmission mode (although the phenomenon seems more intense in ATR mode). When observing anatase in reflectance mode Gonzales [81] also observe the 1st order maxima (after performing Kramers-Kronig correction) on single crystals and nano crystals of anatase.

Afremow [14] observes a sharp band at 358 cm^{-1} instead of the 1st order maxima together with strong broad bands at 544, 657 and 730 cm^{-1}. McDevitt [76] and Farmer [75] also observe a sharp band at ~347, and three broad bands at approximately 520, 700 and 750 cm^{-1}. Karr [15] lists for 2 anatase minerals only one vibration in the range 470-460 cm^{-1}, he does not report any bands for anatase below 400 cm^{-1}.

We observe the 1st order maxima band no matter how we prepare our sample. Whether collecting on powder in ATR mode or in transmission mode, both embedding in PE and applying on PETF (Commercial and home-made). This is thus not just a reflectance ATR observation but it is reproducible with other collection methods but only for our powder titanium dioxide, not for other collected sample spectra mentioned in the literature. Therefore it must be an effect of the size of the powder grain particles, as Gonzales [81] observe this phenomenon on single crystal and nanocrystals but neither Afremow [14], Farmer [75] or McDevitt [76] observed the same 1st order maxima. Instead they observe an actual band.

5.3.2 GREEN PIGMENTS

There are many green colours which has been used as pigments over the centuries. Malachite, vivianite and green earth colours are but a few. But these pigments can all be identified without problems in the MIR region, as non of them are based on metal-oxide or metal-sulphide connections. However, two green oxide pigments of interest in the FIR region, are the hydrated chromium oxide (Cr_2O_3, $2H_2O$) and chromium oxide (Cr_2O_3). Their main bands lie beneath 700 cm^{-1}.

5.3.2.1 HYDRATED CHROMIUM OXIDE AND CHROMIUM OXIDE

Especially chromium oxide (Cr_2O_3) has specific frequencies below 700 cm^{-1}, while hydrated chromium oxide (Cr_2O_3, $2H_2O$) with its incorporated water also has bands in the MIR region. Hydrated chromium oxide is also known as viridian green. Both pigments have been industrially produced as pigments since 1860. Viridian green pigments very often have a problem with impurities in form of borates and chromates due to the manufacture not purifying the pigments well enough. Chromium oxide is much easier to purify and it is more widely used, especially since it was discovered that it has the unusual property of photographing under IR light in the same shade as living foliage and therefore it is the most commonly used green colour for military camouflage [83].

Wavenumber frequencies for both compounds are listed in *Table 5.4*. The observed bands for chromium oxide are in good accordance with the ones observed in Afremow [14], McDevitt [76], Newman [84] and Nyquist [74] for chromium oxide green. We compare our PETF transmission and ATR spectra with those in the literature. A certain shift to lower frequency is expected together with differences in intensity when taking into account the differences between transmission and ATR mode.

Table 5.4: List of frequencies for chromium oxide (Cr_2O_3) and hydrated chromium oxide (Cr_2O_3, $2H_2O$) as reported in literature [14, 74, 76] and observed by us in PETF transmission and ATR mode on powder.

Chromium oxide (Cr_2O_3)					
Newman [84]	**Nyquist [74]**	**Afremow [14]**	**McDevitt [76]**	**Trans observed PETF**	**ATR observed**
	-	1350(w,br)	-	-	-
690(m,sh)	680(m,sh)	660(s,br)	-	-	-
632(s,br)	**634(s)**		**625(s)**	**615(m,sp)**	**607(m,sp)**
	582(s)	580(br)	-	570(w,sh)	566 (w,sh)
566(s,br)	-	**550(s,br)**	**555(s)**	**541(s)**	**518(s,vbr)**
443(m,sp)	**446(w,sp)**	**443(m,sp)**	**435(w)**	**442(w)**	**440(m)**
416(m,sp)	**417(w)**	**412(m,sp)**	**407(w)**	**411(m)**	**402(m)**
	400(m)		-	-	-
	-	**307(w)**		**305(w)**	**307(m)**
	-	180(w,br)	-	-	-

Hydrated chromium oxide (Cr_2O_3, $2H_2O$)			
Newman [84]	**Afremow [14]**	**Trans observed PETF**	**ATR observed**
	1064 (m)	-	-
	795(m)	-	-
635(m,sh)	641(m)	636(m,sh)	633(w)
555(s)	**563(s)**	**577(s,br)**	**537(s,br)**
481(s)	**486(s)**	**473(s,br)**	**454(s,br)**
	-	-	437(m,sh)
420(w)	**421(w)**	**419(m,br)**	**419(m)**
	-	-	354(m,sh)
	-	-	138(w,br)

For hydrated chromium oxide we know from Raman analysis that it contains chromium oxide as well as a small impurity from calcite [18]. The two chromium oxides can easily be distinguished between, as can be observed in *Figure 5.6*.

Our hydrated chromoxide has less defined band shape then the one observed in Afremow, which has better defined bands and less broad bands. This is probably due to the impurity coming from the chromium oxide observed by Raman analysis. In our PETF transmission we also observe a lot of noise bands coming from water vapour below 400 cm^{-1}. Neither Nyquist nor McDevitt lists frequencies for the hydrated chromium oxide, Newman [84] does but in his figure [84] he mistakes the spectrum of chromium oxide with hydrated chromium oxide.

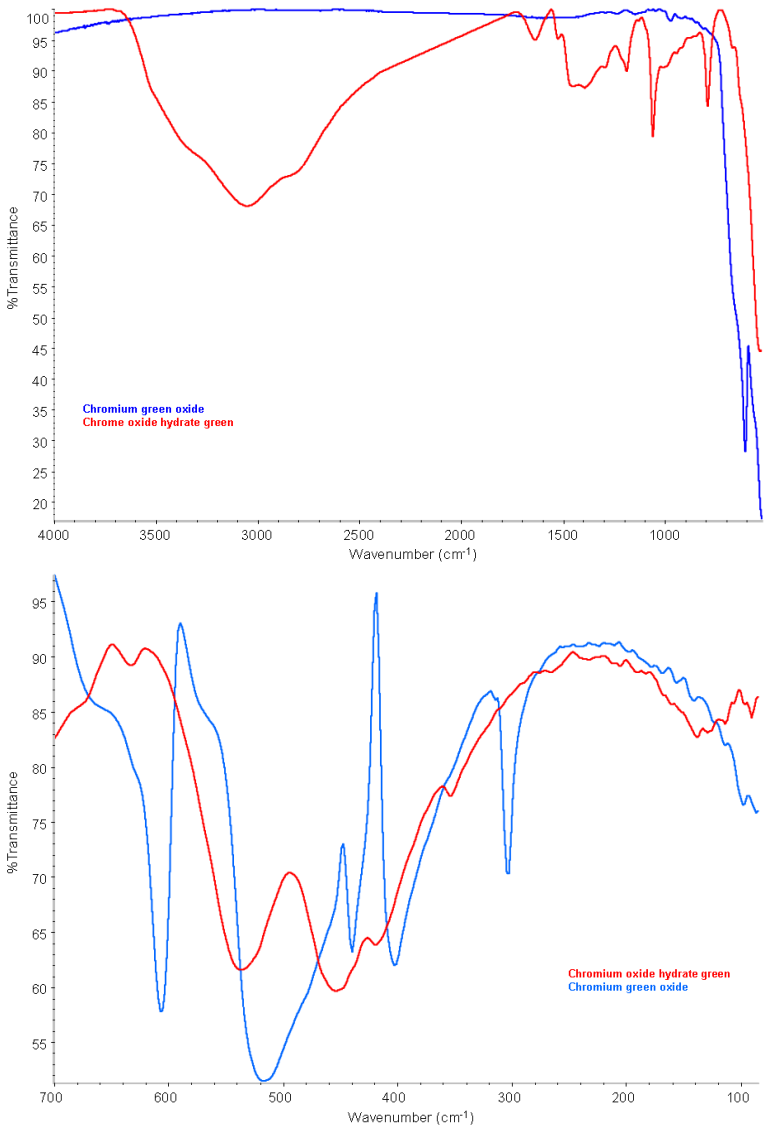

Figure 5.6: ATR IR spectra of hydrated chromoxide and and chromoxide collected in the MIR and FIR region.

We are thus quite sure that our standard pigments are chromium oxide green and hydrated chromium oxide green containing an impurity from chromium oxide.

5.3.3 YELLOW PIGMENTS

For the yellow pigments we have chosen to look closer at the lead yellow pigments known as massicot and litharge. We also look at the arsenic pigments orpiment and realgar and then a series of cadmium sulphides, which change appearance from yellow to orange to red, depending on the co-precipitator present with CdS.

5.3.3.1 MASSICOT & LITHARGE

Massicot and litharge are isomorphic crystal structures of PbO. Litharge has tetragonal and massicot orthorhombic crystal systems. From the Kremer pigmente supplier we have our massicot standard and from OPD we have our litharge standard. But when looking at the two FIR spectra collected in ATR mode we realise quite quickly that they are identical.

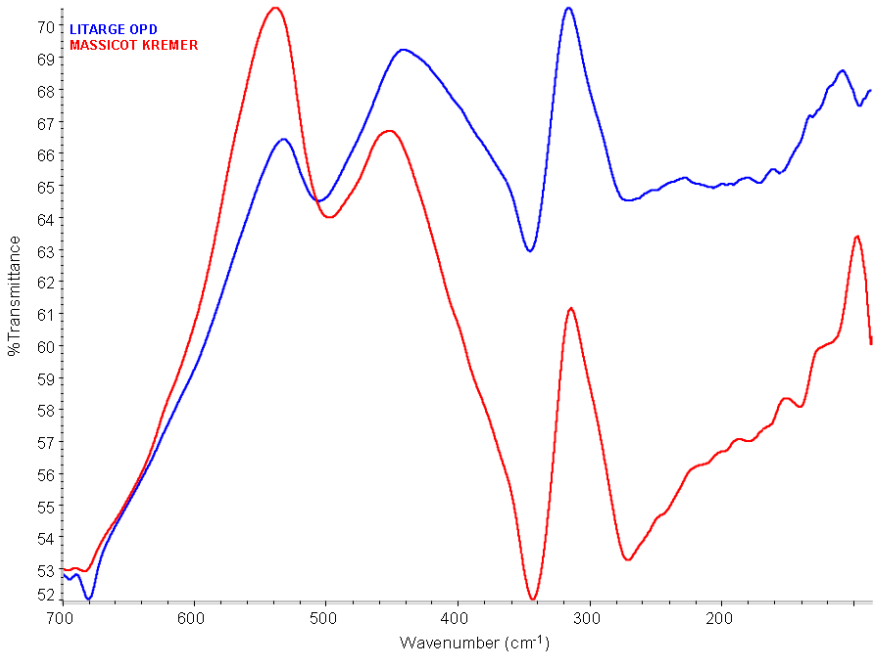

Figure 5.7: ATR FIR spectra of PbO, Litharge from the OPD supplier and Massicot from the Kremer supplier.

The bands observed in the Massicot from Kremer appear at 497(m), 343(s) and 272(s) cm^{-1}. The litharge bands appear in the same place except for the first band at 506 cm^{-1} that has a small shift of 8 cm^{-1}, which could be due to impurities (or precipitation procedure). In the MIR region,

massicot from Kremer have very few (weak) bands at 1390 and 679 cm^{-1} indicating a lead white carbonate as impurity. For litharge from OPD this impurity is also identified as lead white, but in higher concentration. Here, we observe a lot more bands from lead white (1734, 1389, 1044, 864, 759 and 679 cm^{-1}) together with two unidentified bands at 1552 and 1172 cm^{-1}. These impurities probably come from the synthesis of PbO using lead carbonate as starting material. Thus litharge from the OPD supplier is not as pure as the Massicot from the Kremer, but the two substances both contain PbO. McDevitt [76] reports massicot transmission bands at 500(m), 377(s), and 300(s) cm^{-1}, which are in good accordance with the ones we observe in ATR, considering the expected shift to lower wavenumber. Literature [85] of litharge and massicot collected in transmission mode in KBr pellets down to 400 cm^{-1}, reports one band for litharge at 465 cm^{-1} and one band for massicot at 506 cm^{-1}. This is confirmed by Afremow who shows litharge (99% pure) as having bands at 478(m), 355(m,sh) and 300(s) cm^{-1}, which are very different than the observed bands in *Figure 5.7*. Based on [14, 76, 85] we must conclude that both massicot from Kremer and litharge from OPD contains mainly massicot, one with less impurity from lead carbonate than the other. The litharge from OPD is not litharge, but massicot.

5.3.3.2 ORPIMENT & REALGAR

Orpigment and realgar are yellow and orange sulphur pigments used frequent in paint. They can be very difficult to distinguish in the MIR region. In the FIR region this is much easier as their most important bands are observed here, due to the heavy As-atoms present.

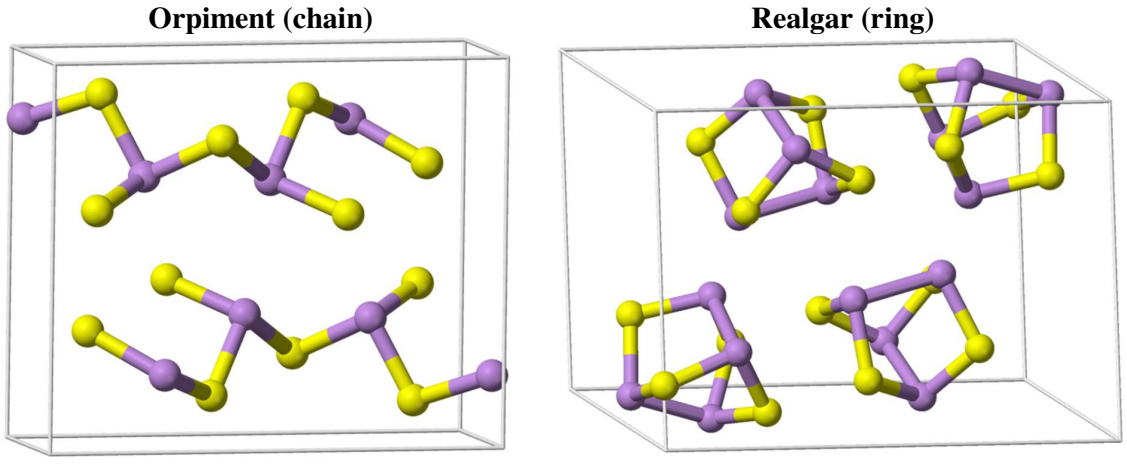

Figure 5.8: The chemical structures of orpiment (As_2S_3) and realgar (α-As_4S_4) depicted in ball-and-stick model, where yellow is sulphur and purple is arsen atoms. Reproduced from [86, 87].

Orpiment has As_2S_3 structure, which is made up of superimposed As_2S_3 layers containing AsS spiral chains. Realgar has As_4S_4 ring structure and is build up of 4 As atomswhich form a tetrahedron and 4 S atoms which form a square. The square of the S cuts through the middle of the As- tetrahedron. The unit cell crystal structures are shown in *Figure 5.8*.

The orange-red realgar (α-As_4S_4) can under the influence of light (UV) change its structure to yellow pararealgar (β-As_4S_4) [88]. For this reason realgar is not applied for outdoor purpose or for mural painting on sunny-side walls etc.

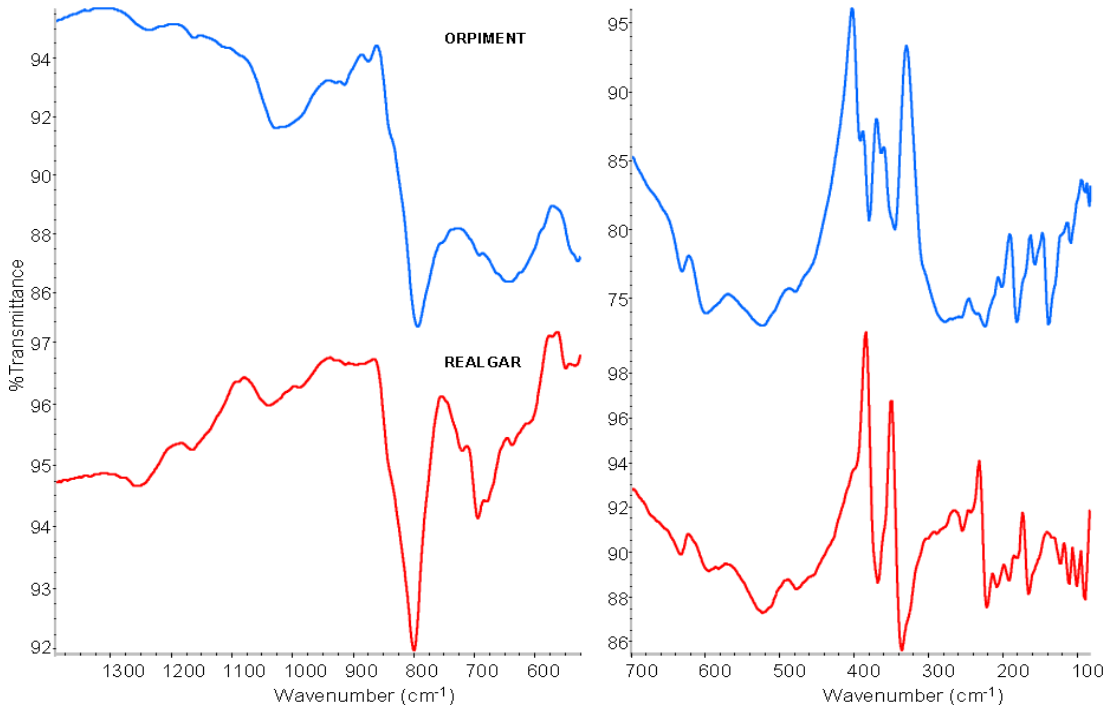

Figure 5.9: ATR MIR and FIR spectra of orpiment (As_2S_3, blue spectrum) and realgar (As_4S_4, red spectrum).

Mineral orpigment and realgar have been investigated in detail by Raman and Infrared (transmission) spectroscopy by Foneris [89], it is also mentioned by Karr [15] (who makes reference to Foneris [89]). The main comparison of our pigment standards has been performed with this literature as it was conducted on pure mineral arsenic sulphur samples. The origin of our pigment samples is unknown, and their purity has yet to be confirmed by other means.

Due to complexity in the crystal of orpiment, Foneris [89] did not assign the bands he observed in this mineral but he concluded, that for both orpiment and realgar, the stretching vibrations are centred around 350 cm^{-1}, bending vibrations centred around 250 cm^{-1} and lattice vibrations are observed below 100 cm^{-1}. Please note that for both orpiment and realgar we observe 1st order maxima band associated with small particle size.

Table 5.5: list of bands for Orpiment (As_2S_3) and realgar (As_4S_4) observed in ATR and compared to Foneris (1969) collected in transmission in the region 400-100 cm^{-1} [89].

Orpiment (As_2S_3)			Realgar (As_4S_4)			
Observed ATR bands (cm^{-1})	**Karr [15] transmission**	**Lit. bands (cm^{-1}) [89]**	**Observed ATR bands (cm^{-1})**	**Karr [15] transmission**	**Lit. bands (cm^{-1}) [89]**	**Interpretation [89]**
			3737(w,sp)			
1233(w)			1257(m)			
1162(w)			1165(m)			
1027(m)			1039(w)			
914(w)						
874(w)			987(w)			
838(m,sh)			**838(m,sh)**			
793(s)			**799(s)**			
750(m,br)						
			719(m,sh)			
			693(m,br)			
			679(m,br)			
631(w,br)			633(m,br)			
599(m,br)			597(m,sh)			
523(w,br)			523(w,br)			
479(w,br)			478(w,br)			
391(m,sh)	390(w)	393(w)				
379(s)	379(m)	381(w)	**374(s,sh)**		**373(s)**	**As-S stretch(E)**
363(m)	362(sh)	361(m)	**367(s)**	**365(m)**	**367(s)**	**As-S stretch(E)**
			358(s,sh)	**355(m)**	358(m)	As-S stretch(A1)
345(s)	345(m)	348(m)	**335(vs)**	**338(s)**	**343(vs)**	**As-S stretch(B2)**
307(m,br)	**300(s)**	**305(s)**	**323(s,sh)**		330(m)	As-S stretch(B1)
			288(w,br)		284(vw,sh)	
277(m,br)			277(w,br)		269(vw)	
256(m,br)			254(m)		258(vw)	
223(s)			**221(s)**		**225(s)**	**S-As-S bend(E)**
			207(m)		211(m)	
201(m)		202(vw)			205(m)	
			191(m)		194(m)	S-As-S bend (B1)
180(s)		183(m)	180(m)		183(m)	S-As-S bend (A1)
168(m,sh)			**164(s)**		**170(s)**	**S-As-S bend (E)**
156(m)		160(vw)	149(w,br)		148(vw)	
138(s)		**139(vs)**			141(vw)	S-As-S bend (B2)
127(w,sh)			122(m)			
108(m)			110(m)			
			100(m)			

By comparison of our FIR spectra with Foneris [89] and Karr [15] we must conclude that we observe the expected bands for arsenic sulphide. However, we also observe other small bands coming from either impurities or bands that have not been mentioned by Foneris [89] and Karr [15]. Those small bands are on the other hand not preventing us from identifying orpiment and realgar as the major component present (estimated 80-95% pure). Especially orpiment seem to have more bands than expected in the FIR region. These can come from an impurity from realgar, since there seem to be some overlapping bands with realgar in the low Far-IR region. But the impurities can only be determined with further analytical studies of the two compounds.

5.3.3.3 CADMIUM SULPHIDES

Cadmium yellow, cadmium orange and cadmium red are modern pigments, which are all based on cadmium sulphide. Cadmium yellow and cadmium red pigments are shown here, they comes from our APR supplier, the purity of the compounds are not known. But we observe quite clearly the presence of a sulphate or silicate by bands in the 1100-1000 cm^{-1} region when collecting ATR spectra in the MIR region. These bands are, however, of a very low intensity and are considered to be small impurities.

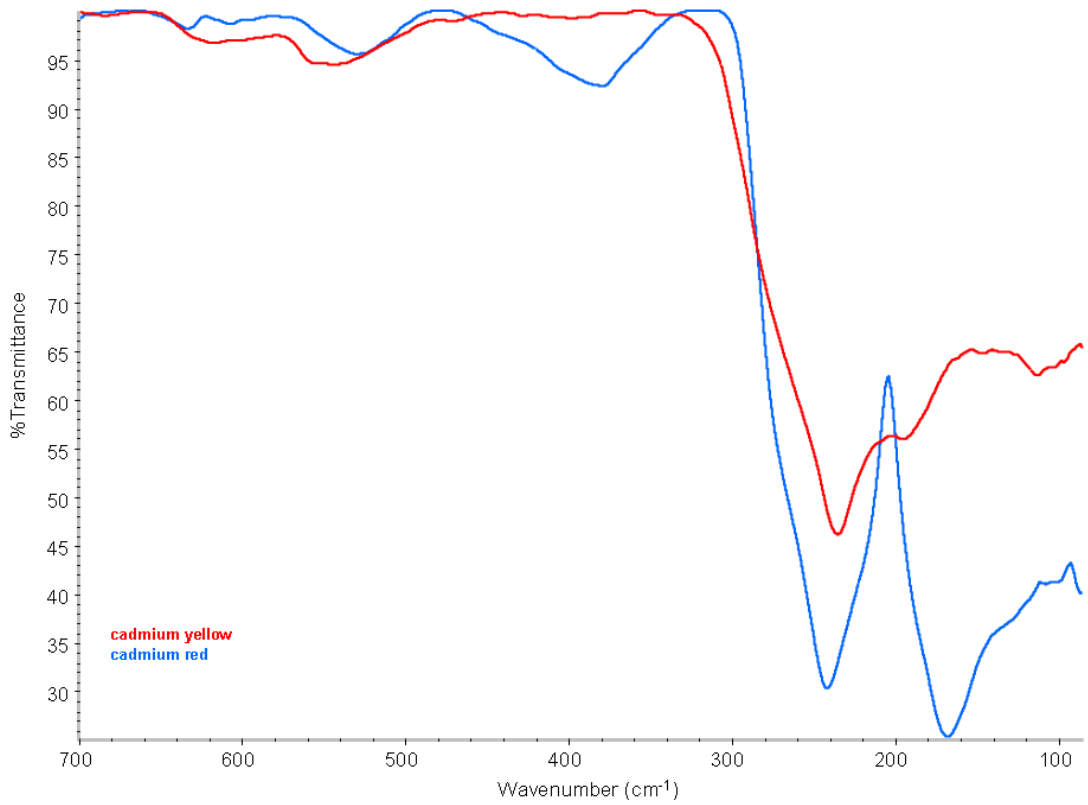

Figure 5.10: ATR FIR spectra of Cadmium Red (Blue spectrum) and Cadmium Yellow (Red spectrum).

Cadmium yellow (CdS) was discovered in 1817. It comes in a variety of shades depending on the degree of calcination. The lighter shades may contain zinc (CdS, ZnS) and the deepest yellows may have traces of selenium (CdSe) incorporated into the crystal. Cadmium red is calcined co-precipitated cadmium sulfide and cadmium selenide (CdS, CdSe). The higher the portion of selenium the more red the pigment is, although the degree of calcination also influences the redness. It was introduced in the early 20th century, as a replacement for the extremely poisonous cinnabar used previously. It is available in a wide range of shades from scarlet to a deep purple [83].

Figure 5.10 shows the ATR FIR spectra of two cadmium sulphides, one yellow and one red. Cadmium yellow has one strong band in the FIR region, where cadmium red is observed as having two strong bands in the FIR region. These two bands are similar in shape to those observed for cinnabar (HgS) but at lower wavenumbers than the CdS.

Table 5.6: list of ATR FIR wavenumbers for cadmium yellow, cadmium red, and cadmium orange compared to Afremow [14].

Afremow [14]	Cadmium yellow ATR	Cadmium red ATR	Cadmium Orange ATR
		633(w),	638(w)
614(vw)	617(w),	607(vw),	610(w)
	545(w),	530(w),	538(w,br)
		380(w),	387(w)
	274(m, sh)	270(m,sh),	277(m,sh)
272(s)	**235(s)**,	**242(s)**	**242(s)**
	195(m,sh	**168(s)**	**176(s)**
	113(m)	-	**-**

The observed bands for cadmium yellow and cadmium red are listed in *Table 5.6*. Both cadmium yellow and cadmium red have small intensity bands in the MIR region, coming from sulphate or silicate impurities. Another cadmium pigment exist in our library, cadmium orange. It has bands similar to cadmium red although they are shifted slightly, which could be due to a difference in particle size or the presence of another impurity, possibly the incorporated ZnS as mentioned abouve. The bands observed at ~380 and ~170 cm^{-1} for cadmium red and cadmium yellow is suspected of originating from a Cd-Se vibration, since we expect the cadmium red and orange to contain this, unlike cadmium yellow. Unfortunately, we have no standard to confirm this assignment.

The only literature which list band frequencies for cadmium red is Afremow [14], although they only observe one strong band due to their cutoff at 200 cm^{-1} in transmission spectroscopy. As the observed band at 272 cm^{-1} is a strong absorbing band we would expect the shift from transmission to ATR to be significant and we do observe a significant shift for this band of ~30 cm^{-1}.

5.3.4 BLACK PIGMENTS

Three black corrosion minerals were investigated by MIR and FIR spectroscopy, both in transmission and in ATR mode. They are covellite (CuS), chalcocite (Cu_2S) and galena (PbS). The purity of covellite and chalcocite have been confirmed by powder XRD as being approximately 95% pure. Galena was not confirmed by XRD because there was not enough grains to perform XRD. The black galena grains was removed as an impurity from the white anglesite ($PbSO_4$)

crystals, and not surprisingly we observe weak bands coming from anglesite in the ATR MIR spectrum of galena. By Raman analysis we observe galena with anglesite and litharge (PbO) as impurities.

However, all three have bands of very weak or non-existing intensity as can be seen in *Figure 5.11*. Their baselines are also very noisy throughout the entire range due to the low intensity bands. Small water vapour bands appear from 400 cm^{-1} and down.

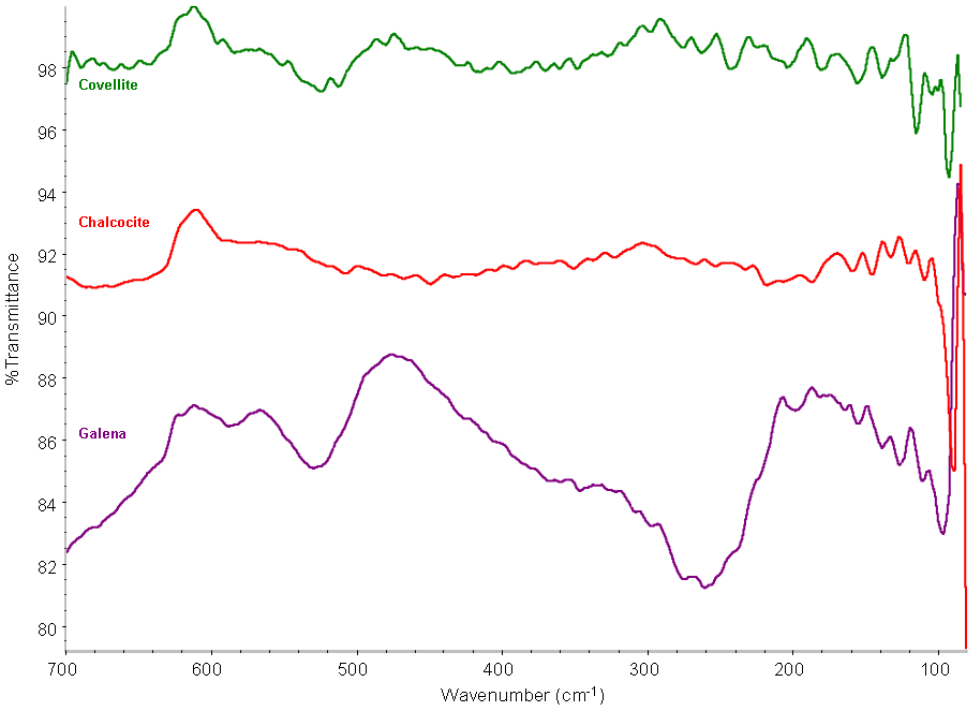

Figure 5.11: ATR FIR spectra of Covellite (CuS), chalcocite(Cu_2S) and Galena (PbS)

For both galena and covellite Karr [15] reports no absorption for these two minerals, so we are surprised when we observe some weak bands for galena at 529 and 216 cm^{-1}. But this cannot be confirmed as originating from galena, as in literature it is listed as being without absorption bands. The bands from anglesite are observed at higher wavenumber and the bands from the litharge impurity are expected at 478(m), 355(m,sh) and 300(s,br) cm^{-1} (in transmission). We cannot confirm that the bands observed in the spectrum of galena really originate from galena, the bands however, do not appear to come from the impurities present. When observing galena in transmission in PE we observe weak bands at 476 and 153 cm^{-1}. These bands cannot come from the same compound as we know from theory that when going from transmission to ATR we expect the same or a lower wavenumber position, not a higher wavenumber.

Thus we conclude the bands observed in the spectrum of galena is a mystery, most probably coming from an unknown impurity, and covellite and chalcocite as minerals without significant IR absorption.

5.3.5 BLUE PIGMENTS

There are no blue oxides or sulphide pigments in our standard library database. Instead we show here two of the most easily recognisable pigments; Prussian blue and azurite. Prussian blue comes in many variants known as Prussian blue (PB) analogues, we compare our PB analogue, called milori blue, to those listed in literature. Mineral azurite is here compared both to literature but also to the mineral malachite, as they are both copper carbonates.

5.3.5.1 PRUSSIAN BLUE

Prussian blue has the dubious honour of being the first artificial pigment in history of pigments. It was first invented in Berlin in 1704 by Diesbach, but very quickly the alkaline pigment spread all over Europe, which is evident in the many names giving to it i.e. Berlin blue, Paris blue, Antwerp blue, Chinese blue, Milori blue etc [90]. Normal Prussian blue is an almost blue black pigment, although if it is co-precipitated with zinc it has a lighter shade (and is often called Antwerp blue), and when it is prepared with an bleaching oxidizing agent it has a reddish coppery lustre [90]. Thus, it is a blue pigment with many possible colour shades dependent on production receipts.

The general formula for Prussian blue is $Fe(NH_4)Fe(CN)_6$, xH_2O but it comes in many different analogues, dependent on the producer of the pigment. They come as single complexes or double complexes. The single complexes has the general formula $M_2[M^1(CN_6)]$, while the double complexes has the general formula $M_3[M^1(CN_6)]_2$ where M is Fe^{3+}, Ni^{2+}, Co^{2+}, Zn^{2+}, Cd^{2+}, and M^1 is Fe^{2+} or Fe^{3+}.

From the works of Ghosh [91] (reprinted in *Table 5.7*) collected of Prussian blue analogues in transmission, we know that single complexes generally have the C-N stretching vibration under 2100 cm^{-1}, and the Fe-C-N bending vibration in the range 530-470 cm^{-1}. For double complexes the CN stretching vibration is usually split in two, one below 2200 cm^{-1} and one just below 2100 cm^{-1}, while the Fe-C-N bending vibration is observed in the range 450-430 cm^{-1}. Thus it is possible in most case to detect whether the analogue is a single or double complex when applying IR spectroscopy.

Table 5.7: List of IR frequencies of Prussian Blue anlogues collected in transmission (2200-70 cm^{-1}) reprinted from Ghosh [91], compared with our Milori blue standard from Kremer, collected in ATR mode.

PB Analogs	ν(CN)	ν(FeC)	δ(FeCN)	δ (CFeC), lattice etc
$Co_2[Fe(CN)_6]$	2081(s,br)	596(s), 555(w)	476(sh), 461(m)	249(s), 234(s), 200(s)
$Co_3[Fe(CN)_6]_2$	2118(s,br)	593(w), 537(m)	434(m)	212(s)
$Cu_2[Fe(CN)_6]$	2095(m,br)	595(m)	494(m)	262(m,br), 214(w)
$Cu_3[Fe(CN)_6]_2$	2177(s,br), 2101(m,br)	545(s,br)	444(s,br)	242(m,br), 212(w)
$Ni_2[Fe(CN)_6]$	2096(m,br)	596(m)	476(m)	256(s), 223(s)
$Ni_3[Fe(CN)_6]_2$	2171(s,br), 2105(m,br)	550(w)	440(s)	248(s), 186(w)
$Zn_2[Fe(CN)_6]$	2100(m)	603(s,br)	527(w), 492(m,br), 476(w)	210(m)
$Zn_3[Fe(CN)_6]_2$	2188(m), 2167(m), 2100(w)	592(w), 544(s,br)	430(s,br)	206(s,br), 196(sh), 174(m)
$Cd_2[Fe(CN)_6]$	2062(s,br)	594(s)	500(w), 444(s)	234(m), 174(m)
Prussian blue	2080(s,br)	599(m,br)	512(sh), 494(s,br)	250(s,br)
Turnbull's blue	2083(s,br)	598(m,br)	512(sh), 498(s,br)	250(s,br)
Berlin's green	2172(m,br), 2083(s,br)	598(m,br), 550(m,br)	508(s,br), 445(w,br)	250(s,br)
Milori blue ATR	2063(s,br)	602(m)	510(m,sh), 491(s,br), 479(s,sh)	254(m,sh), 219(s,br)

As a peculiarity the FeC stretching band observed at approximately 600 cm^{-1} is strong in our spectrum (both in transmission and ATR). According to Wilde [92] this band is strong if the Prussian blue pigment comes from the soluble part of the Prussian blue synthesis, while the insoluble part of the Prussian blue synthesis only has a very weak band at ~600 cm^{-1}. The soluble part has a higher percentage of $KFe(CN)_6$ present in the matrix. One could thus speculate that the ~600 cm^{-1} band is from the K-Fe-C bending vibration and not from the Fe-C bending vibration as stated in Ghosh [91].

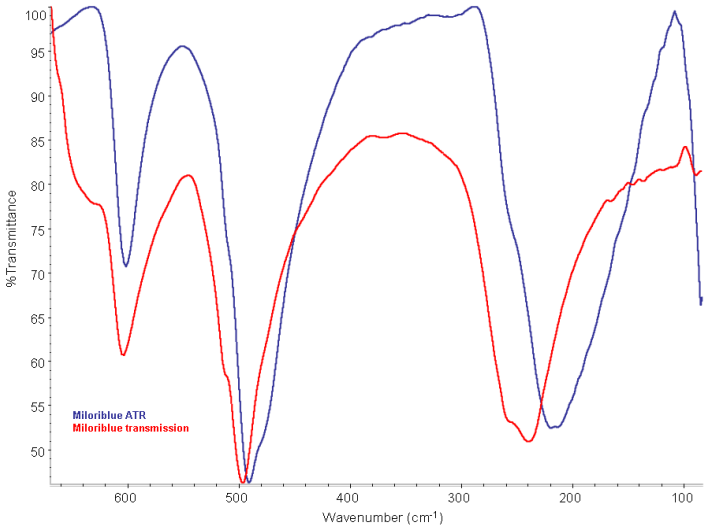

Figure 5.12: Spectra of miloriblue from Kremer Pigmente collected in ATR (blue) and transmission (red) mode.

Our standard Prussian blue comes from Kremer and is called Milori blue. The observed spectrum of milori blue collected in ATR mode correspond very well to the Prussian and Turnbull blue analogues (which is assumed identical based on [92] despite different production receipts), indicating that our Milori blue was produced in a similar manner. The expected spectral differences between transmission and ATR mode for strong absorbing bands are observed for the δ C-Fe-C bending and lattice vibrations below 300 cm^{-1} .

5.3.5.2 AZURITE AND MALACHITE

Azurite ($Cu_3(CO_3)_2(OH)_2$) and malachite ($Cu_2CO_3(OH)_2$) are probably the two most often used mineral pigments. Azurite is a blue mineral, while malachite is green, but their chemical formulas are very similar. They are both copper carbonates with monoclinic crystal system, azurite has 2 formula units in one crystal cell, while malachite has 4 molecular units in its crystal cell. They are in nature very often found together in the same mines, the minerals very often contain impurities and inclusions unique for the areas where they are found..

Our minerals comes by courtesy of the geological museum at the University of Bologna, who have also conducted powder XRD analysis to confirm their purity. Azurite is found to be 98% pure and malachite 95%. We also have both azurite and malachite from all the suppliers mentioned in ***Table 5.1***, some are synthetic produced under names such as bremer blue (azurite) or have even been synthetic precipitated by the students of our M2ADL lab (malachite). But the minerals by courtesy of the geological museum are the only one to have been verified for purity by powder XRD analysis, thus these are the ones we compare with literature.

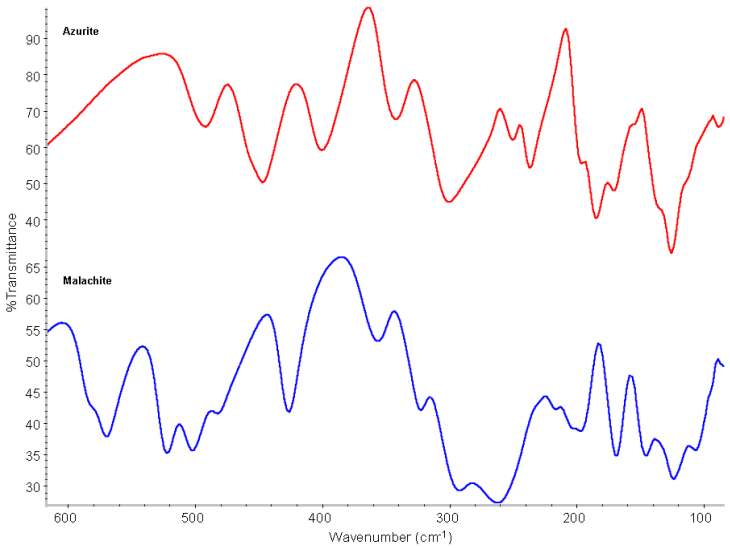

Figure 5.13: ATR FIR spectra of azurite (red) and malachite (blue).

Table 5.8: List of band positions for azurite and Malachite from literature [75, 93] compared to our minerals collected in transmission and ATR

Azurite					**Malachite**				
Assignm. [75, 93]	**Frost [93]**	**Farmer [75]**	**Trans**	**ATR**	**Assignment [75, 93]**	**Frost [93]**	**Farmer [75]**	**Trans**	**ATR**
OH stretch	3559				OH stretch	3504		3499	3480
OH stretch	3424	3425	3424	3424	OH stretch	3409	3400	3404	3399
OH stretch	3422				OH stretch	3325	3320	3313	3311
OH stretch			3358	3351	$\nu_1 + \nu_4$			1805	1806
OH stretch	3271							1603	
			2553	2552	ν_3 B_2	1519 1491	1500	1498	1498
$\nu_1 + \nu_3$	2530				ν_3 A_1	1420 1388	1400	1419 1390	1423 1383
			2498	2497	ν_1	1096	1095	1097	1096
$\nu_1 + \nu_3$	2414						1045	1048	1044
			1881	1857			875	873	868
$\nu_1 + \nu_4$	1860				ν_2 symm	821	820	821	818
			1832	1834	ν_2 anti sym	804	803		
2 ν_2	1670							776	775
ν_3 A_1	1445	1490	1493 1465	1486 1462	ν_4 B_2	750	748	749	748
ν_3 B_2	1415	1415	1414	1403	ν_4 A_1	712	710	710	711
ν_1	1088	1090	1090	1090	Cu-O stretch	580	580	583	582
		1035			Cu-O stretch	570	570	571	570
		952	953	949	Cu-OH stretch	528	528		
ν_2 anti sym	836	837	837	830	Cu-OH stretch	522	522	523	522
ν_2 symm	816	817	815	814	Cu-O stretch		505	504	502
ν_4 B_2	762	769	767	768	Cu-OH stretch		485	485	482
ν_4 A_1	754	747	743	739	Cu-X stretch	428	425	429	427
Cu-O stretch	494	495	495	492	Cu-X stretch	418	418		
Cu-OH stretch	459	455	457	447				356	357
Cu-O stretch	397	400	404	401	Cu-X stretch	337	337		
Cu-OH stretch		345	346	342	Cu-OH bend	325	325	326	323
	317				Cu-OH bend		295	299	292
O-Cu-OH bend	306	305	308	300	Cu-OH bend	278	278	272	262
	256		253	250				-	216
	251				OH-Cu-X	206	206	206	203
O-Cu-OH bend	235	240	240	237				195	197
	225				O-Cu-X	176	176	172	169
	218				OH-Cu-X	152	152	150	145
	209					142			
Oop bend	199	194	199	197	O-Cu-X	132	132	128	124
	188		189	184				107	106
	179							91	93
Oop bend	172	179	172	170					
			-	154					
		140	140	135					
		128	130	125					
			-	119					
			90	88					

In the MIR region the main vibrations observed are the carbonate vibrations, but due to both pigments having the heavy copper incorporated, we observe many vibration bands in the FIR

region, originating from Cu-O, Cu-OH, O-Cu-OH stretching and bending vibrations, together with lattice vibrations, which can be seen in *Figure 5.13*, recorded in ATR mode.

Frost [93] and Farmer [75] have both listed wavenumber frequencies for these two minerals, both in the MIR and FIR region collected in transmission mode. We have collected spectra of azurite and malachite in both transmission and ATR mode, and we observe only few differences. The main differences is in intensities of the bands, the wavenumbers are almost identical. *Table 5.8* lists the band positions for azurite and malachite from Frost [93] and Farmer [75] in transmission and our minerals in transmission and ATR.

There is great congruency between both Farmer [75], Frost [93] and our minerals, but small differences are noticed. These discrepancies probably originating from small impurities incorporated into the mineral structure. The differences observed between Frost [93] and us can be explained by the source of the minerals being different and these differences are what we observe in the MIR and FIR region. The source of Farmer's minerals are not reported in [75].

Table 5.9: Source of minerals Frost [93], Farmer [75] and us.

	Azurite	**Malachite**
Farmer [75]	Unknown	Unknown
Frost [93]	Tsumeb mine, Namibia, Africa	Broken Hill mine, Australia
Our source	Chessy, France	Katang, Zaire (Congo)

One could speculate that the FIR region could be used to determine the source of mines by analysing the incorporated impurities that are observed in the FIR region. However, more knowledge about impurities together with petrological information from several mines are needed in order to confirm such supposition.

5.3.6 RED PIGMENTS

Four red pigments are shown here, which are of interest for the FIR region. Minium (Pb_3O_4), Hematite (Fe_2O_3), cuprite (Cu_2O) and cinnabar (HgS). Both the minium and hematite comes from Zecchi, the cuprite is supplied by the Geological Museum, University of Bologna and the cinnabar comes from various suppliers that will be discussed in the cinnabar subsection.

5.3.6.1 MINIUM

Minium, also known as red lead (Pb_3O_4), is a toxic pigment used since the ancient Roman period. *Figure 5.14* shows the pigment collected in transmission mode in PE and on powder in ATR mode.

The bands observed in transmission are in good agreement with both Afremow [14], Nyquist [74], and McDevitt [76], although we observe small shifts of 2-10 cm^{-1}, which can be explained by differences in particle size or impurity present in our standard. Afremow's [14] minium is listed as being 97% pure, with 3% PbO impurity (a natural impurity from the calcination preparation). We also observe bands which could originate from lead carbonate bands at 1397 and 678 cm^{-1} when collecting in ATR mode, similar bands are observed by Nyquist [74]. They are however, very weak bands, which come from an impurity. Miniums own bands are strong and they are all observed below 600 cm^{-1}, as can be seen from ***Table 5.10***, which list all the frequencies.

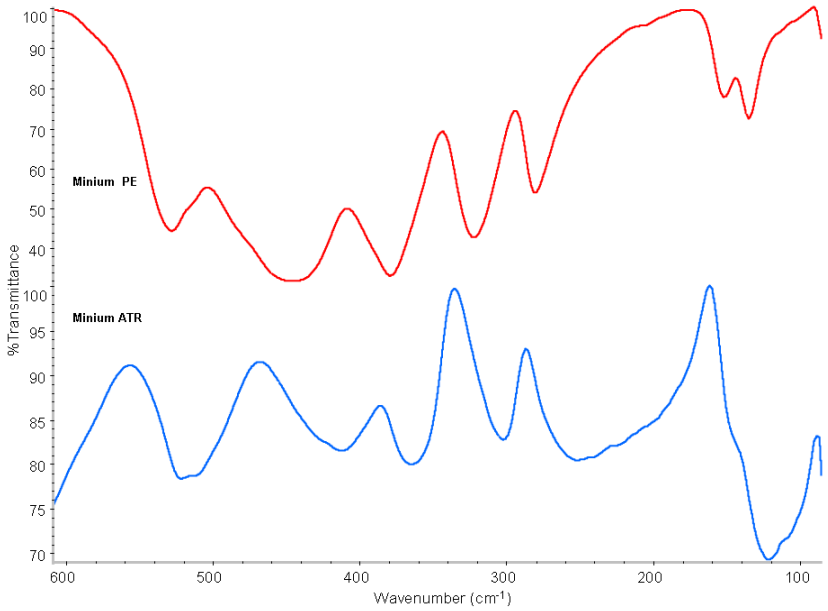

Figure 5.14: FIR spectra of minium collected in transmission (red) and ATR (blue).

In the ATR spectrum of minium we observe the bands appear to be 'broad nosed' and not sharp, which could indicate excess amount of powder has been placed on the ATR crystal. We compare our ATR spectrum with that of Vahur [32], who reports minium mixed with linseed oil (1:1 ratio) as having bands at 528, 454, 381, 328 and 280 cm^{-1}. This is very close to the ones observed in transmission. The differences observed in out spectra between collection in transmission and in ATR mide (shifts within 5-30 cm^{-1}) must then be caused by excess powder on the crystal.

Table 5.10: List of vibration frequencies for minium as reported in litrature by Nyquist [74], McDevitt [76] and Afremow [14] and recorded in transmission in PE and on powder by ATR mode.

Nyquist [74]	McDevitt [76]	Afremow [14]	Transmission/PE	Vahur [32] ATR	ATR on powder
1400(vw)	-	-	-		1397(vw,br)
-	-	-	-		991(vw,br)
720(vw)					
680(vw)	-	-	-		678(vw,sh)
660(vw)	650(w)	-	-		-
530(s)	**525(s)**	**531(s)**	**528(m)**	**528(s)**	**522(s)**
	-	515(vw, sh)	514(w,sh)		510(s)
455(s)	**445(s)**	**456(s)**	**447(s,br)**	**454(s)**	**413(m)**
380(s)	**380(s)**	**384(s)**	**380(s)**	**381(s)**	**365(s)**
325(s)	**320(m)**	**332(m)**	**323(s)**	**328(s)**	**302(m)**
283(m)	-	**293(w)**	**281(m)**	**280(s)**	**252(s,vbr)**
230(w,sh)	-	-	206(vw)		-
154(m)	-	-	152(m)		146(m,sh)
137(m)	-	-	**135(m)**		**122(s)**
	-	-	-		107(s,sh)

When comparing our observed vibrations of minium with those listed in literature we must conclude our standard contain minium and it is reasonable pure.

5.3.6.2 HEMATITE

Hematite (Fe_2O_3) is one of the most common red pigment applied in Cultural Heritage objects, right from the early days of cave and rock paintings, to the renaissance in frescoes and paintings, up to present day in ceramics, concrete, bricks, glass and painting. Hematite is part of a very large family known as the iron oxides, listed in *Table 5.11*. The iron oxides cover a wide range of colours, yellow, green, red, brown and black with a multitude of hues. They are non-toxic and as pigments they have many popular attributes. They are exceptionally stable, non-fading and highly resistant to acids and alkalis and can therefore be exposed to outdoor conditions, i.e. rock painting [94].

Table 5.11: The iron oxides, reprinted from [94].

Oxide–hydroxides and hydroxides	*Oxides*
Goethite α-FeOOH	Hematite α-Fe_2O_3
Lepidocrocite γ-FeOOH	Magnetite Fe_3O_4 ($Fe^{II}Fe^{III}_2O_4$)
Akaganéite β-FeOOH	Maghemite γ-Fe_2O_3
Schwertmannite $Fe_{16}O_{16}(OH)_y(SO_4)_z \cdot n\ H_2O$	β-Fe_2O_3
δ-FeOOH	ε-Fe_2O_3
Feroxyhyte δ′-FeOOH	Wüstite FeO
High pressure FeOOH	
Ferrihydrite $Fe_5HO_8 \cdot 4\ H_2O$	
Bernalite $Fe(OH)_3$	
$Fe(OH)_2$	
Green Rusts $Fe^{III}_x Fe^{II}_y (OH)_{3x+2y-z} (A^-)_z$; $A^- = Cl^-$; ½ SO_4^{2-}	

In almost every corner of the world, the Sahara, central Australia, South Africa, southern France, northern Spain and along the Silk road, evidence of age-old cultures can be witnessed by cave and rock paintings. In prehistoric times the hematite pigment, mainly in earth and ochre form, was applied to the cave wall without previous treatment. About 2000 BC sintering of the raw ochre and earth pigment was well established and had resulted in an amazing tonality range of yellow, brown, red and black colours all containing iron oxides in various form [94].

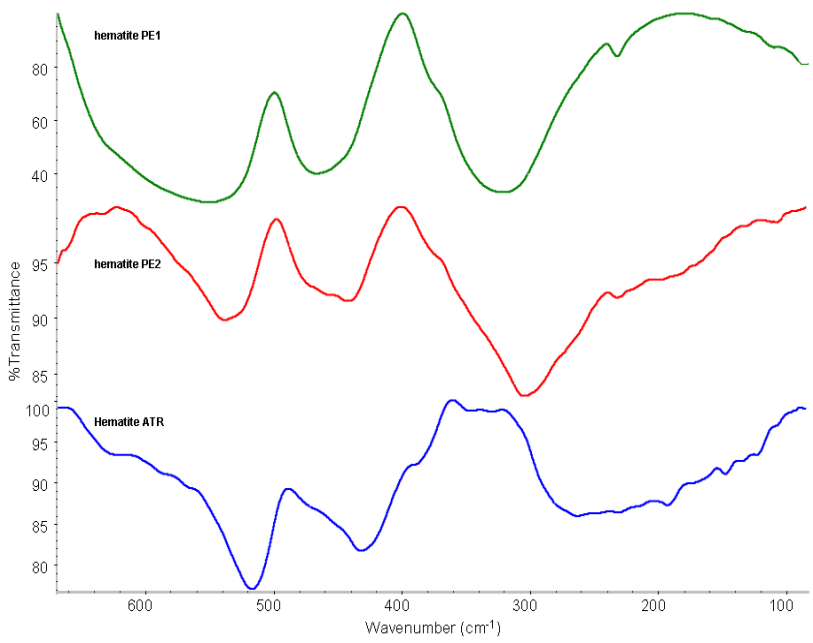

Lat_{vib} [66]	PE1	PE2	ATR
A_{2u}	-	657	-
	627	-	623
	-	569	-
	551	-	**-**
E_u	-	**538**	**517**
	467	465	-
E_u	-	**442**	**432**
A_{2u}	373	371	387
E_u	**320**	**304**	-
	-	**-**	**263**
E_u	232	232	231
	-	-	192
	-	-	147

Figure 5.15: FIR Spectra of Hematite from Zecchi. Hematite 1 and 2 have been collected in PE in transmission mode, while hematite ATR, has been collected on the hematite powder in ATR mode. The vibrations are listed in the table, with assignment of lattice vibrations after [66], and with the strongest vibrations marked in bold.

Figure 5.15 shows the FIR spectra of hematite collected in transmission and ATR spectroscopy. The table in *Figure 5.15* lists the observed wavenumbers and the lattice vibrations for D^6_{3d} symmetry as assigned by [66]. In the two transmission spectra we see quite clearly that there is a significant difference in shape, intensity and band shifts when comparing high (PE1) and low (PE2) hematite concentration in the PE pellet. PE1 has probably also been ground too much since we also notice loss of definition in the spectrum, i.e. the shoulder bands that we observe in PE2 are not present in PE1. Hematite spectra collected in ATR mode again show the expected difference compared to a transmission spectrum, noticeable in shift of bands, intensity differences and asymmetric band shape (most noticeable in the broad band at 263 cm^{-1}). Vahur [32] reports ATR spectra of red pigments containing hematite (mixed with linseed oil in 1:1 ratio) but none of them are pure compounds. They are pompei red, red earth, reddish caput mortuum and venetian red pigments with silicate clay material, gypsum and other minerals as reported impurities. Their band

positions are therefore not discussed here, but they are similar to our collected ATR spectrum, with observed shifts of 5-10 cm^{-1}.

This particular hematite comes from our pigment supplier Zecchi. From Raman analysis of this pigment we know that it is very pure, only a small amount (2-5 %) of amorphous carbon is present as an impurity.

Still the bands of hematite observed in our FIR region can vary a great deal depending on particle size, temperature, amount of grinding and how the hematite was produced. *Table 5.12* lists 9 other synthetic hematite standards compared to PE1 and PE2. They have all been collected by transmission spectroscopy. As can be observed the three strongest bands of hematite can shift over a large range, depending on temperature, particle size, and starting product for the synthesis. These observations of hematite spectra leads to the conclusion that a hematite standard as such do quite simply not exist. The average band values for hematite can be calculated to 550 ± 24.5, 459 ± 19 and 324 ± 26 cm^{-1}, based on the band values listed in *Table 5.12* from our IR bands and literature [66, 95]. Karr [15] reports the frequency range for 10 hematite minerals, which are listed in the end of *Table 5.12*. Here we observe much less fluctuation in the band values than between the synthetic produced hematite.

Table 5.12: list of the three strongest bands for hematite as reported in literature [66, 95] compared to PE1 and PE2. All samples have been collected in transmission.

Sample	Band (cm^{-1})	Band (cm^{-1})	Band (cm^{-1})	Comments	ref
H1-1	571	469	339	Heating synth maghemite 650°C for 3 H	[95]
H1-2	534	451	306	Heating synth goethite 320°C for 3 H	[95]
H2-1	565	473	342	Ferrihydrite precipitated	[95]
H3-1	574	478	352	Ferrihydrite precipitated	[95]
A(600°C)	525	440	300	Heating goethite at 600°C	[66]
B(700°C)	530	442	305	Heating goethite at 700°C	[66]
C(800°C)	530	450	318	Heating goethite at 800°C	[66]
D(950°C)	540	470	335	Heating goethite at 950°C	[66]
E(prolonged grinding)	560	470	342	Heating goethite at 950°C + prolonged grinding	[66]
PE1	551	467	320	Heating of hematite + PE in hot (180°C) anvil die + higher concentration than PE2 + prolonged grinding.	
PE2	569	442	304	Heating of hematite + PE in hot (180°C) anvil die	
Average Fe_2O_3	**550 ± 24.5**	**459 ± 19**	**324 ± 26**	Expected band region of synthetic produced hematite	
10 minerals	**550-540**	**471-469**	**333**	Frequency range of 10 hematite minerals	[15]

Idealised hematite (Fe_2O_3) has hexagonal (rhombohedral) structure, similar to corundum (Al_2O_3) structure. In red ochre sources hematite can have small amount of iron substituted with aluminium in the crystal structure. This can also cause bands shifts in the spectra of hematite as well as cause the tonality of hematite to become lighter with increased aluminium substitution [95].

5.3.6.3 CUPRITE

Cuprite (Cu2O) is a very common red corrosion product formed on archaeological copper or bronze objects. As a mineral it has a very beautiful deep red colour and is thus very recognisable on metal objects. The green malachite is an equally common copper corrosion product formed on bronze objects.

In *Figure 5.16* we show three ATR spectra. One of the mineral cuprite, one of the mineral malachite and one is a mixture of the two in a 1:1 ratio. Both minerals have been analysed by powder XRD analysis, where we learn that cuprite is pure and malachite is 95% pure with approximately 5% impurity coming from hematite and cuprite. The ATR spectrum of cuprite has two strong bands at 603 and 143 cm^{-1} [96, 97]. Also a 1^{st} order maxima band is observed at 663 cm^{-1}. Smaller and very weak shoulder bands are observed at 516, 484 and 433 cm^{-1}.

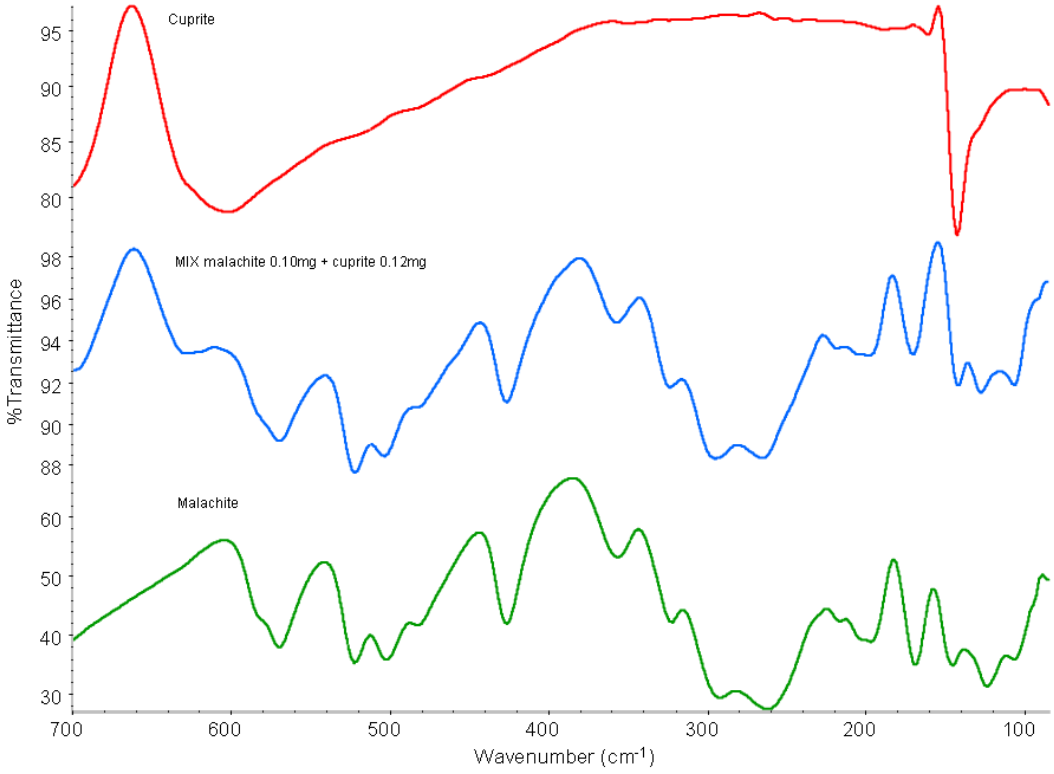

Figure 5.16: FIR spectra of mineral cuprite (red), mineral mixture of 0.12 mg cuprite and 0.10 mg malachite (blue) and mineral malachite (green). Collected on powder in ATR mode.

In *Figure 5.16* we observe what happens to the cuprite band at 146 cm^{-1} in a mixture with malachite. It is quite clear that in a mixture with malachite it will be difficult to confirm the

presence of cuprite, were it not for the band at 603 cm^{-1} and the 1st order maxima band at 663 cm^{-1}. Without it we could not positively confirm the presence of cuprite, as the sharp cuprite band expected at 146 cm^{-1} has disappeared completely. The same 1st order maxima band is observed in a transmission spectrum collected by Afremow [14] for a 97% pure cuprite at 680 cm^{-1}, with bands observed at 626 (s, br) and 425 (w, sh) cm^{-1} (no bands collected under 200 cm^{-1}). Cuprite transmission spectrum collected by Nyquist [74] observe no 'maxima' band but they collect many bands, the two strongest are at 620 and 147 cm^{-1}, with many weak broad bands at 520, 430, 340, 250 and 85 cm^{-1}.

As 1st order maxima bands are a function of particle size, this band cannot be expected to appear in a more coarse sample of cuprite, which basically means that finding cuprite in a mixture with malachite could be difficult.

5.3.6.4 CINNABAR

One of the pigments that we are particular interested in investigating in the FIR region is the red cinnabar, which historically is one of the most important in painting history, right from Early Chinese bone inscription (2000 B.C.) to Egyptian Fayum painting and Roman wall painting (1-3 century A.D.) to the Italian medieval and renaissance ages (Bellini, Titian & Botticelli) [98]. When the pigment source comes from nature the general custom is to name it cinnabar (mineral name), when the pigment has been synthesized it is generally called vermillion [98].

Cinnabar, which has the chemical formula HgS, is nowadays considered unhealthy and is almost impossibly to buy without proper authorization. It is therefore also difficult for modern painters to purchase the pigment. In the old days (before health restrictions) the only restrictions on the purchase of a pigment was financial restrictions. Cinnabar is historically one of the most expensive pigments (together with Lapis Lazuli) and also one of the pigments attributed most symbolic status. Every man (with money) could afford to commission a painting from a artist but only the very rich and very powerful could afford to have the painter use cinnabar and lapis lazuli.

Identification of cinnabar cannot be performed by IR in the normal MIR range, as HgS like CdS, does not have active bands in this region. But it has active bands in the Far-IR region and therefore we should be able to identify it using ATR or transmission FIR spectroscopy.

Table 5.13: List of 4 different Cinnabar standards and their sources.

Cinnabar Pigment		**Source**
A	Cinnabar, id no 10625	Kremer Pigmente GmbH & Co. KG, Germany
B	Cinnabar, Chinabox no 17	Xi'an Marked, China
C	Cinnabar, Imperiale Scuro (Lot no 42809)	Unknown Source, **nicknamed 'Imperiale'**, from Italy
D	Cinaprino, Dark	Phase (Prodotti per il Restauro), Italy

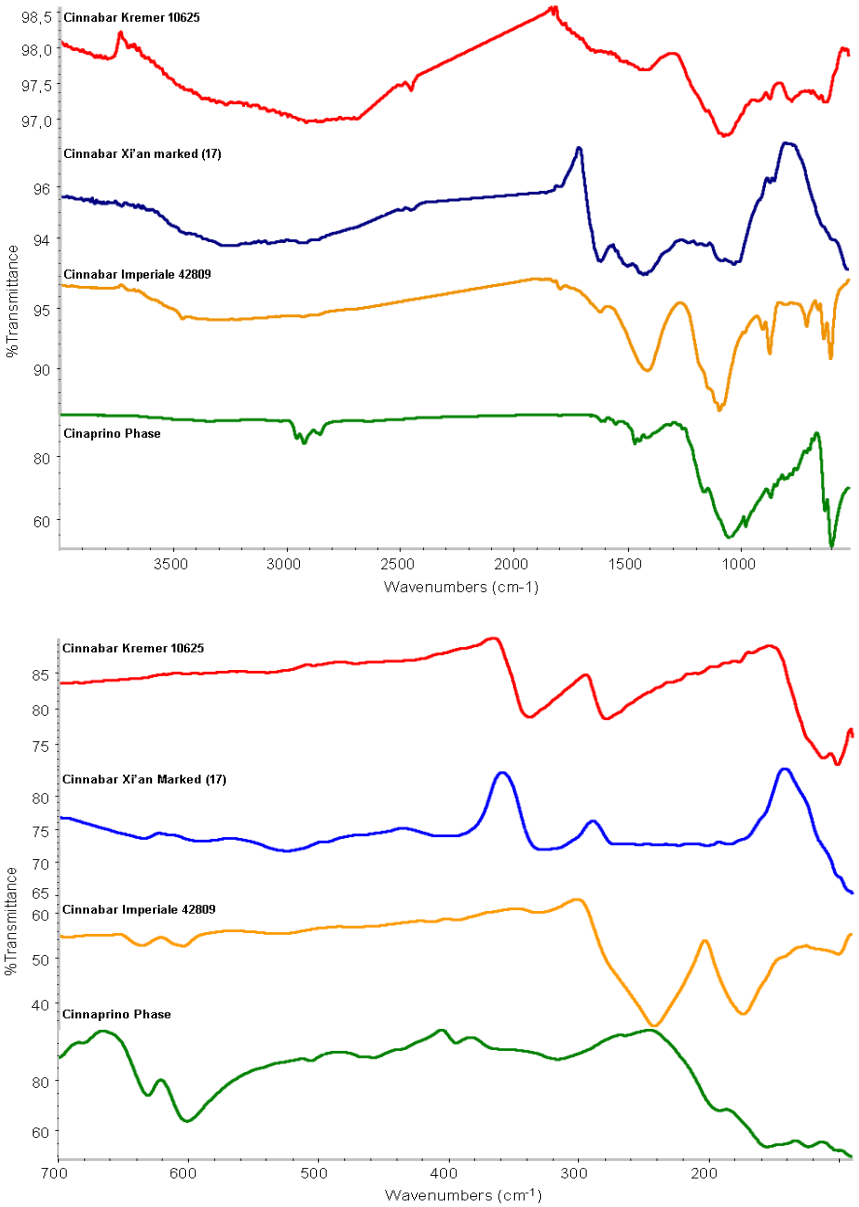

Figure 5.17: ATR MIR and FIR spectra collected of 4 different cinnabar pigments coming from A) Kremer Pigmente 10625 (Germany), B) Xi'an Marked (China), C) 'Imperiale' (Italy), and D) Phase (Italy).

In our laboratory we have three cinnabar standards from different suppliers and one Italian cinnabar-like pigment called cinaprino. Table 5.13 list the sources of the 4 cinnabar standards of which we have collected ATR spectra (MIR and FIR region) for our library database.

When looking at the ATR spectra of the 4 cinnabar standards, it quickly becomes clear that the 4 standards are not identical to one another. In the MIR region the 4th standard (cinaprino) is the only one with strong bands. Here, we also observe organic bands (CH-stretching region 3000-2800 cm^{-1} and CH-bending region 1600-1400 cm^{-1}). These bands do not have strong absorbance, which makes us conclude it is only present in a small amount. But the bands present at 1100-1000 cm^{-1} are strong and could be assigned to a sulphate compound.

The other three standards have only very weak bands in the MIR region, which means either that we are looking at overtone bands or that we observe small impurities in the standards. All three have relatively strong bands in the FIR region.

In the FIR region we observe only few bands. We observe similarities between the Kremer cinnabar and the cinnabar purchased on the Xi'an marked, although also band broadening caused by too much powder on the ATR crystal is observed. The Kremer cinnabar and the 'Imperiale' cinnabar both have two strong bands in the FIR region but the bands have shifted 100 cm^{-1} to lower wavenumber. The fourth spectrum also have two strong bands but shifted to a higher frequency than the cinnabar of Kremer or Xi'an marked.

As a curiosity when we compare the 'Imperiale' cinnabar with spectra in our FIR library we have a 90% congruency with standard Cadmium Red pigment APR 6626. This means that 'Imperiale' is a fake cinnabar sold to artists as cinnabar, probably due to the 'health' restrictions on sale of real cinnabar (although cadmium also cannot be considered healthy).

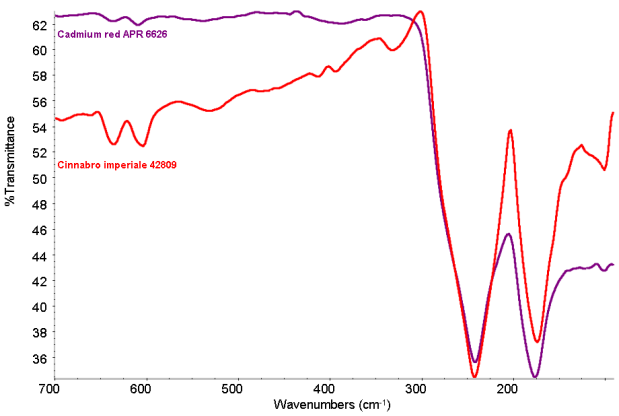

Figure 5.18: Library comparison between cinnabar 'Imperiale' and Cadmium Red no 6626 from the Artist Pigment Range (APR) of W.G. Ball Ltd.

In order to verify what is mercury and what is cadmium, we analyze the four cinnabars with our Artax X-Ray Fluorescence (XRF) instrument from Brucker with a molybdenum source. The experiments are carried out under helium atmosphere in order to observe the lighter elements (sulphur, silicium ect.). The Voltage is set for 17 kV, the current to 1200 μA with a collection time of 300 seconds collected in the range 0-50 keV for all four standards. The collected XRF spectra can be seen in Figure 5.19 and the results are listed in Table 5.14.

In two of the cinnabar standards, the one from Kremer Pigmente 10625 and the one from the Xi'an marked, we observe the presence of mercury. Both have silicium present as an impurity. However, the cinnabar from Xi'an marked also have a large impurity from titanium and calcium.

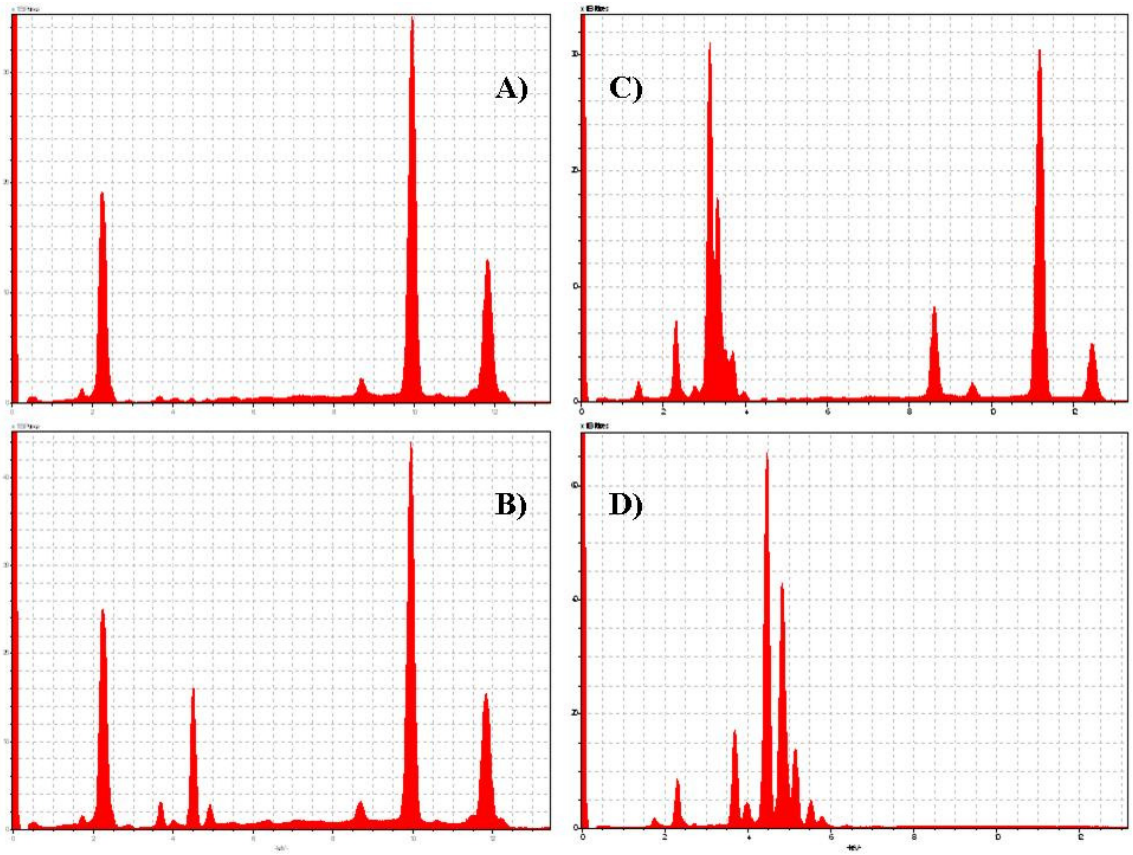

Figure 5.19: The XRF spectra of 4 cinnabar pigments sold from A) Kremer Pigmente 10625 (Germany), B) Xi'an Marked (China), C) 'Imperiale' (Italy), and D) Phase (Italy).

The 'imperiale' and cinaprino have no mercury present at all. The 'imperiale' has cadmium and selenium as the two strongest elements, while zinc and sulphur are present as secondary elements. This confirms the FIR comparison with the cadmium red pigment APR 6626 seen in *Figure 5.18*, that 'imperiale' is in reality a cadmium red pigment probably consisting of a CdS-CdSe-ZnS complex.

Table 5.14: List of the 4 cinnarbar standard and their XRF results

Cinnabar Souce	**Primary element**	**Secondary element**	**Trace element**
A) Kremer Pigmente	Hg	Si	Ca, Ba
B) Xi'an Marked (17)	Hg	Ti, Ca, Si	Fe, K,
C) 'Imperiale'	Cd,Se	Zn, S	Ba
D) Phase	Ba	S, Ca	K, Fe, Si

The cinaprino from Phase is neither a mercury nor a cadmium compound. It consist mainly of barium, but also sulphur and calcium is present, which could indicate the cinaprino is a barium

sulphate compound. This is confirmed by the vibrations observed in the MIR spectrum in *Figure 5.17*D [84].

Sulphur is only detected with certainty in the 'imperiale' and the cinaprino pigments. In the cinnabar from Kremer and Xi'an marked sulphur is not detected because the K_α-line of sulphur is covered by the strong M_α- and M_β-line of mercury. Organic components cannot be detected by XRF analysis.

The spectra of cinnabar from Kremer have also been collected in transmission mode, both embedded in PE and applied on a thin film (commercial PETF), and in both spectra we observe the three main features at 346, 284, 125 (129 for the PETF) and 87 cm^{-1}, which is in accordance with published literature [28, 74, 97, 98]. The observed bands are assigned to E (246, 284, 87 cm^{-1}) and A_2 (125 cm^{-1}) symmetries according to [28]. However, in the PETF spectra we also observe a broad band at 494 cm^{-1}, which is not from cinnabar (or the impurities). It is suspected to be a false band signal, possible a reflection of the smooth and glossy surface of the commercial PETF.

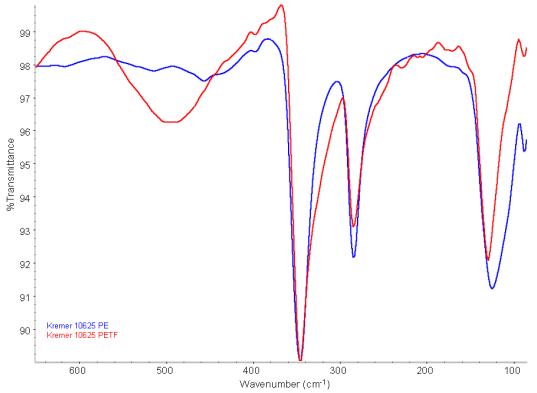

Figure 5.20: FIR spectra of cinnabar collected in transmission mode embedded in PE and applied on a PETF.

In ATR we observe the bands of cinnabar (from Kremer) at 338(m), 279(m), 125(m,sh), 112(s), 101(s) and 86(s) cm^{-1}, which can be seen in *Figure 5.17*. The bands observed in ATR by Vahur [32] reports cinnabar (mixed with linseed oil 1:1 ratio) as having bands at 342 and 284 cm^{-1}. This is in good agreement with our observed bands and are also very close to the wavenumbers observed in transmission. In transmission we only observe the band at 125 cm^{-1}, while in ATR we observe this splitting into three bands at 125, 112 and 101 cm^{-1}. The splitting of the band is also observed in [28]. We know from chapter 4 that the amount of cinnabar placed on the ATR crystal is very important, which is why we observe the broadening of the cinnabar from the Xi'an marked in *Figure 5.17*, where there is too much powder on the ATR crystal.

CHAPTER 6 PRELIMINARY TESTS: COMPARATIVE STUDIES

6.1 BINDING MEDIA

An experiment is conducted in order to determine the influence of binding media in the FIR region. First, spectra are collected of pure binding media in the MIR and FIR region in ATR mode on binding media which has dried on microscopic glass plates for more than a year. Next we collect spectra of binding media mixed with pigment in order to observe if the binding media is visible in the FIR region.

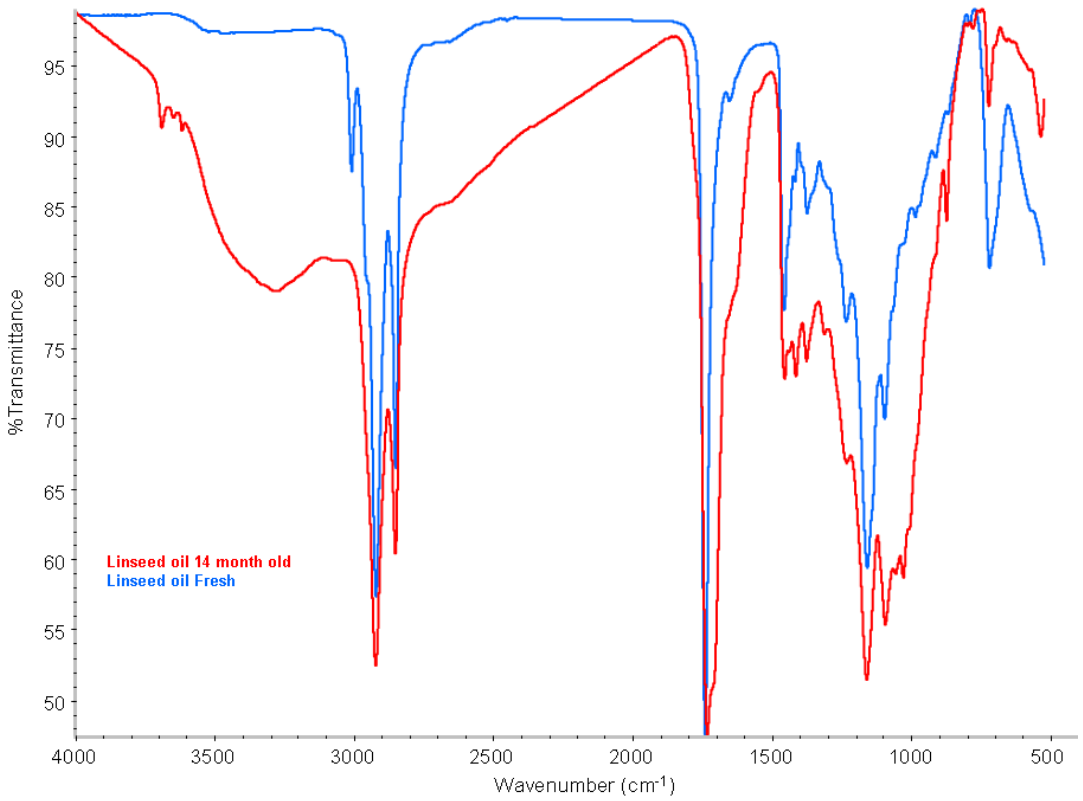

Figure 6.1: ATR MIR spectra of fresh (blue) and 14 month dry (red) linseed oil.

In order to collect the spectra of binding media, several standard binding media, as listed in *Table 6.1*, are prepared by the M2ADL students according to [90, 99] by applying the binding medium on a microscopic glass plate and leaving it to dry. The reason for leaving it to dry is the obvious that there are major differences between fresh and dry binding media, as can be observed in *Figure 6.1*. Note especially how the extreme sharp ester band at 1739 cm^{-1} becomes more broad as the acid is formed, which is visible in the 14 month old oil by the shoulder band at 1714 cm^{-1}. Note also that OH-stretching is formed in the dry oil while the alkene CH-stretching vibration at 3008 cm^{-1} has disappeared from the fresh oil as the C=C bonds are hydrolysed during drying.

Table 6.1: list of binding media subjected to IR spectroscopy, which have been applied on a microscopic glass plate and left to dry for more than 1 year.

Binding media	**Source/surplier**	**Date of application**
Linseed oil	Zecchi colori e belle arti, via dello Studio 19r, 50122 Firenze, Italy	05.12.2007
Tung oil	Xi'an marked (China)	18.03.2004
Rabbit glue	Unknown	22.02.2008
Fish glue	l'ARTISTICA	22.02.2008
Egg white tempera	Local supermarket	23.11.2007
Egg yolk tempera	Local supermarket	23.11.2007

The minimum time for drying is 1 year for our binding media, before collecting the spectra in ATR mode in both MIR and FIR region, which can be seen in *Figure 6.2*. Wavenumbers for all binding media are listed in *Table 6.2* collected in ATR mode.

Table 6.2: List of wavenumbers (cm^1) for binding media, linseed oil, tung oil, egg tempera (white and red), fish and rabbit glue, collected in ATR mode.

Linseed oil 05.12.2007	**Tung oil 18.03.2004**	**Tempera egg red 23.11.2007**	**Tempera egg white 23.11.2007**	**Fish glue 22.02.2008**	**Rabbit glue 22.02.2008**
3400(w,br)	3400(w,br)	3281(m,br)	3284(m,br)	**3248(s,br)**	**3272(s,br)**
2924(s)	**2954(m,sh)**	3007(m)	3067(m)	**3068(s,br)**	3070(m,br)
2853(m)	**2916(s)**	2952(m)	2955(m)	**2978(s,br)**	2935(m,br)
1734(s)	**2849(s)**	**2921(vs)**	**2922(vs)**	2873(m,sh)	2872(m,sh)
1714(s,sh)	**1731(s,sh)**	**2851(s)**	**2852(s)**	2651(m,sh)	2652(m,sh)
1629(m,sh)	**1704(s)**	**1741(s)**	**1742(s)**	1627(vs)	**1626(s)**
1457(m)	1629(m,sh)	**1632(s)**	**1636(s)**	**1538(s)**	**1520(s)**
1414(m)	1460(m)	1539(m)	1538(m)	**1443(s)**	**1445(s)**
1376(m)	1412(m)	1458(m)	1455(m)	**1405(s)**	1403(m,sh)
1235(s,sh)	1378(m)	1416(m)	1415(m)	1337(m)	1332(m)
1151(s)	1235(m,sh)	1400(m)		1236(m)	1235(m)
1094(s)	**1164(s)**	1379(m)	1378(m)	1202(m)	1169(m)
978(s)	**1094(s)**	1233(m)	1231(m)	**1077(s)**	1080(m)
874(m)	975(s)	**1161(s)**	**1161(s)**	1030(m,sh)	1029(m)
723(m)	875(m)	**1088(s)**	**1084(s)**	975(m)	980(w,sh)
579(w)	723(m)	**1063(s)**	**1062(s)**	874(w)	873(w)
537(m,br)	579(w)	970(m)	970(m)		633(w)
466(m)	547(w,br)	874(w)	874(w)	595(vw)	587(vw)
432(m,sh)	**492(m)**	824(w)	824(w)	548(w,sh)	547(w,sh)
398(w)	**463(m,sh)**	719(m)	718(w)	**523(w,br)**	**526(m,br)**
360(w,sh)	427(w,sh)	**695(m,sh)**	697(w)		503(w,sh)
340(m,sh)	397(w)	580(w)	632(w,br)	467(w)	466(w,br)
312(s,br)	**314(m,br)**	500(w,br)	578(m,sh)		430(vw)
276(m,sh)	275(m)	**454(m,br)**	**522(m,br)**	401(vw)	400(w)
228(m)	254(m)	427(sh)	463(m,sh)	**333(m,sh)**	**329(m,br)**
103(s)	229(m)	**391(m)**	425(w,sh)	**303(m,br)**	**306(m,br)**
91(s)	148(w)	260(m,br)	**311(w,br)**		
	101(m,sh)	235(m,br)	224(m,sh)		
	89(s)	210(m,br)	192(m,sh)		
		181(m,br)	**144(s,br)**		
		150(m,br)	125(m,sh)		
		132(m,br)	**114(s)**		

The content of oil is a mixture of triglyceride esters, which contains both saturated and unsaturated acids. The acids present in the oil depends on the source of the oil, i.e. linseed oil contains stearic, ($C_{17}H_{35}COOH$), palmitic ($C_{15}H_{31}COOH$) and arachidic ($C_{19}H_{39}COOH$), oleic ($C_{17}H_{33}COOH$), linolic ($C_{17}H_{31}COOH$) and linolenic ($C_{17}H_{29}COOH$) acids in varying amount, while tung oil instead of linolenic acid has mainly eleostearic acid ($C_{17}H_{31}COOH$) present in the trigyceride [90, 100].

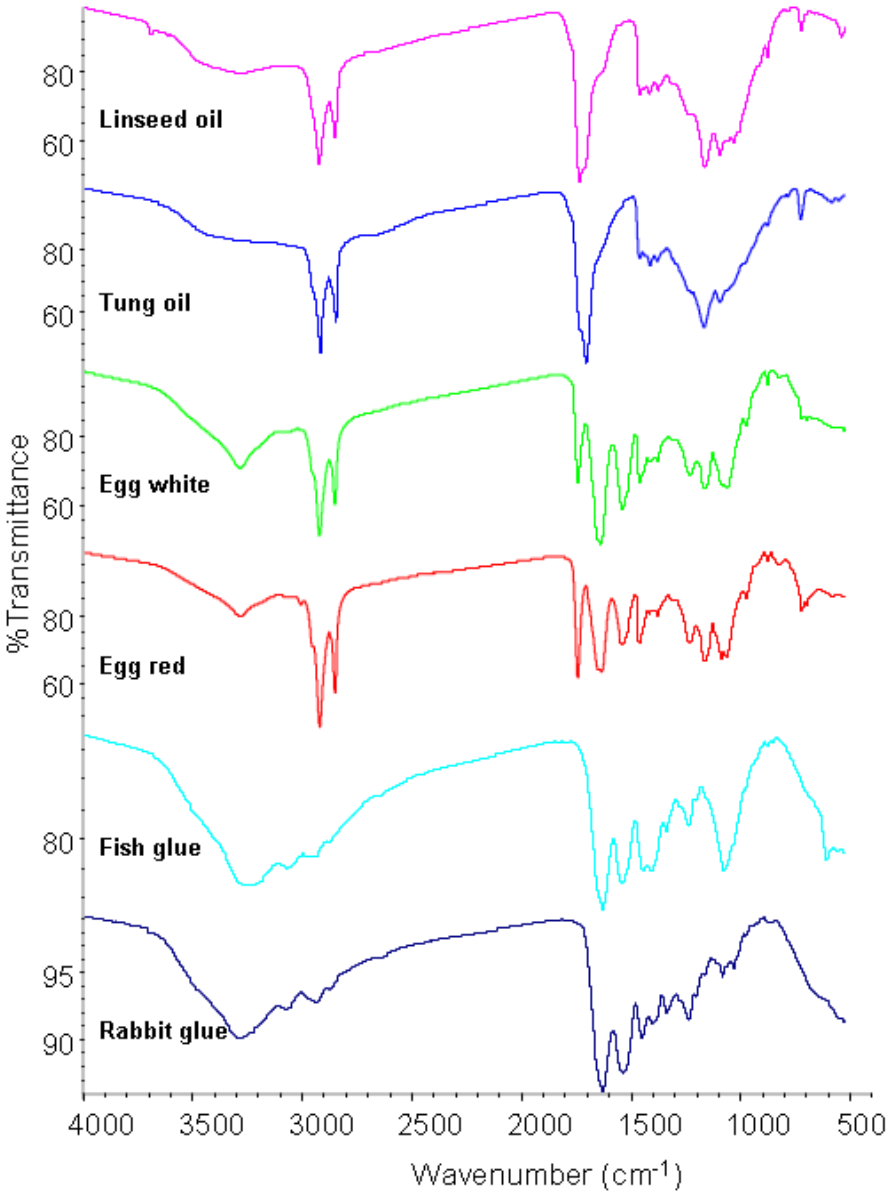

Figure 6.2: ATR MIR spectra of various binding media, linseed oil, tung oil, egg white, egg (yolk) red, fish glue and rabbit glue.

Figure 6.3 shows the collected ATR spectra of linseed oil and tung oil. In the MIR region we observe the only difference between the linseed and tung oil is the intensity of the C=O stretching

vibration region for the ester C=O vibration and the acid C=O vibration [40, 101]. For the linseed oil, the bands observed are at 1734(s) and 1714(s,sh) cm^{-1}, while for the tung oil it is 1731 (s,sh) and 1704(s) cm^{-1}, the intensity of these two bands are reverse. The bands collected of linseed oil in ATR mode are in good congruency with the ones reported in literature for transmission [102] with only small shift 5-10 cm^{-1} observed between the two methods.

The ester and acid bands observed in the oils confirms that tung oil contains more acid after 4½ years of drying, while the linseed oil still contains more ester after only 1 year of drying. One year of drying the binding media is thus not enough for comparison with i.e. binding media in old 1400 century master pieces.

In the FIR spectra of linseed and tung oil in *Figure 6.3* we observe quite specific band vibrations for the linseed oil indicating something inorganic, while for the tung oil the bands appear more to our expectations, as very weak and undefined bands. This difference can perhaps be explained by the small percentage of added salt in linseed oil, which should speed up the drying. Gettens [90] writes that it is normal to add both lead, manganese and cobalt salts (0.1-0.3%) in linseed oil, which could explain the significantly different FIR spectra observed between the two types of oil. Upon collecting the spectrum of fresh linseed oil a second time (not shown), the linseed oil in the FIR region looks very similar to that of tung oil, with very weak and undefined bands, not inorganic components seems to be present. The only difference this time is the band at 495 cm^{-1} observed in tung oil. This band is not observed in linseed oil.

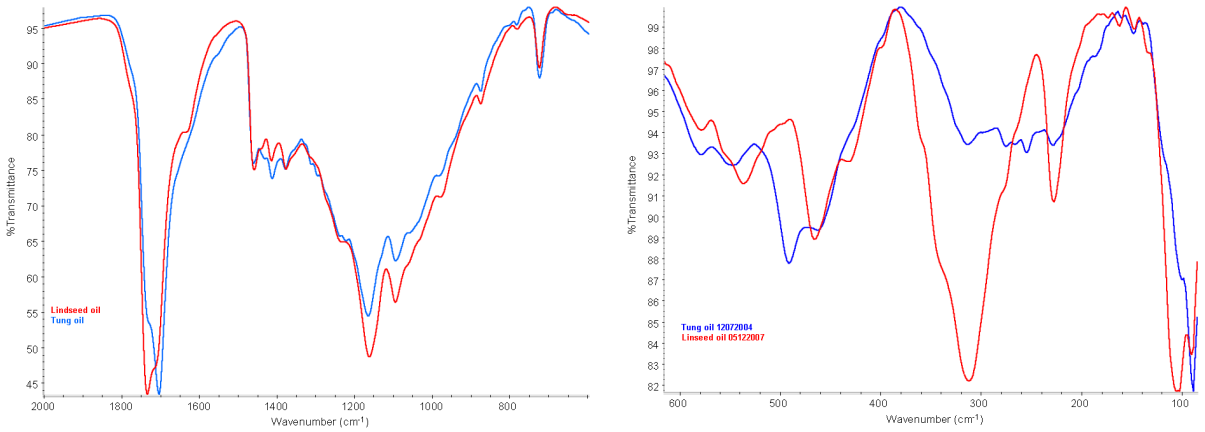

Figure 6.3: ATR MIR and FIR spectra of linseed oil (red) and tung oil (blue). By the time of ATR collection the linseed oil has dryed for 14 month, the tung oil for 4½ years on microscope glass.

In order to collect a spectrum in the FIR region of the binding media it is sometimes necessary to scratch the thin binding media film off the microscope glass. When collecting direct on the thin film while it is still on the microscope glass, we accidentally record the spectrum of the microscope glass together with that of the binding media. This is due to the refractive index of the thin film of

the binding media (n_i ~1.4-1.5) [90], which is very close to the refractive index of the ATR crystal (n_{diam} = 2.4). When the refractive index of the binding media is close to that of the ATR crystal, it facilitates higher penetration into the thin film than intended. The IR beam penetrates from 2.3 µm at 500 cm^{-1} to 12.3 µm at 90 cm^{-1} into the thin film, see chapter 2, Figure 2.11. This is occasionally more than the thickness of the thin film layer applied on the microscope glass. Scratching the thin film off the microscope glass is however not necessary when there are pigment mixed with the binding media, since the presence of the pigment makes the paint layer much thicker and thus we do not observe the microscope glass when we collect the spectra direct on the paint layer on the microscope glass.

Glue contains proteins mainly made from animal gelatin, *Table 6.2* lists the wavenumber frequencies for rabbit and fish glue, both have very similar bands throughout the IR region. Egg tempera can be made from both egg white and egg yolk, they both have similar bands in the MIR region but distinct differences are observed in the FIR region, caused by the differences in proteins and lipids present in the egg white and egg yolk.

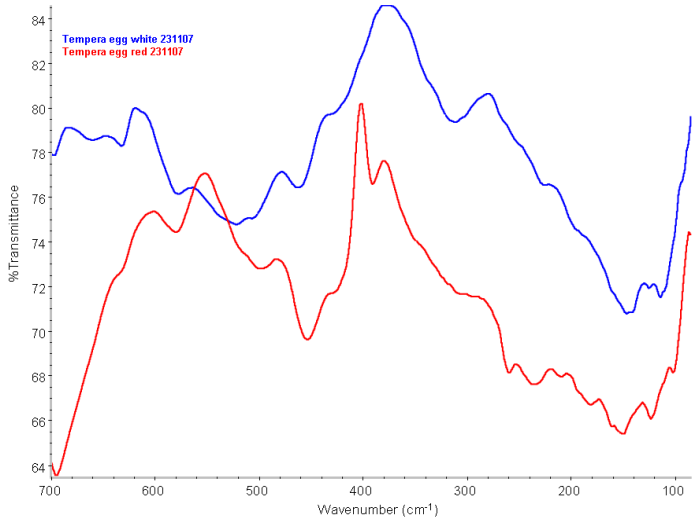

Figure 6.4: ATR FIR spectra of egg white and egg yolk.

So by merely collecting ATR spectra of oil, tempera and glue one should think that distinguishing between the binding media would be easy. In the MIR region this is a distinct possibility but in the FIR region the intensities of the binding media are generally weak. Remembering that most binding media are only present in small amounts in painting, it could be a problem observing binding media in the FIR region when the intensities are already weak, in a pigment-binder mixture where the binding media is only present in low concentrations.

Several standard pigments mixed with binding media have been prepared and applied on microscope glass plate by the students of M2ADL. The preliminary test is to ascertain if we observe the binding media in the FIR region in the test mixtures. We known that binding media in the MIR region can be observed since the binding media has strong bands in this region, but do the binding media interfere with interpretation in the FIR region. *Figure 6.5* show the malachite-tempera interaction collected in the MIR and FIR region directly on the microscope glass plate.

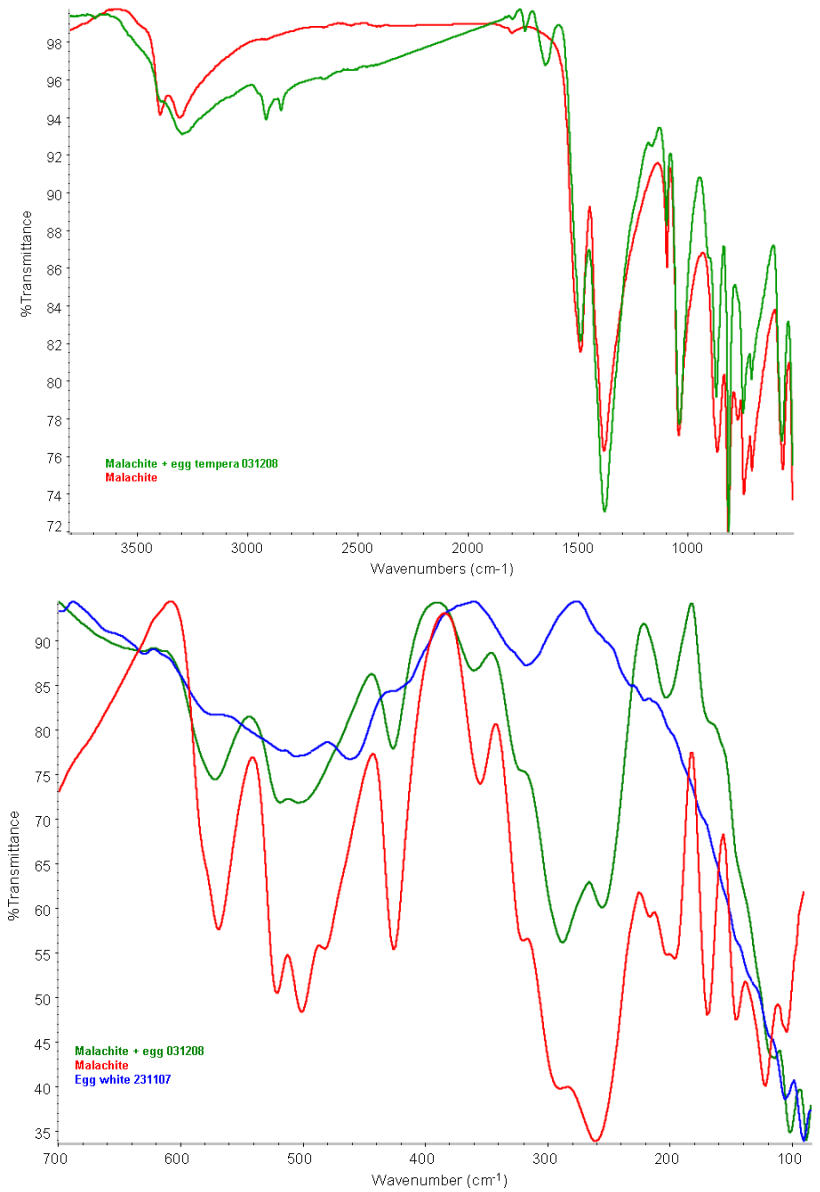

Figure 6.5: ATR MIR and FIR spectra of malachite (red), egg white (blue) and a mixture of malachite and egg tempera (green).

In the MIR region we observe vibrations originating from both malachite and egg tempera, but the bands originating from egg tempera are quite weak compared to the intense bands coming from

malachite. The bands originating from egg tempera are observed in the OH, NH and CH stretching region and the C=O and C=C stretching vibrations at 1742 and 1632 cm^{-1}, but no bands from the binding media is observed lower, due to the relatively intense bands coming from the malachite pigment.

As suspected in the FIR region, when egg tempera is mixed with malachite, we do not observe specific bands originating from egg tempera. We only observe bands coming from the malachite standard. However, we notice a band broadening of malachite bands. Below 200 cm^{-1}, where egg tempera has a beginning cut-off, the lattice vibrations we should be seeing from malachite have lost their definition and have become weak and almost disappeared.

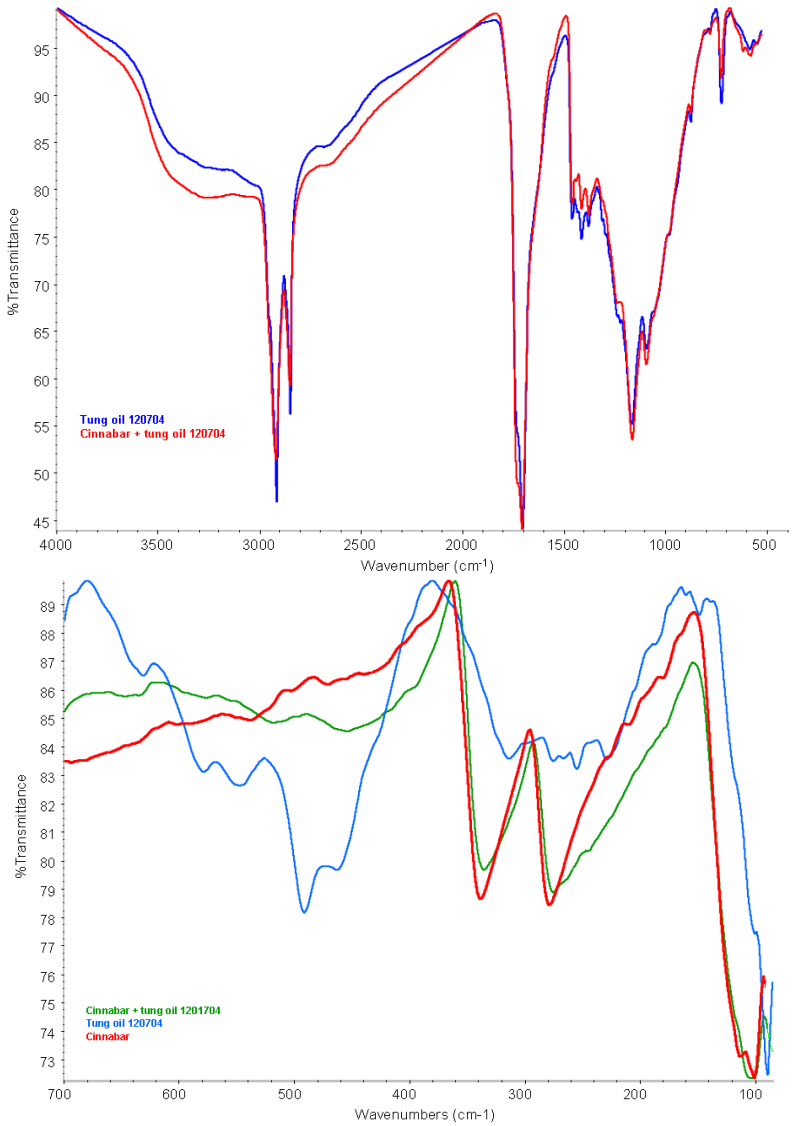

Figure 6.6: ATR spectra of cinnabar, tung oil, and cinnabar with tung oil as binding media (dry 4½ year).

Figure 6.6 shows the cinnabar-tung oil interaction. In the MIR region we observe only the presence of the tung oil This is not surprising since cinnabar has no absorption is this region. The

situation is opposite in the FIR region. Here we observe the cinnabar quite clearly with no bands present from the tung oil. We do, however, observe a broadening of cinnabar bands, which could be caused by the oil or too high concentration of cinnabar on the ATR crystal.

We must conclude that the MIR region is excellent for determining organic binding media. But in the FIR region we do not observe the organic binding media when combined with an inorganic pigment. This is due to the relatively weak bands coming from the organic binding media in the FIR region. Small band broadening effects are observed.

6.2 THE M2ADL DIDACTIC TEST TABLETS

From the preliminary test of binding media in the FIR region previously we known to expect band broadening in the FIR region, but no bands from the binding media is expected. To further explore the pigment-binder interaction in the FIR region we move from paint on microscopic glass plate to paint on test samples. At the same time we explore methods of sampling when collecting in transmission and ATR spectroscopy. For transmission spectroscopy we sample our test tablets for embedding in PE. The same PE pellets are then collected normally and by testing them in our new beam condenser. This means collecting spectra on a smaller sampling area. We also test the pigment-binder interaction on lab-made PETF. In ATR we test surface contact, as well as testing enhancing the depth of penetration with a water droplet. We also compare surface contact with micro sampling.

Figure 6.7: A selection of some of the M2ADL didactic tablets used by the students to practice micro sampling techniques.

The chosen test samples for further testing of the pigment-binder interaction are the M2ADL didactic tablet. They are mainly used for teaching students of this University department how to

perform micro sampling techniques as well as micro chemical tests. The M2ADL tablets was originally made by the teaching staff but has over the years been supplied with new tablets made by the more experienced students. The tablets are anywhere between 5 months and 5 years old and vary in length between 1 cm and 12 cm long.

6.2.1 THE M2ADL TABLET EXPERIMENTS

The tablets, whose schematic cross-section can be seen in *Figure 6.8*, have a stone base of approximately 1 cm calcareous stone (Maastricht stone), a thick layer of gypsum (bound with glue) followed by a thin layer of animal glue (rabbit glue), which ensures better binding with the upper paint layer. The paint layer is made up of only one paint layer. The paint layer is a mixture of a pigment

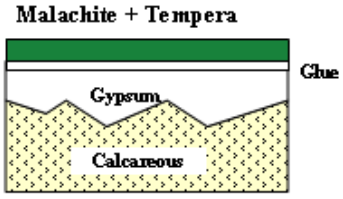

Figure 6.8: Shematic cross-section of the didactic tablets

with a binding media, which is either linseed oil, egg tempera or rabbit glue. The entire list of didactic tablet with pigment and binding medium can be seen in *Table 6.3*.

The tablets have been short named by the teaching staff according to consecutive numbers, one or two initials of the pigment name and first initial of binding medium (i.e. 4BPC, tablet no. 4 with BP Bianco di Plumbum (Italian for lead white) and C for Colla (glue in Italian).

The M2ADL tablets have been used to evaluated 6 different methods, which are listed in Table 6.4; Three methods using ATR spectroscopy and three methods using transmission spectroscopy. The purpose is to evaluate the pigment-binder interaction, to check the created databases as well as to evaluate and compare the different methods applied.

The first method applied is direct contact between the surface of the tablet and the diamond ATR Smart Orbit crystal. Imagining that the contact with the ATR crystal can sometimes be a problem due to non-planarity of the sample

Table 6.3: the list of didactic M2ADL tablets with pigments and binding media.

Sample	Pigment	Binder
0MS	Maastricht Stone (limestone)	
1G	Ground (Gypsum)	
2GC	Gypsum	Animal Glue
3OC	Yellow Ochre	Animal Glue
4BPC	Lead white	Animal Glue
5BPT	Lead white	Tempera
6BPO	Lead white	Oil
7BZT	zinc white	Tempera
8MC	Malchite	Animal Glue
9MT	Malchite	Tempera
10CT	Crysocolla	Tempera
11MIT	Minium	Tempera
12AT	Atacamite	Tempera
13CIO	Cinnabar	Oil
14MO	Malchite	Oil
15ET	Hematite	Tempera
17CIT	Cinnabar	Tempera
18OT	Yellow Ochre	Tempera
19PT	Prussian blue	Tempera
20VT	Verdigris	Tempera
21OO	Yellow Ochre	Oil
22OC	Yellow Ochre	Animal Glue
24BOT	Ultramarine Blue	Tempera

surface, the second method attempts to enhance the signal by applying a drop of water on the ATR crystal before achieving contact with the M2ADL tablet. In the third method, we have scratched powder from the surface of the tablet and examined the powder on the ATR crystal. These three methods have all been performed in the normal IR (MIR) and in the Far-IR (FIR) region covering the range 4000-525 cm^{-1} and 700-90 cm^{-1}.

Table 6.4: The 6 methods by which the M2ADL didactic tablets have been investigated.

#	Method	ATR MIR region	ATR FIR-region	Transmission FIR region
1	Surface contact	x	x	
2	Water enhanced surface contact	x	x	
3	Powder on ATR crystal	x	x	
4	Powder on PE pellet			x
5	Powder embedded in PE			x
6	Powder embedded in PE using 4xBeam Condenser			x

In the fourth method we again scratch powder from the surface of the tablets, but this time we examine the powder by brushing it on the surface of a PETF. In the fifth method we embed some scratched-off powder in a PE pellet. And finally in the sixth method, we examine the same PE pellet as in the fifth method (with embedded pigment in PE) but are analysing the PE pellet by using the 4x Beam Condenser. The beam condenser is new to our laboratory. Its purpose is to make it possible to examine a smaller area in transmission than normally. The normal area which the IR beam is investigating in transmission is 8 mm; with the use of the beam condenser this area is now reduced to 2 mm. These last three methods have only been carried out in transmission mode covering the FIR region 670-90 cm^{-1}.

6.3 RESULTS FOR THE M2ADL TABLETS

Here, a few of the spectra collected from various tablets will be reviewed and the above mentioned methods evaluated.

6.3.1 TABLET 0MS – MAASTRICHT LIMESTONE

As a curiosity we collect spectrum of the tablet stone itself, known as Maastricht limestone ($CaCO_3$). Maastricht limestone is a soft and very porous (> 40%) limestone, containing numerous large bioclasts (mainly carbonate sea shells) bound together by clear crystalline sparite cement

(carbonate > 4 µm in grain size) [103]. When applying pressure with the ATR arm the tablet stone breaks upon almost no pressure from the smart orbit arm. Thus applying pressure with the smart orbit arm must be dealt with carefully on all tablets in order not to break them.

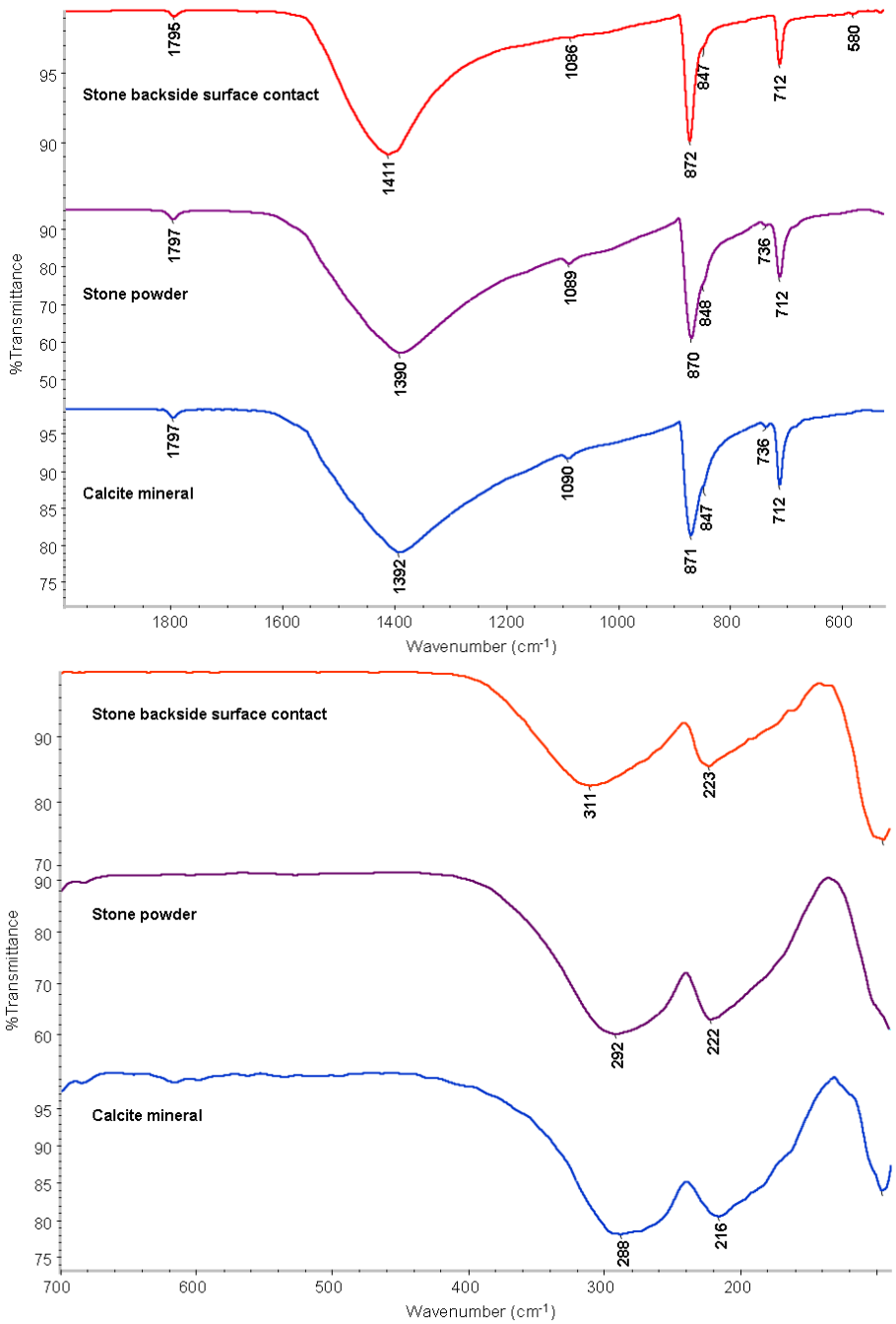

Figure 6.9: ATR spectra of 0MS, the Maastricht stone used as background for all the paint layer, direct surface contact (red) powder removed from the stone (purple) compared to mineral calcite (blue).

ATR spectra of the stone material collected while in surface contact with the ATR crystal and on powder removed from the stone is observed in *Figure 6.9*. We focus on the two bands at

approximately 1400 and 300 cm^{-1}. Shifts are observed in these two strong bands when comparing surface contact with powder removed from the stone. The bands shift from 1411 to 1390 cm^{-1} and 311 to 292 cm^{-1}. In both bands we observe a shift of about 20 cm^{-1}, which is well over the expected differences (considering spectral resolution are only 4 cm^{-1}).

Both spectra are compared to our calcite from a mineral source collected on powder on the ATR crystal. There are no differences in recording, the experimental settings and the spectral resolutions are identical. However, the only difference between these to ways of collecting is the contact ATR achieved between the stone, and the powder.

In chapter 5.3.1.1. we observed that precipitation moves vibrations to a higher wavenumber while crystallised mineral moves the same vibration to a lower wavenumber. Despite the fact that we have seemingly good contact between the crystal and the solid sample (no noise observed in the baseline) we observe a shift to lower wavenumber when examining the same sample as powder. This can only be explained by the difference in amount of pressure applied on the solid sample and the powder sample, and the fact that the solid limestone is (very) porous while the examined powder sample is just a few grains (squeezed flat between the ATR crystal and the ATR arm).

We further note that this observed shift between solid and powder happens in the exact same bands where we also observe changes between collected transmission and ATR spectra of calcite. This, ATR theory tell us, only happens in the strongest absorbing bands.

6.3.2 TABLET 2GC – GYPSUM WITH ANIMAL GLUE

When collecting directly on the surface of the tablet we achieve no signal, due to bad contact between the tablet and the ATR crystal. Therefore we try to enhance the signal with water, and we get a relatively good signal from gypsum and from water. The enhanced water contact spectrum has had the spectrum of liquid water subtracted, hoping it was possible to completely subtract the water from the sample spectrum. As can be observed in *Figure 6.10*, the water bands in the MIR region cannot be completely removed from the 2GC water enhanced spectrum. We observe only the presence of glue by one weak band at approximately 1540 cm^{-1}. No other bands from glue are observed. We notice also that a few bands shift wavenumbers, approximately to 3-5 cm^{-1} higher, when comparing the water enhanced spectrum with the powder spectrum. We observe also gypsum and glue (by the band at 1540 cm^{-1}) when examining the powder removed from 2GC, and this spectrum is naturally free of interfering water bands (but we observe the expected OH stretching vibrations from the gypsum).

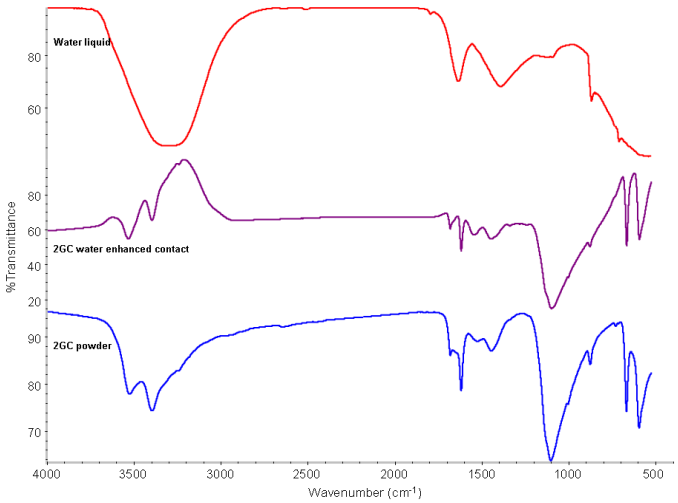

Figure 6.10: ATR MIR spectra of liquid water (red). 2GC water enhanced contact (purple) and powder removed from 2GC (blue).

6.3.3 TABLET 11MIT – MINIUM WITH EGG TEMPERA

In the ATR MIR spectra we observe tempera heavily under the influence of the strong background coming from minium, which include calcite and silicate impurities and a 1st order maxima band originating from the small particle size of the minium powder. As minium has no actual bands in this region, we do not observe minium in the MIR region.

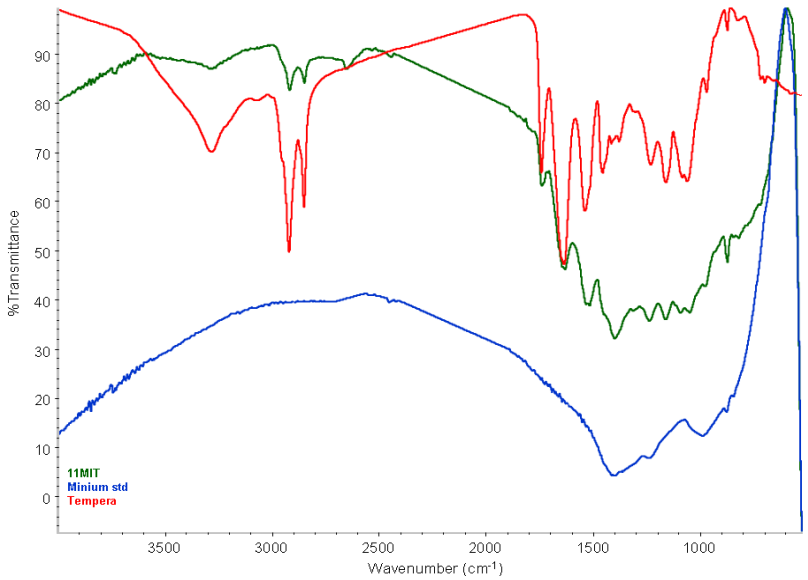

Figure 6.11: ATR MIR spectra of tablet 11MIT (green), minium standard (blue) and egg tempera (red).

When observing the 11MIT collected in ATR in *Figure 6.12* we observe many small changes. First when comparing the powder standard of minium (green) with the powder sample 11MIT (blue), we notice that 11MIT moves bands at 500 and 410 cm^{-1} to a higher wavenumber. The shift is small (2-8 cm^{-1}) but still observable, and the binding medium must be the cause of the change. When comparing the sample 11MIT powder (blue) with 11MIT surface contact (orange) we observe particular the band at 420 cm^{-1} moves to higher wavenumber and becomes visibly broader. This must be the effect of the pressure applied as observed before for the 0MS sample. When comparing the 11MIT surface contact (orange) with 11MIT water enhanced contact (red), we notice particularly the bands centred at 360 and 300 cm^{-1} shifting 5-10 cm^{-1} towards lower wavenumbers. Below 250 cm^{-1} the water enhanced spectrum has more changes from the surface contact, notice particularly the change in frequency of the 1st order maxima band. These effects must be caused by the water adding an extra element to Harrick's equation, specifically the refractive index of the sample, the ATR crystal and that of the water.

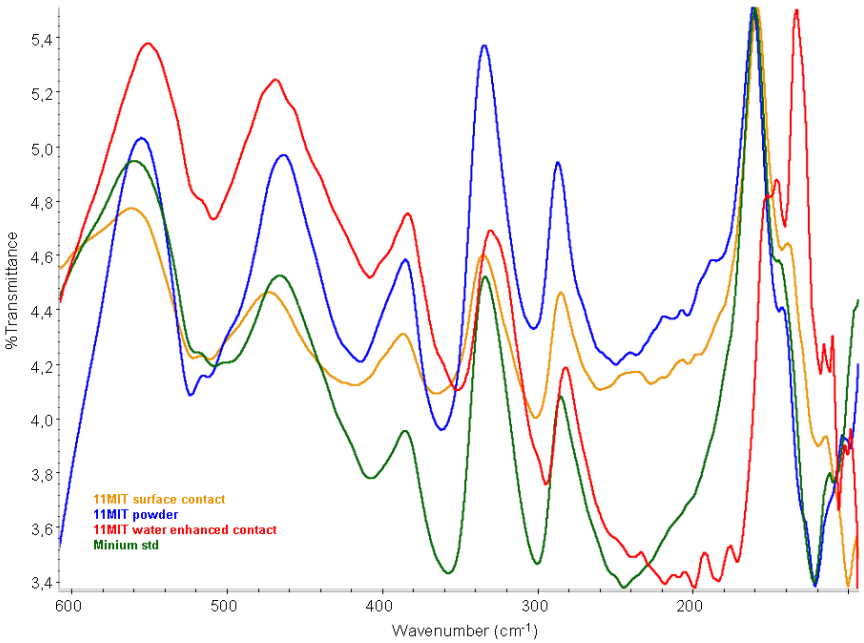

Figure 6.12: ATR FIR spectra of 11MIT collected with surface contact (orange), powder (blue), water enhanced surface contact(red) and a spectrum of the powder minium standard (green).

In the FIR region we detect no specific differences whether we collect in normal transmission mode or apply the beam condenser in transmission mode, although we notice a little more noise on the baseline when using the beam condenser. When applying the 11MIT sample on a PETF we again collect a spectrum of the smallest of particles and therefore we observe higher definition (i.e. shoulder bands are more visible) of the bands than when embedded in PE. We observe no bands

from egg tempera in the FIR transmission neither do we observe any influence from the tempera in form of band broadening or shift of bands.

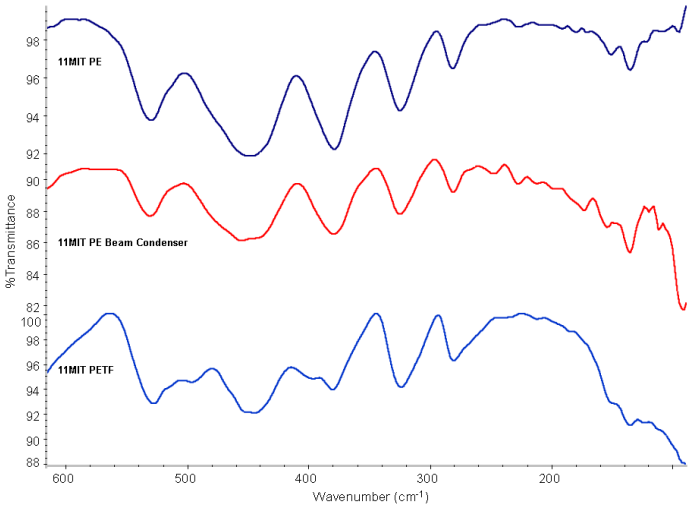

Figure 6.13: FIR transmission spectra of powder from tablet 11MIT in PE (dark blue), in PE with the beam condenser (red) and collected on PETF (ligh blue).

6.3.4 TABLET 14MO – MALACHITE WITH LINSEED OIL

In the ATR MIR region we have no problem identifying the binding medium as linseed oil and the pigment as malachite on the powder sample. When applying surface contact with the tablet we appear to have interference coming from calcite, probably due to powder from the soft tablet itself on the surface of the stone. But still we are able to collect spectra of both linseed oil and malachite.

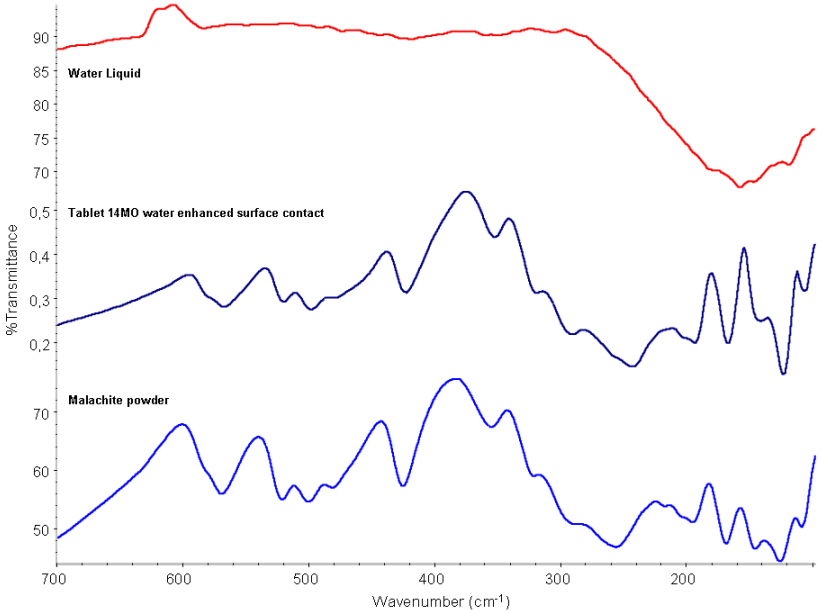

Figure 6.14: FIR spectra of water (red), tablet 14MO water enhanced surface contact (Dark blue) and malachite powder standard from Zecchi (light blue).

In the FIR region we have no problem identifying the pigment as malachite as can be observed in *Figure 6.14*. When trying to enhance the signal with water, we again observe malachite but we also notice a small shift of 14 cm^{-1} in one of the malachite bands, the band at 256 cm^{-1} moves to 242 cm^{-1}. This band is not from the binding media as we observe no other bands from the oil in the FIR region. It could be that the malachite used for the tablet is different from the 6 malachite standards present in our FIR library, see the region 340-200 cm^{-1} in *Figure 6.15*, which shows 6 malachite standards with different origins, both natural (mineral) and synthetic produced from various suppliers.

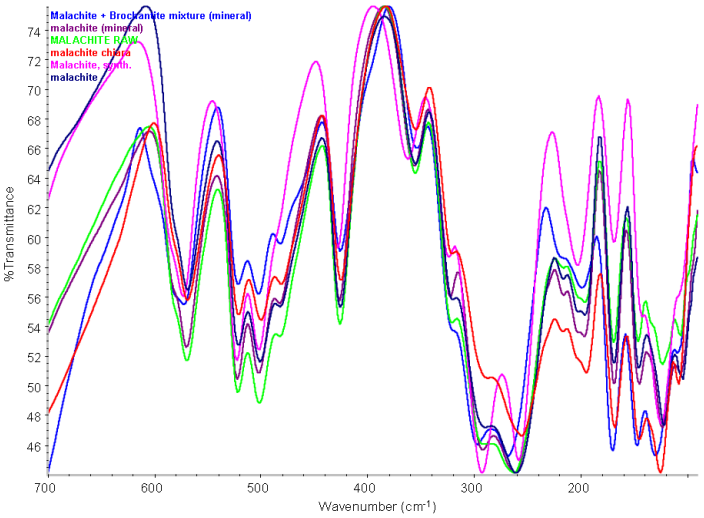

Figure 6.15: ATR FIR spectra of malachite from 6 different sources (synthetic and mineral origin), showing difference in lattice bands in the region 340-200 cm^{-1}.

6.3.5 TABLET 17CIT – CINNABAR WITH EGG TEMPERA

From chapter 5.3.5.4 we known to be alert when we talk of cinnabar, since not all standards sold as cinnabar actually contain HgS. The first examination is in the MIR region, here we observe the tablet in direct surface contact with the ATR crystal and on powder removed from the surface examined on the ATR crystal, compared to our library standard of cinnabar imperiale.

In Figure 6.16 in 17CIT, we observe the binding medium, tempera by bands observed at 1737 and 1626 cm^{-1}, together with a small amount of calcite observed by bands at 1414, 873 and 710 cm^{-1}. What appears to be silicate is observed in the spectra by strong bands at 1053 cm^{-1}. When compared to our library it matches very well with our cinnabar imperiale standard, which we discovered in section 5.3.5.4, figure 5.17, does not contain cinnabar but cadmium red with impurities from calcite and silicate.

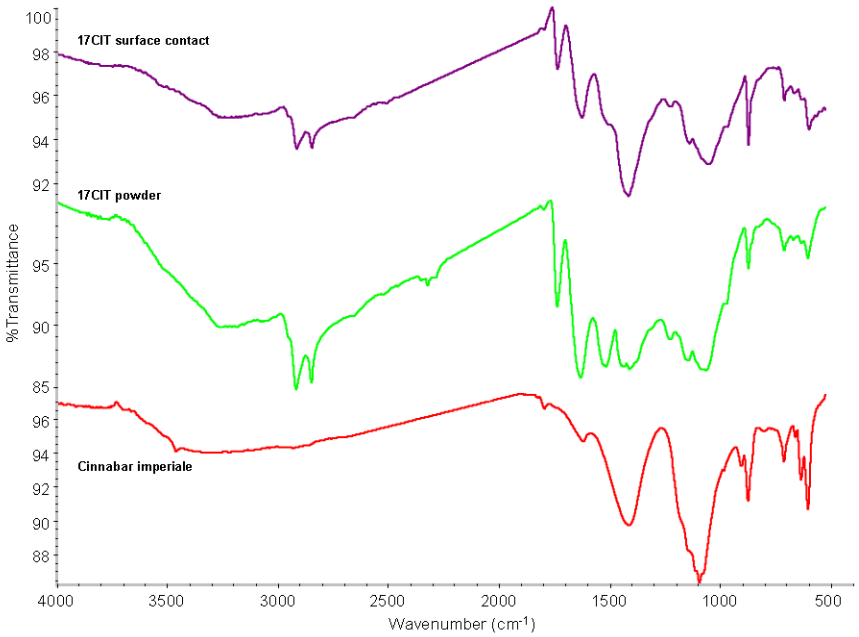

Figure 6.16: ATR MIR spectra of tablet 17CIT collected with direct surface contact (purple) and powder removed from the tablet (green), compared to cinnabar imperiale standard (red).

In the FIR region we have problems achieving good signal from the ATR crystal when performing surface contact with the sample as can be seen in *Figure 6.17*. When removing powder from the tablet we have no problems collecting a spectrum. The pigment is easily identified as cadmium red and not the expected cinnabar.

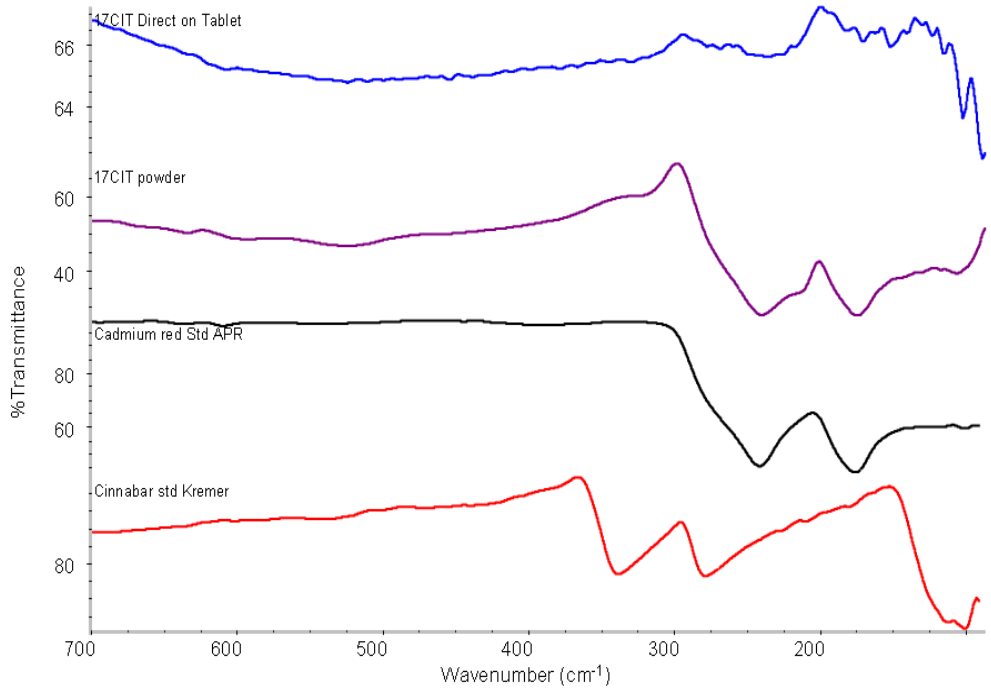

Figure 6.17: ATR FIR spectra of 17CIT surface contact (blue), 17CIT powder(purple), compared to Cadmium red (black) and cinnabar (red) from our library.

6.3.6 TABLET 19PT – PRUSSIAN BLUE WITH TEMPERA

No significant changes are observed in the spectra of 19PT whether in transmission or ATR mode, MIR or FIR region, with water enhanced contact, direct surface contact, or powder removed from the surface, embedded in PE normally or using the beam condenser or applied on PETF. The only differences observed in these spectra lie in the baselines and the amount of water vapour observed. For PETF and when using the beam condenser more water vapour was observed. Otherwise no shift or significant band broadening was observed between the methods.

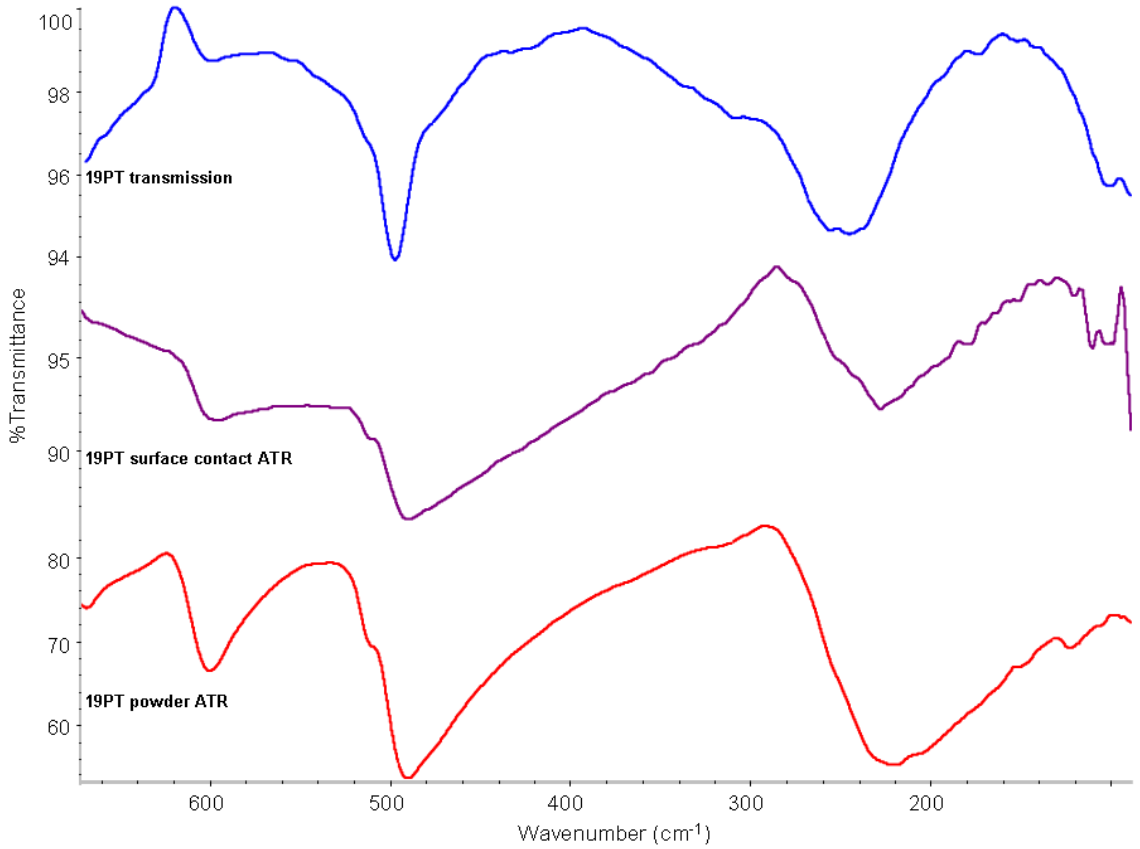

Figure 6.18: IR spectra of tablet 19PT, prusian blue with tempera, collected in transmission (blue), direct surface contact ATR (purple) and powder ATR (red).

6.3.7 TABLET 20VT - VERDIGRIS WITH TEMPERA

With Verdigris we have, in the MIR region, no problem with identifying verdigris and the binding media, egg tempera, whether we apply surface contact, water enhanced surface contact or

powder removed from the surface. In the FIR region, we have a bad surface contact where we observe a lot of noise, but are still able to identify verdigris. In ATR mode on powder removed from the surface we also have no problem identifying verdigris. But water enhanced ATR FIR works very badly due to band broadening, the actual verdigris band have very low intensity. The desired effect of water enhancing the surface penetration is here not observed. It is contemplated whether too much water was applied to the crystal before bringing the water drop in contact with the tablet, causing almost no verdigris bands to be observed, or rather they are observed but have very weak intensity and very low definition.

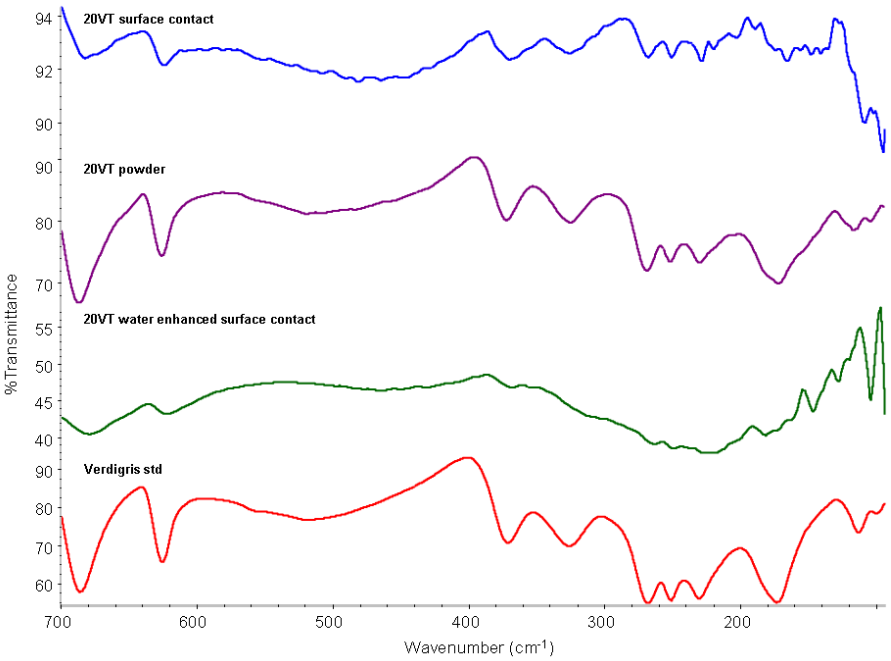

Figure 6.19:ATR FIR spectra of tablet 20VT in surface contact (blue), powder removed from the surface (purple), water enhanced surface contact (green) and verdigris powder standard (red).

In FIR transmission the PE pellet shows no bands, neither in normal transmission nor when applying the beam condenser. It is thought the pellet has to low concentration of verdigris. There is no problem with analysing the PETF in transmission mode, here we clearly observe the bands from verdigris.

6.4 DISCUSSION

In all the examined tablets we managed to identify the pigment and the binder using one or more of the 6 methods applied. In only a few case were we surprised at the result. When investigating 4BPC, we expected to find animal glue but instead found egg tempera as the binding

medium. We did not discover cinnabar in any of the two cinnabar tablets, 13CIO and 17CIT. In the case of 13CIO we found a still unidentified silicate compound, whose spectra in both MR and FIR region are almost similar to that of smalt (glass coloured blue by cobalt salts), which could possible be an ultramarine red. For 17CIT we also fail to identify cinnabar but instead we find cadmium red, which was also the case of the cinnabar 'imperiale' that was discussed previously in chapter 5.3.5.4.

Table 6.5:Results interpretation using ATR and transmission in the FIR region and ATR in the MIR region.

Sample	Pigment & Binder	ATR MIR region	ATR FIR-region	Transmission FIR region
0MS	Maastricht stone	calcite	calcite	calcite
1G	Gypsum	Gypsum	Gypsum	Gypsum
2GC	Gypsum, Glue	Glue, Gypsum	Gypsum	Gypsum
3OC	Yellow Ochre, Glue	glue, silicate	yellow ochre	yellow ochre
4BPC	*Lead white, Glue*	*Tempera*	Lead white	Lead white
5BPT	Lead white, Tempera	tempera	Lead white	Lead white
6BPO	Lead white, Oil	oil	Lead white	Lead white
7BZT	zink white, Tempera	tempera	zinc white	zinc white
8MC	Malchite, Glue	glue, malachite	malachite	malachite
9MT	Malchite, Tempera	tempera, malachite	malachite	malachite
10CT	Crysocolla, Tempera	tempera, silicate	crysocolla	crysocolla
11MIT	Minium, Tempera	tempera, 1st order maxima band	minium	minium
12AT	Atacamite, Tempera	tempera, atacamite	atacamite	atacamite
13CIO	*Cinnabre, Oil*	*linseed oil*	*? identical to smalt*	*? identical to smalt*
14MO	Malchite, Oil	linseed oil, malachite	malachite	malachite
15ET	Hematite, Tempera	tempera	hematite	hematite
17CIT	*Cinnabar, Tempera*	*tempera, calcite, silicate*	*cadmium red (imperiale)*	*cadmium red (imperiale)*
18OT	Yellow Ochre, Tempera	tempera, silicate	yellow earth	yellow earth
19PT	Prussian blue, Tempera	tempera, Prussian blue	Prussian blue	Prussian blue
20VT	Verdigris, Tempera	tempera, verdigris	verdigris	verdigris
21OO	Yellow Ochre, Oil	linseed oil, calcite, silicate	yellow ochre	yellow ochre
22OC	Yellow Ochre, Glue	glue, silicate	yellow ochre	yellow ochre
24BOT	Ultramarine Blue, Tempera	tempera, silicate (quartz-like)	ultramarine blue	ultramarine blue

Surface contact in ATR mode (MIR and FIR) sometimes fails to give any results simply because the sample is not planar enough. Occasionally we do get some signal, making it possible to identify the pigment (present in large percentage) but the signals are too weak to identify the binding media used (present in small percentage). A second consideration is the risk of destroying the sample accidentally by applying too much pressure by the smart orbit arm. This is indeed an important consideration as the stone tablets are made of a soft and porous stone material. In case the sample is a valuable piece of art, this has to be considered carefully before starting the experiments.

When analysing the collected spectra we notice that it matters *how* these collections are performed. When the ATR crystal are in contact with a solid sample or with a powder sample, it is possible to detect shifts in bands in both MIR and the FIR region, the shift from powder to solid goes towards a higher wavenumber. This would make it difficult do distinguish between similar crystal structures, like calcite and smithsonite which both have calcite crystal structure, and the difference between the two calcite structures are very small as we known from chapter 5.3.1.1.

Additionally, the binding media seem to have some influence on the FIR spectrum, causing band broadening and small shifts. But not always. This can then only be interpreted in the way that the amount of binding medium in the sample plays an important role together with the absorbing qualities of the pigment. Band broadening caused by binding media was not observed in the MIR region.

The malachite from 14MO in *Figure 6.15* shows us that differences are to be expected between crystals lattices (even in the same material) when working in the FIR region. *Figure 6.15* shows us 6 malachite standards that has different lattice vibrations in the range from 340 -200 cm^{-1}.

Using water enhanced signals is possible, but also slightly confusing, as you always have the bands from water interfering with your interpretation of the spectral bands in the MIR region. Water has no bands in the FIR region. Heavy mathematical spectral manipulation can quite possible solve this problem, but this is time-consuming (it also alters the original spectrum and hence, you loose spectral information). Also, one must take into account that water can cause discolouring of the painted surface, ring marks from were the water touched the surface, and also leave an imprint of the ATR crystal on the moist surface. The contact time between sample and water has to be as short as possible to avoid this to happen. On most of the M2ADL tablet the water marks evaporate and the discolouring seems to disappear over time. These problems do not occur with all samples and it seem very much to depend on what type of binding medium has been applied (glue seems to be the worst) but all this has to be considered when deciding to use water to enhance the ATR contact with a sample.

While conducting these experiments it has happened that the paint layer stuck to the ATR crystal when removing the stone tablet from the ATR after spectral collection. This has happen on several occasions when glue was the binding media. This also has to be considered carefully before starting experiments involving valuable artwork.

Water enhanced spectra can be an advantage when no contact is possible on the solid sample, but differences is sometimes observed in the FIR spectra. We notice differences i.e. minium, in the form of shift to lower wavenumber for the observed 1st order maxima. This is quite clearly an effect caused by the ATR theory, where we are introducing a third refractive element to Harrick's

equation (chapter 2). Normally Harrick's equation has only two refractive elements to consider, that of the sample and that of the ATR crystal, now we are introducing that of the liquid water into that equation.

In FIR transmission we observe very little changes, and those changes that we do observe have to do with the fact that we are using PE instead of PETF, where the particle sizes are mixed in PE whereas with PETF's only small particle sizes remains on the surface of PETF. This can be a serious advantage when dealing with very broad bands (Zinc white and smalt has clearly more defined bands when using PETF than when using PE). However, the experiments with the very broad bands on PETF are not yet completed.

Table 6.6: Spectral evaluation of the 6 different methods for ATR and transmission spectroscopy (4x best, 1x worst).

Method	**ATR MIR region**	**ATR FIR-region**	**Transmission FIR region**
Surface contact	xxx	xxx	
Water enhanched surface contact	xx	xx	
Powder on ATR crystal	xxxx	xxxx	
Powder on PE pellet			xxx
Powder embedded in PE			xxxx
Powder embedded in PE using 4xBeam Condenser			x

The idea of the beam condenser is to condense the IR beam on a smaller area thereby minimising the sample amount necessary by making pellets with a smaller diameter. But in practice we noticed that the signal intensity was always very low and the noise intensity equally higher compared to the normal signal intensity. Due to the way the beam condenser compartment is built (proximity of mirrors to sample holder and the lid of the sample compartment) you have a considerably higher risk of observing water bands in the FIR region than when using normal transmission or ATR in the FIR region. Every time you open the lid you let out the dry air inside, thus requiring more time for stabilising the atmosphere inside the beam condenser. The beam condenser seems to be build for MIR region investigations and not for FIR region ones, since the water vapour is not equally important in the MIR region. This has yet to be tested.

CHAPTER 7 CASE STUDIES

7.1 INTRODUCTION

Three case studies will be presented here. The samples originate from mural paintings and from corrosion products found on archaeological bronze artefacts. One case concerns just a few examinations performed in FIR transmission spectroscopy while the rest of the sampling have been performed in ATR mode, mainly because the we wanted to explore the entire region (MIR and FIR) on the same sample. In these cases only a few grains have been removed from the samples in order to collect the spectra.

7.2 ABBAZIA DEL MONTE, CESENA, ITALY

The monastery Abbazia S. Maria del Monte (Abbey Saint Mary of the mountain) in Cesena was founded in ca. 1050. In January 1337 the fundament of the monastery was damaged by earthquake, which was further seriously damaged during a second earthquake in 1768. Due to the earthquakes the monastery has been architecturally consolidated several times during the centuries. Some of the original choir was demolished and the cupola was reinforced. As part of the restorations the painter Giuseppe Milani (1716-1798) painted the cupola in 1773-74. The painting in the cupola has recently been restored.

Figure 7.1: Part of the mural painting covering the Cupola in Abbazia del Monte, Cesena, Italy, showing an 'Angel on a red cloud' with a smaller angel in green clothing turning away in the left part of the picture.

Samples from Abbazia del Monte have been investigated by FIR transmission spectroscopy by embedding in a PE pellet [18]. In this case, all the samples have with varying success been

investigated by µATR spectroscopy on cross-section (unpublished material) and we observe in these cross-sections mainly silicate material, i.e. red, yellow and green earth, calcite, and gypsum.

7.2.1 RED SAMPLE AM1

The red layer in sample AM1 observed in a cross-section by µATR investigations cannot be assigned due to penetration of the embedding polyester resin into the top layer of the sample. Only the organic embedding resin is visible. Therefore it was attempted to assign the pigment by using FIR transmission spectroscopy.

Sample AM1 is a pale red and white sample taken from a dotted area of a reddish cloud beneath the angel seen in *Figure 7.1* and seen in close-up in *Figure 7.2*.

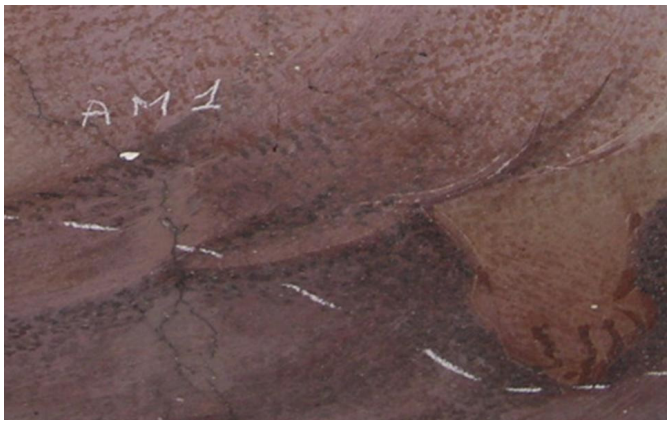

Figure 7.2: Close up of sampling area AM1'Angel on a red cloud'.

Two PE pellets were made from this sampling. It was impossible to avoid white grains when selecting the grains for pellet making so some were mixed with the red grains. AM1a was more red coloured than AM1b. Approximately 0.3-0.5 mg of sample have been used for preparation of the PE pellets.

The FIR spectra of sample AM1a and AM1b from Abbazia del Monte, together with mineral samples of calcite, quartz and hematite from Zecchi is shown in *Figure 7.3*.

The AM1a sample, the sample more red than AM1b, has bands at 540, 460, 440, 315, 227 and 103 cm^{-1}. Bands at 315, 227 and 103 cm^{-1} can be assigned to calcite indicating its use as binder for the preparation of the mural paintings. The strong band of hematite expected at 304 cm^{-1} and the small band at 231 cm^{-1} is unfortunately overlapped by the very strong calcite bands. However, very small band observed in AM1a at 540, 460 and 440 cm^{-1} could indicate the presence of hematite. These two very small bands are not present in the less red sample AM1b. The AM1b sample have bands at 538, 466, 395, 371, 317, 227 and 109 cm^{-1}. Here we observe strong bands coming from calcite (317, 227 and 109 cm^{-1}) and the bands at 467, 395 and 368 cm^{-1} can be positively assigned to quartz. The relatively intense band at 537 cm^{-1} has yet to be identified but it probably derives from a second silicate structure diverse from the pure quartz structure present in the AM1 sample. Hematite cannot be confirmed in AM1b as the band at 440 cm^{-1} is missing or completely overlapped by the observed quartz band at 467 cm^{-1}.

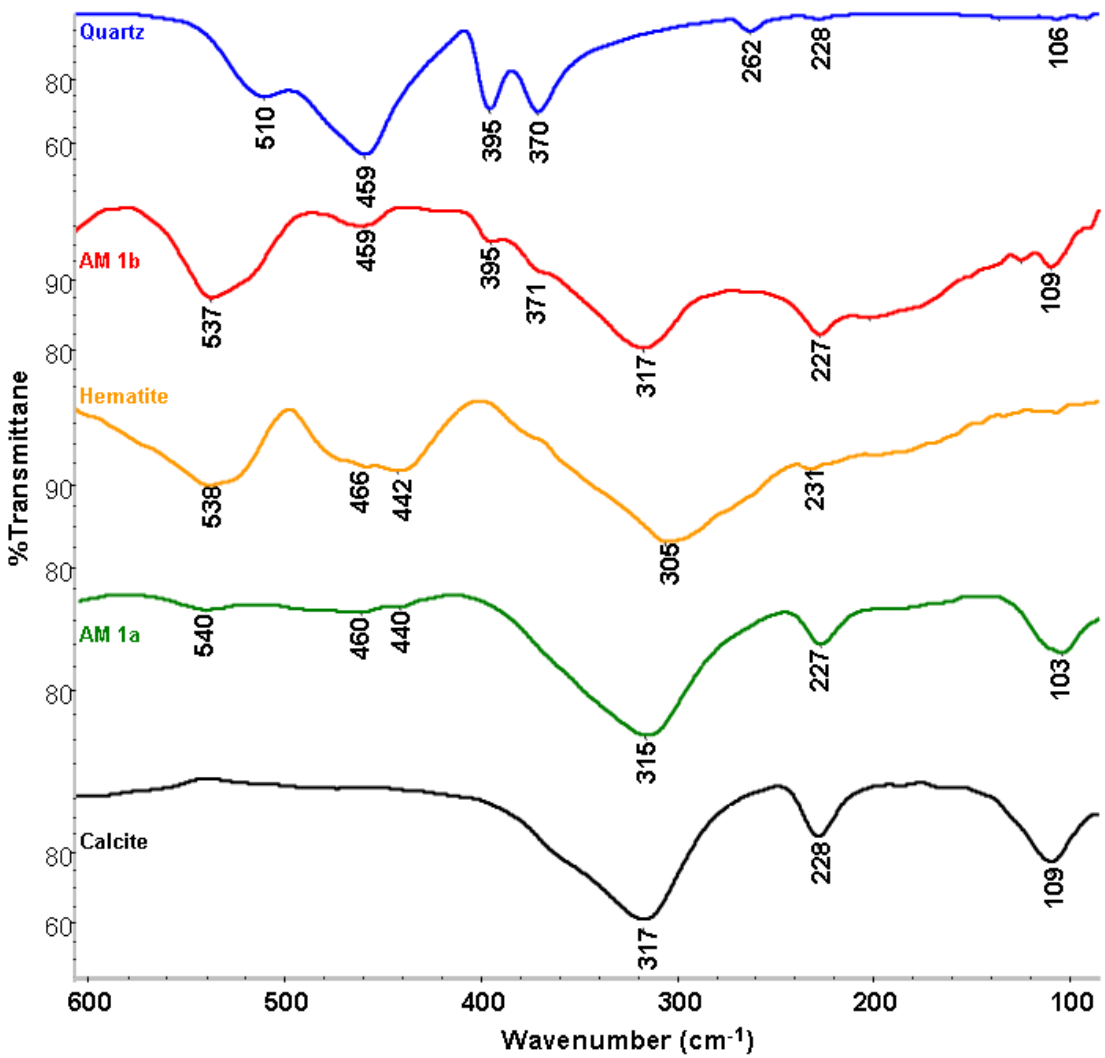

Figure 7.3: FIR spectra of mineral quartz (blue), sample AM1b (red), hematite from zecchi (orange), sample AM1a (green) and mineral calcite (black) collected in the region 600-90 cm^{-1}.

We conclude that the red AM1 sample is a complex material containing large amount of calcite coming from the preparations of the mural paintings but it also contains small amounts of quartz and hematite, indicating a red earth or ochre pigment used for colouring with a red tonality the cloud under the Angel.

7.2.2 GREEN SAMPLE AM15

The second sample from Abbazia del Monte is from the same area as AM1, but is a green sample from the angel turning away in ***Figure 7.1***, this is repeated in ***Figure 7.4a***, and a close up of sampling area is observed in ***Figure 7.4b***. It is collected in µATR on the cross-section without problems and is identified as a green earth silicate with many defined bands at 1100, 1065, 1015 and 960 cm^{-1}. Here we also collect a FIR transmission spectrum of the green sample AM15, which

is shown in Figure 7.5. We compare sample AM15 to mineral calcite (blue spectrum) and one of the few green earth standard pigments available in our library from Kremer Pigmente called Bohemian

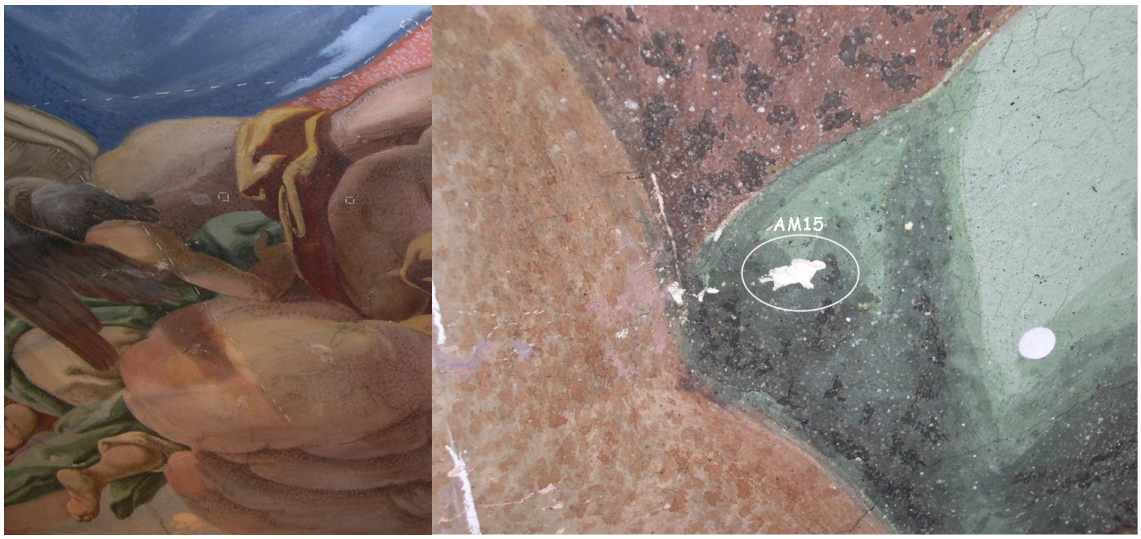

Figure 7.4: Pictures of sampling area AM15, A) the angel turning away dressed in green garment, B) close up of green sampling area.

The standard Bohemian green earth is, according to Kremer Pigmente, a natural green earth pigment (glauconite) containing Al-, K-, Mg-, Ca- and Fe-Silicate. The MIR region (collected in ATR) shows only the presence of a silicate by bands at 3500, 1635, 961, 835, 799 and 700 cm^{-1}, it is considered pure as no obvious pollution bands has been observed in the spectrum. The standard, however, is not identical to the one recorded of our AM15 in µATR in the MIR region. The vibrations observed in the FIR region are the lattice vibrations observed from the silicate.

By comparing the FIR spectra in *Figure 7.5* we see that the sample AM15 contains calcite, observed by bands and 314, 227 and 105 cm^{-1}. It also clearly contain a green earth with similar lattice structure to that of the Bohemian std, visible by bands at 500, 458 and 440 cm^{-1}. The band observed at 536 cm^{-1} was also observed in the above red AM1b sample and is though to be part of (another) silicate vibration. Very weak bands at 179 and 154 cm^{-1} are also observed.

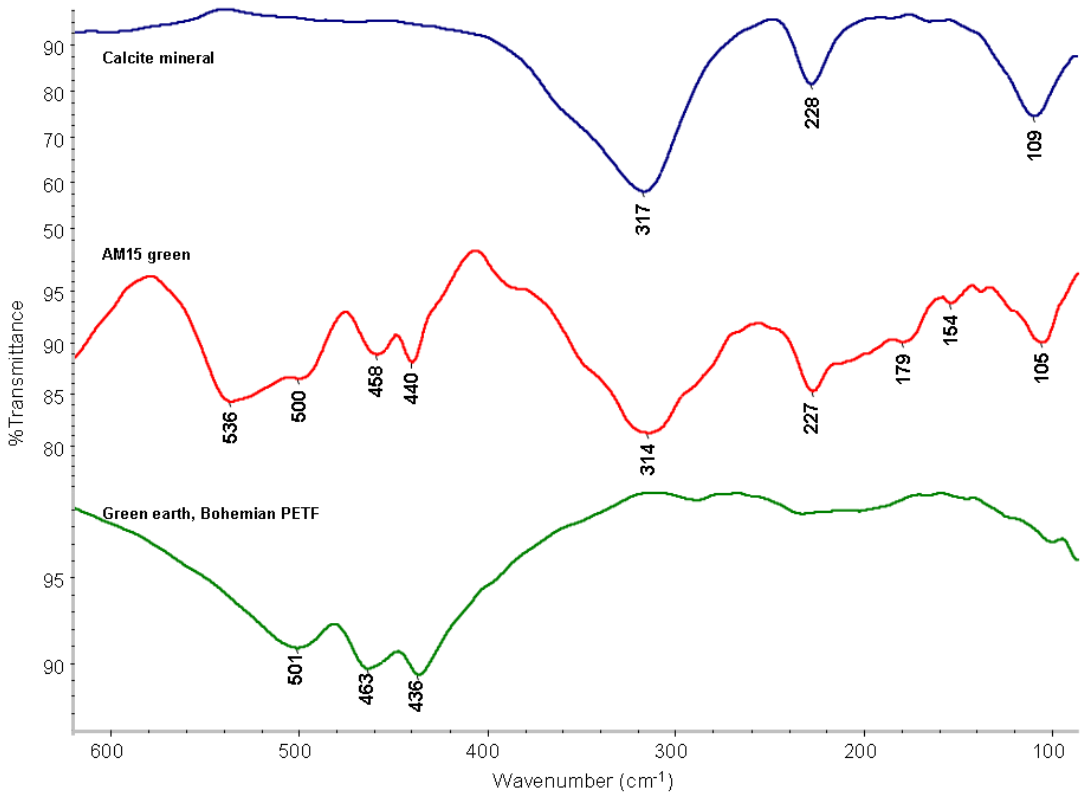

Figure 7.5: FIR spectra of calcite (blue), green sample AM15 (red) and green earth std (green) collected in transmission (the green earth std on PETF).

For both samples AM1 and AM15 we conclude that they contain calcite, probably from the preparations of the mural paintings, and they both contain siliceous material. In the case of the red sample AM1 this information was not available when examining the cross-section by μATR, as the cross-section was penetrated by embedding polyester resin in the top layer. In sample AM1 in the FIR region we also observe hematite. For the green AM15 we confirm the findings of silicate and calcite collected both by μATR and FIR transmission.

7.3 THUBCHEN LAKHANG TEMPLE IN LO MANTHANG, NEPAL

By order of King Bkra.shis.mgon the Thubchen Lakhang monastery was built in 1470 and completed by 1472. It was built in rammed mud and wood forming approximately a planar square. Several restorations have been performed during the past centuries. Some restoration work was performed by King Aham bSam.grub.dpal.'bar in the 1660s after an earthquake. Debris have accumulated on the floor due to upper parts collapsing during various earthquakes. A large portion of the north wall collapsed in 1815 and was rebuilt inwards linked to the existing portion by a short wall in rammed mud. This intervention is attributed to Queen Padma.bhu.ti and King 'Jam.dpal dgra.'dul. The new north wall was again rebuilt in mud-brick after the 1898 earthquake. The north

wall was prolonged towards the east, forming a north-eastern chamber. Some repairs were carried out during the late 1950s.

Figure 7.6: Pictures of the Thubchen Lakhang monastery seen from the outside and the decorated and painted hall after reconstruction.

The Thubchen Lakhang temple and the mural painting inside the temple can only be described as being in a very bad condition. Several places the mural painting was collapsed due to earthquakes and this has lead to pieces of the mural painting being on the ground instead of on the wall. The samples available can basically be described as clay support with paint, which were picked up from the ground in the temple for various analyses in an attempt to restore the temple back to its original state as part of the Upper Mustang Cultural Heritage Conservation Project.

Figure 7.7: The clay stones used for building the rammed mud wall and as support for the mural painting.

The support for all the painting was a clay material of a grey, yellow and red colour. The pictures of the grey and red clay materials can be seen in *Figure 7.7*. The clay support are approximately 5x5 cm. *Figure 7.8* shown the ATR MIR and FIR spectra of the red clay material compared to that of red Bole and China Clay. Gettens [90] describes red Bole as "about identical with China clay", and based on the MIR spectra we must agree that red bole and China clay are very alike and both are very alike the red clay mterial used as substrate for the mural paintings. Looking at the FIR spectra we observe both similarities as well as differences between the three. Neither three have been analysed further for contents of impurities.

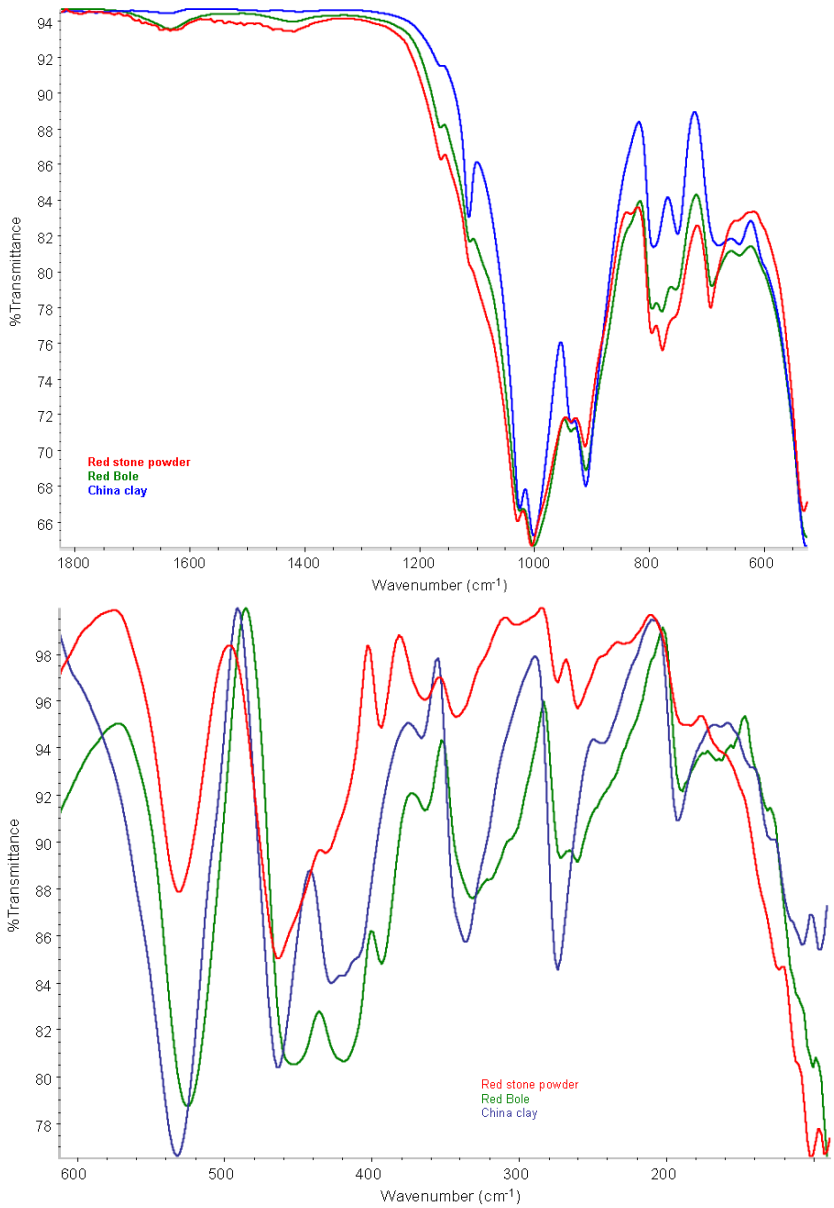

Figure 7.8: ATR spectra of red clay support (red) compared to Red Bole (green) and china clay (blue)

The support contains various paint layers. Grains from the top paint layer have been removed from the surfaces for ATR analysis.

Already published material about the Thubchen Lakhang temple in Lo Manthan gives us an idea of the expected colour palette used by the Nepalese artists [104]. The samples were investigated by microRaman analysis on cross-sections and inclusions found in paint layers. Some of the pigments found were azurite, malachite, lapis lazuli, cinnabar and pararealgar [104].

7.3.1 SAMPLE NNEW1

Sample NNEW1 is from the East Wall and it contains blue colourations, dark blue and light blue. The dark blue grain is quickly identified in both the MIR and FIR region as azurite. The FIR region can be observed in *Figure 7.10*. Our light blue grain sample NNEW1 is compared with a standard of lapis lazuli from Kremer pigmente and the red clay support in *Figure 7.11*. The lapis lazuli standard is almost pure lazurite when compared to the ATR spectrum published in the Rruff database [105], no calcite is observed in our standard, which is otherwise normal for lapis lazuli (and observed in the spectrum published in the Rruff database [105]).

Figure 7.9: Photo of sample NNEW1 showing light and dark blue colouration on the surface.

We are thus not sure our lapis lazuli standard is really a pure lapis lazuli.

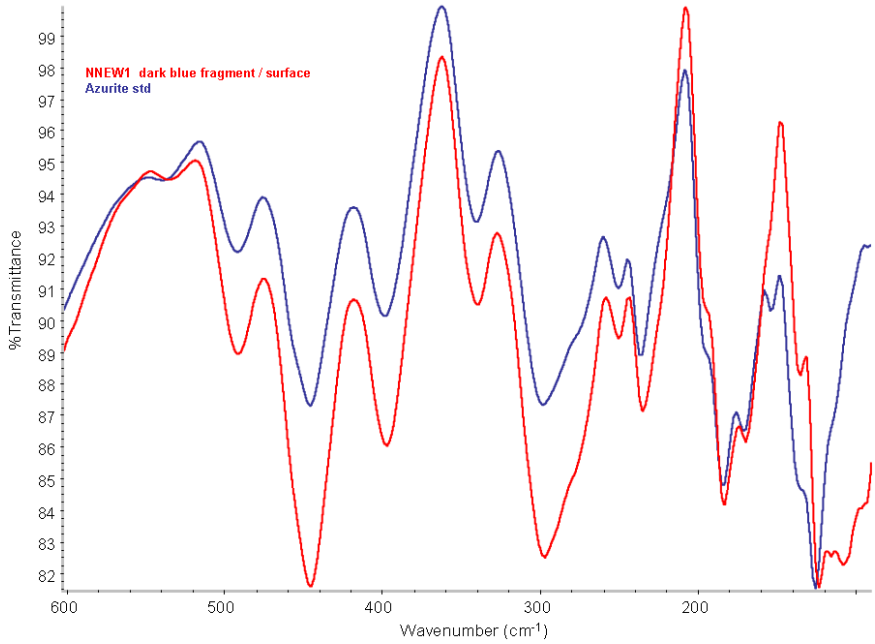

Figure 7.10: ATR FIR spectrum of sample NNEW1 blue fragment (red) compared to a standard azurite sample (blue).

In our NNEW1 light blue sample we identify a siliceous material observable by a band at 1007 cm^{-1}, which does not match that of lapis lazuli. It looks very similar to the red clayous support, however. In the NNEW1 sample we also identify calcite by bands at 1415, 874 and 711 cm^{-1} in the MIR region and 306, 227 and 103 cm^{-1} in the FIR region. In the FIR region we observe very weak bands, two of them are at 533, 468 and 394 cm^{-1}. The bands are similar to those originating from the red clayous support but small shifts of bands are noticed; the bands from lapis lazuli are not comparable with the ones observed in the light blue grain sample from NNEW1.

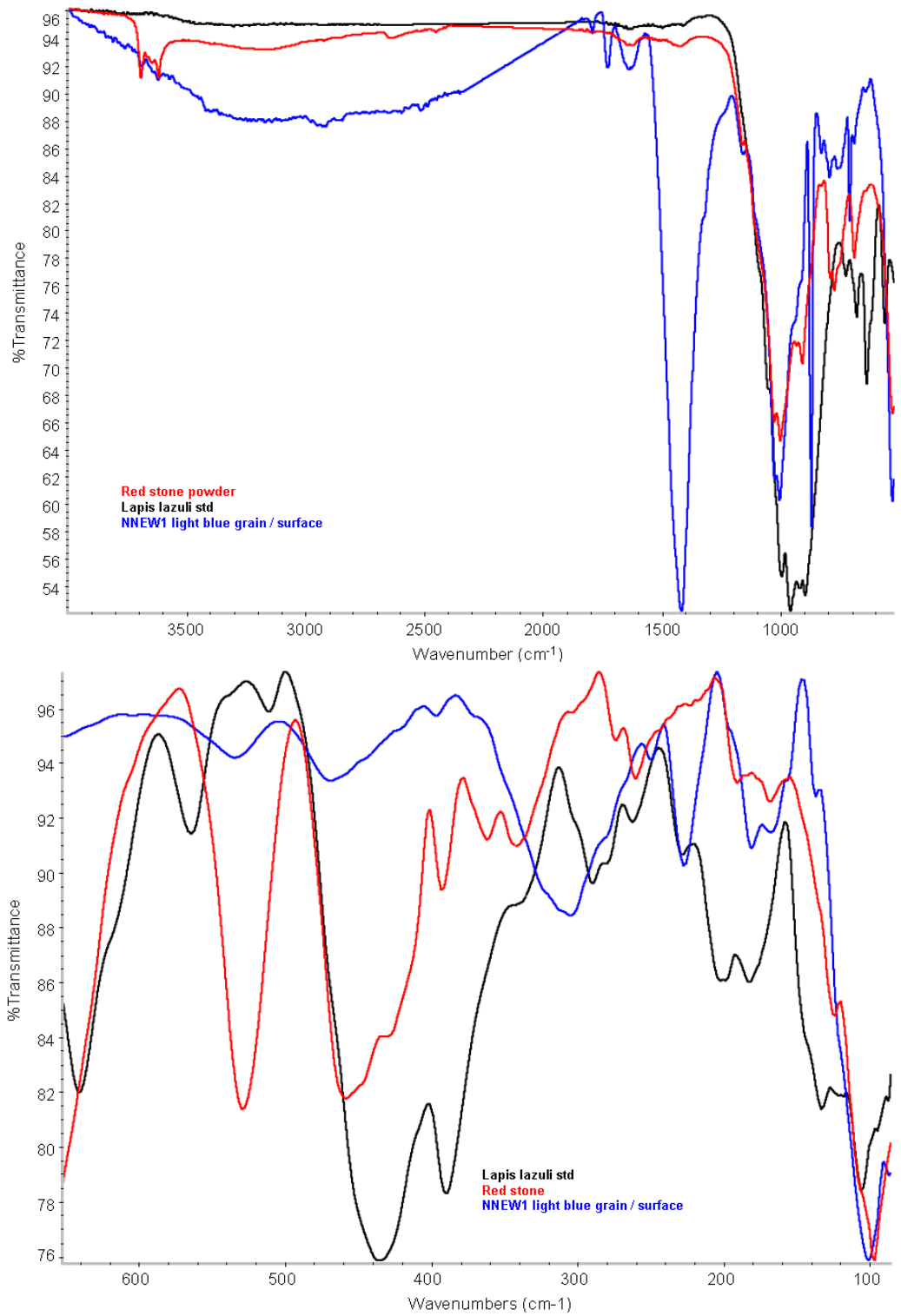

Figure 7.11: ATR region collected of sample NNEW1, a light blue grain (blue) compared to the red clayous support (red) and lapis lazuli std (black)

This is a general trend among all the samples taken from the surfaces of samples from the Thubchen Lakhang temple, that we observe only vibrations which are identical or similar (with small shift observed) to the bands observed from the red clayous support. In a few cases we observe

azurite or calcite but none of the expected pigments, pararealgar, lapis lazuli or cinnabar, were found.

Figure 7.12: Mural painting from Thubchen Lakhang temple, before and after restoration (and after removal of over-paintings), showing the evidence that water has run down the mural painting for years leaving a visible layer of clay on the surface of the painting.

As the monastery is built in rammed mud (the red and white clay support observed in *Figure 7.7*) one could imagine that when it rains, the water mixed with mud slowly seeps through the mud walls and distributes over the mural paintings, making a very thin layer of mud on the surface. A part of the mural wall painting can be seen in *Figure 7.12*, (before and after restoration), which shows the clear signs of water having penetrated from above and run down the wall. The thin mud layer is not a problem when analysing the cross-sections made from these samples by Raman spectroscopy [104], and in a few cases a thin transparent layer is observed on top of some of the cross-sections.

In 8 samples, regardless of the colour of the grain removed from the surface of the samples, only clay or siliceous material are recorded with ATR spectroscopy in the MIR and FIR region. The samples are from the east wall (NNEW1 and TEWC), from the south wall (samples NNSW7,

NNSW8, NNSW9, NNSW10, and NNSW15) and from the north wall (TENW-A). Some spectra show also the presence of azurite or calcite but no other compounds are detected.

In these cases we have found one of the limitations by applying ATR spectroscopy to the surface of a sample. The IR beam in ATR spectroscopy penetrates 3-5 µm in the MIR region (more in the FIR region depending on the refractive index of the sample). When a thin clayous layer is covering (or even has penetrated into) the surface of the mural painting, then this explains why we almost only observe clayous material when removing pigment grains from the surface for ATR analysis.

We seem to have more luck identifying pigments applied by Nepalese artist with these next samples. Possible due to less rain seeping down the wall in other areas of the temple.

7.3.2 SAMPLE T2

The T2 sample is from a blue drapery from the west wall of the Thubchen Lakhang temple. Sampling area is shown in *Figure 7.13* together with a cross-section of the sample (original magnification 200x). The cross-section reveals the sample is not pure blue, as is observed from the sampling area photo, but it is blue-brown with small inclusions of green crystals.

Figure 7.13: Photo of sampling area of T2 on blue drapery and microscopic photo of cross-section of sample T2 (original magnification 200x) showing dark blue/brown layer with inclusions of green crystals.

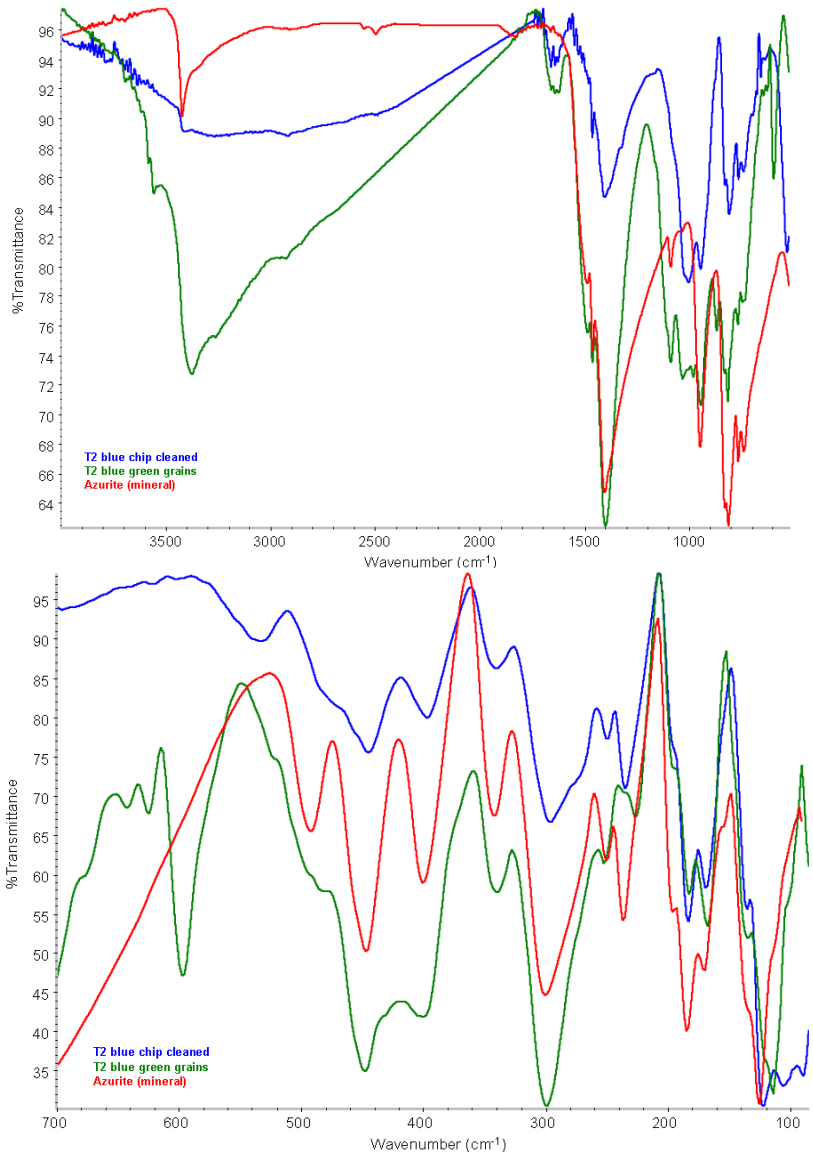

Figure 7.14: ATR MIR and FIR spectra of T2 blue cleaned chip (blue) and mixture of blue and green grains (green) compared to mineral azurite (red).

When collecting spectra we investigate a blue chip, a mixture of blue and green gains and a few green particles by ATR spectroscopy. The blue chip removed from the T2 sample was dirty with clay material on the surface. It is therefore necessary to gently wash the surface with water before collecting spectra (after allowing the chip to dry).

The mixture of blue and green grains has slightly different spectra than the blue chip. But in both samples we identify azurite when comparing with mineral azurite standard as seen in *Figure 7.14*. In the MIR region we observe the presence of silicate by bands at 1030 cm^{-1} from both T2 samples, the blue chip and the mixture of blue and green grains. But only in the mixture of the blue and green grains do we observe a sharp band at 3650 cm^{-1}, which originate from free OH stretching vibrations. In the FIR region we observe in the mixture of blue and green grains a prominent band

at 600 cm^{-1}. This band is not present in the sample from the blue chip, it also do not come from the azurite. The differences observed could come from two diverse silicate present in the two blue samples or, more likely, it comes from the green grains present in the blue and green sample.

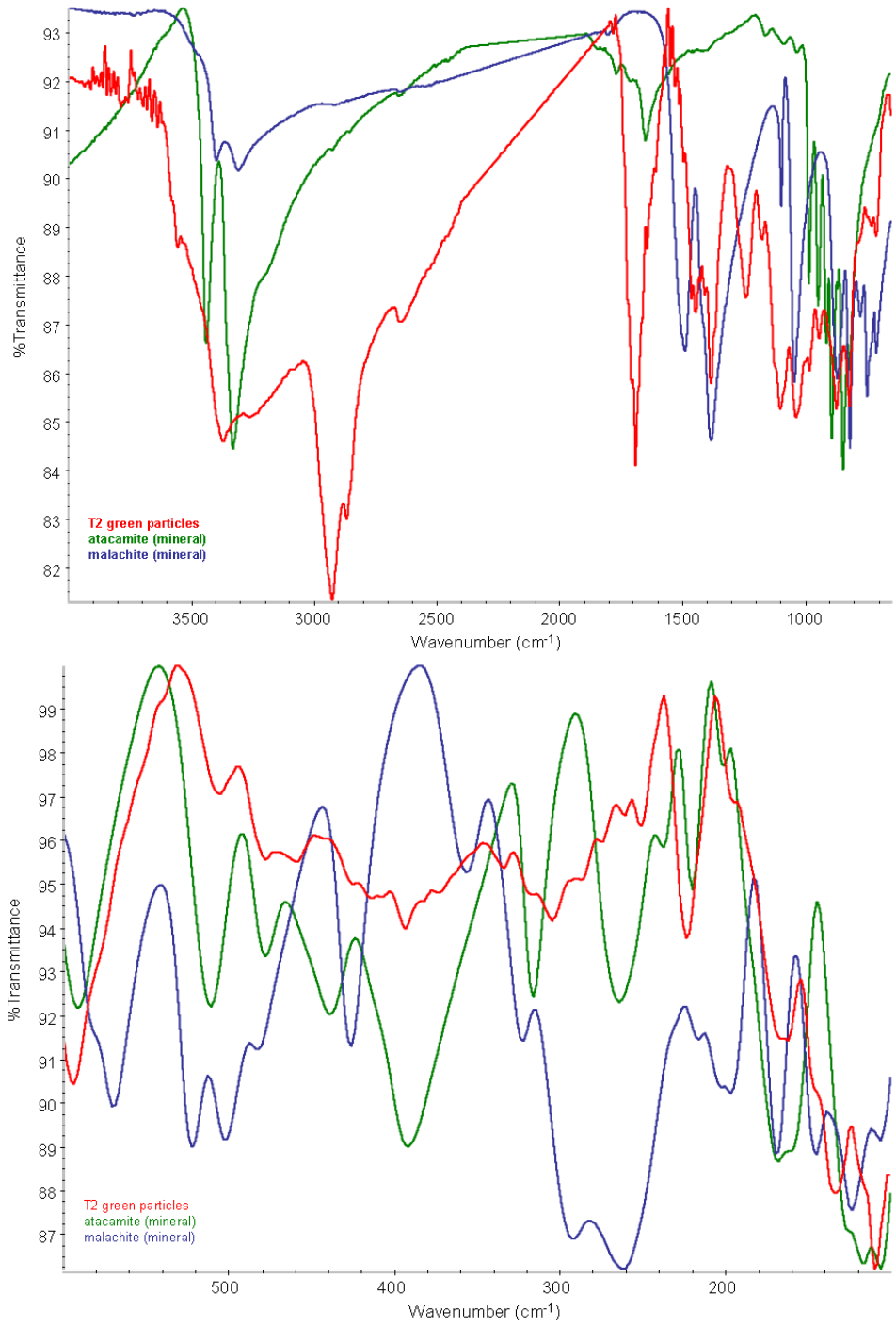

Figure 7.15: ATR MIR and FIR spectra of T2 sample of green particles (red), compared to atacamite (green) and malachite (blue)

Very few green particles are successfully removed from the T2 sample for ATR investigations in the MIR and FIR region as can be seen in *Figure 7.15*. In the green T2 sample an organic compound is present. Most prominent are the bands at 2927 and 2868 cm^{-1} from CH stretching vibration and carbonyl (amide I) stretching vibration at 1691 cm^{-1}, and amide II at 1644 cm^{-1}, together with CH-CH vibrations at 1383, 1240 and 1036 cm^{-1}. Previous published results of the green layer performed by µATR spectroscopic examination of the T2 sample directly on the cross-section [11], the green is identified as malachite with high content of a free fatty acid (oil binding media) with a carboxylate C=O stretching at 1710 cm^{-1}, and ester by band at 1735 cm^{-1}, and proteinaceous material observed by amid I and amid II bands at 1641 and 1539 cm^{-1} together with silicate (strong Si-O band at 990 cm^{-1}) [11].

Table 7.1: List of vibrations for 1 Herbertsmithie, 2 Paratcamite, 3 Clinoatacamite, 4 atacamite, 5 Botallackite collected in transmission 4000-400 cm^{-1} (reprinted from [106]) compared to our unknown green particle sample T2 collected in ATR mode (not all T2 vibrations are mentioned).

1	2	3	4	5	**ATR sample T2 green (cm^{-1})**
				3520 s, sp	
3410 sh	3450 s, sp	3450 s, sp	3450 s, sp	3440 sh	3557
3380 vs, sp	3380 vs, sp	3360 s	3360 w, sh	3420 s	3369
3320 sh	3310 s, fsp	3310 s	3340 vs		
			3190 w, br		
970 sh	972 m	984 s, sp	982 s, sp		981
945 s, fsp	943 s, fsp		946 s, sp		
		920 s, sp	922 s, sp		943
		902 vw			
		888 vw	890 s, sp		873
		860 s, sp	862 w	853 s	
	812 m, br	822 ms	845 s, sp	815 s, sp	820
753 s, br	750 s			778 s, fbr	
				703 s, fbr	729
597 w, br	590 w, br	572 ms	590 s	525 s, sp	711
	510 sh	512 s	510 s	502 s, sp	
460 s	460 vs	448 vs	475 s	450 ms, sp	594
	400 m	405 s	438 s	418 s	505
		380 sh	390 vs	385 s	477
					459
					393
					223

s = strong, m = medium, w = weak, sh = shoulder, sp = sharp, br = broad, v = very, f = fairly.
1. Herbertsmithite, Mina Los Tres Presidentes, Chile. Off specimen 22 of Table 1. Cu/Zn = 3.1.
2. Paratacamite, Kali Kafi mine, Iran. Off WHP 593/374. Cu/Zn = 9.4.
3. Clinoatacamite, Levant mine, Cornwall. Off RSWB 69-304.
4. Atacamite, Mina la Farola, Chile. Off RSWB 77-50.
5. Botallackite, Levant mine, Cornwall. Off RSWB 74-244.

These already published results [11] are not in agreement with our ATR spectroscopic observations, which could be due to serious degradation of the malachite or due to another compound present, possibly a copper chloride compound. We observe amid I and amide II bands at

1641 and 1539 cm^{-1}, but not at the same wavenumbers as already reported in [11]. Neither do we observe free fatty acid and ester bands at 1710 and 1735 cm^{-1} respectively. Malachite have some bands which are in agreement with the green particles from T2 but there are also prominent strong malachite bands missing, mainly the band at 1491 cm^{-1}. *Figure 7.15* shows the ATR spectra of green particles from T2, compared to malachite and atacamite. From the literature we know that degradation of blue azurite can turn into green pigments like clintoatacamite ($Cu_2Cl(OH)_3$) [107], or paratacamite ($Cu_3(Cu,Zn)(OH)_6Cl_2$) [108] in the presence of chloride from a humid environment. We have already observed clay material on the surfaces of some samples originating from rain washing down over the Thubchen Lakhang mural painting. It is thus quite possible that the azurite has degraded to a copper chloride compound.

Unfortunately, we do not have the basic copper chloride clintoatacamite, paratcamite or botallackite as standards for detailed spectroscopic library comparison to confirm or eliminate the presence of one of these copper chloride mineral pigment.

IR vibrations of 5 copper chloride compounds collected in transmission for herbertsmithite, paratacamite, clintoatacamite, atacamite and botallackite are listed in the literature [106], they are listed in *Table 7.1*. However, we are still not able to completely identify exactly the components of our T2 green compound. Most probably the green inclusion T2 is a complex mixture of several copper chloride compounds together with the organic amide compound. Further investigations are required, together with ATR collection of standard copper chloride degradation compound, in order to closer determine the content of the green T2 sample.

7.3.3 SAMPLE NNSW10

A red and blue sample from the south wall are examined by ATR spectroscopy. The blue pigment is identified as azurite mixed with a silicate material (not shown), while the red sample is identified as a clayous silicate material similar to China Clay. This can be observed in *Figure 7.17*. Bands from hematite (which could explain the red colour) are not observed. If hematite bands are present they are overlapped by the bands from the China Clay present in the sample. Some other

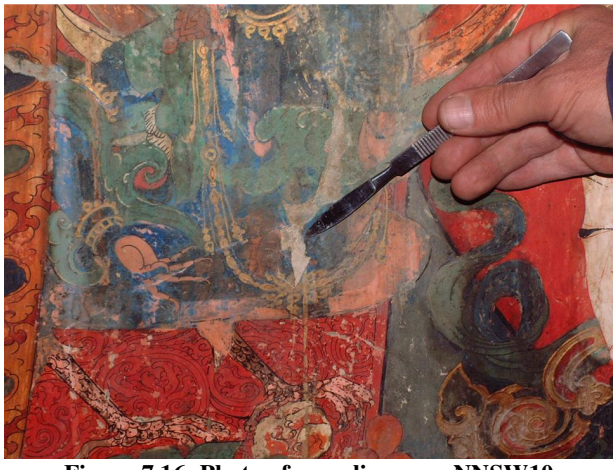

Figure 7.16: Photo of sampling area NNSW10

compound is also present in the sample, mainly seen by the broad OH stretching vibration at 3500-2800 cm^{-1}, by bands at 1656, 1514 and 1400 cm^{-1} as well as small shifts observed in the FIR region compared to the bands of the China clay standard.

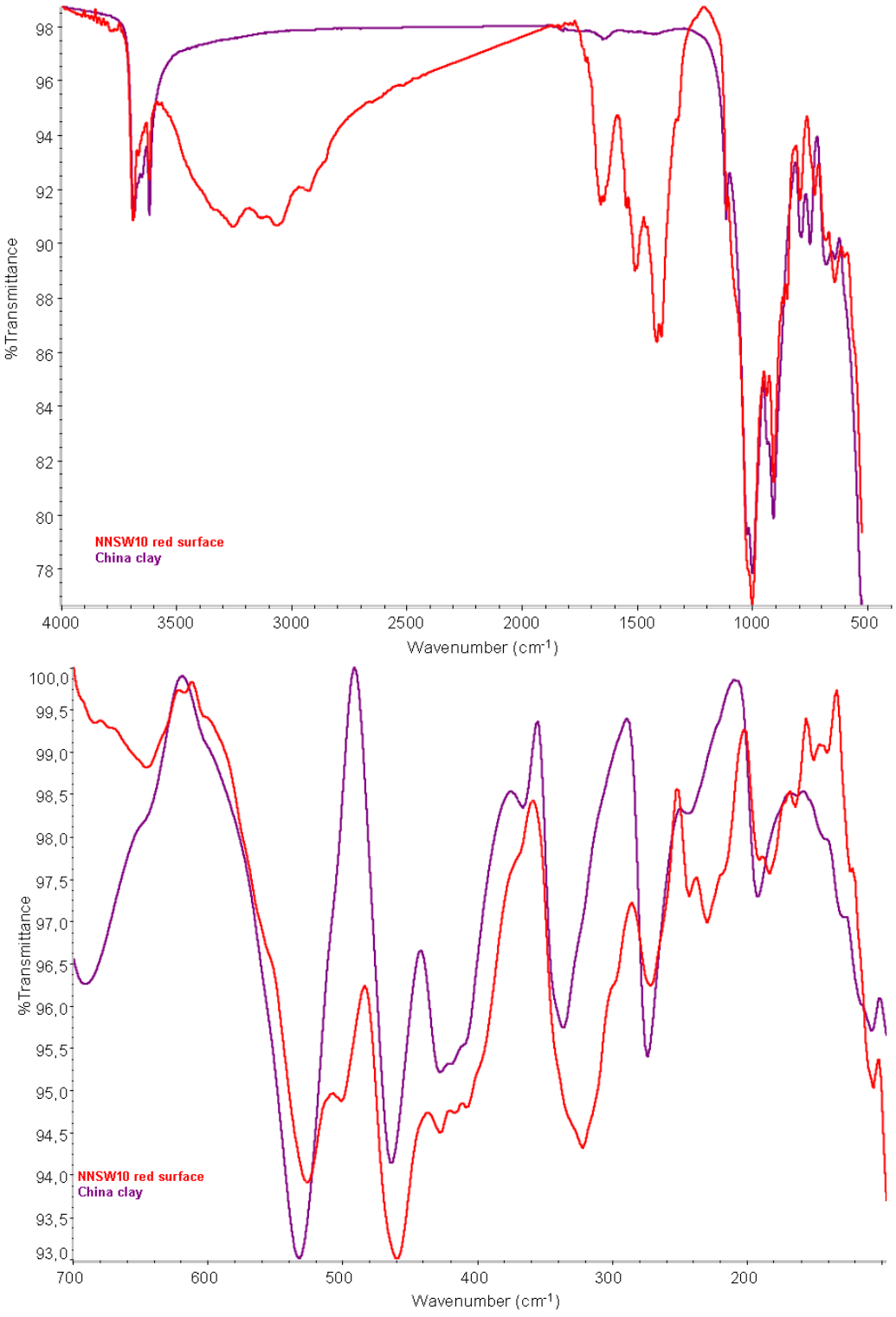

Figure 7.17: ATR MIR and FIR spectra of NNSW10 red surface (red) compared to China Clay standard (purple).

7.3.4 SAMPLE T17, RED AND BLUE LAYER

Sample T17 is a red and blue chip from the south wall. It is part of the decoration for Buddha's halo. A close up of the sampling area is shown in *Figure 7.18*. Here, no obvious clay material (mud) has seeped down the wall to cover the mural painting. We investigate both the red and blue colour on a small chip by applying surface contact between the chip and the ATR crystal. The chip is white on the backside as can be observed in the after sampling picture in *Figure 7.18*.

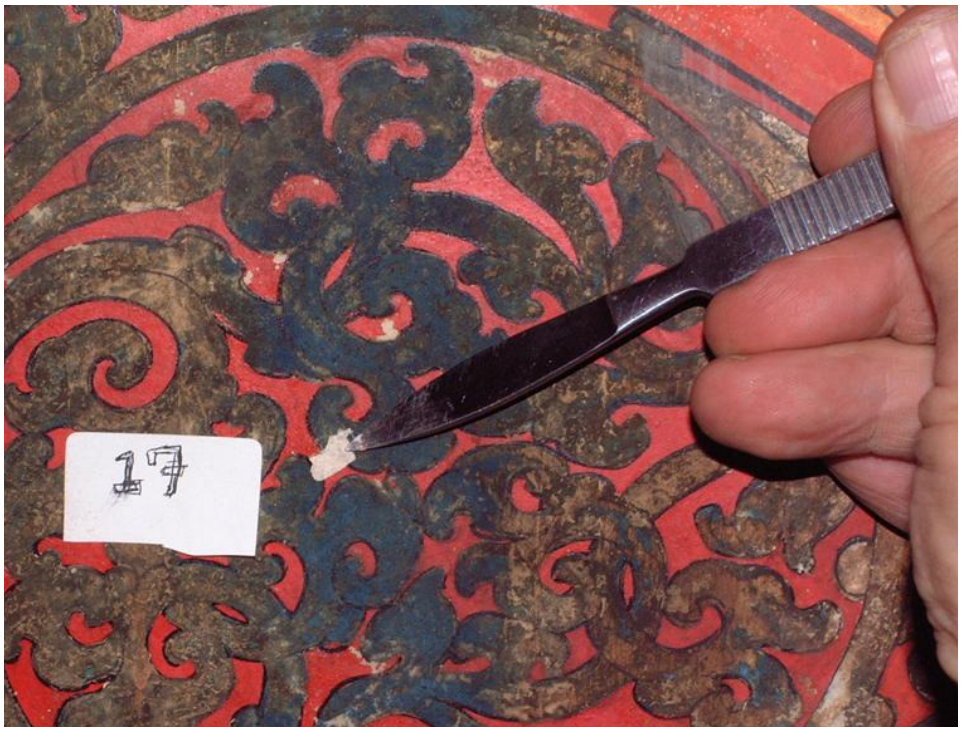

Figure 7.18: Sampling area T17 (South wall, after sampling), showing the red and blue pigments which are part of the decoration of Buddha's halo.

For the red sample in the MIR region we observe calcite, silicate and glue as the organic binding media when performing surface contact. However, the signal intensity is very low and heavy noise is observed on the baseline as can be seen in *Figure 7.19*. Calcite is observed by bands at 1410, 875 and 714 cm^{-1}, the glue is observed by weak bands at 1630 and 1520 cm^{-1}, while the silicate is observed by the band centred at 1030 cm^{-1}.

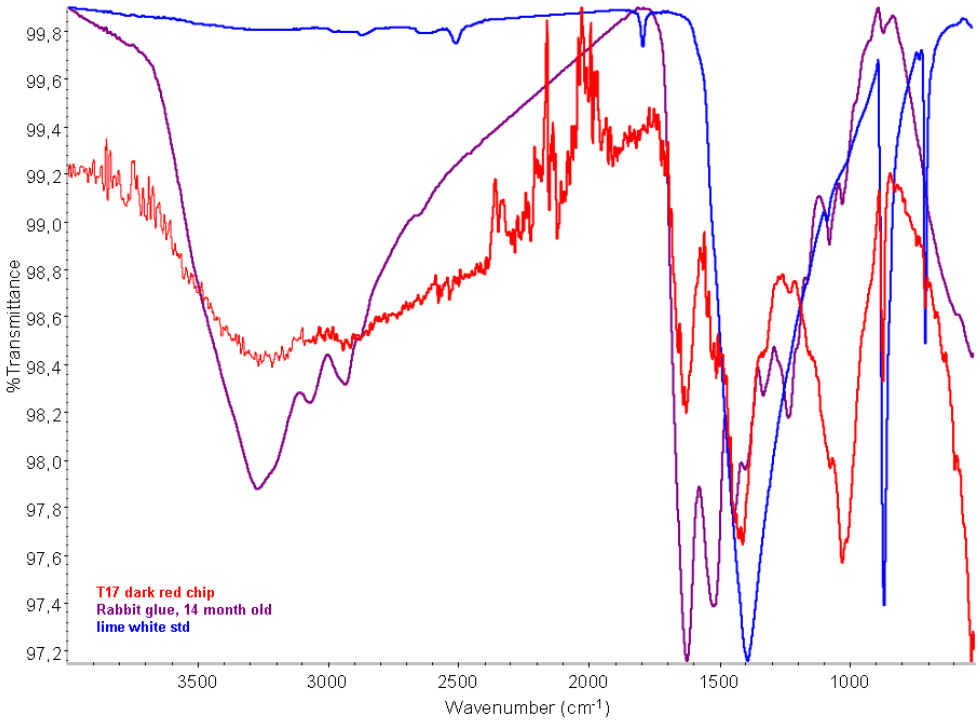

Figure 7.19: ATR MIR spectra of dark red sample T17 (red), compared to rabbit glue (purple) and calcite (blue).

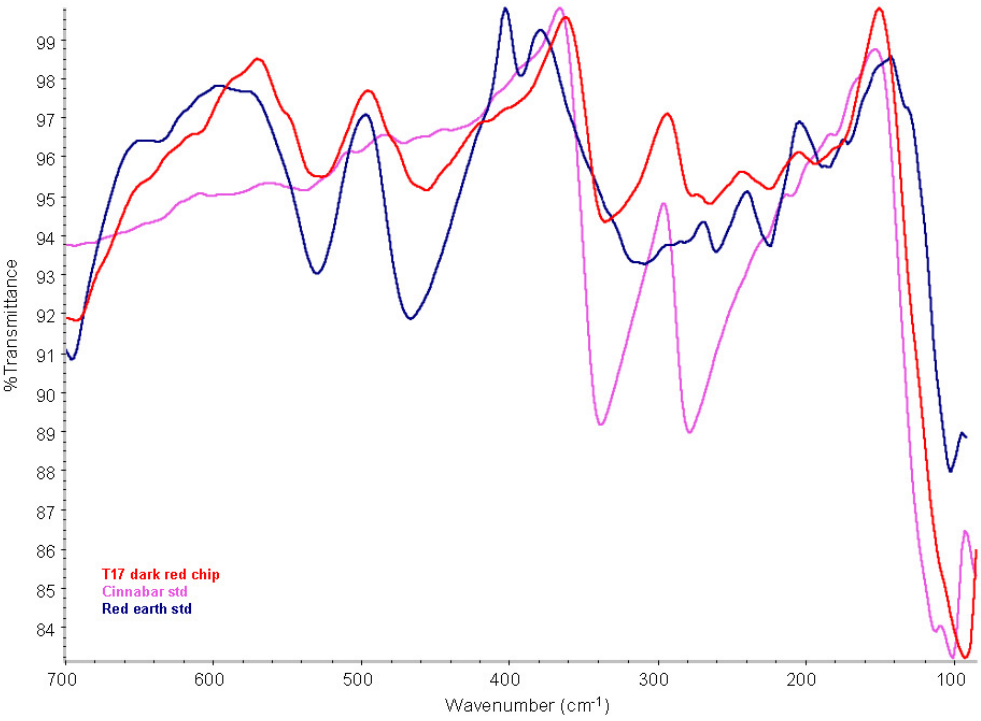

Figure 7.20: ATR FIR spectra of red chip sample T17 (red), compared to cinnabar std (purple) and a red earth std (blue).

The same dark red chip is also examined in the FIR region by surface contact. Here we observe much less noise in the spectra, than in the MIR region. We compare the spectrum of sample T17 to that of cinnabar and red earth. Red earth is present in our sample by bands observed at 529,

457 and 315 (shoulder) cm^{-1}, bands which are all typical of hematite. Bands from cinnabar are observed at 336, 278, 111 (shoulder) and 98 cm^{-1}. The presence of mercury is confirmed by SEM-EDAX (Scanning Electron Microscopy and Energy Dispersive Spectroscopy) investigation on the red layer of a cross-section of sample T17.

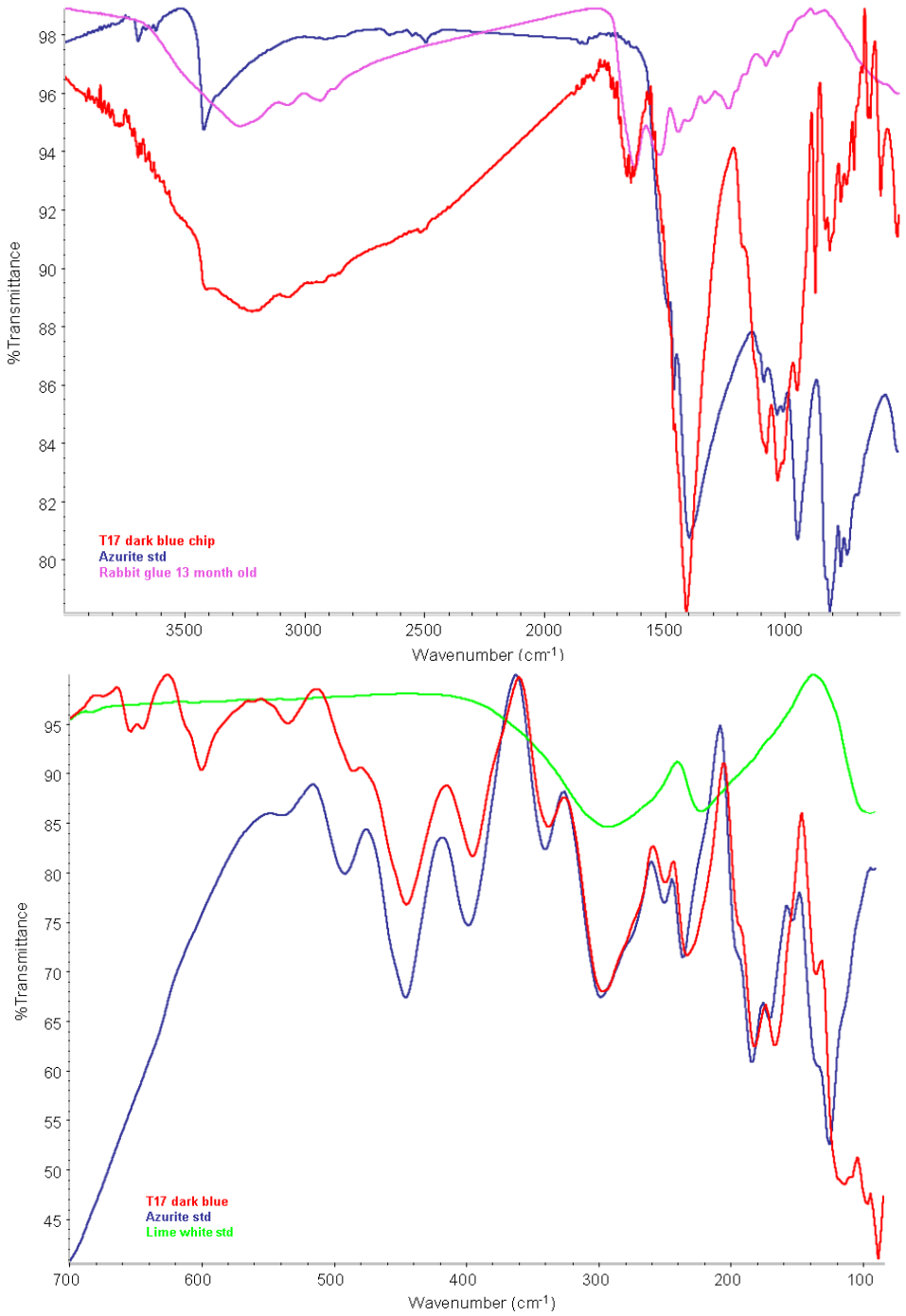

Figure 7.21: ATR MIR and FIR spectra of blue sample T17 (red), compared to azurite (blue), rabbit glue (purple) and calcite (green). Calcite is observed in the MIR region by sharp bands at 875 and 711 cm^{-1} but no bands are observed in the FIR region.

Similarly we investigate the blue layer from sample T17. In the MIR region we observe weak bands originating from glue, small amount of calcite (from the white substrate underneath) and the blue pigment which we identified as azurite.

The glue is observed by weak OH and CH stretching bands in the region 3300-2800 cm^{-1} and C=C vibration at 1640 cm^{-1}. Calcite is observed in the MIR region by sharp bands at 875 and 712 cm^{-1}. The CO stretching vibration of calcite at 1410 cm^{-1} is coinciding with the carbonate vibration of azurite. Calcite is not observed in the FIR region the calcite bands are completely covered by the azurite bands. The baseline in the blue sample T17 is very different from the standard azurite pigment, significant differences in band intensity are noted, especially in the region 1200-600 cm^{-1}. In this region the azurite band positions are in complete agreement with the bands observed in the blue sample T17, but the intensities are clearly different. Although we identify azurite we clearly also observe the presence of another compound. This is confirmed by three unidentified bands observed at 654, 645 and 600 cm^{-1} (a region where neither azurite nor calcite have any band absorption). Azurite is also observed in the FIR region by many bending and lattice vibrations. We note that in the very low FIR region, from 240-90 cm^{-1} the intensity of bands from the blue sample T17 sample and the azurite sample are dissimilar. This could be due to the still unidentified compound.

The cross-section of the blue layer has also been examined by SEM-EDAX. Here copper is the major component with small amount of calcium, potassium, silicium and aluminium present. This confirms azurite as the major component in the blue paint layer. The presence of potassium, silicium and aluminium combined with observable variations in the 1200-600 cm^{-1} baseline, diverse intensity of bands, as well as the three unidentified bands at 654, 645 and 600 cm^{-1}, make us conclude the unidentified compound is a siliceous material present in small amount.

7.3.5 SAMPLE T22, RED PIGMENT

Sample T22 is a dark red sample which in the MIR region only have bands at 1400, 875 and 711 cm^{-1} indicating the presence of calcite, and bands associated with a silicate, where the most prominent bands are at 1004 and 912 cm^{-1}. In the FIR region we again confirm calcite and red earth silicate by comparing the red sample with calcite and a red ochre standard, as can be seen in *Figure 7.22*. In the T22 sample we observe hematite by bands at 531, 464, 429 and 332 (shoulder) cm^{-1}. The bands at 395 and 373 cm^{-1} are from the silicate indicating the silicate has quartz-like structure. This is also confirmed in the MIR region (not shown) where we observe small quartz bands at 796 and 778 cm^{-1}. Bands at 306 and 223 cm^{-1} are originating from the calcite.

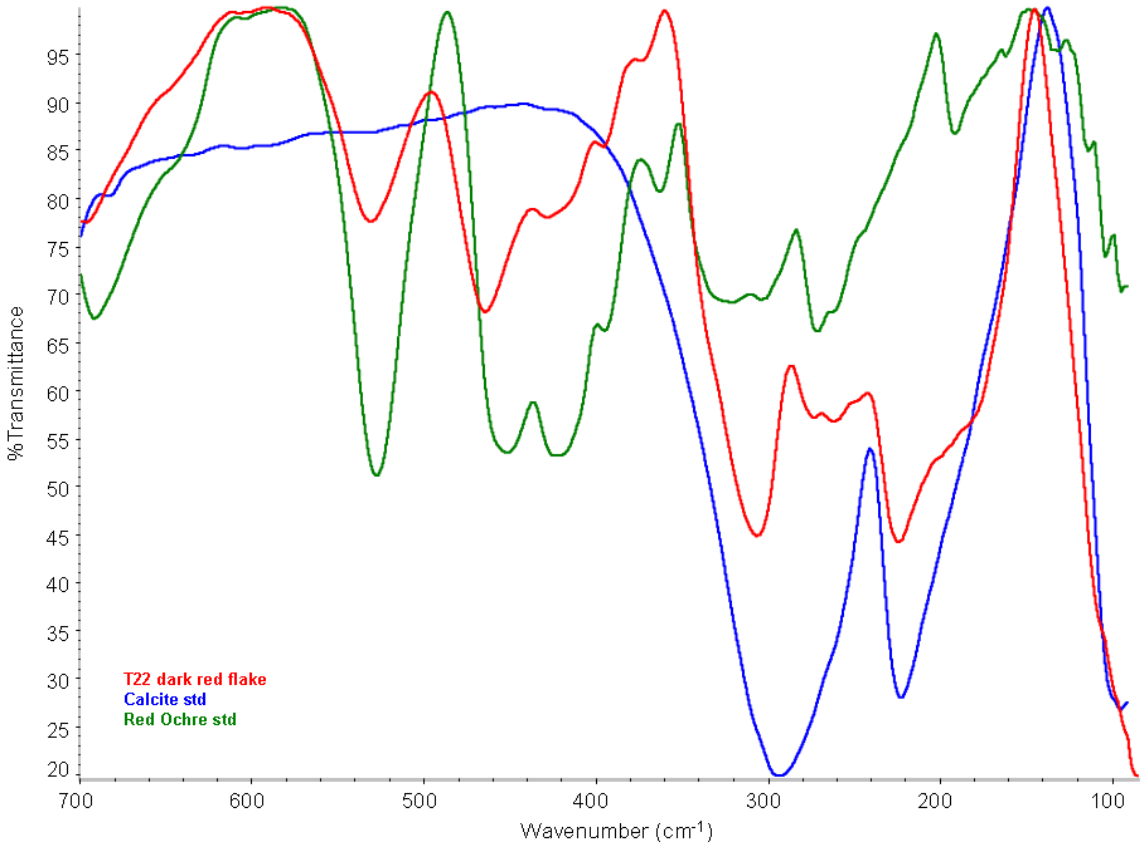

Figure 7.22: ATR FIR spectra of the dark red sample T22 (red) compared to calcite standard (blue) and red ochre standard (green).

The pigments identified by ATR spectroscopy as the colours employed by the Nepalese artist are azurite, red ochre (hematite), cinnabar, China clay and calcite. Malachite has not been identified but what appears to be a green degradation product of azurite, mixtures of basic copper chlorides, are observed. Glue is observed as the binding media. Silicate appears to be present in almost all the samples, either as a clayous material covering the surface of the samples coming from the rain seeping through the roof down the walls of rammed mud or present as silicate pigment, like red and green earth pigments.

7.4 LIANGDAI, SHAANXI PROVINCE, CHINA

In april 2005 in Liangdai, Village of Hancheng City, Shaanxi Province, China, a three-month field excavation started, which revealed a cemetery with a total of 103 tombs. Four grand graves with passages and 17 chariot pits was found, where two of the grand graves belongs to a ruler and his wife who lived during the early part of the Spring and Autumn Period (770-476 BC).

Figure 7.23: Pictures from the 2005 excavation in Liangdai, China.

Judging from the size, shape and structure of the tombs as well as abundant funerary objects, archaeologists determined that the cemetery, which covers a total area of 330.000 m^2, was for the burial of members of the aristocracy of a kingdom dating back approximately 2,800 years from the late Western Zhou (c.1100-c.771 BC) to the early Eastern Zhou Dynasty (770-256 BC). However, the findings seem to be in conflict with the Historical Records written by Sima Qian of the Western Han Dynasty (206 BC-AD 25), as it says that the area where the newly-found ancient tombs are located was the land of the State of Liang. From the inscription on the bronze wares uncovered from the grave of one ruler, it is written that the ruler was the Duke of Rui. The city now known as Hancheng was then known as land of the State of Rui instead of Liang. Archaeologists are still trying to determine the ruler and more investigations and information are needed for confirmation [109].

Figure 7.24: Pictures of excavated bronze objects from Liangdai, China, showing bronze ornaments and bells.

The excavation revealed a large number of funerary objects made of bronze, jade and gold from three graves and one pit. Articles exposed from the graves include more than 600 pieces of bronze ware as well as numerous gold vessels and lacquer ware, many with carved dragon patterns, a symbol of ruling in ancient China. More than 500 pieces of intricately carved jade were found in the tomb of the wife of the ruler. These include jade jewellery inlaid with precious stones and jade carvings of silkworms and tortoises.

7.4.1 SAMPLE LB10, BRONZE TUBES WITH NET DECORATIONS

From inside the bronze tube we remove a few light green grains. We investigate the same grains in both MIR and FIR region by ATR spectroscopy.

From the MIR region we identify malachite with some oil. The extreme sharp band observed at 1733 cm^{-1} indicate the presence of an ester, as there are no shoulder band at lower frequency (1715 cm^{-1}) to indicate the presence of an acid. This is then a fresh oil we observe. We also note that none of the observed CH stretching bands are located above 3000 cm^{-1}, which indicates that the oil is saturated.

Figure 7.25: Pictures of sample LB10 showing the corrosion on the surface and inside the tube. The tube is approximately 2 cm long and 1 cm broad.

In the FIR region we again observe malachite but we also observe clear signs of degradation of the crystal lattice. The range 340-200 cm^{-1} we know from chapter 6 to be different depending on the source of malachite so here we would expect differences. But the other regions, from 600-340 and 200-90 cm^{-1}, are very similar when comparing the 6 different sources of malachite in chapter 6. In our LB10 sample, however, we observe loss of definition and bands disappearing. Observe the band at 170 cm^{-1} which should be present but is almost gone in the LB10 sample. Also, the region 600-340 cm^{-1} has less definition, the band at 500 cm^{-1} is reduced to a shoulder band. This means that clear evidence of crystal degradation is taking place.

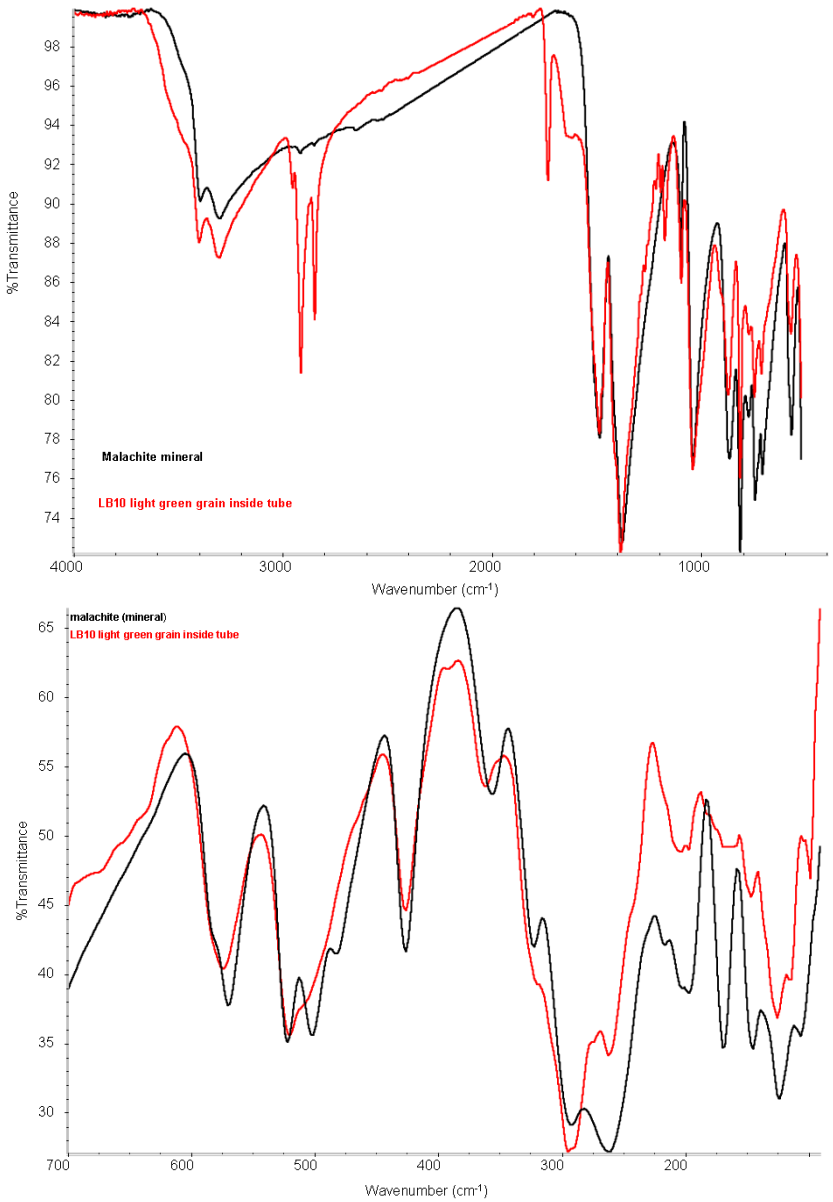

Figure 7.26: ATR spectra of green sample from LB10 (red) and malachite (black). In the MIR region we observe malachite and oil In the FIR region we observe clearly loss of definition (band at 500 cm^{-1}) and the disappearance of band at 170 cm^{-1}, which indicates a beginning degradation of the crystal lattice in malachite.

7.4.2 SAMPLE LB8, LINCHPIN FROM CHARIOT WHEEL

A linchpin is locking pin inserted crosswise, it is the part that serves to hold together the end of an axle wheel of the chariots found in Liangdai. Sample LB8 is a fraction broken off from the linchpin, corroded on the surface with green corrosion.

Figure 7.27: Pictures of sample LB8, bronze fractions broken off from the linchpin.

From surface investigations of the sample LB8 we conclude like with LB10, that the surface is corroded with malachite. The presence of silicate is also detected in the MIR region by a broad band at 1050 cm^{-1}, and by bands at 466 and 395 cm^{-1} in the FIR spectrum.

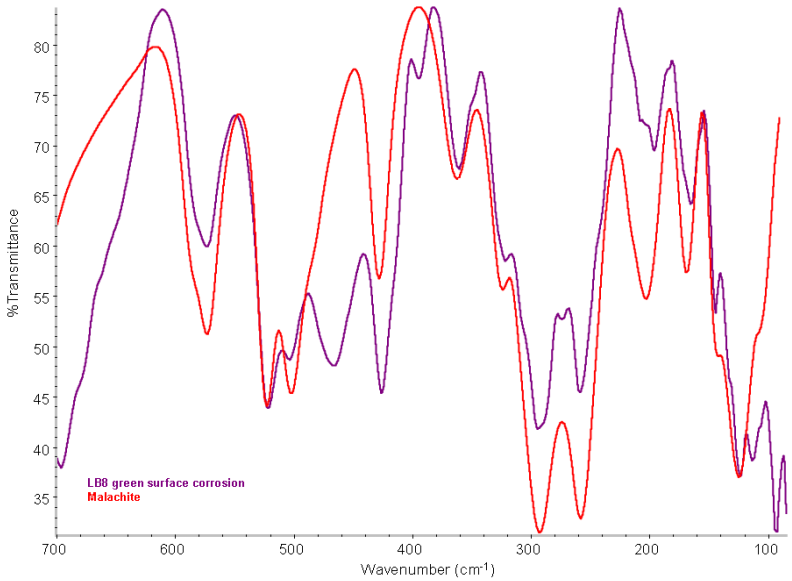

Figure 7.28: ATR FIR spectrum of LB8 green surface corrosion (red) compared to amalachite standard (purple). Besides malachite also a silicate compound is observed by bands at 466 and 395 cm^{-1}.

Just below the surface there are red-brown grains, which in the MIR region appears to have a carbonaceous structure similar but not identical to malachite. It could be so degraded that several

vibration features are missing as can be seen in *Figure 7.29*. The bands observed in the MIR region are of very low intensity compared to the intensity observed in the FIR region. In the FIR region we do not observe any malachite but we identify cuprite by bands at 603 and 145 cm^{-1}. Cuprite is observed in both the MIR and FIR region due to the 1st order maxima band at 663 cm^{-1}. Another unknown compound is observed in the FIR region, which has one broad band centred around 500 cm^{-1} and two small bands at 273 and 233 cm^{-1}.

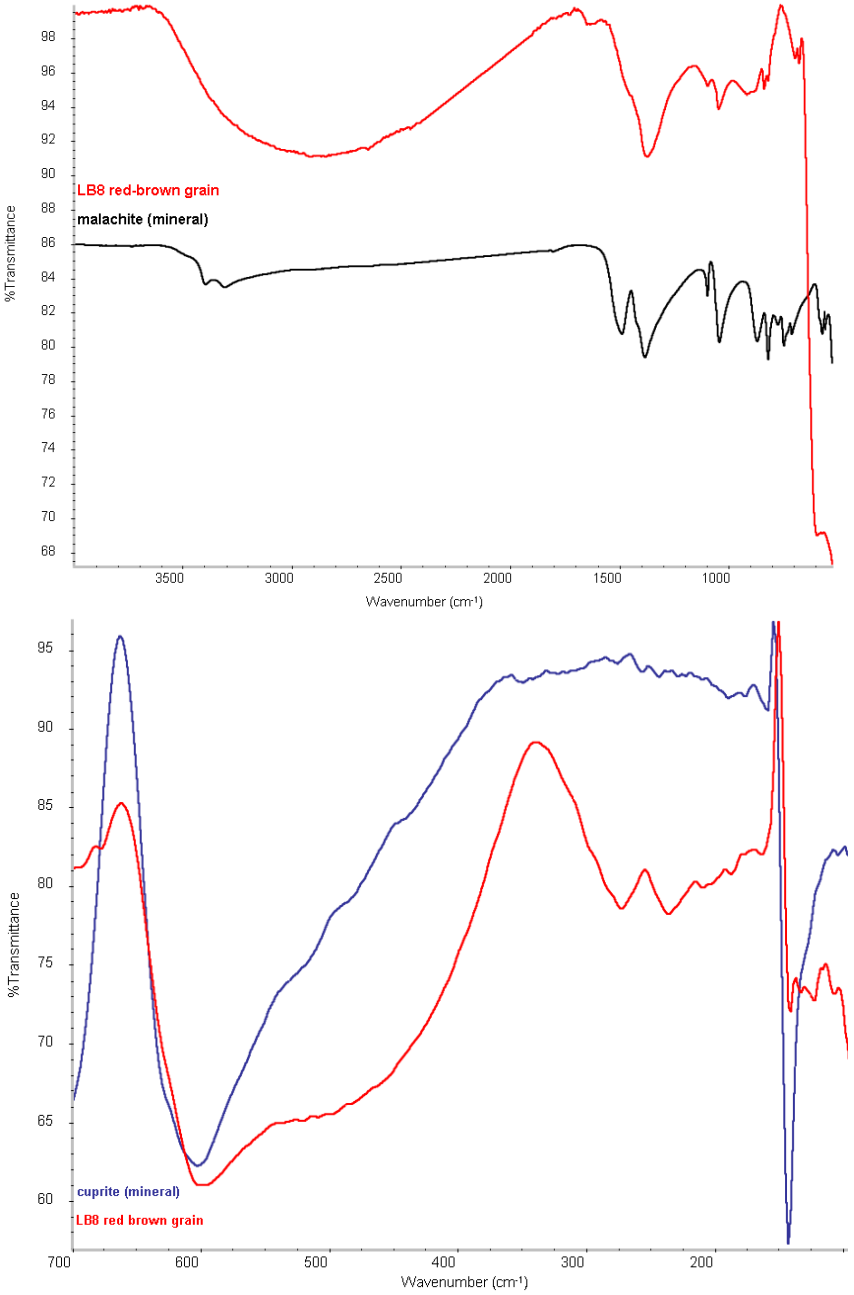

Figure 7.29: ATR spectra of sample LB8 (red) compared to malachite (black) in the MIR region and compared to cuprite (blue) in the FIR region.

7.4.3 SAMPLE M27, RED POWDER FROM SARCOPHAGUS

Reddish powder sample M27 comes from the surface of a sarcophagus, found in one of the tombs. The powder is spread in the tomb and on the sarcophagus in order to keep away the evil spirits, this is a Chinese tradition. As can be observed in the picture of the powder sample M27, the powder is not homogeneous in colour, it consist of brown, grey, orange, and red colour variations.

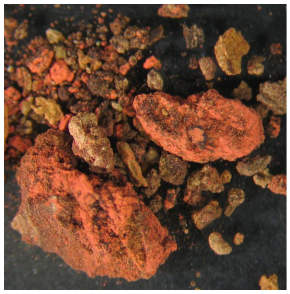

Figure 7.30: Picture of the red brown powder from sample M27

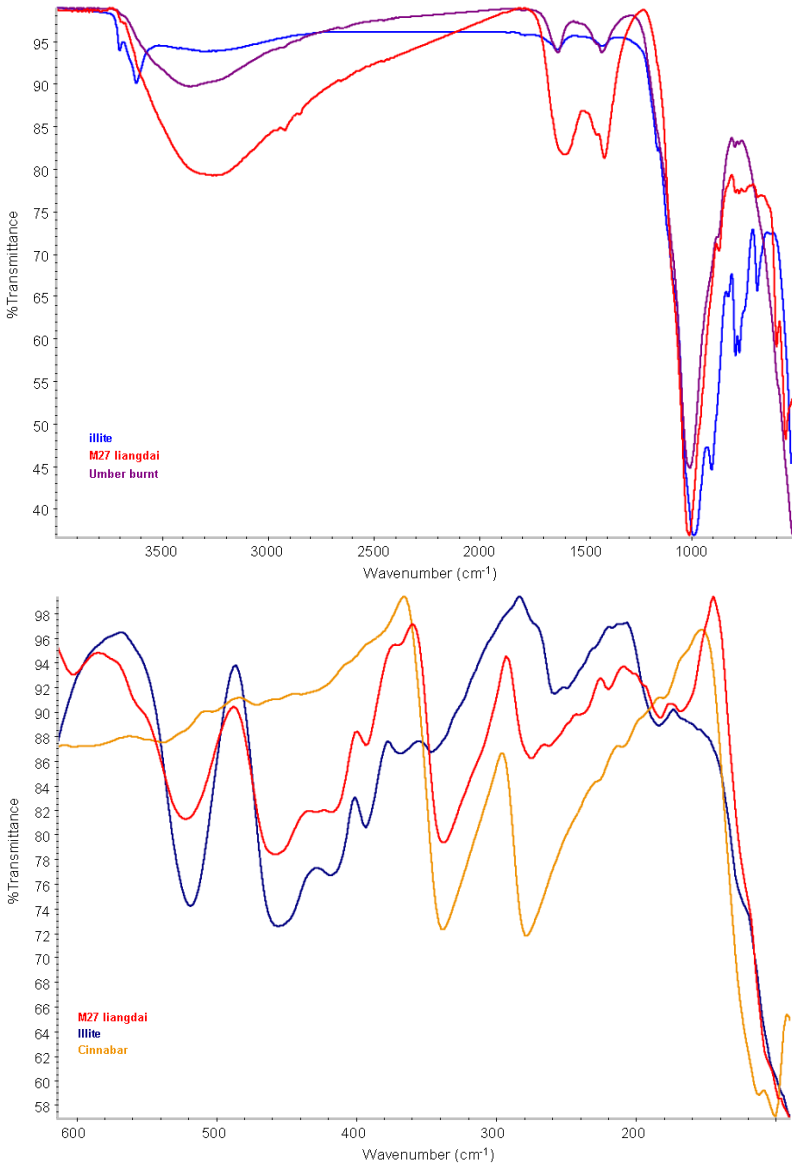

Figure 7.31: ATR Spectra of sample M27 (red) compared to burnt umber (purple), and illite (blue) in the MIR region and cinnabar (orange) and illite (blue) in the FIR region.

The first sample is red-brown coloured. In the MIR region we identify the red-brown powder as a siliceous material very similar to that of burnt Umber, which is a clayous silicate containing iron and manganese oxides. We also compare it to illite, a clayous silica containing both complex bonded and free water. Sample M27 has the broad OH-vibrations centred at 3350 cm^{-1}, which indicate all its water is bonded. When comparing to grey illite we observe the illite has free OH-vibrations seen at 3700-3600 cm^{-1}, it also has much more defined bands, i.e. the bands below 800 cm^{-1} (quartz), than sample M27.

By observing M27 in the MIR region, it is clearly a silicate whose internal molecular vibrations are similar to that of burnt umber. A small amount of organic material is also present in M27, it is observed by the very weak CH stretching bands below 3000 cm^{-1}.

In the FIR region the red-brown sample M27 is identified as cinnabar (HgS) by bands at 340 and 280 cm^{-1}. But also bands at 520, 465 and 397 cm^{-1} are observed, confirming the presence of clayous silica material very similar to those vibrations observed for illite (but not similar to the vibrations of burnt umber).

In a second sample from M27, more red than the first, we observe (with much stronger bands) the presence of the cinnabar. The silicate however, is present in much lower concentration in both MIR and FIR region. In the samples here from Liangdai, China, we observe typical corrosion products from archaeological bronze objects, azurite, malachite, cuprite and the red cinnabar powder traditionally used for ceremonial burials. In the case of malachite in the MIR region we observe no detectable signs of degradation while we in the FIR region observe missing bands in malachite indicating the degradation of the lattice structure. In the FIR region we are also able to detect the crystal structure of the silicate as belonging to the illite family by observing the lattice vibrations.

CHAPTER 8 CONCLUSIONS

8.1 RESUMÉ

The differences observed between samples collected in transmission and ATR spectroscopy are intensity differences, shift of bands to lower frequency and distortion of the band shape. These dissimilarities are known from literature concerning the MIR region. We substantiate that these variations are also observed in the FIR region. Since characteristic bands of standard pigments can be so different in appearance it is thus necessary to create a library database of standard spectra collected in both ATR as well as in transmission in the FIR region for comparison with unknown samples.

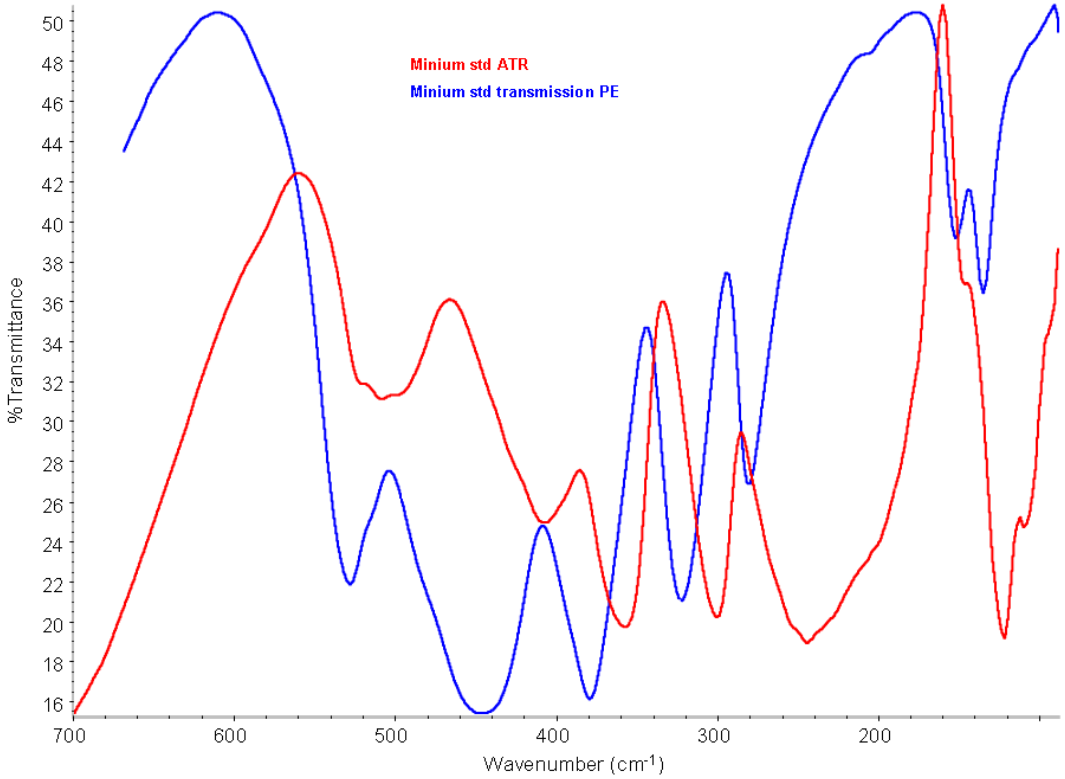

Figure 8.1: FIR spectra of minium (Pb_3O_4) collected in transmission (blue) and ATR (red). Considerable shifts are noticed.

One example is the red minium (Pb_3O_4) standard collected in transmission (blue) and ATR (red) it is quite obvious that significant shifts has occurred together with distortions of the band shape. Although the majorities of inorganic pigments change very little, in the range of 2-10 cm^{-1}, there are the occasional pigments, like the minium, which change significantly due to many coinciding factors. One being the differences in theory between transmission and ATR, which states that only the strong absorbing bands will shift frequency, and minium has such very strong bands in the FIR region.

In ATR spectroscopy the depth of penetration is deeper in the FIR region than in the MIR region. We should thus be able to achieve better spectra with less noise on the same amount of sample in the FIR region compared to spectra collected in the MIR region. This is an advantage when working with small quantities of sample, as is often the case when working with cultural heritage samples.

Our instrument has been optimised for FIR spectroscopic investigation. The main features for FIR collection is the solid substrate beamsplitter together with the higher energy output of the Globar light source, and the DTGS detector, which combines to collect better spectra with less noise in the FIR region, than ever seen before in the literature. We define the FIR region, as the region in which the solid substrate beamsplitter and the DTGS detector with PE window has been employed. In ATR the region is 700-90 cm^{-1} and in transmission the region is 670-90 cm^{-1}. Similarly, we define the MIR region, as the region where spectra was collected using the normal DTGS detector with KBr beamsplitter. The MIR region in ATR is 4000-525 cm^{-1} and in transmission it is 4000-400 cm^{-1}. There is a small overlap between the two regions.

Having both transmission and ATR as possible options of investigation in the FIR region, make the Thermo Nicolet 5700 a versatile investigative tool.

Table 8.1: Experimental set-up for collection of spectra in ATR spectroscopy in FIR and MIR mode and FIR transmission spectroscopy of thick pellets and thin films after optimization experiments.

PARAMTERS	**ATR Attenuated Total Reflection**		**FIR TRANSMISSION**	
	MIR	**FIR**	**FIR pellets**	**FIR thin film**
Sample compartment	Insert Smart Object	Insert Smart Object	Main Compartment	Main Compartment
Detector	DTGS	DTGS Polyethylene	DTGS Polyethylene	DTGS Polyethylene
Beamsplitter	KBr	Solid Substrate™	Solid Substrate™	Solid Substrate™
Source	Globar	Globar	Globar	Globar
Accessory	Smart orbit/diamond	Smart orbit/diamond	None	None
Window	None	PE	PE	PE
Max range (cm^{-1})	4000	700	670	670
Min range (cm^{-1})	525	90	90	90
N° of Scans/spectrum	64	64	64	64
Spectral resolution (cm^{-1})	4	4	4	4
Gain	Autogain	Autogain	Autogain	1
Mirror velocity (cm/s)	0,6329	0,6329	0,6329	0,9494
Calibration	Environmental RH (background)	Environmental RH (background)	Water vapour	Water vapour

The signal to noise ratio is improved immensely by lowering the mirror velocity from faster velocity settings. The only exception is for collection using the PE thin film. This requires a quicker mirror velocity and a lower gain, because of the very nature of the thin film. Unfortunately slowing

the moving mirror down also means increasing the time necessary for collecting one spectrum. One spectrum containing 64 scans at a mirror velocity of 0.6326 cm/s takes 96 seconds. Table 8.3 list the experimental set-up of the spectrometer after completing the optimization experiments.

We must conclude that the background is not stable over a long period of time, and hence it is necessary to always subtract the background when collecting a sample spectrum. The order of collecting the background also influences the quality of the spectra as experiments mentioned above has shown. Collecting the background first and the sample spectrum second, gives better quality spectra than the reverse order due to higher energy output.

Applying the GPG is necessary in both FIR and MIR spectroscopic collection of spectra. After the GPG has been switched on, the humid environment inside the spectrometer is stable enough for collection after approximately 30 min of purging. But once the GPG has been switched on for a ½ hour there are no longer any problems with water vapour bands in the FIR spectrum. Peak value must be checked before commencing any collection of spectra. If the experimental method or the beamsplitter is changed during the work day, then it is imperative to align the interferometer for maximum intensity signal.

The reproducibility is found in the region 700-90 cm^{-1} for ATR spectroscopy and 670-90 cm^{-1} for transmission spectroscopy. Below 90 cm^{-1} the spectra have unreliable and fluctuating bands arriving from the instrument background.

Some spectral manipulation is performed on all spectra collected in both ATR and transmission mode. We do not apply any zero-filling, but we employ the Happ-Genzel apodization algorithm to all collected spectra. Smoothing of spectra are especially applied when water bands are present in the spectrum or when harmonic vibrations disturb the spectrum. Normally smooth 5-9 is applied in the FIR region, while smooth 7-13 is applied in the MIR region.

Advanced ATR correction and Kramer-Kronig transformation algorithm was attempted in order to transform the ATR spectrum of cinnabar to a transmission spectrum. Neither was satisfactory enough in simulating transmission spectra. It is therefore still necessary to collect standard pigments using both techniques for building a digital library database.

In transmission we have chosen to use PE as the embedding medium because PE is transparent in the same region where our solid substrate beamsplitter is transparent. PE gives us an added region from 240-100 cm^{-1}, which we would not have if we where using CsBr as embedding medium. However, PE requires heating in order to be transparent to the infrared beam, this means also that the sample will be briefly exposed to the heat while producing the PE pellets. This is a problem if the sample is heat sensitive, especially for compounds containing H_2O, -OH and -NH. In many cases, inorganic pigments and minerals have higher melting points than that of the PE. For

those pigments and corrosion minerals we do not observe any structural changes. Changes are, however, observed in pigments containing H_2O, -OH and -NH. The changes are not always observed in the lattice vibration region but also sometime just in the OH stretching region (above 3000 cm^{-1}). This indicate changes in the molecule which do not affect the crystal structure of the compound.

Vivianit, an iron phosphate with water incorporated in the structure, was the pigments which showed the biggest differences in the FIR region. Some of the water is lost during the temperature experiments and we quite clearly see the difference before and after heating. To generalise, this means that we can expect structural changes in all samples which has incorporated water into the structure, when we examine the sample embedded in a PE pellet in transmission mode. It is therefore necessary to use one of the other options, PE thin films in transmission or ATR spectroscopy, for identifying samples with incorporated structural water.

PE itself is an excellent example of observed structural changes. When comparing the semitransparent PE pellet to the completely transparent PE thin film, we observe quite clearly a change in the structure. We observe the presence of new bands, shift of bands and changes in intensity.

The purpose of the PETF is to avoid exposing the sample to heat altogether by brushing the sample onto a PETF. The thin film is either commercially available or can be produced in the laboratory. The laboratory made PETF is produced from the same PE which is used for producing the normal PE pellets. Higher temperature and pressure are necessary to produce the thin film. The thin films requires no sample preparation, only powder or powder in an organic solution brushed onto the surface of the PETF. This is a fast and easy method for collection in the FIR region. But the PETFs are extremely sensitive to water vapours. Interpretation of weak bands appearing in PETF spectra must therefore be performed with caution.

The upper and lower limits for ATR and transmission mode are presented in **Errore. L'origine riferimento non è stata trovata.**. Malachite was selected as a representative standard for medium intensity compounds in the FIR region.

Table 8.2: Upper and lower limits for collection of std. malachite in transmission and ATR

	MIR ATR	**FIR ATR**	**FIR Trans (embedding)**
Lower limit	<0.04 mg	<0.04 mg	0.3% (~0.21 mg)
Std. samples	~0.1-0.2 mg	~0.1-0.2 mg	0.3-2.1% (~0.2-1.5 mg)
Maximum limit	>0.5 mg	>0.5 mg	>3.3% (~2.38 mg)

For ATR spectroscopy, both in the MIR and FIR region, the lower spectral identification limit is less than 0.04 mg of malachite. This is a factor of 10 better than for transmission. The normal

amount used for ATR is approximately 0.1-0.2 mg, while it is 0.2-1.5 mg for transmission. For ATR there is a natural upper limit in that if more than 0.5 mg is placed on the ATR crystal, it quite simply covers the entire crystal. It has not been attempted to find the upper limit visible in the spectra, because we work with cultural heritage materials, i.e. often only small amounts are available.

Following these sample preparation for both ATR and transmission we are now ready to begin spectral collection of standards in order to build a library database for comparison with samples from cultural heritage objects.

When building up the library it is necessary to known the standards as well as the impurities present in the standards, and if the impurities are present in such amount than they might influence the spectrum, i.e. observing vibrational bands from the impurities. Generally if the impurities are present in more than 5-10 % you should expect to observe them. It also depends on how absorbing the bands of the impurities are, are they strong absorbing, you should expect to seem them at the very least as a shoulder; are they low absorbing, they will perhaps only cause band broadening even if present in high concentration.

From the comparison of three compounds called cinnabar and one called cinaprino we have learned an important lesson; that it is difficult to trust your suppliers. The pigments you buy as a standard may have one name which makes you expect mercury sulphide, but the contents can be something quite different. The same can be said of our litharge and massicot standards.

It is therefore, unfortunately, necessary to check the standards by other means for contents and also for impurities. This can be achieved by Raman analysis or, if the pigment has a crystal structure (not amorphous), XRD analysis can also be performed with success determining the purity of the crystal. XRF analysis is also good for elemental analysis, but if the standard contains organic substances the XRF is not useful, which we observed in the cinaprino standard.

The same crystal systems, i.e. calcite and smithsonite, gives very similar spectral vibrations, which can make it difficult to distinguish between the two, especially if you have a mixture, if you are not attentive. We also learned from comparison of our mineral with wavenumbers in the literature, that precipitated calcite moves the wavenumber frequency higher while mineral calcite moves the frequencies lower. This is a general trend observable both in Raman and IR spectroscopy. Hematite is an excellent example that temperature and production method of a standard can heavily influence the vibrations observed in the spectra. By comparing mineral azurite and malachite we observe that impurities facilitates the possible assignment of mineral provenance.

We observe a few time the 1st order maxima band present in oxides and sulphides. Occasionally this band is also observed in literature. The 1st order maxima band is a result of overlapping

reflection with an actual band frequency, it is mainly observed when the powder pigment is ground to very small particles. The particle size is not always controllable by us, as most pigment standards are delivered already grounded from the supplier. Some standards are grounded to very specific particle sizes in order to achieve various shade of colour, as the colour generally becomes lighter with smaller particle sizes.

When looking at binding media it is no surprise that we can observe binding media in the MIR region even when mixed with strong absorbing pigments. But we observe no bands from the binding media in the FIR region although we do observe band broadening of the pigment vibrations.

After the comparative studies of the M2ADL tablet are complete we must conclude that the best way of examining the didactic test tablets is by scratching powder from the samples and then examining the powder, either by ATR (MIR or FIR) or in transmission mode, by either embedding the powder in PE or applying dust particles from the powder on the surface of a transparent PE pellet. Surface contact can also be used but the weaker components, in our case the binding medium, is not always observed due to bad contact and baseline noise. Water enhancing the signal can work but it is not reliable and there are still too many unknowns in the equation. The beam condenser, although brilliant in theory, requires a lot more practical testing before optimum utilisation is achieved in the FIR region.

When we perform transmission spectroscopy on our samples from Abbazia del Monte we are able to confirm in one sample what was already observed in the MIR region by a second technique, µATR spectroscopy on cross-section. In the second sample the same µATR technique had failed to give us any information due to penetration of the embedding medium into the sample, but also here we succeed in getting the required information, that is the characterisation of read and green earth pigments.

From the Thubchen Lakhang monestary in Nepal we had high hopes for finding pigments like lapis lazuli, pararealgar and cinnabar. Unfortunately, due to the bad state of the sample material, most samples coming from the mural paintings had been covered by a thin layer of clay material similar to the clay used for the construction of the walls and roof. When removing small grain samples for ATR collection, the clay material was present in almost every sample collected. We do however, manage to identify some of the colours employed by the Nepalese artist. The pigments identified are azurite, cinnabar, hematite (red ochre), calcite and China clay. Green inclusions in a blue layer is found to be basic copper chlorides, a degradation product of azurite.

The bronze corrosion products analysed from Liangdai, China gives us added information about the state of the lattices structures when we observe the FIR region. We expect a certain degree of

degradation due to the fact that the objects have been excavated after numerous years in the soil. By using the FIR region for analysis, we learn whether the crystal structures are degraded with missing bands or that they are comparable to pure mineral structures.

8.2 CONCLUSIONS

Both transmission and ATR spectroscopy can be used in the FIR region. Both has advantages and disadvantages.

Transmission spectroscopy is perhaps the method with most disadvantages. The biggest disadvantage is that you can cause a structural change in the pigment, when you heat the pigment together with the PE to form the pellet. Especially if the pigment contains water or hydroxide some degree of structural change must be expected to happen in the pigment which we observed in chapter 4. As no heat is required in the ATR method, this is a major advantage over the transmission method.

A major disadvantage for the ATR method is the lack of literature of collected spectra, which to a certain degree is available in transmission mode. The literature is not available down to 90 cm^{-1}, which is our lower limit of collection for both transmission and ATR spectroscopy, but it is available down to 300-200 cm^{-1} for most compounds.

In ATR there is little (or no) preparation time of the sample, while in transmission you have to embed the sample in PE under heating or, if you use the PETF, you have to apply the powder onto the PETF. Normally this does not take any time but if your sample has a high content of binding material it is not possible to brush it on the PETF, you have to dissolve the sample in an inert liquid first, apply it on the PETF and wait for it to dry.

Table 8.3: Advantages and disadvantages for transmission and ATR spectroscopy.

Procedure:	**Transmission method**		**ATR method**	
	Advantage	**Disadvantage**	**Advantage**	**Disadvantage**
Heat required		yes	no	
Literature available	yes			no
Preparation time	no (PETF)	yes (PE)	no	
Surface contact	no			yes
Sample:				
Solid		no	yes	yes
Liquid	yes		yes	
Powder	yes		yes	
Lowest amount	0.3%*		0.04 mg*	

*on malachite samples

A potential disadvantage of the ATR is that the method requires surface contact. In most cases this is not a problem, with powder or liquid there are no problems, but with a solid sample a certain degree of problem will arise due to the sample-ATR crystal interface. Most time the contact will just result in noise on the baseline, but in other cases, due to the sample not being planar, contact is not obtainable. In transmission there is no surface contact, samples must be in powder or liquid form, embedded in PE or applied to PETF. Solid samples cannot be examined by transmission. Table 8.3 gives an overview of the advantages and disadvantages mentioned here.

Too much amount placed on the ATR crystal or too much powder embedded in the PE can cause band broadening and loss of band definition. When examining powder in chapter 4, we also determined the lower limit for malachite embedded in PE or placed on the ATR crystal. ATR is determined to be a factor of 10x better than transmission when comparing amount of sample employed. If we go any lower in amount the noise from the instrument could cause interference for band interpretation in the spectra making it difficult to interpret vibration bands.

ATR and transmission spectroscopy are both excellent methods when working with small quantities of samples removed from cultural heritage objects.

In infrared spectroscopy there are already established procedure using μATR in the MIR region on cross-sections [11, 20] which gives a excellent idea of what pigments a painter has applied to his canvas, layer after layer. But μATR analysis of cross-sections comes short, due to technical limitation caused by a detector cut-off at 650 cm^{-1}. Below 650 cm^{-1}, as we have seen, is where all the important oxides and sulphides of heavy metals have there most prominent vibrations bands, i.e. like minium, massicot, cinnabar, cuprite, orpiment and realgar. In many cases the scientist would then turn to micro-Raman spectroscopy for observing the pigments just mentioned [110] and for analysing cross-sections [13, 79, 104]. However, also for examining cross-sections by micro Raman spectroscopy there are limitations in the form of fluorescence, which is very often caused by degrading binding media present in the paintlayer.

This is then where the two methods, transmission spectroscopy and/or ATR spectroscopy in both MIR and FIR region, can step in and assist in the identification of oxides and sulphides used in paint and pigments. Optimum examination of a sample from an artwork would be to use both IR and Raman spectroscopy to enable the scientist to have a complete picture of the pigments and binding media used by the artist.

IR spectroscopy is but one of many ways to examine particles removed from artworks. As the tree of methodology is showing us in Figure 8.2, once you select your sampling area on the artwork

and remove micro particles from the artwork (making proper photo documentations) there are many possible ways of analysing your sample; each method has its strength and weaknesses.

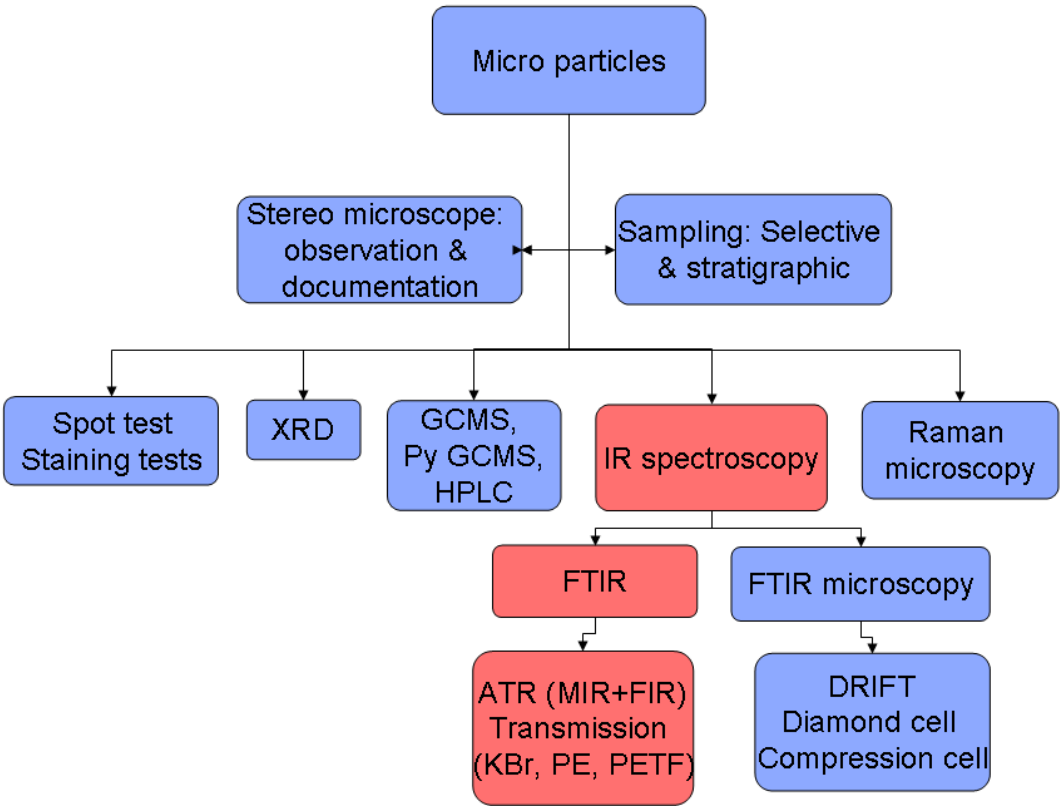

Figure 8.2: Tree of metodology for micro particles removed from an artwork.

When applying chemical spot test on your chemicals you can detect elements present but not the structures nor do you have any information about impurities. With X-Ray Diffraction (XRD) you can determine the crystal structures but only if the structure is crystalline and not amorphous. GCMS and similar related methods are required in order to completely identify the organic compounds present, particular the binding media applied in paintings.

IR and Raman spectroscopy are complementary methods, where Raman always has had the advantage when identifying the heavy oxides and sulphides due to the Raman region (3500-100 cm^{-1}). The only problem with Raman has been fluorescence, which can make interpretation of bands difficult. IR spectroscopy has, as already discussed in previous chapters, had problems with beamsplitters and detector cut-off at 400 cm^{-1} in the past. All of which made it difficult to observe the heavy oxides and sulphides used as paint materials. However, with new beamsplitter material (solid substrate) combined with a DTGS detector, it is now possible to collect IR spectra of particles in the region 4000-90 cm^{-1} employing both ATR and transmission spectroscopy. The big advantage is the price of this extended region, as it is available at a reasonable affordable prices in accessory

equipment to an already existing FTIR spectrometer (in our case the Nicolet 5700 spectrometer from Thermo Scientific).

8.3 FURTHER DEVELOPMENTS

The next development in FIR spectroscopy would be to collect spectra in the FIR region on cross-section of a sample. This is not impossible but unfortunately still a very expensive endeavour.

The combination of a microscope with the FIR region requires some technical improvements, mainly higher energy source and a different combination of detector and beamsplitter are required. So far these improvements are only available in synchrotron radiation facilities; one synchrotron beamline (U10A) is available at NSLS, Brookhaven laboratories, Upton, NY, USA. This beamline makes it possible to collect microscopic areas of a cross-section in the range 700-25 cm^{-1}. This is possible only due to the high amount of energy created in the synchrotron facility.

The use of the micro-IR spectrometer with the capability of collecting vibrational bands in the FIR region 700-25 cm^{-1}, together with micro IR-spectroscopy or μATR spectroscopy in the MIR region 4000-650 cm^{-1}, would thus give a complete chemical map of a cross-section from a painting, covering in total the 4000-25 cm^{-1} region. This would cover both organics as well as inorganic components present in the cross-section.

However, this is still only possible in a synchrotron facility and a better, cheaper and more manoeuvrable energy source would have to be invented before this would be feasible.

Instead, the possibility available to us at this point in time in the FIR region is that which is described here in the project. Here we can collect the vibrational bands of oxides and sulphides from pigments and corrosion products in the FIR region by transmission and ATR spectroscopy by removing individual grain samples from the sample surfaces. It has been performed with remarkable ease and with relative low cost accessory to an already existing spectrometer.

ACKNOWLEDGEMENTS

There is a lot of people I would like to extend my gratitude, without whose cooperation this project would never have been realised.

My supervisor, colleagues and the students at M2ADL, University of Bologna, Ravenna Campus. Initial PE experiments with forming the pellets, first directly on the hotplate, later in the anvil die, was carried out by master student Simone Capelli, in our M2ADL department, University of Bologna, Italy.

Prof. Andrea Saccani from the Applied Chemistry and Materials Science department, University of Bologna, Italy, was very helpful in determining he exact melting point of our PE by using DSC.

Prof. Pietro Baraldi from the department of Chemistry, University of Modena, Italy, and Prof. Concezio Fagnano, from the department of Biochemistry, University of Bologna, Italy, has kindly shared their standard pigments as well as their knowledge of the standard pigments with us, in order for us to collect as many spectra as possible of inorganic pigments in the FIR region.

Prof. Concezio Fagnano, Biochemical department, University of Bologna, Prof. Pietro Baraldi, Chemistry department, University of Modena and Prof. Emilio Castellucci at LENS, University of Florence, for good advise and scientific discussions.

Prof. Fagnano was also kind enough to conduct Raman analysis using a 488 nm laser on a number of standard pigments in order to identify the impurities.

Dr. Daniella Pinna from the Pinacota Nationale, Bologna, Italy, allowed me to collect Raman Spectra of selected pigments using their 785 nm Micro-Raman spectrometer.

Our collection of corrosion products comes by courtesy of Prof. Vanna Minguzzi from the Geological museum, University of Bologna, Italy, who was not only kind enough to supply the standards, but has also performed DTA and powder XRD analysis on the same standards for verification and purity analysis.

My family and friends for always being there for me despite the distance between us.

This project has been carried out with the support of the European Union within the Marie Curie EST action, contract EPISCON, MEST-CT-2005-020559.

REFERENCE

1. Aaby, B.; Gregory, D.; Jensen, P.; Smith Sørensen, T. *In-situ bevaring af oldsager i Nydam Mose (In-situ conservation of relics in Nydam Bog)*; National Museum of Denmark: 1999; pp 35-44.

2. Herschel, F. W., Investigations of the powers of the prismatic colours to heat and illuminate objects. *Philos. Trans. R. Soc. London,* **1800,** 90, (49), 255-283.

3. Sheppard, N., The Historical Development of Experimental Techniques in Vibrational Spectroscopy. In *Handbook of Vibrational Spectroscopy*, Chalmers, J.; Griffiths, P., Eds. John Wiley & Sons: 2001; Vol. 1, pp 1-32.

4. Jiang, E. Y., *Advanced FTIR Spectroscopy: Principles, Experiments and Application*. Thermo Scientific Publication: 2007; p 52.

5. Stimson, M. M.; O'Donnell, M. J., The Infrared and Ultraviolet Absorption Spectra of Cytosine and Isocytosine in the Solid State. *Journal of the American Chemical Society* **1952,** 74, (7), 1805-8.

6. Dent, G., Preparation of Samples for IR Spectroscopy as KBr Disks. In *The Internet Journal of Vibrational Spectroscopy*, Wiley & Sons: 1996; pp 3-6.

7. Cooley, J. W.; Tukey, J. W., An algorithm for machine calculation of complex Fourier series. *Math. Comp.* **1965,** 19, 297–301.

8. Homepage of Nobel Prizes http://nobelprize.org/. (Access Date: June 4th 2009),

9. Harrick, N. J.; du Prè, F. K., Effective Thickness of Bulk Materials and of Thin Films for Internal Reflection Spectroscopy. *Applied Optics* **1966,** 5, (11), 1739-1743.

10. Harrick, N. J., Electric Field Strengths at Totally Reflecting Interfaces. *Journal of the Optical Society of America* **1965,** 55, (7), 851-857.

11. Mazzeo, R.; Joseph, E.; Prati, S.; Millemaggi, A., Attenuated Total Reflection–Fourier transform infrared microspectroscopic mapping for the characterisation of paint cross-sections. *Analytica Chimica Acta* **2007,** 599, (1), 107-117.

12. Mazzeo, R.; Joseph, E.; Minguzzi, V.; Grillini, G.; Baraldi, P.; Prandstraller, D., Scientific investigations of the Tokhung-Ri tomb mural paintings (408 A.D.) of the Koguyo era, Democratic People's Republic of Korea. *Journal of Raman Spectroscopy* **2006,** 37, 1086-1097.

13. Kendix, E.; Nielsen, O. F.; Christensen, M. C., The use of micro-Raman spectroscopy in architectural paint analysis. *Journal of Raman Spectroscopy* **2004,** 35, (8-9), 796-799.

14. Afremow, L. C.; Vandeberg, J. T., High Resolution Spectra of Inorganic Pigments and Extenders in the Mid-Infrared Region from 1500 to 200 cm^{-1}. *Journal of Paint Technology* **1966,** 38, (495), 169-202.

15. Karr, C. J., *Infrared and Raman Spectroscopy of Lunar and Terrestrial Minerals*. Academic Press: New York, NY (USA), 1975; p 376.

16. Kendix, E.; Moscardi, G.; Mazzeo, R.; Baraldi, P.; Prati, S.; Joseph, E.; Capelli, S., Far infrared and Raman spectroscopy analysis of inorganic pigments. *Journal of Raman Spectroscopy* **2008,** 39, (8), 1104-1112.

17. Kendix, E.; Prati, S.; Joseph, E.; Sciutto, G.; Mazzeo, R., ATR and transmission analysis of pigments by means of far infrared spectroscopy. *Analytical and Bioanalytical Chemistry* **2009,** 394, (4), 1023-1032.

18. Kendix, E.; Prati, S.; Mazzeo, R.; Joseph, E.; Sciutto, G.; Fagnano, C., Far Infrared Spectroscopy in the Field of Cultural Heritage. *e-PRESERVATIONScience (IRUG8 conference proceedings)* **2009,** accepted for publication.

19. Kendix, E. L.; Prati, S.; Mazzeo, R.; Joseph, E.; Sciutto, G., Far Infrared Spectroscopy of Pigments in Art. *Meddelelser om Konservering (Announcement about Conservation)* **2008,** 2, 3-10.

20. Mazzeo, R.; Prati, S.; Quaranta, M.; Joseph, E.; Kendix, E.; Galeotti, M., Attenuated total reflection micro FTIR characterisation of pigment–binder interaction in reconstructed paint films. *Analytical and Bioanalytical Chemistry* **2008,** 392, 65-76.

21. Shugar, G. J.; Ballinger, J. T.; Dawkins, L. M., *Chemical technicians' ready reference handbook*. 4th ed.; 1996; p 992.

22. Lide, D. R., *CRC Handbook of Chemistry and Physics*. 89th ed.; CRC Press: Boca Raton, USA, 2008.

23. http://teaching.shu.ac.uk/hwb/chemistry/tutorials/molspec/irspec1.htm. (Dec.),

24. Singh, J. Lattice vibrations: Scattering of phonons. http://www.cambridge.org/resources/052182379X/2064_ch06.pdf

25. Maddams, W., The Background to Sample Preparation for Infrared Transmission Measurements on Solids. In *The Internet Journal of Vibrational Spectroscopy*, Wiley & Sons: 1996; pp 6-12.

26. Tsang, J.-S.; Cunningham, R. H., Some Improvements in the Study of Cross Sections. *Journal of the American Institute for Conservation* **1991,** 30, (2), 163-177.

27. Neri, F.; Saitta, G.; Chiofalo, S., A simple procedure to remove the interference fringes from optical spectra. *Journal of Physics E: Scientific Instruments* **1987,** 20, (7), 894-896.

28. Zallen, R.; Lucovsky, G.; Taylor, W.; Pinczuk, A.; Burstein, E., Lattice Vibrations in Trigonal HgS. *Physical Review B* **1970,** 1, (10), 4058-470.

29. Liang, W. Y.; Yoffe, A. d., Transmission Spectra of ZnO Single Crystals. *Physical Review Letters* **1968,** 20, (2), 59-62.

30. *ATR - Theory and Applications*; Pike Technologies: Madison, 2005; pp 1-3.

31. Bradley, M.; Izzia, F., ATR in the Far-Infrared Region - A Simple Tool for Analysis of Heavy Metals in Polymers and Incinerator Ash. *Thermo Scientific Application Note* **2008,** 50828.

32. Vahur, S.; Knuutinen, U.; Leito, I., ATR-FT-IR spectroscopy in the region of 500-230 cm^{-1} for identification of inorganic red pigments. *Spectrochimica Acta Part A: Molecular and Biomolecular Spectroscopy* **2009,** 73, (4), 764-771.

33. Keune, K. Binding medium, pigments and metal soaps characterised and localised in paint cross-sections. Paint
Binding medium
Cross section, Amsterdam, 2005.

34. Averett, L. A.; Griffiths, P. R.; Nishikida, K., Effective Path Length in Attenuated Total Reflection Spectroscopy. *Analytical Chemistry* **2008,** 80, (8), 3045–3049.

35. Lucania, J. P.; Berets, S. L.; Milosevic, M.; Gremlich, H.-U.; Schmitt, J. *The Identification of Geological Samples Using Single Reflection Diamond ATR FTIR Spectroscopy*; Harrick Applications Bulletin, november 2008, 2008; p 21.

36. Kulesza, P. J.; Malik, M. A.; Denca, A.; Strojek, J., In Situ FT-IR/ATR Spectroelectrochemistry of Prussian Blue in the Solid State. *Anal Chemistry* **1996,** 68, 2442-2446.

37. Humecki, H. J., *Practical Guide to Infrared Microspectroscopy*. Marcel Dekker, Inc.: New York, USA, 1995; Vol. 19, p 472.

38. Nunn, S.; Nishikida, K., Advanced ATR Correction Algorithm. *Thermo Scientific Application Note* **2003,** 01153.

39. Smith, B. C., *Fundamentals of Fourier transform infrared spectroscopy*. CRC Press: Boca Raton, 1996; p 202.

40. Pavia, D. L.; Lampman, G. M.; Kriz, G. S., *Introduction to spectroscopy*. 2nd ed.; Harcourt Brace College Publishing: 1996; p 511.

41. Naylor, D. A.; Boreiko, R. T.; Clark, T. A., Mylar beam-splitter efficiency in far infrared interferometers: angle of incidence and absorption effects. *Applied Optics* **1978,** 17, (7), 1055-1058.

42. Griffiths, P. R.; de Haseth, J. A., *Fourier Transform Infrared Spectrometry*. 2nd ed.; Wiley-Interscience, a John Wiley & Sons, Inc., Publication: 2007; p 529.

43. Angino, E. E., Far Infrared (500-30 cm^{-1}) Spectra of some Carbonate Minerals. *The American Mineralogist* **1967,** 52.

44. Vidrine, D. W.; Anderson, C. R. Silicon Beamsplitter (rigid far-IR beamsplitter utilizing ordinary double-side-polished silicon wafers). US Patent No. 4,632,553, 1986.

45. Manduca, N., Personal Communication with Technician from Thermo Scientific. In 2009.

46. Kok Chemware http://www.sanderkok.com/techniques/ir/. (Last accessed June 2009),

47. Finch, A., *Chemical Applications of Far Infrared Spectroscopy*. Academic Press Inc (Jun 1970): 1970; p 277.

48. Anderson, A.; Wong, L. Y., Crystal field splitting in the far infrared spectrum of rhombic sulfur. *Canadian Journal of Chemistry* **1969,** 47, 2713-2715.

49. Becucci, M.; Bini, R.; Castellucci, E.; Eckert, B.; Jodl, H. J., Mode Assignment of Sulfur α-S_8 by Polarized Raman and FTIR Studies at Low Temperatures. *The Journal of Physical Chemistry B* **1997,** 101, (12), 2132.

50. Shimadzu Application *Kramers- Kronig Transform and Applications*; p 2.

51. Thermo Scientific Algorithms - Kramers-Kronig Transform. http://www.thermo.com/com/cda/resources/resources_detail/1,2166,13331,00.html (June 2009),

52. Dressel, M.; Gompf, B.; Faltermeier, D.; Tripathi, A. K.; Pflaum, J.; Schubert, M., Kramers-Kronig-consistent optical functions of anisotropic crystals: generalized spectroscopic ellipsometry on pentacene. *Optics Express* **2008,** 16, (24), 19770-19778.

53. Thermo Scientific http://www.thermo.com/com/cda/resources/resources_detail/1,2166,13331,00.html.

54. Kok Chemware Sanderkok Infrared Spectroscopy techniques. http://www.sanderkok.com/techniques/ir/ (May 15 2009),

55. Parkhutik, V.; San-Jerónimo Martínez, M.; Gómez Senent, E., Processing of Infrared Spectroscopy Data on Thin Porous Films Using Software "Prospect". *Journal of Porous Materials* **2000,** 7, (1-3), 239-242.

56. Clark, F. R. S.; Moffatt, D. J., The Elimination of Interference Fringes from Infrared Spectra. *Applied Spectroscopy* **1978,** 32, (6), 547-549.

57. Hirschfeld, T.; Mantz, A. W., Elimination of Thin Film Infrared Channel Spectra in Fourier Transform Infrared Spectroscopy. *Applied Spectroscopy* **1976,** 30, (5), 552-553.

58. Gerbaux, X.; Hadni, A.; Tazawa, M.; Villegier, J. C., Far-infrared spectra of magnesium oxide. *Applied optics* **1994,** 33, (1), 57-59.

59. May, L.; Schwing, K. J., The Use of Polyethylene Disks in the Far Infrared Spectroscopy of Solids. *Applied spectroscopy* **1963,** 17, (6), 166-166.

60. de Langen, M.; Prins, K. O., NMR investigation of phase transitions in polyethylene in the vicinity of the hexagonal high pressure phase. *Polymer* **2000,** 41, (3), 1175-1182.

61. Hikosaka, M.; Tsukijima, K.; Rastogi, S.; Keller, A., Equilibrium triple point pressure and pressure-temperature phase diagram of polyethylene. *Polymer* **1992,** 33, (12), 2502-2507.

62. Oral, E.; Godleski Beckos, C.; Muratoglu, O. K., Free radical elimination in irradiated UHMWPE through crystal mobility in phase transition to the hexagonal phase. *Polymer* **2008,** 49, (21), 4733-4739.

63. Farmer, V. C.; Russell, J. D., Effects of particle size and structure on the vibrational frequencies of layer silicates. *Spectrochimica Acta* **1966,** 22, (3), 389-398.

64. Sato, K.; Kurosawa, F.; Kammori, O., Effect of Particle Size on Infrared Spectra of Inorganic Powders. *Bulletin of the Chemical Society of Japan* **1969,** 42, (12), 3593-3596.

65. Schiele, C.; KHalfar, K., Cold pressing of polyethylene Disk. A new Technique. *Applied Spectroscopy* **1965,** 19, (5), 163-164.

66. Rendon, J. L.; Serna, C. J., IR spectra of Hematite: The effect of particle size and shape. *Clay Minerals* **1981,** 16, 375-381.

67. Rodgers, K. A.; Kobe, H. W.; Childs, C. W., Characterization of Vivianite from Catavi, Llallagua Bolivia. *Mineralogy and Petrology* **1992,** 47, (2-4), 193-208.

68. Giron, D., Thermal analysis and calorimetric methods in the characterisation of polymorphs and solvates. *Thermochimica Acta* **1995,** 248, 59.

69. Endoh, T.; Kurihara, Y., Influence of Pb impurity on melting point and metallography of Sn-5wt%Sb alloy. *Electronics and Communications in Japan (Part II: Electronics)* **1998,** 81, (1), 12.

70. Fellmuth, B.; Hill, K., Estimating the influence of impurities on the freezing point of tin. *Metrologia* **2006,** 43, (1), 83.

71. Thomsen, V.; Schatzlein, D.; Mercuro, D., Limit of Detection in Spectroscopy. *Spectroscopy* **2003,** 18, (12), 112-114.

72. McNaught, A. D.; Wilkinson, A., *IUPAC Compendium of Chemical Terminology (the "Gold Book").* 2nd ed.; Blackwell Scientific Publications: Oxford, 1997.

73. Nakamoto, K., *Infrared and Raman Spectra of Inorganic and Coordination Compounds, Parts A & B*. 6th ed.; Wiley-Interscience: New York, 2009.

74. Nyquist, R. A.; Kagel, R. O., *Infrared Spectra of Inorganic Compounds (3800-45 cm^{-1}).* Academic Press: New York, 1971; p 495.

75. Farmer, V. C., *The Infrared Spectra of Minerals*. Mineralogical Society Monograph 4: London, 1974; p 539.

76. McDevitt, N. T.; Baun, W. L., Infrared Absorption Study of Metal Oxides in the Low Frequency Region (700-240 cm^{-1}). *Spectrochimica Acta* **1964,** 20, 799-808.

77. Damen, T. C.; Porto, S. P. S.; Tell, B., Raman Effect in Zinc Oxide. *Physical Review* **1966,** 142, (2), 570.

78. Burgio, L.; Clark, R. J. H., Library of FT-Raman spectra of pigments, minerals, pigment media and varnishes, and supplement to existing library of Raman spectra of pigments with visible excitation. *Spectrochimica Acta Part A: Molecular and Biomolecular Spectroscopy* **2001,** 57, (7), 1491-1521.

79. Kendix, E. NIR-FT-Raman spectroscopic investigations of: 1. Cross-sectional paint analysis of historic buildings. 2: Seashells from snails & mussels (in Danish). Institute of Chemistry, University of Copenhagen, 2004.

80. Katiyar, R. S.; Dawson, P.; Hargreave, M. M.; Wilkinson, G. R., Dynamics of the rutile structure. III. Lattice dynamics, infrared and Raman spectra of SnO2. *J. Phys. C: Solid State Phys.* **1971,** 4, (15), 2421-2431.

81. Gonzales, R. J. Raman, Infrared, X-ray, and EELS Studies of Nanophase Titania. Virginia Polytechnic Institute and State University, Blacksburg, Virginia, 1996.

82. Berreman, D. W., Infrared Absorption at Longitudinal Optic Frequency in Cubic Crystal Films. *Physical Review* **1963,** 130, (6), 2193-2198.

83. Johansen, T. http://www.paintmaking.com. (2009 August),

84. Newman, R., Some Applications of Infrared Spectroscopy in the Examination of Painting Materials. *Journal of the American Institute for Conservation* **1979,** 19, (1), 42-62.

85. White, W. B.; Roy, R., Infrared Spectra-Crystal Structure Correlations: II. Comparison of simple polymorphic Minerals. *THE AMERICAN MINERALOGIST* **1964,** 49, 1670-1687.

86. http://en.wikipedia.org/wiki/Orpiment.

87. http://en.wikipedia.org/wiki/Realgar.

88. Douglass, D. L.; Shing, C.; Wang, G., the light induced alteration of realgar to pararealgar. *American Mineralogist* **1992,** 77, 1266-1274.

89. Foneris, R., the infrared and raman spectra of realgar and orpiment. *THE AMERICAN MINERALOGIST* **1969,** 54, 1062-1074.

90. Gettens, R. J.; Stout, G. L., *Painting materials*. 2nd ed.; Dover Publications, Inc: New York, 1966; p 333.

91. Ghosh, S., Infrared spectra of the Prussian blue Analogs. *Journal of Inorganic and Nuclear Chemistry* **1974,** 36, (11), 2465-2466.

92. Wilde, R. E.; Ghosh, S. N.; Marshall, B. J., The Prussian blues. *Inorganic Chemistry* **1970,** 9, 2513-2516.

93. Frost, R. L.; Martens, W. N.; Rintoul, L.; Mahmutagic, E.; Kloprogge, J. T., Raman spectroscopic study of azurite and malachite at 298 and 77 K. *Journal of Raman Spectroscopy* **2002,** 33, (4), 252-259.

94. Cornell, R. M.; Schwertmann, U., *The Iron Oxides*. 2nd ed.; Wiley-VCH, GmbH & Co. KgaA: 2003; p 694.

95. Kosmas, C. S.; Franzmeier, D. P.; Schulze, D. G., Relationship among derivative spectroscopy, color, crystallite dimensions, and Al substitution of synthetic goethites and hematites. *Clays and Clay Minerals* **1986,** 34, (6), 625-634.

96. Heltemes, E. C., Far-Infrared Properties of Cuprous Oxide. *Physical Review* **1966,** 141, (2), 803.

97. Karr, J., Clarence; Kovach, J. J., Far-Infrared Spectroscopy of Minerals and Inorganics. *Applied Spectroscopy* **1969,** 23, (3), 219-223.

98. Gettens, R. J.; Feller, R. L.; Chase, W. T., Vermilion and Cinnabar. *Studies in Conservation* **1972,** 17, 45-69.

99. Thomsen Jr., D. V., *The Craftman's Handbook "il Libro dell' Arte" Cennino d'Andrea Cennini*. 3rd ed.; Dover Publications Inc.: New York, 1960.

100. Friend, J. N., *The Chemistry of Linseed Oil*. Gurney & Jackson: London, 1917; p 112.

101. Joseph, E. Application of FTIR Microscopy To Cultural Heritage Materials. Università di Bologna, Ravenna, 2009.

102. Lazzari, M.; Chinatore, O., Drying and oxidative degradation of linseed oil. *Polymer Degradation and Stability* **1999,** 65, (2), 303-313.

103. Dreesen, R.; Dusar, M., Historical building stones in the province of Limburg (NE Belgium): role of petrography in provenance and durability assessment. *Materials Characterization* **2004,** 53, (2-4), 273-287.

104. Mazzeo, R.; Baraldi, P.; Lujàn, R.; Fagnano, C., Characterization of mural painting pigments from the Thubchen Lakhang temple in Lo Manthang, Nepal. *Journal of Raman Spectroscopy* **2004,** 35, (8-9), 678-685.

105. Downs, R. T. In *The RRUFF Project: an integrated study of the chemistry, crystallography, Raman and infrared spectroscopy of minerals.*, 2006; Program and Abstracts of the 19th General Meeting of the International Mineralogical Association in Kobe, Japan. O03-13: 2006.

106. Braithwaite, R. S. W.; Mereiter, K.; Paar, W. H.; Clark, A. M., Herbertsmithite, Cu3Zn(OH)6Cl2, a new species and the definition of paratacamite. *Mineralogical Magazine* **2004,** 68, 527-539.

107. Vandenabeele, P.; Lambert, K.; Matthys, S.; Schudel, W.; Bergmans, A.; Moens, L., In situ analysis of mediaeval wall paintings: a challenge for mobile Raman spectroscopy. *Anal. Bioanal. Chem.* **2005,** 383, (4), 707-712.

108. Dei, L.; Ahle, A.; Baglioni, P.; Dini, D.; Ferroni, E., Green degradation products of azurite in wall paintings: Identification and conservation treatment. *Studies in conservation* **1998,** 43, (2), 80-88.

109. CNR.CN Aristocratic Cemetery of the Zhou Dynasty in Liangdai Village, Shaanxi Province. (december, 2005),

110. Edwards, H. G. M.; Farwell, D. W.; Lee, J. S.; Fredericks, P. M., Vibrational spectroscopic study of the contents of a chest excavated from the wreck of the HMS Pandora. *Spectrochimica Acta Part A: Molecular and Biomolecular Spectroscopy* **2003,** 59, (10), 2311.